Titre: Title:	Investigation of Waste Rock Segregation and Heterogeneity During Disposal Using Field Observation, Experimental Tests and Discrete Element Simulations
Auteur: Author:	Peiyong Qiu
Date:	2022
Type:	Mémoire ou thèse / Dissertation or Thesis
Référence: Citation:	Qiu, P. (2022). Investigation of Waste Rock Segregation and Heterogeneity During Disposal Using Field Observation, Experimental Tests and Discrete Element Simulations [Thèse de doctorat, Polytechnique Montréal]. PolyPublie. https://publications.polymtl.ca/10755/

URL de PolyPublie: PolyPublie URL:	https://publications.polymtl.ca/10755/
Directeurs de recherche: Advisors:	Thomas Pabst
Programme: Program:	Génie minéral

POLYTECHNIQUE MONTRÉAL

affiliée à l'Université de Montréal

Investigation of waste rock segregation and heterogeneity during disposal using field observation, experimental tests and discrete element simulations

PEIYONG QIU

Département des génie civil, géologique et des mines

Thèse présentée en vue de l'obtention du diplôme de *Philosophiæ Doctor*

Génie minéral

December 2022

POLYTECHNIQUE MONTRÉAL

affiliée à l'Université de Montréal

Cette thèse intitulée:

Investigation of waste rock segregation and heterogeneity during disposal using field observation, experimental tests and discrete element simulations

présentée par **Peiyong QIU**

en vue de l'obtention du diplôme de *Philosophiæ Doctor*

a été dûment acceptée par le jury d'examen constitué de :

Richard SIMON, président

Thomas PABST, membre et directeur de recherche

Li LI, membre

Esteban SÁEZ, membre externe

DEDICATION

To my family

To my homeland

ACKNOWLEDGEMENTS

I would like to express my deepest gratitude to my supervisor Prof. Thomas Pabst for his dedicated support, guidance, and encouragement throughout the process of this project. His plentiful knowledge and experience, and overall insights in this field always encourage and inspire me to overcome difficulties. He is always willing and enthusiastic to assist in any way he could, with understanding, thoughtfulness and patience. Especially, I appreciate that he has generously spent a lot of time in discussing various aspects of this project throughout the years. I greatly appreciate all that I have learned from him, and I believe all these would strongly improve me and be good memory in my life.

I would like to thank Prof. Li Li and Vincent Martin for their evaluation of my pre-doctoral report. Their professional questions and suggestions helped this project so much. Many thanks to Prof. Li Li again for being the committee member, and great thanks to other committee members including Prof. Esteban Sáez, Prof. Richard Simon and my supervisor Prof. Thomas Pabst.

I acknowledge the financial support from Natural Sciences and Engineering Research Council of Canada (NSERC), Fonds de recherche du Québec-Nature et Technologies (FRQNT), Research Institute of Mines and Environment (RIME UQAT-Polytechnique), and the industrial partners of RIME UQAT-Polytechnique. Specially, I would like to thank our partners at Canadian Malartic mine for acquiring field observation data for this project.

I would like to thank my colleagues in RIME group who were present and supported me throughout the years. Many thanks go to Noura EI-Harrak who gave laboratory training course, taught me to conduct laboratory tests, and helped to manage the test materials and equipment. I would like to thank Patrick Berneche for his professional and experienced help and suggestions for the laboratory tests. I am also thankful to Karim Essayad who generously shared test materials, field data and technical documents. I also express thanks to other colleagues for their help and kindness. I must name some of them: Abtin Jahanbakhsh Zadeh, Adrien Dimech, Akram Deiminiat, Antoine Laverdière, Chuan Fan, Jian Zheng, Karine Sylvain, Moïse Rousseau, Monica Monzon, Ngoc Dung Nguyen, Pengyu Yang, Ruofan Wang, Shengpeng Hao, Tom Crouzal, Xin Chen, Yulong Zhai, and Yuyu Zhang (I apologize to them who are not named).

I would like to thank my friends outside of RIME group for their help, trust, and sharing happiness with me. Special thanks to Dongze Zheng, Jianguo Wang, Liya Ma, Yang Cao, Yang Zhang. Many thanks to Prof. Liyun Tang and Prof. Di Wu for heir help during these years. I also thank Juanjuan Zheng for sharing technical documents with me.

Finally, I would like to express my sincere thanks to my family for the unconditional love and strong support with consistent trust!

RÉSUMÉ

Les opérations minières génèrent de grandes quantités de roches stériles, qui sont généralement déposées en surface à proximité des sites de production. La disposition des roches stériles à l'aide de la méthode de déversement avec épandage au butoir (push dumping) et la méthode de déversement à la benne (end dumping) entraîne généralement une ségrégation importante, créant des structures hétérogènes complexes dans les haldes à stériles et augmentant les risques d'instabilité géotechnique et géochimique. La caractérisation et l'évaluation de la ségrégation des stériles selon différentes méthodes de construction et hauteurs des gradins sont cependant extrêmement difficiles en raison des grandes dimensions des haldes, de l'instabilité des pentes abruptes et de la difficulté à déterminer la masse et la taille des particules grossiéres et irrégulières.

L'objectif principal de ce projet était donc d'évaluer l'impact de disposition des roches stériles sur leur ségrégation et leur l'hétérogénéité dans les haldes et de proposer des recommandations pour réduire la ségrégation et améliorer la stratégie de d'entreposage. Cette recherche inclut aussi des objectifs secondaires qui visaient à caractériser la ségrégation et l'hétérogénéité des roches stériles dans les haldes et à évaluer la ségrégation dans différentes conditions opératoires lors du stockage.

Des observations sur le terrain faisant l'objet d'une caractérisation des roches stériles ont été réalisées en analysant la distribution granulométrique le long de la pente de la halde à l'aide d'une analyse d'images obtenues par drones. Des simulations à la base de la méthode des éléments discrets à l'aide de PFC3D ont ensuite été menées à l'aide du code PFC3D pour simuler le comportement de l'écoulement des roches stériles lors du stockage. Une nouvelle méthode de calibration du modèle a été proposée pour simuler de manière fiable la ségrégation des roches stériles à l'échelle du laboratoire et du terrain. Cette méthode comprenait la calibration du modèle à l'aide de essais d'angle de repos et la validation à l'aide des essais de ségrégation pour les modèles à l'échelle du laboratoire, puis a été mise à l'échelle pour les modèles de terrain. Des modèles numériques ont finalement été utilisés pour évaluer la ségrégation et l'hétérogénéité des roches stériles sous divers facteurs d'influence tels que les méthodes de construction et la hauteur des gradins.

Les roches stériles caractérisées par des observations sur le terrain ont indiqué une ségrégation et une hétérogénéité importantes le long de la pente des haldes à stériles. Les résultats ont montré que la ségrégation et l'hétérogénéité latérale pouvaient entraîner une forte variabilité (différence d'un à deux ordres de grandeur) de la conductivité hydraulique saturée et plus généralement des propriétés géotechniques des stériles sur le terrain. Le contrôle de la ségrégation est donc apparu plus bénéfique pour améliorer la stabilité des haldes.

L'approche de calibration proposée dans cette recherche s'est avérée facile à utiliser et efficace pour simuler la ségrégation des roches stériles à différentes échelles, comme le prouve la validation en laboratoire et sur le terrain. Ces résultats encourageants ont confirmé que les modèles numériques PFC3D pourraient être utilisés pour extrapoler ces observations préliminaires à des échelles plus larges et pour évaluer et comparer différentes méthodes de construction en fonction de diverses contraintes opérationnelles. Des recommandations pour contrôler la ségrégation et améliorer la stratégie de disposition ont été proposées sur la base de ces résultats.

Les hauteurs des gradins simulées (10 m à 25 m) et les charges utiles des camions miniers (300 t et 600 t) ont un effet limité sur la ségrégation des stériles.

Dans cette étude, la méthode de déversement avec épandage au butoir tend à créer plus de ségrégation que la méthode de déversement à la benne, car cette dernière a généré des vitesses initiales plus élevées, ce qui, à son tour, a contribué à réduire la ségrégation des roches stériles. La raison en était la hauteur relativement limitée des gradins qui devait être inférieure à 25 m pour réduire les instabilités géotechniques et le temps de simulation. Dans ces conditions, l'accumulation d'énergie pendant le flux de particules a moins d'effet sur la ségrégation que l'énergie initiale.

L'optimisation de la distribution granulométrique des particules des roches stériles (avant déposition) et le contrôle de la vitesse de poussée semblent efficaces pour limiter la ségrégation des stériles. L'utilisation d'un facteur de poudre plus important ou le concassage des plus grosses particules est donc recommandé pour homogénéiser et contribuer à limiter la ségrégation des stériles. L'augmentation de la vitesse de poussée peut également réduire la ségrégation au sommet de la pente, mais l'effet sur la distribution des stériles au bas de la pente est plus limité.

La disposition latérale avec déversements séquentiels a été recommandée pour réduire la ségrégation des roches stériles sur le terrain. L'espacement des déversements a eu un effet limité sur la ségrégation des stériles, tant qu'il est resté suffisamment petit pour assurer des interactions entre chaque déversement.

Cette étude a été menée pour des hauteurs de gradins limitées et des sites miniers spécifiques, et d'autres recherches sont recommandées pour valider ces résultats sur d'autres sites miniers avec des stériles et des conditions d'exploitation différents. Cependant, l'approche utilisée dans cette recherche pourrait être directement extrapolée à d'autres sites pour l'étude de la ségrégation des stériles.

Les résultats de ces recherches devraient contribuer à améliorer le plan de dépôt des stériles sur les sites miniers en exploitation et futurs. Les recommandations proposées pourraient permettre de contrôler la ségrégation et d'homogénéiser les stériles lors de leur stockage, et ainsi d'améliorer la stabilité géotechnique et géochimique des haldes.

ABSTRACT

Mining operations generate large amounts of waste rock which are generally disposed of on the surface. Waste rock disposal using push-dumping and end-dumping methods usually leads to significant segregation, creating complicated heterogeneous structures in waste rock piles and increasing risks for both geotechnical and geochemical instability. Characterization and evaluation of waste rock segregation under different construction methods and bench heights are, however, extremely challenging because of the large dimensions of the piles, the instability of the steep slopes and the difficulty to determine the mass and size of large and irregular particles.

The main objective of this project is therefore to assess the effect of waste rock disposal on waste rock segregation and heterogeneity in waste rock piles and to propose recommendations to reduce segregation and improve disposal strategy. This research also included main specific objectives which aim to characterize waste rock segregation and heterogeneity in piles, and to evaluate segregation under various operational conditions during disposal.

Field observations for waste rock characterization were conducted by analyzing particle size distribution (PSD) along the slope of a waste rock pile using image analysis on drone pictures. Discrete element simulations using PFC3D were then conducted to simulate waste rock flow behaviour during disposal. A new model calibration method was proposed to reliably simulate waste rock segregation at both laboratory and field scales. This method included model calibration using repose angle tests and validation using segregation tests for laboratory scale models, and was then upscaled for field models. Numerical models were finally used to evaluate waste rock segregation and heterogeneity under various influence factors such as construction methods and bench heights.

Waste rock characterized by field observations indicated significant segregation and heterogeneity along the slope of waste rock piles. Results showed that segregation and lateral heterogeneity could result in high variability (one to two orders of magnitude difference) of the saturated hydraulic conductivity and more generally of the geotechnical properties of waste rock in the field. Controlling segregation appeared therefore beneficial to improve pile stability.

The calibration approach proposed in this research proved easy to use and efficient to simulate waste rock segregation at various scales, as proven by laboratory and field validation. These

encouraging results confirmed PFC3D models could be used to extrapolate these preliminary observations to larger scales and to evaluate and compare different construction methods depending on various operational constraints. Recommendations to control segregation and improve disposal strategy were proposed based on these results.

Simulation results showed that bench heights (10 m to 25 m) and mine truck payloads (300 t and 600 t) had limited effect on waste rock segregation in this study.

In this study, push-dumping method tended to create more segregation than end-dumping method because end-dumping method generated greater initial velocities, which, in turn, contributed to reduce segregation. The reason was the limited bench heights which usually be smaller than 25 m to reduce geotechnical instabilities and simulation time. In these conditions, the energy accumulation during particle flow had less effect on segregation than the initial energy.

Optimizing waste rock PSD (before deposition) and controlling push velocity seemed efficient to limit waste rock segregation. Using a greater powder factor or crushing the largest waste rock particles was therefore recommended to homogenize waste rock and contribute to limit waste rock segregation. Increasing push velocity could also reduce segregation at the top of the slope but the effect on waste rock distribution at the bottom of the slope was more limited.

Lateral disposal with sequential dumps was recommended to decrease waste rock segregation in the field. Dump spacing had limited effect on waste rock segregation, as long as it remained small enough to ensure interactions between each dump.

This study was conducted for limited bench heights and specific mine sites, and more research is recommended to validate these results on other mine sites with different waste rock and operational conditions. However, the approach used in this research could be directly extrapolated to other sites for waste rock segregation investigation.

The results of this research should contribute to improve the deposition plan of waste rock on operating and future mine sites. The proposed recommendations could help to control segregation and homogenize waste rock during disposal, and therefore improve geotechnical and geochemical stability of piles.

TABLE OF CONTENTS

LIST OF TABLES

LIST OF FIGURES

LIST OF SYMBOLS AND ABBREVIATIONS

A	Particle area (mm)
a	Long axis (mm)
b	Medial axis (mm)
c	Short axis (mm)
c'	Effective cohesion (kPa)
C_C	Coefficient of curvature (-)
C_H	Segregation indicator (-)
C_U	Coefficient of uniformity (-)
d	Specimen diameter (mm)
d	Sieve aperture size (mm)
D_{10}	Particle diameter corresponding to 10% passing (mm)
D_{15}	Particle diameter corresponding to 15% passing (mm)
D_{30}	Particle diameter corresponding to 30% passing (mm)
D_{50}	Particle diameter corresponding to 50% passing (mm)
D_{60}	Particle diameter corresponding to 60% passing (mm)
D_{75}	Particle diameter corresponding to 75% passing (mm)
D_{80}	Particle diameter corresponding to 80% passing (mm)
D_{95}	Particle diameter corresponding to 95% passing (mm)
D_c	Diameter of the smallest circumscribing circle (mm)
D_e	Equivalent particle diameter (mm)
D_i	Diameter of the largest circumscribing circle (mm)
D_{max}	Maximum particle diameter (mm)

E	Effective modulus (Pa)
F_{max}	Maximum Feret's diameter (mm)
F_{min}	Minimum Feret's diameter (mm)
F_n^l	Linear normal force (N)
F_d	Damping force vector (N)
F_t	Generalized force (N)
G_S	Specific gravity (-)
h	Height of pile (bench) (m)
h'	Modified coefficients of uniformity (-)
h''	Modified coefficients of uniformity (-)
H	Measured height of waste rock cone (mm)
H'	Simulated height of waste rock cone (mm)
k^*	Stiffness ratio (-)
k_1	Fitted parameter (-)
k_2	Fitted parameter (-)
k_n	Normal stiffness (N/m)
k_s	Shear stiffness (N/m)
k_{sat}	Saturated hydraulic conductivity (cm/s)
k_r	Rolling resistance stiffness (N·m)
logd	Logarithmic mean particle size (-)
M	Mass (kg)
M'	Updated rolling resistance moment (N·m)
N	Particle number (-)
P	Particle perimeter (mm)

R	Effective contact radius (mm)
R'	Equivalent roughness (-)
S	Equivalent strength (kPa)
u_w	Pore water pressure (kPa)
v	Velocity vector (-)
V	Particle volume (mm^3)
W	Specimen width (mm)
α	Local damp (-)
β	Particle density (kg/m^3)
β_n	Normal critical-damping ratio (-)
β_s	Shear critical-damping ratio (-)
θ	Repose angle (°)
λ	shape factor (-)
μ	Friction coefficient (-)
μ_r	Rolling friction coefficient (-)
σ_n	Normal stress (kPa)
σ'_n	Effective normal stress (kPa)
τ	Shear strength (kPa)
τ_p	Peak shear stress (kPa)
φ'	Effective friction angle (°)
φ_b	Basic friction angle (°)
χ	Segregation degree (-)
$\Delta\theta$	Relative rotation increment (-)
Δt	Timestep (s)

AMD	Acid mine drainage
CD	Consolidated drained test
CI	Coarsening index
CND	Contaminated neutral drainage
CQ	Coarsest quartile
CU	Consolidated undrained test
DEM	Discrete element method
FQ	Finest quartile
MPM	Material point method
PFEM	Particle finite element method
PSD	Particle size distribution
UCS	Uniaxial compressive strength
WRP	Waste rock pile
RSI	Relative Segregation index
SI	Segregation index
SI_P	Perfect segregation state
SPH	Smoothed particle hydrodynamics method

LIST OF APPENDICES

CHAPTER 1 INTRODUCTION

1.1 Background

Large volumes of waste rock are produced during mining activities, and are commonly deposited in large piles that can exceed 150 m in height, and cover several square kilometers in area (Aubertin, 2013; Amos et al., 2015; Hajizadeh Namaghi et al., 2015). The particle size distribution (PSD) of waste rock is widely graded ranging from clayey and silty particles to cobbles, boulders and meter-sized blocks (Morin et al., 1991; James et al., 2013). The management and reclamation of such large size waste rock piles represent a challenge for the mining industry (Bussière et al., 2020).

The deposition of waste rock with a wide PSD generally causes segregation: coarse blocks tend to move downwards to the toe of the pile while fine particles remain closer to the deposition point near the crest of the pile (Nichol, 1986; Morin et al., 1991; Herasymuik et al., 2006). End-dumping method is considered to produce more segregation than push-dumping method because of more initial energy in the waste rock with end-dumping method (Aubertin, 2013). Segregation is also expected to increase with the pile height because of greater energy and moment for larger particles when they move on a longer slope (Tang et al., 2004; Gharat, 2019). So waste rock piles are usually constructed using small benches to improve geotechnical stability, reduce segregation and enhance operation safety, but the cost for transportation and disposal may therefore also increase (Aubertin, 2013; Hawley et al., 2017).

Fine particles can move through the voids between larger particles and sink down towards lower layers, while larger particles move faster and further in the upper layer with relatively higher momentum driven by gravity (Dolgunin et al., 1995; Cheng et al., 2019). Stratification then develops as inclined fine-grained and coarse-grained layers forms along the external pile surface (Fala et al., 2005). Stratification also occurs at the surface of benches where waste rock can be crushed and compacted by the regular circulation of heavy equipment during construction, thus creating less permeable horizontal layers (Anterrieu et al., 2010; Aubertin, 2013; Broda et al., 2017). Waste rock within piles can therefore present a high degree of heterogeneity (Anterrieu et al., 2010; Lahmira et al., 2017; Maknoon et al., 2021).

Waste rock segregation and stratification bring uncertainties to the hydro-geotechnical and geochemical properties such as the shear strength and hydraulic conductivity (Fala et al., 2012; Lahmira et al., 2016; Zevgolis, 2018). Shear strength is a key parameter indicating the geotechnical stability of waste rock piles, and is strongly affected by the heterogeneous distribution of waste rock in terms of PSD and compactness (Barton, 1982; Gupta, 2016; Andjelkovic et al., 2018). The hydraulic conductivity may vary by several orders of magnitude, resulting in high degree variabilities of the water flow and water retention capacity within waste rock piles (Appels et al., 2018; Raymond et al., 2021). The presence of oxygen and water in waste rock piles can oxidize reactive minerals such as sulfides in waste rock and generate acid mine drainage (AMD) (Akcil et al., 2006; Qureshi et al., 2016). Large water fluxes favored by the high permeability of waste rock may contribute to a rapid transport of contaminated water to the environment, bringing risks to the geochemical stability of waste rock piles in terms of acid mine drainage (AMD) (Aubertin et al., 2008; Pedretti et al., 2020; St-Arnault et al., 2020).

Much effort was put to characterize the segregation and stratification of waste rock both in the laboratory and field (Nichol, 1986). However, these investigations are often limited to small size scales (usually smaller than 0.5 m) because of the difficulties and risks to access the pile slopes, and the limited precision of measurement techniques for large blocks (Shepherd, 1989; Ayres et al., 2006; Gupta, 2016). Consequently, common characterization techniques such as sieving analysis are often not applicable to quantitatively characterize waste rock segregation in the field.

Discrete element method (DEM) provides another efficient way to overcome such limitations and to quantify the segregation of granular material by simulating simultaneously different segregation mechanisms including rolling, sieving and percolation (Combarros et al., 2014; Cheng et al., 2019; Su et al., 2019). However, some challenges for DEM applications at field scale remain, including the heavy calculation pressure, the representativity of particles (which geometry often requires to be simplified) and the determination of input parameters (Ai et al., 2011; Roessler et al., 2019; Coetzee, 2020). The representativeness of the simulation models for the field application remains controversial considering the extremely large particle volumes and sizes. Consequently, calibration is needed to provide reliable simulation models for the investigation of waste rock segregation in the field. Also, most research focused on the effect of heterogeneity on the hydro-geotechnical and geochemical properties of waste rock (Fala et al.,

2012; St-Arnault et al., 2020). However, limited research is conducted to quantitatively characterize the segregation and the effect of main influence factors such as construction method and pile height. Multi-scale techniques including field observation, laboratory tests and numerical simulations are therefore required to investigate the heterogeneous distribution of waste rock in piles and the corresponding effect on the geotechnical and hydrological properties.

1.2 General and specific objectives

The main objective of this research was to assess the effect of waste rock disposal on waste rock segregation and heterogeneity in waste rock piles and to propose recommendations to reduce segregation and improve disposal strategy.

To achieve this goal, several specific objectives were also proposed:

1. Develop a particle shape model to estimate waste rock diameters and masses using image analysis.
2. Characterize waste rock segregation and lateral heterogeneity statistically along the slopes of waste rock pile in the field.
3. Characterize waste rock properties (characteristic diameters, segregation degree) as a function of the position along the slope of waste rock pile.
4. Propose a new method to calibrate and validate discrete element simulation models and to accelerate the calculation time for waste rock disposal simulations.
5. Assess the effect of construction method, bench height, and operational influence factors such as push velocity and mine truck payload on waste rock segregation.
6. Propose operational recommendations to limit waste rock segregation during disposal.

Scientific hypothesis

Waste rock disposal can be improved by controlling segregation to homogenize waste rock distribution in waste rock piles

1.3 Content of the thesis

Chapter 1 introduces the context of this project and presents the research background, research needs, research question and hypothesis, and the general and specific objectives of this thesis.

Chapter 2 presents a literature review of waste rock disposal including material hydrogeological and geotechnical properties, construction methods, segregation and heterogeneity. Waste rock properties such as particle size distribution, repose angle and friction angle, bulk density, and hydraulic conductivity are presented. The commonly used construction methods such as end-dumping and push-dumping methods are described. Segregation mechanisms, influence factors and indices used to evaluate the segregation degree are introduced. Finally, the main methods to evaluate the segregation including experiments and numerical simulations are discussed.

Chapter 3 presents the methodology of field observation, laboratory tests and numerical simulations used in this research. The basic properties such as specific gravity and particle shape were firstly characterized, and these results were also exhibited. Waste rock segregation and lateral heterogeneity was characterized in the field using image analysis. Simulation models were calibrated and validated using repose angle tests and segregation tests in the laboratory. The calibrated models were finally used to simulate the flow behaviour of waste rock at field scale. Waste rock segregation was finally investigated considering the effect of various influence factors including construction method, bench height, and relevant operational factors such as push velocity and payload of mine trucks.

Chapter 4 presents detailed processes and results of the field characterization of waste rock segregation and lateral heterogeneity using image analysis. 42 images of the waste rock slope, covering a 1400 m long area at Canadian Malartic mine, were analyzed to characterize waste rock segregation. Laboratory calibration was conducted to determine the particle shape factor α, which was then used to estimate the diameters of particles on the pictures, and to determine the PSD curves in different sections along the slopes of the waste rock pile. Waste rock segregation was analyzed using characteristic diameters and segregation degree from the top to the bottom of the slope. Lateral heterogeneity was also characterized along the lateral direction of the slopes.

Chapter 5 presents the process of a new method to calibrate and validate the discrete element models carried out with PFC3D (Itasca) for waste rock segregation simulations. Experimental tests such as repose angle tests and segregation tests were conducted in the laboratory to calibrate and validate simulation models. Calibrated models were then extrapolated to reproduce the

segregation properties (e.g., characteristic diameters, segregation degree) during waste rock disposal in the field.

Chapter 6 presents detailed simulations of waste rock disposal in the field and the effect of various influence factors such as construction method and bench height on waste rock segregation. Construction methods including push-dumping and end-dumping methods were mainly simulated for waste rock disposal. Various influence factors including bench heights (10 to 25 m), mine truck payloads (300 t and 600 t), push velocities (0.1 to 0.6 m/s), lateral disposal, and waste rock PSD were mainly investigated. Segregation degree (χ) and relative particle diameters (D_{10} / D_{10}', D_{50} / D_{50}', D_{95} / D_{95}') from the top to the bottom sections of the slope were compared. A relationship between the segregation degree and the bench height was proposed. Some operational recommendations were then proposed to control segregation.

Chapter 7 presents a general summary of the results, discussion, conclusion and recommendations for further research.

1.4 Contributions and originality

The main contribution of this study was to improve the understanding of waste rock segregation during disposal under different operational factors such as construction method and bench height.

Waste rock segregation and heterogeneity was statistically characterized at field scale by analyzing the waste rock slope (covering a 1400 m long area) using image analysis. Diameters and masses of waste rock particles on the slope were determined for segregation and lateral heterogeneity investigation. A new method was proposed to calibrate and validate simulation models for waste rock disposal simulations. This method can simply calibrate the simulation models for segregation investigation by measuring the repose angles of tested granular materials. In addition, this method can accelerate the calculation time for waste rock disposal simulations in industrial level using discrete element method. Calibrated simulation models can then be used to reproduce the process of construction methods and provide a better insight on the heterogeneous distribution of waste rock from an operational point of view.

The characterization of waste rock segregation and heterogeneity remains a challenge for researchers and the industry, and the work in this project is therefore original in many aspects.

This project combined different techniques including field observations, experimental tests, and extensive discrete element simulations. This thesis quantitatively analyzed waste rock segregation under various operational influence factors. A relationship between segregation degree and bench height was proposed. End-dumping and push-dumping methods were simulated to investigate the vertical segregation and lateral heterogeneity of waste rock during disposal. Many operational factors such as mine truck payload, push velocity and lateral disposal were mainly investigated. The research results in this project will be helpful to control segregation for waste rock disposal on the surface or in open pit.

CHAPTER 2 LITERATURE REVIEW

2.1 Waste rock generation and management

Surface and underground mining operations involve a series of processes including blasting, excavation, hauling, waste storage and ore milling. Blasting breaks intact rock into pieces, making transport of rocks possible for storage or further processing (Price et al., 2010; MEND, 2015). Both surface and underground mines produce large amounts of waste rock. For example, an estimated total of 450 Mt of waste is placed on the waste rock pile at Canadian Malartic mine with the storage volume of 230 Mm^3 (Lehouiller et al., 2020). The Lac Tio open-pit mine is located 43 km north of Havre-Saint-Pierre (Quebec, Canada). Around 72 Mt of waste rock have been produced and disposed in piles around the Lac Tio mine (Martin et al., 2017). West Line Creek pile covers a surface area of about 2.7 km^2 with a pile height reaching 115 m, and contains about 2.1×10^6 billion bank cubic meters of waste rock (Mahmood et al., 2017).

Waste rock management is a challenge for the industry to consider environmental, economic and safety issues. Many different approaches are used to manage waste rock such as in-pit disposal (MEND, 2015), co-disposal of waste rock and tailings (Demers et al., 2021), underground backfill (Belem et al., 2008), or valorization (Sylvain et al., 2019). The most common management approaches, however, remain the disposal of waste rock in surface piles and in open pits (Azam et al., 2006; Abrosimova et al., 2015; Wilson et al., 2018).

2.1.1 Waste rock piles

Large waste rock piles are usually constructed with benches of 10 to 25 m high (Aubertin, 2013). Different construction methods are used for waste rock disposal depending on the topography of the storage area, foundation conditions, available equipment, and overall pile design (Maknoon, 2016; Puell Ortiz et al., 2017). Four main methods are usually used for waste rock disposal, including end dumping, push dumping, free dumping, and dragline (Morin et al., 1991; McLemore et al., 2009):

End dumping: End-dumping method (Figure 2.1a) is the most frequently used method to build waste rock piles (Aubertin, 2013; Tomaschitz et al., 2018). Waste rock is dumped from the truck on the top edge of the waste rock pile and falls down along the slope. The mass of waste rock

dumped from each truck usually ranges between 40 and 400 tons. End dumping method usually causes segregation with more coarser particles moving further to the bottom of the pile and smaller particles tending to remain near the top of the slope (Nichol, 1986; Zhang et al., 2017). End dumping method usually creates relatively loose slope surface since waste rock is dumped freely without mechanical compaction (Boakye, 2008). Stratification also occurs when waste rock particles flow along the slope with fine layer and coarse layer advanced alternatively (Hawley et al., 2017; Raymond et al., 2021).

Push dumping: Push-dumping method (Figure 2.1b) is used to built waste rock piles by dumping waste rock close to the crest of the pile and then pushing them in the slope using dozers (Moffitt, 2000; Pearce et al., 2016). Push dumping method provides less initial energy to waste rock compared to end-dumping method, and therefore induces less segregation. Previous research indicated that about 40% of the largest particles accumulate at the base of the slope with push-dumping method, compared to about 75% with end-dumping method (Nichol, 1986; Morin et al., 1991). Larger particles are distributed more randomly during pushing and resurfacing. The slope of waste rock pile can be reshaped in push-dumping method, creating higher (or lower) slope angles (Raymond et al., 2021).

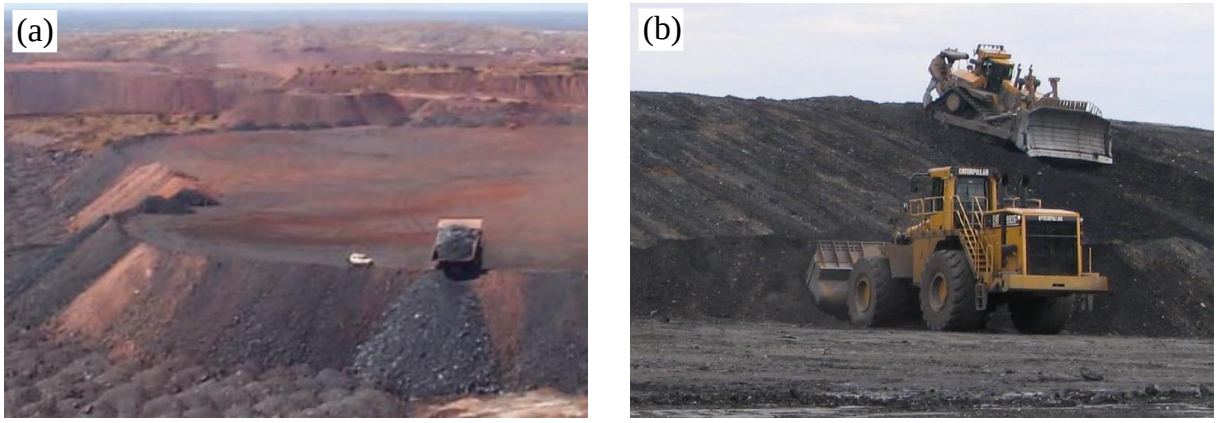

Figure 2.1: (a) End dumping method and (b) push dumping method for waste rock pile construction (a and b were taken from Pearce et al. 2016 and Paul et al. 2011, respectively)

Free dumping method: Free-dumping method is typically used to dispose of waste rock as small heaps on the pile surface, and dozers and compactors then level and compact the surface (Fala et al., 2003). Free dumping method is usually used to built piles with lower heights at the early stage of the operations. The technique is then often replaced by end dumping or push dumping methods to deposit waste rock on the leveled surface. Segregation caused by this method is not significant but high variation in the physical properties of waste rock (e.g., bulk density) can be observed because of the different degrees of compactness (Tachie-Menson, 2006).

Dragline: Draglines are primarily used for coal mines and open-pit operations (Rai et al., 2011; Mohammadi et al., 2016). Dragline spoils are deposited directly on the pile surface, and the effect on compaction and segregation is usually limited (Nichol, 1986).

Construction methods such as end-dumping and push-dumping methods usually cause significant segregation, creating complicated heterogeneous structures and increasing the risk for hydrogeotechnical instabilities (Anterrieu et al., 2010; Broda et al., 2017; Lahmira et al., 2017) (see section 2.3). Waste rock usually contain reactive sulfidic minerals, acid mine drainage (AMD) may be produced when these sulfidic minerals are oxidized and contaminate the surrounding environment (Aubertin et al., 2008; Qureshi et al., 2016; Pedretti et al., 2020). However, waste rock reactivity was out of the scope of this thesis and will not be further discussed here.

2.1.2 In-pit disposal

In-pit disposal is an attractive alternative technique to surface disposal which consists in depositing mine waste (i.e., waste rock and tailings) directly into the open pits. In-pit disposal of waste rock could be beneficial in terms of environmental, physical, financial, and social aspects (Ayres et al., 2006; MEND, 2015; Bussière et al., 2020), and more particularly to:

- Isolate wastes permanently and reduce the possible acid generating and metal leaching from mine wastes. In-pit disposal can also help restoring the mine site to pre-mining conditions and the site aesthetics can be improved on closure.

- Improve the long-term geotechnical stability of mine waste store sites, stabilize pit walls, eliminate potential accidental solids release, and reduce waste management care and maintenance.
- Reduce the need of tailing dams. The large amount of tailings can be stored in the pit so that there is no risk of dam failure (Lumbroso et al., 2019), no cost for tailing dam construction and maintenance and relevant liquefaction (James et al., 2017).
- Reduce the long-term management care and maintenance of mine wastes that are disposed on the surface.

Two main strategies, namely top-down disposal and bottom-up disposal, are usually considered for in-pit disposal depending on the topography, cost and engineering schedule (Joseph et al., 2007; Bar et al., 2020):

Top-down disposal: Waste rock is dumped on the top of a progressively advanced slope. Waste rock is usually in a relatively loose state (Lahmira et al., 2017).

Bottom-up disposal: Waste rock is dumped into small heaps on the bottom of the pit and then leveled and compacted into thin bench. New waste rock is continuously dumped on the existing surface and compacted into new layers (Zevgolis, 2018).

The choice of a disposal strategy directly affects the waste rock piles' geotechnical stability and has significant economic impacts (Spitz et al., 2019a), but can be complicated under different considerations.

Bottom-up disposal usually leads to denser waste rock because of repeated compaction and operation for each bench. The slope of waste rock dumped with top-down disposal is close to the natural repose angle in a loose state, which leads to a lower factor of stability (Williams, 1996).

The noise and large uncertainties regarding the internal structure of waste rock pile also bring great challenges to in-pit disposal when top-down disposal is applied.

Segregation is usually more significant with top-down disposal than bottom-up disposal. Coarse particles tend to accumulate close to the toe because of higher initial momentum when they fall down along a higher slope in top-down disposal (Nichol, 1986). This is not the case with bottom-

up disposal in which waste rock is dumped and compacted layer by layer, resulting in less segregation.

Progressive reclamation is complex for piles constructed with top-down disposal because waste rock pile is accessible only at the end of the disposal. On the contrary, bottom-up disposal allows progressive or temporary reclamation during disposal, increasing the safety of waste rock pile for mine closure or if the backfilling operations last several years (Zevgolis, 2018).

Bottom-up disposal is also more complex to plan, requires a larger fleet of vehicles, increases gas consumption and maintenance costs (for roads and ramp, but also for haul trucks which are not designed to drive downwards) (MEND, 2015).

Open pit can reach hundreds of meters depth, and the haul road is mainly designed to transport ore rock up to the surface for waste storage and metallurgical processing (MEND, 2015). However, in-pit disposal needs to transport waste rock back into the pit when bottom-up disposal is used, increasing the risk to transportation and accelerating the deterioration of equipment.

In practice, in-pit disposal is therefore often complex to implement because of operational and technical challenges in terms of mining cycle, safety, hydrological aspects and other site specific aspects (MEND, 2001, 2015). Waste rock disposed in pits may interact with the groundwater when the mine waste is not adequately isolated from the local environment, bringing risks to the generation of acid mine drainage (AMD) and surrounded environment pollution (Villain et al., 2014; Barfoud et al., 2019; Rousseau et al., 2022). There are also other general limitations to in-pit disposal independently of the deposition methods. For example, the tendency of disposed mine wastes to consolidate over the long-term results in surface settlement after, and thus a need for prolonged backfilling (Puhalovich et al., 2011; Villain, 2014).

In general, waste rock disposal including surface disposal and in-pit disposal, generates different degrees of waste rock segregation and stratification depending on the selected construction methods. As a consequence, waste rock distribution in terms of PSD, porosity (or compactness) and settlement, exhibits high degree of uncertainties.

2.2 Geotechnical and hydrogeological properties of waste rock

2.2.1 Particle size distribution

waste rock PSD is widely graded ranging from clayey and silty particles to cobbles, boulders and meter-sized blocks (Aubertin, 2013; James et al., 2013; Smith et al., 2013a). The maximum particle diameter of waste rock in the field can reach several meters (Figure 2.2). Waste rock uniformity coefficient C_U (= D_{60} / D_{10}) is usually larger than 20 and even up to 440 (Gamache-Rochette, 2004; Fala et al., 2005; Aubertin, 2013). The typical grading characteristics for waste rock are summarized in Table 2.1. The uniformity coefficient C_U is often considered a practical and easy-to-use criterion to estimate possible segregation of a coarse material during disposal, and a greater C_U (usually $C_U > 3$) is generally deemed to indicate a higher segregation risk (Langroudi et al., 2015).

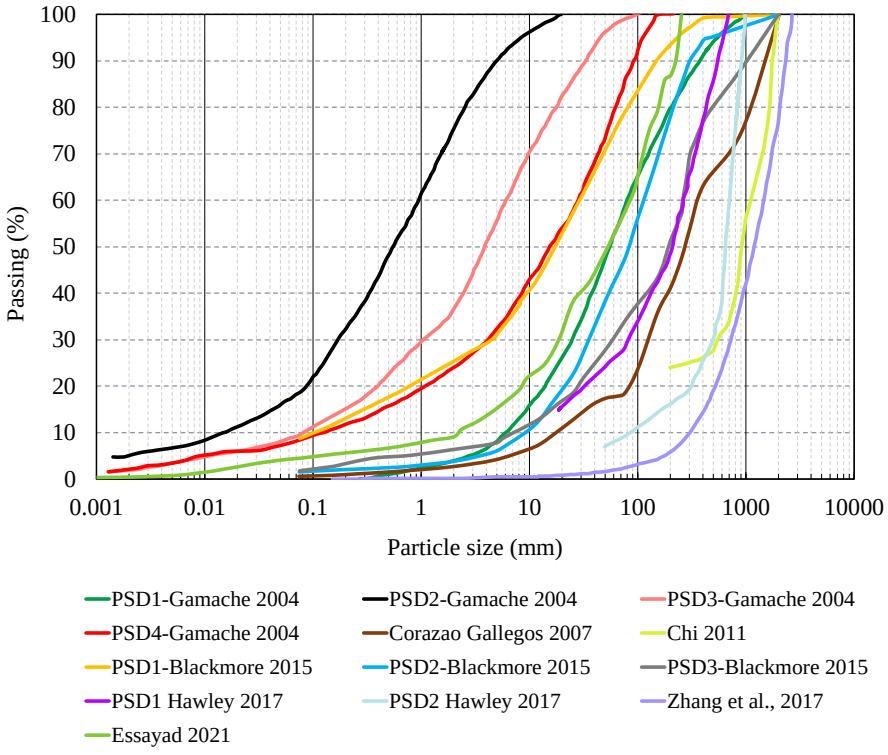

Figure 2.2: PSD curves of waste rock in the field. The details of the gradation characteristics are summarized in Table 2.1.

Table 2.1: Gradation characteristics of waste rock in the field.

D_{max} (mm)	D_{60} (mm)	D_{50} (mm)	D_{30} (mm)	D_{10} (mm)	C_U (-)	C_C (-)	Reference
20-1000	0.9-79	0.6-55	0.2-25	0.01-6	13-228	1.3-5	Gamache-Rochette (2004)
2000	370	273	127	18	21	2.5	Corazao Gallegos (2007
2000	1106	913	548	-	-	-	Chi (2011)
2000	29-261	18–193	4-60	0.1-9	13-284	1.2-6.6	Blackmore (2015)
590-980	264-704	210–647	82-496	86	8	4	Hawley et al. (2017)
2660	1461	1190	727	304	4.8	1.2	Zhang et al. (2017)
254	86.1	57.1	18.6	2.2	39.1	1.8	Essayad (2021)

Sieve analysis (ASTM D6913) for the coarse fractions (> 0.075 mm), combined with wet sieving (ASTM C117) and hydrometer tests (ASTM D7928) for fine fractions (< 0.075 mm), are traditionally used to characterize the PSD of waste rock (and other mine wastes) in the laboratory. But the limited sieve sizes and practical difficulties may lead to the collection of unrepresentative samples, which do not reflect the whole sizes of waste rock in the field (Hawley et al., 2017). Image analysis is therefore a useful alternative which allows to determine waste rock PSD (Fernlund, 2005; Amos et al., 2015; Dipova, 2017). Image analysis can provide both quantitative and qualitative information of PSD and shape characteristics (Zhang et al., 2017). Different tools can be used for image processing such as 3D laser scanner (Sun et al., 2014), Computed Tomography (CT) imaging (Zhang et al., 2018), Scion Image (Wijekoon et al., 2008), or ImageJ (Masad et al., 2005; Kumara et al., 2012; Ohm et al., 2013). 3D scanner and CT imaging are not well suited to analyze field waste rock particles because these apparatuses are in small dimensions and can not test several tonnes of waste rock for PSD determination.

The main limitation of image analysis is that pictures are taken in 2-dimensions and do not give information on the particle mass (Mora et al., 1998; Kwan et al., 1999). Each particle mass can be evaluated by estimating its volume multiplied by its specific gravity. Particles are then assumed

to have standard geometries such as cubes, spheres, rectangular prisms and ellipsoids (Raschke et al., 1997; Kumara et al., 2012; Dipova, 2017), which allow to easily estimate their volume from 2D projections, and shape models such as ellipsoid model, Feret's diameter model, and sphere model were specifically developed for that purpose (Kumara et al., 2012).

The sphere model (Figure 2.3a) converts the measured particle area (A) to the equivalent particle diameter of a sphere (D_e, $D_e = 2 \times \sqrt{A/\pi}$), which is used to calculate the particle volume (Li et al., 2005). Sphere model is easy and fast when a large number of particles are analyzed such as waste rock in the field (Shanthi et al., 2014; Zhang et al., 2017).

Feret's diameter model (Figure 2.3b) defines the long and medial axes as the maximum and minimum Feret's diameters. Maximum Feret's diameter (F_{max}) is the longest distance between any two points along the particle boundary, and minimum Feret's diameter (F_{min}) is the minimum caliper diameter of the particle (Ferreira et al., 2012; Hamzeloo et al., 2014). The minimum bounding rectangle is the expression of the maximum extents of a 2-dimensional object that fits in a rectangle, which can then be used to obtain the dimensions of the fitted ellipse (Ferreira et al., 2012).

The ellipsoid model consists in fitting a particle in an ellipse using the long and short axes in the projected area. The 3-D ellipsoid particle is represented by a long (a; Figure 2.3c), a medial (b; Figure 2.3 c and d) and a short axis (c; Figure 2.3d). The volume (V) of an ellipsoid is then calculated by (Kumara et al., 2012):

$$V = \frac{4}{3}\pi \times \frac{a}{2} \times \frac{b}{2} \times \frac{c}{2} \tag{2.1}$$

However, the 2-D projected area provides only the long and medial axes. The short axis c is hidden in the out of plane dimension and has to be estimated using a shape factor λ (λ = c / b) (Đuriš et al., 2016). Particles from the same source are usually deemed to exhibit similar shape characteristics and the shape factor is therefore assumed to be constant for a same material, independently of the particle size (Mora et al., 1998; Dipova, 2017).

Finally, particle diameter in sieving analysis corresponds to the size of the square sieve aperture (d in Figure 2.3), but some particles could pass through the diagonal of the corresponding square sieve aperture. Consequently, particles passing through a given sieve can be larger than the sieve size. An equivalent particle diameter (D_e) is usually introduced in image analysis to match the definition of particle diameter and sieve opening (Kumara et al., 2012; Dipova, 2017). The equivalent particle diameter for the ellipsoid model is calculated by (Ohm et al., 2013):

$$D_e = \sqrt{(b^2 + c^2)/2} \tag{2.2}$$

Where D_e: equivalent particle diameter (mm); b and c: medial and short axis (mm).

The equivalent particle diameter for Feret's diameter model is calculated by:

$$D_e = F_{min}/\sqrt{2} \tag{2.3}$$

Where F_{min}: Minimum Feret's diameter (mm).

These particle shape models have been widely used to determine the particle size distribution of waste rock in the field (Bhatia et al., 1990; Dipova, 2017; Zhang et al., 2017). These models are all built based on different simplifications, resulting in differences of particle diameters and mass estimations. In this study, these shape models would also be used for waste rock characterization, and the difference of these models would be compared in this project (see details in chapter 4).

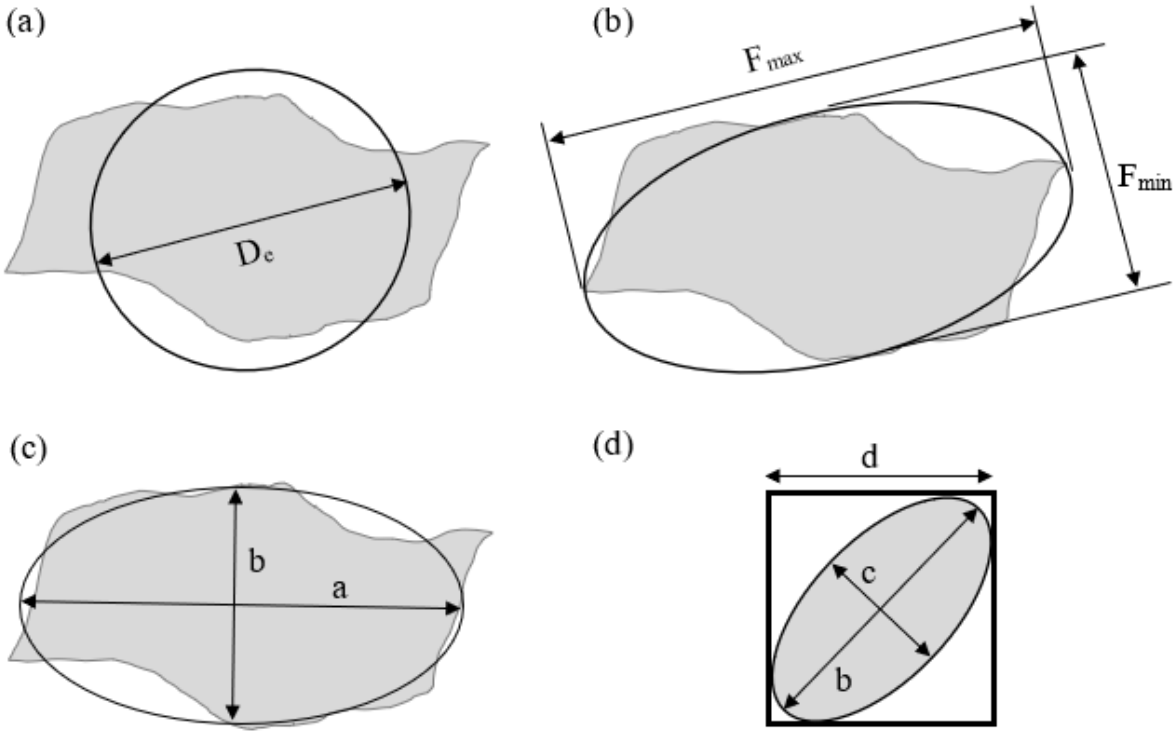

Figure 2.3: Typical shape models of waste rock. (a): Sphere model with the equivalent particle diameter D_e. (b): Feret's diameter model, with F_{min} and F_{max} representing the minimum and maximum distance between any two points along the particle boundary. (c): Ellipsoid model, with a and b representing the long and medial axis of the projected particle area. (d): One particle passing through the square sieve aperture. Length d represents the size of the sieve aperture. c represents the short axis of the particle (Adapted from Ohm et al 2013).

2.2.2 Particle shape

Particle shape highly affects the assemblies and the friction properties of granular material (Barton, 1982; Azema et al., 2010; Carrasco et al., 2022). Particle shape is mainly characterized using shape descriptors such as circularity (also sphericity) (Blott et al., 2008), roundness (Zheng et al., 2015), elongation and flatness (Azema et al., 2010; Carrasco et al., 2022).

The degree of sphericity is originally expressed as the ratio of the surface area of a particle to that of a perfect sphere with equal volume (Wadell, 1932). Sphericity is used to evaluate the degree to which the particle shape approximates that of a real sphere (Bagheri et al., 2015). The circularity

indicates a perfect circle with a value of 1.0, while indicates an increasingly elongated shape as the circularity approaches 0. However, surface area is often difficult to measure on irregular granular particles (e.g., waste rock and rockfill). So circularity is an alternative shape descriptor to estimate the sphericity of particles based on the projected 2-dimension particle (Blott et al., 2008). The sphericity can range between 0.6 and 0.7 for crushed rock (Sun et al., 2014)

The roundness is originally defined as the ratio of the average radius of curvature of particle corners to the radius of the maximum inscribed circle (Wadell, 1932). Roundness quantifies the sharpness of particle corners (Zheng et al., 2015). For example, roundness close to 0.0 means angular particle and close to 1.0 means well-rounded particles. However, identification of curved corners is difficult because the outline of a gravel particle includes various scales of curvature. So some simplified formulae are also used to estimate the roundness of granular particles based on the dimension of the projected area of a particle (Kuenen, 1956). Angularity is considered as the opposite of roundness (Blott et al., 2008). Waste rock particles are characterized as angular and very angular particles (Azam et al., 2009).

The elongation (= b / a) and flatness (= c / a) represent the three dimensions of a particle (Bagheri et al., 2015). An elongation degree of close to 0.0 means extremely elongated particles and close to 1.0 means non-elongated particles. Similarly, A flatness degree of close to 0.0 means extremely flat particle and close to 1.0 means non-flat particles. The elongation can widely range between 0.3 and 0.9, and the flatness can range between 0.07 and 0.6 for waste rock particles (Ovalle et al., 2020). Some others report that the elongation is greater than 0.5, with a mean of around 0.75, while flatness ranges between 0.2 and 1.0 (Linero et al., 2017)

The main shape descriptors are summarized in Table 2.2 and Figure 2.4. These shape descriptors are still widely used for granular particles (e.g., waste rock, rockfill) (Hamzeloo et al., 2014; Vangla et al., 2018; Sozzi et al., 2021; Zhang et al., 2021). The shear strength and the dilation of the granular material increase with increasing irregularity and elongation (Xu et al., 2021). An increase of roundness from 0.1 (very angular) to 1 (well rounded) can also produce a decrease of the critical state friction angle of sandy soils from 40º to 28º (Cho et al., 2006).

Table 2.2: Formulae used for shape descriptors calculation. P: the perimeter of the particle (mm); A: the area of the particle (mm^2); D_i: the diameter of the largest inscribed circle (mm); D_c: the diameter of the smallest circumscribing circle (mm). a, b, c: the longest, medial, and short axis of a particle (mm). The details of these values are shown in Figure 2.4.

Shape descriptor	**Formula**	**Range**	**Reference**
Elongation	b/a	0 - 1	Kuenen (1956)
Flatness	c/a	0 - 1	Blott et al. (2008)
Circularity	$4\pi A/P^2$	0 - 1	Cox (1927)
Circularity / Roundness	$4A/(\pi a^2)$	0 - 1	Pentland (1927)
Circularity	$4A/(\pi {D_c}^2)$	0 - 1	Tickell (1932)
Circularity	$\sqrt{4\pi A/P^2}$	0 - 1	Wadell (1933)
Circularity	$\sqrt{D_i/D_c}$	0 - 1	Riley (1941)
Circularity	P^2/A	> 4π	Janoo (1998)
Sphericity	$(bc/a^2)^{1/3}$	0 - 1	Krumbein (1941)
Sphericity	$(c^2/ab)^{1/3}$	0 - 1	Sneed et al. (1958)
Roundness	$\Sigma(\mathrm{r}/\mathrm{D_i})/\mathrm{N}$	0 - 1	Wadell (1933)
Roundness	D_c/b	0 - 1	Kuenen (1956)

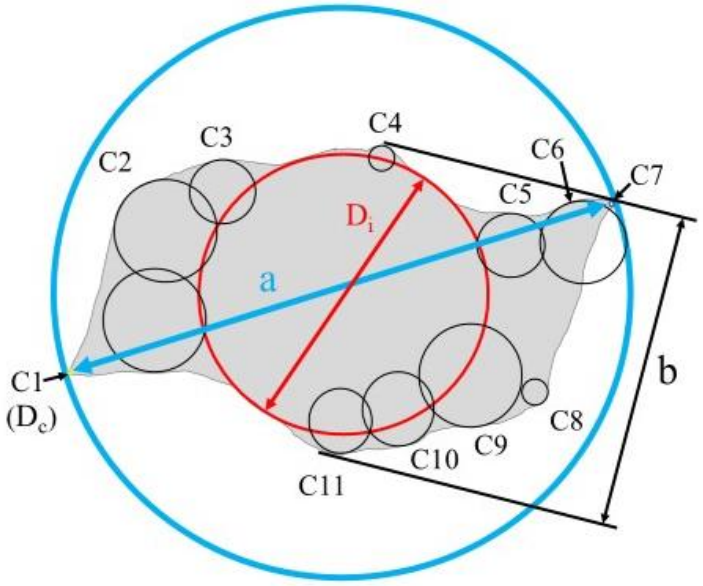

Figure 2.4: Schematic illustration of shape characterization based on a projected particle (in grey). C1 – C11: corners of the particle (mm). Black circles are used to indicate the radius of the curvature of the corners. Corner C1 indicates the smallest circumscribing circle with diameter D_c. The red circle represents the largest inscribed circle with the diameter of D_i. a and b represent the longest and medial axis of this particle. Short axis c is hidden in the projected area and is not shown in this figure.

2.2.3 Specific gravity, density and porosity

The specific gravity (G_S) can range between 2.4 and 4.8 or more for waste rock (Bussière, 2007; Essayad, 2021). The dry bulk density of waste rock can range between 1600 and 2700 kg/m^3 (Williams, 2001; Adams et al., 2007; Bay, 2009). Waste rock bulk density highly depends on the compactness of the material, which is heterogeneously distributed within waste rock pile (Wickland et al., 2010; Weil et al., 2016). Waste rock porosity can range between 0.15 and 0.55 (Adams et al., 2007; Bay, 2009). Table 2.3 presents some values of specific gravity, bulk density, and porosity of waste rock material reported in the literature.

Table 2.3: Basic geotechnical properties of waste rock in the field.

Mine site	Dry density (kg/m^3)	Wet density (kg/m^3)	Specific gravity	Porosity	References
WISMUT GmbH	1630 - 2100		2.64 - 2.75	0.31 - 0.40	Hockley et al. (2003)
Goldstrike mine	1960	2040	2.48 - 2.68	0.26	Martin et al. (2004)
Davis mine	2650	-	-	0.35 - 0.55	Adams et al. (2007)
Golden Sunlight Mine	1500 - 2100	-	-	0.23 - 0.26	Azam et al. (2007)
Antamina mine	2330	2400	1845	-0.11 - 0.45	Corazao Gallegos (2007); Vriens et al. (2019)
-	1570 - 1608	-	2.78 - 2.83	0.45	Azam et al. (2009)
Antamina mine	1845 - 2000	-	2.894	0.15 - 0.45	Bay (2009)
Canadian Malartic mine	1500 - 2310	-	2.71 - 2.81	0.16 - 0.35	Essayad (2021)

2.2.4 Saturated hydraulic conductivity

Waste rock saturated hydraulic conductivity (k_{sat}) usually varies between 10^{-6} m/s and 10^{-2} m/s depending on several factors such as porosity, PSD (Chapuis, 2004; Wickland et al., 2010; Wilson et al., 2022). Table 2.4 presents various k_{sat} of the waste rock material from different mine sites. The variations of saturated hydraulic conductivity could result in preferential flow within waste rock piles (Fala et al., 2005; Fala et al., 2012; Neuner et al., 2013). Sometimes, one or two orders of magnitude difference in the hydraulic conductivity can make water flow along irregular and diverted paths (Lahmira et al., 2016, 2017).

Standard permeability tests including constant head tests and variable head tests are mainly used in the laboratory according to the ASTM standards (ASTM, 2006, 2007, 2016b). But it is

difficult to precisely conceptualize the experimental system because the experiment specimens are usually in small scales and contain only limited particle size, and the pore structures of laboratory specimens are sometimes different to the field conditions (Benson et al., 2007). Infiltration tests (Lessard, 2011; Pieretti et al., 2022) and geophysical investigation (Anterrieu et al., 2010; Dimech et al., 2019; Dimech et al., 2022) are mainly used to determine the saturated hydraulic conductivity in waste rock pile. It is also challenging to operate on the large scale waste rock pile under complicated field condition (Gorakhki et al., 2022). Many predictive models have been proposed to estimate k_{sat} based on the geotechnical properties (e.g., D_{50} and void ratio) such as Hazen model (Hazen, 1991), Kozeny-Carman (KC) model (Chapuis et al., 2003) and Kozeny-Carman Modified (KCM) model (Mbonimpa et al., 2002). These models can well predict waste rock saturated hydraulic conductivity (Gamache-Rochette, 2004; Peregoedova, 2012; Lanoix et al., 2017; Essayad, 2021).

Table 2.4: Values of hydraulic conductivity of waste rock from literature.

Mine site	**k_{sat} (cm/s)**	**References**
Goldstrike mine	6×10^{-3}	Martin et al. (2004)
Mine at south Carolina	2×10^{-2}	Fines (2006)
Golden Sunlight Mine	2×10^{-3} - 5×10^{-3}	Azam et al. (2007)
Antamina mine	1×10^{-4} - 3×10^{-4}	Corazao Gallegos (2007)
Lake Tio mine	4×10^{-3} – 1×10^{-1}	Peregoedova (2012)
Diavik mine	1	Neuner et al. (2013)

2.2.5 Repose angle

The bench slopes in a waste rock pile usually form at waste rock repose angle, which could widely range between 30° and 40° (Burnley, 1993; Xu et al., 2017; Zhang et al., 2017). An average repose angle for free-dumped or end-dumped (see section 2.2) cohesionless rockfill

ranges between 35° and 40° with a typical value of 37° (Quine, 1993; Williams et al., 2008). Repose angles for different waste rock piles are presented in Table 2.5.

Loose-dumped waste rock slopes are usually subjected to rainfall, resulting in decrease of the geotechnical stability. The friction angle is sometimes estimated using the repose angle (Linero et al., 2007; Blight, 2010; Spitz et al., 2019b). However, material's repose angle represents the loosest packing state or the friction angle at the critical state (Williams, 1996). The friction angle is expected to be 4° to 6° higher than the repose angle of the material on loose-dumping, because of the effects of overburden stress (Xu et al., 2017).

The repose angle of granular material can also be used to calibrate discrete element models because it can give an indication of the material flowability and is directly related to particle intrinsic properties such as the friction and rolling (Roessler et al., 2019). The repose angle in simulation models is mainly controlled by friction coefficient (Just et al., 2013; Combarros et al., 2014), rolling resistance coefficients (Iwashita et al., 1998; Roessler et al., 2019) and contact damp (Yan et al., 2015; Santos et al., 2016a) (see details in section 2.3.4).

Table 2.5: Values of repose angles for different waste rock. D_{max} [L]: Maximum particle diameter.

Repose angle (°)	**D_{max} (m)**	**Bench height (m)**	**References**
32-37	-	140	Burnley (1993)
34-40	-	75-90	Quine (1993)
37-38	-	50-400	Moffitt (2000)
38	-	-	Azam et al. (2007)
38	> 0.9	15	Smith et al. (2013a; 2013b)
37	1.5	10	Gervais et al. (2014)
30-40	2.66	20	Zhang et al. (2017)

2.2.6 Shear strength

Waste rock shear strength varies with the geotechnical properties such as PSD, porosity and water content, which increases uncertainties and risks for geotechnical instability of waste rock piles (Iabichino et al., 2014; Zevgolis, 2018). According to Mohr-Coulomb failure criterion (Coulomb, 1776; Mohr, 1900), shear strength of a granular soil can be defined as:

$$\tau = c' + (\sigma_n - u_w) \tan \varphi' \quad (2.4)$$

Where: c': the effective cohesion (kPa); φ': the internal friction angle (°); σ_n: the total normal stress on the plane of failure (kPa); $(\sigma_n - u_w)$: the effective normal stress on the plane of failure (kPa); u_w: the pore water pressure (kPa).

Effective cohesion occurs because of the presence of cementing materials such as clay minerals and the precipitation of secondary minerals (Boakye, 2008). The effective cohesion is usually close to zero for waste rock (< 5 − 10 kPa) because of the small amount of clay (Aubertin, 2013). Waste rock friction angle typically ranges between 21º and 62º depending on the condition of the targeted materials (Raymond et al., 1978; Indraratna et al., 1998; Azam et al., 2009; Aubertin, 2013). The friction angle is typically correlated to many factors such as compactness state, PSD, particle shape, roughness and water content. (Marschi et al., 1972; Barton, 1982; Gupta, 2016).

Waste rock friction angle highly relates to the normal stress (also confining stress in triaxial test). The peak friction angle generally decreases with normal stress because waste rock particles under lower stress are more prone to displacement and rotation, leading to dilatancy and an increase of the friction angle (Indraratna, 1994; Andjelkovic et al., 2018; Zevgolis, 2018). Increasing normal stress can also result in the crushing of large particles and reduction of friction angle (Bard et al., 2011; Zhao et al., 2012).

The friction angle strongly depends on particle shape, and waste rock with more angular and / or elongated particles have higher strength than rounded particles (Xiao et al., 2019). Particle shape varies with particle size (Linero et al., 2017), and waste rock presenting a wider PSD enhances

particle interlocking effect and therefore increase the shear strength (Nguyen et al., 2015; Carrasco et al., 2022).

The effect of particle size on the friction angle is still controversial among researchers, and some consider the increase of maximum particle size increases the friction angle (Simoni et al., 2006; Fakhimi et al., 2011; Kim et al., 2014), while others indicate that the friction angle decreases with increasing the maximum particle size (Pankaj et al., 2013; Honkanadavar et al., 2014). There are also different suggestions that the intermediate-size particle has more influence on the shear strength than the oversize particles (Wang et al., 2013).

Waste rock shear strength can be determined using laboratory and field tests, and estimation models. Field tests usually require large volume of material and complicated test processes (Oyanguren et al., 2008; Coli et al., 2011). So, scaling-down techniques used in the laboratory tests, including direct shear test and triaxial test, are still the main methods to determine waste rock shear strength (Fox et al., 2011; Ovalle et al., 2014; Deiminiat et al., 2022).

2.2.6.1 Direct shear tests

Direct shear test is usually used to determine waste rock shear properties in the laboratory considering its easy operation (ASTM, 2011a). The maximum particle diameter (D_{max}) in the specimen should be less than 1/10 of the width (W) and 1/6 of the initial specimen thickness (ASTM, 2011a). The maximum particle size is approximately 5 mm for small-scale direct shear test with a typical initial width (or diameter) of 50 mm (Bareither et al., 2008; Kim et al., 2014; Ziaie Moayed et al., 2016). A minimum W / D_{max} of 10 is still considered not large enough to provide reliable test results (Deiminiat et al., 2022). As a consequence, regular direct shear test setups are not applicable for mine waste rock that typically ranges from clay to large boulders of several meters in diameter (Fakhimi et al., 2011; Gupta, 2016). Direct shear devices are therefore redesigned and extended to test the shear strength of granular material and their applications are listed in Table 2.6.

Table 2.6: Maximum particle diameters and specimen sizes for direct shear tests

Material	Specimen size (mm)	D_{max} (mm)	Shear rate (mm/min)	Vertical stress (kPa)	Reference
Soil–rock mixture	600 × 600 × 400	300	6 - 8	-	Xu et al. (2011)
Accumulation Soil	500 × 500 × 400	20 - 60	0.5	100 - 250	Wang et al. (2013)
Granular	300 × 300	15.9	0.0001 - 10	98 - 294	Kim et al. (2014)
Waste rock	300 × 300 × 200	20	0.09	100 - 300	Alias et al. (2014)
Sand	300 × 300 × 154	-	-	109 - 218	Ziaie Moayed et al. (2016)
Rockfill	800 × 800 × 650	100 - 125	-	250 - 2090	Andjelkovic et al. (2018)
Waste rock	720 × 720 × 720	100			Linero et al. (2020)
Waste rock	300 × 300 × 180	6	1.5	50 - 150	Deiminiat et al. (2022)

2.2.6.2 Triaxial tests

Triaxial tests, such as consolidated undrained (CU) triaxial test (ASTM, 2011b) and consolidated drained (CD) triaxial test (ASTM, 2011c), are also commonly used methods to determine the shear strength of coarse materials (Hawley et al., 2017). The sample-size ratio (d/D_{max}), defined as the ratio of the specimen diameter (d) to the maximum particle size (D_{max}), is usually recommended to be larger than 6 (ASTM, 2011b; Fox et al., 2011). A sample-size ratio of 5 is also recommended to eliminate the effect of shear strength overestimation (McLemore et al., 2009). Many large-scale tests are therefore conducted to overcome the limitation of oversize particles, and typical applications are presented in Table 2.7.

Table 2.7: Maximum particle diameters and specimen sizes used for triaxial tests. D: diameter; H: height of specimens.

Material	**D_{max} (mm)**	**Shape**	**Specimen size (mm)**	**Reference**
Rockfill	180	Cylinder	1130 (D) × 2500 (H)	Marsal (1967)
Rockfill	152	Cylinder	915 (D) × 2286 (H)	Marachi (1969); Marschi et al. (1972)
Rockfill	25.4 - 38.1	Cylinder	300 (D) × 600 (H)	Indraratna et al. (1993)
Waste rock	200	Cylinder	1000 (D) × 2000 (H)	Linero et al. (2007)
Granular soil	10	Square	120 × 120 × 60	Shi et al. (2010)
Accumulation Soil	10	Cylinder	100 (D) × 200 (H)	Wang et al. (2013)
gravel material	40	Square	230 ×230 × 500	Lenart et al. (2014)
Rockfill	40/160	Cylinder	250 (D) × 375 (H); 1000 (D) × 1500 (H)	Ovalle et al. (2014)

2.2.6.3 Other failure criteria

Experimental results also show that the strength envelopes of geomaterials are usually characteristically nonlinear (Charles et al., 1980; Indraratna et al., 1993). The non-linearity model is therefore proposed for cohesionless materials showing a non-linear relationship between the normal and shear stresses (De Mello, 1977):

$$\tau_P = k_1 \sigma_n^{k_2} \tag{2.5}$$

Where: τ_P: the peak shear stress (kPa); σ_n: the normal stress (kPa); k_1 and k_2: Characteristic parameters.

Parameters k_1 and k_2 are obtained by curve fitting. These fitted parameters don't exhibit clear physical significance but are dependent on the stress unit, which may vary for different applications (Indraratna et al., 1993; Haselsteiner et al., 2017). The larger values of parameters a and b can be attributed to the higher stress range (e.g., σ_n = 5 MPa) (De Mello, 1977).

Barton proposed the following equation to determine the effective friction angle of waste rock (Barton, 1982):

$$\varphi' = R' \cdot \log(S/\sigma'_n) + \varphi_b \tag{2.6}$$

Where R′ waste rock equivalent roughness (-); S: waste rock equivalent strength (kPa), respectively; σ'_n: the effective normal stress (kPa); φ_b: the basic friction angle (°).

The equivalent strength S depends on the characteristic diameter D_{50} and the uniaxial compressive strength (UCS) of rock mass. The equivalent roughness R depends on the after-compaction porosity n of the waste rock, as well as on the origin, roundedness, and smoothness of the waste particles. φ_b can be obtained from tilt tests on waste rock. The details on the determination of these parameters can be found in Barton model (1982). The peak friction angles determined using direct shear tests could be 2° to 8° greater than those measured with triaxial tests (Wu et al., 2008; Asadzadeh et al., 2009).

2.3 Waste rock segregation

In the process of waste rock segregation during the construction of waste rock piles using various construction methods, fine particles can move through the voids between larger particles and sink down towards lower layers, while larger particles move faster and further in the upper layer with relatively higher velocity driven by gravity (Dolgunin et al., 1995; Cheng et al., 2019). Stratification then develops as inclined fine-grained and coarse-grained layers formed along the external pile surface (Fala et al., 2005). Stratification also occurs at the surface of benches where

waste rock can be crushed and compacted by the regular circulation of heavy equipment during construction, thus creating less permeable horizontal layers (Anterrieu et al., 2010; Aubertin, 2013; Broda et al., 2017). Segregation and stratification then lead to high degree of spatial variations of waste rock within piles, i.e., a high degree of heterogeneity (Fala et al., 2012; Lahmira et al., 2017; Maknoon et al., 2021).

Waste rock segregation can directly affect the spatial distribution of geotechnical and hydrogeological properties including porosity, density, volumetric water content, and shear strength of waste rock, thus increasing the risk for localized water flow and geotechnical instabilities (Lahmira et al., 2017; Appels et al., 2018; Pedretti et al., 2020). Matrix water flow mainly occurs in fine-grained layers because of a higher water retention capacity, while preferential water flow is mostly concentrated in the coarse-grained layers because of a larger porosity (Peregoedova et al., 2014; Amos et al., 2015; Martin et al., 2017). Waste rock shear strength also varies within waste rock pile because the particle size and compaction degree of waste rock highly determine the magnitude of the structural component of strength, which affects the shear resistance in much the same way as interlocking effect between particles (Barton, 1982; Frossard et al., 2012). Oxygen may flow through large voids and reach reactive wastes, and large water fluxes bring risks to the geochemical stability of waste rock piles in terms of acid mine drainage (AMD) and contaminated neutral drainage (CND) (Aubertin et al., 2008; Pedretti et al., 2020; St-Arnault et al., 2020).

These spatial variations of hydro-geotechnical and geochemical properties, induced by segregation, bring challenges to the disposal safety regarding the structure stability and construction safety. Thus, understanding and controlling segregation can be beneficial to the waste rock disposal.

2.3.1 Segregation mechanisms

Segregation during granular flow can be commonly observed in different fields such as debris flow (Takahashi et al., 1992), landsides (Shen et al., 2016a; Cheng et al., 2019), heap leaching pile construction (Zhang et al., 2017), disposal of waste rock (and rockfill) in waste rock pile and dam constructions (Fala et al., 2005; Asmaei et al., 2018). In all these cases particle segregation is controlled by a number of different mechanisms and these mechanisms are listed in table 2.8. The

mechanisms such as rolling, sieving effect and percolation are mainly discussed (Drahun et al., 1983; de Silva et al., 2000; Sutherland, 2003).

(1) Rolling effect

Rolling effect is considered one of the dominant mechanisms in governing the segregation in heap formation (Figure 2.5a) (Drahun et al., 1983; Benito et al., 2014; Asachi et al., 2018). Larger particles have a greater capability of rolling over obstacles when they roll down along an inclined surface (Sutherland, 2003). As a consequence, larger particles tend to move further to the bottom of inclined slopes while smaller particles remain closer to the top, therefore leading to particle segregation. Rolling effect is highly related to particle sphericity and rounded particles will more easily roll along inclined slopes than flat particles (Roskilly et al., 2010; Shimosaka et al., 2013). Irregular particles, such as waste rock and rockfill, will be subject to interlocking among the particles and prevent them from free flowing (Tang et al., 2007; Fan et al., 2017).

(2) Sieving effect

Sieving effect (Figure 2.5b) is considered another dominant mechanism controlling the segregation in waste rock pile, allowing smaller particles to flow through a sliding layer composed of larger particles (Kenney et al., 1993; Sutherland, 2003; Tang et al., 2004). Sieving segregation occurs when a graded material (e.g., waste rock) flows along the inclined slope, resulting in a continuous opening and closing of variously sized pore spaces (Sutherland, 2003). Then, smaller particles sink down through the voids between larger particles when particles flow toward the bottom of the inclined slope. Sieving effect is significant when large particles represent a high proportion of the material and form a moving layer (de Silva et al., 2000). This is typically the case for waste rock in the field where particles larger than 10 cm can account for 80% of the total mass (Corazao Gallegos, 2007)

(3) Percolation

Percolation allows smaller particles to move through the voids between larger particles because of vibrations (Jain et al., 2013; Khola et al., 2016; Tirapelle et al., 2021). Some factors including size ratio, shape and surface roughness change the packing and interlocking state, and therefore affect the percolation phenomenon (Stephens et al., 1978a, 1978b; Tang et al., 2007; Khola et al., 2016). Percolation exhibits similar behaviour to sieving effect, but is usually distinguished

because it results from vibrations, instead of requiring a moving layer in sieving effect. However, precisely distinguishing percolation and sieving during waste rock disposal can be tedious as they may happen together and present similar flow behaviour (Tang et al., 2005). Segregation induced by percolation and sieving also results in stratification during waste rock disposal (Fan et al., 2012).

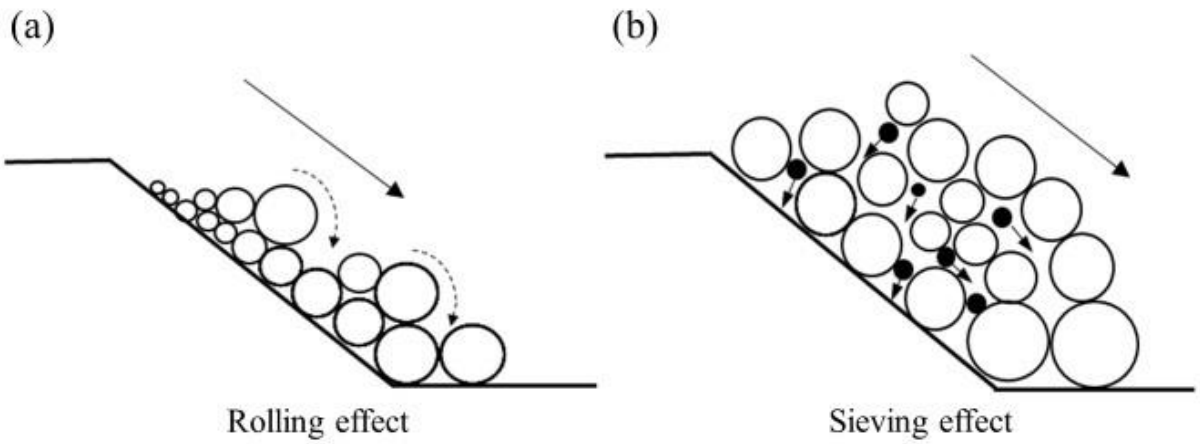

Figure 2.5: The dominant segregation mechanisms in granular flow. (a): Rolling segregation where larger particles move further because of greater momentum. (b): Sieving effect with smaller particles also sink down through the voids between larger particles when particles flow toward the bottom of the inclined slope. (Adapted from Sutherland, 2003)

Table 2.8: The mechanisms of segregation.

Mechanism	Description	Application	Effect on waste rock segregation	References
Rolling	Larger particles have a greater capability of rolling over obstacles when rolling down along an inclined surface.	Heap; WRP	Dominant	Drahun et al., (1983); Benito et al., (2014)
Sieving	Low proportion of smaller particles can pass through the voids between particles.	Heap; WRP	Dominant	Sutherland (2003); Fan et al., (2011)
Percolation	Smaller particles move through the void between larger particles induced by vibration.	Hopper; Silo; WRP	Important	Hashim et al. (2008); Khola et al., (2016)
Impact	Impact, either between particles or between particle and boundary, alter the flow paths of particles.	Silo; Heap; WRP	Important	Mosby et al. (1996); Jiang et al., (2018)
Inertial effect	Larger particles will discharge further away from the end of the inclined chute than smaller particles.	Silo; Heap; WRP; Chutes	Limited (occur during end-dumping from the truck)	de Silva et al. (2000); Fung et al., (2003)
Agglomeration	Fine particles are agglomerated, and flow bound together because of the presence of water.	Not specified. Material containing fine particles and water	Limited	Sutherland (2003); Tang et al., (2004)
Concentration-driven displacement	Fine particles move more actively than larger particles and therefore tend to concentrate in some local areas.	drum mixers; rotary kilns; pharmaceutical industry	Limited (only when large proportion of fines occurred)	Kuo et al. (2016); Santos et al., (2016b)
Repose angle effect	Repose angle effect occurs when different materials are dumped sequentially on a heap. Materials with a repose angle smaller than the slope can roll down to the bottom of the heap, while materials with a greater repose angle will tend to remain close to the deposition point.	Heap; WRP (possible)	Limited (only when materials have different densities)	de Silva et al. (2000); Sutherland, (2003)

Table 2.8 (continued): The mechanisms of segregation. WRP: waste rock pile.

Mechanism	Description	Application	Effect on waste rock segregation	References
Embedding	particles inertia causes larger or denser particles to penetrate a layer on the surface of the material at the apex of a heap, and become embedded there.	Heap	Limited (stockpiling processes under a high pouring rate)	Mosby et al. (1996); Ketterhagen et al. (2008)
Air current	Finer particles tend to move to the side of the silo driven by air flow, leaving larger proportion of coarser particles in the center.	Silo	Not relevant (application in underground backfilling is not clear)	Zigan et al. (2007); Zigan et al. (2008)
Fluidization	Fine particles become aerated during the filling process and larger particles pass through the aerated fine layers.	Silo	Not relevant (application in underground backfilling is not clear)	Feng et al. (2007); Engblom et al. (2012)
Displacement	Larger particles tend to move upward under low frequency and high amplitude vibrations, and move downwards under high frequency and low amplitude vibrations.	Not specified. Graded material under vibration	Not relevant	Huerta et al. (2004); Kudrolli (2004)
Push-away	The material with a lower density can be pushed aside when the denser material falls on it. Size effect is not considered.	Heap	Not considered (the relative density (G_S) is assumed the same for the same mine)	Tanaka (1971); Félix et al. (2004).

In summary, many mechanisms affect the segregation in granular flow in nature, but only limited mechanisms play an important role on waste rock segregation during disposal, such as sieving, rolling, percolation and impact. These mechanisms usually lead to segregation synchronously. Some mechanisms including inertial effect, repose angle effect, agglomeration, concentration-driven displacement and embedding sometimes occur under some specific conditions. Other

mechanisms including air current, fluidization, displacement and push-away are neglected in waste rock segregation.

2.3.2 Factors affecting segregation

Segregation is significantly influenced by waste rock physical properties, construction methods, and some environmental conditions such as rainfall. These factors affecting segregation are described in Table 2.9. Among these factors, particle size distribution, construction methods and bench height (or pile size) are mainly discussed for waste rock segregation during disposal.

Waste rock physical properties are usually assumed the same for a certain mine site, except the effect of waste rock PSD, which usually covers a wide size span and shows a high degree of uncertainty. The coefficient of uniformity C_U and the coefficient of curvature C_C can be used to evaluate the segregation potential (Asmaei et al., 2018). For example, a greater C_U (or C_C) tends to induce a higher segregation potential. However, C_U is sometimes considered not reliable to evaluate segregation because particles coarser than D_{60} are actually more prone to segregation (Messerklinger et al., 2011). Consequently, modified coefficients of uniformity, i.e., $h'' = D_{90} / D_{15}$ and $h' = D_{90} / D_{60}$ are proposed to more realistically evaluate particle size distribution in terms of segregation risk (Burenkova, 1993). Therefore, C_h ($= h'' / h'^2 = (D_{60})^2 / (D_{90} \times D_{15})$) is also proposed as an indicator to evaluate the segregation potential of granular material with wide particle size distributions (Langroudi et al., 2015). A higher C_h (or h'') indicates a higher segregation potential (Burenkova, 1993).

Laboratory experiment reports the bottom of the slope contains about 40% of the maximum particles with push-dumping method and 75% with end-dumping method (Nichol, 1986). Waste rock piles are usually constructed using benches of a recommended maximum height of 25 m with the objective to reduce segregation and increase the physical stability of the slopes (Anterrieu et al., 2010; Aubertin, 2013; Dawood et al., 2013). Segregation tends indeed to increase with the slope length of the waste rock pile (Nichol, 1986). However, no report is found to quantitatively analyze the effect of construction method and bench height on waste rock segregation in the field.

Table 2.9: Summary of the influence factors affecting granular segregation.

Influence factors	Description	Consequence	References
Physical properties	•Particle size distribution (C_U, C_C) •The proportion of coarse particles •Particle shape •Particle specific gravity (G_S)	•Higher C_U and C_C indicated higher segregation potential. •Interlocking effect of irregular particles with different elongation and roundness. •Different G_S may cause segregation controlled by push-away, embedding, and repose angle effect.	Stephens et al. (1978a); Massol-Chaudeur et al. (2002); Tang et al. (2007); Khola et al. (2016); Fan et al. (2017); Asachi et al. (2018)
Construction methods	•End-dumping and push-dumping method •Bench height of waste rock pile	•Different initial energy during waste rock disposal with different construction methods. •Segregation tends to increase with the slope length of the waste rock pile.	Nichol (1986); Anterrieu et al. (2010); Aubertin (2013); Dawood et al. (2013)
Environmental conditions	•Rainfall •Water content •Vibration	•Agglomeration segregation and concentration-driven displacement segregation may occur with the presence of water. •Displacement segregation and percolation segregation may occur under vibration.	Tang et al. (2004); Hashim et al. (2008).

2.3.3 Segregation characterization

Quantitative characterization of waste rock segregation provides the basis to analyze the hydrological properties (e.g., water flow) and geotechnical properties (e.g., shear strength) within heterogeneous waste rock piles. The segregation of waste rock in the field can be difficult to characterize because of the following reasons:

- Waste rock piles are usually in large dimensions and constructed with benches with slope angles around 35° to 40°, making waste rock piles complicated for investigation. So,

access to the steep slopes of waste rock piles can be dangerous (Burnley, 1993; Williams et al., 2008).

- The surface layer of the slope is normally in loose state because the waste rock is dumped freely and no compaction is conducted on the slope surface. Also, waste rock piles are usually subjected to rainfall, tending to reduce to the geotechnical stability of loose-dumped waste rock slopes (Xu et al., 2017; Zevgolis, 2018).
- Waste rock particles usually exhibit irregular shapes and the maximum particle diameter can reach 2 m, making it complicated to precisely determine the size and mass of large waste rock particles (Fines et al., 2003; Zhang et al., 2017; Dwumfour et al., 2020).

Image analysis provides an efficient alternative to overcome the limitations above. The details of image analysis can be found in section 2.2.1. The segregation of granular materials is usually characterized based on the particle size distribution using characteristic diameters such as D_{10}, D_{50}, D_{80} (Blight, 2010; Zhang et al., 2017), and segregation degree (χ) (Kenney et al., 1993).

(1) Segregation characterization based on characteristic diameters

Characteristic diameters D_{10}, D_{50}, D_{80} in different segregated zones can be used to characterize the segregation of waste rock in the field (Zhang et al., 2017). The increase of these characteristic diameters indicates a trend that particles become coarser. The absolute values of D_{10}, D_{50}, D_{80} vary with mine sites and no typical ranges can be specified. The segregation can also be evaluated using D_{50} with considering the spatial variation of particles with different sizes (Béket Dalcé et al., 2019).

The relative particle sizes such as D_{50} / D_{50} (max), defined as the ratio of D_{50} at any distance away from the deposition point to the maximum D_{50} of the total material (Blight, 2010). This index is originally used to characterize the segregation in a tailing storage facility filled with slurried tailings. D_{50} / D_{50} (max) ranges between 0 and 1, and indicates coarser material with higher D_{50} / D_{50} (max). Relative particle size can clearly exhibit the segregation state of the material at any position of the investigated piles. The relative particle size works on the basis of the continuously graded material so that characteristic diameters can be extracted.

(1) Segregation characterization based on the PSD curve

Segregation degree from Kenney (1993)

Logarithmic mean particle size (logd, calculated using equation 2.7) provides an approximation of the area to describe the geometry of the entire distribution curve (Kenney et al., 1993). For example, $\log d_{FQ}$ represents the shaded green area for PSD curve FQ in Figure 2.6.

$$\log d = \sum_{i=1}^{n} (P_i - P_{i-1}) \log \sqrt{D_i \cdot D_{i-1}} \quad (2.7)$$

Where D_i and D_{i-1} (mm): consecutive particle sizes with corresponding passing P_i and P_{i-1}.

Segregation index (SI) is then used to quantify the extent of segregation in a soil mass based on the logarithmic mean particle size (Kenney et al., 1993):

$$SI = \log (d_C/d_F) = \log d_C - \log d_F \quad (2.8)$$

Where $\log d_C$ and $\log d_F$ (-): the logarithmic mean particle size of the coarse zone and fine zone of the segregated material. The segregated coarse and fine zones are selected depending on the specific applications (Sutherland, 2003). For example, the top section represents the fine zone and bottom section represents the coarse zone in Figure 2.6.

Relative segregation index (RSI) is defined as the ratio of the segregation index (SI_{test}) of the segregated material to the segregation index calculated for perfect segregation state (SI_P) (Kenney et al., 1993):

$$RSI = \frac{SI_{test}}{SI_P} = \frac{\log d_C - \log d_F}{\log d_{CQ} - \log d_{FQ}} \quad (2.9)$$

Where $\log d_{FQ}$ and $\log d_{CQ}$ (-): the logarithmic mean particle size of the finest quartile and coarsest quartile, which are defined under a perfect segregation state.

Perfect segregation is defined as a state occurred when the finest zone (finest quartile) contains only particles smaller than D_{25} of the original gradation, and the coarsest zone (coarsest quartile) contains only particles larger than D_{75} of the original gradation (Westland, 1988; Kenney et al., 1993). The PSD curve of the coarsest quartile (CQ in Figure 2.6) is established by removing particles smaller than D_{75} of the original gradation, which is calculated as $P_{CQ} = 4P_0 - 300$, where P_0 is the passing percentage at the original gradation (curve O in Figure 2.6). The PSD curve of the finest quartile (FQ in Figure 2.6) is established by removing particles larger than D_{25} of the original gradation, which is calculated as $P_{FQ} = 4P_0$.

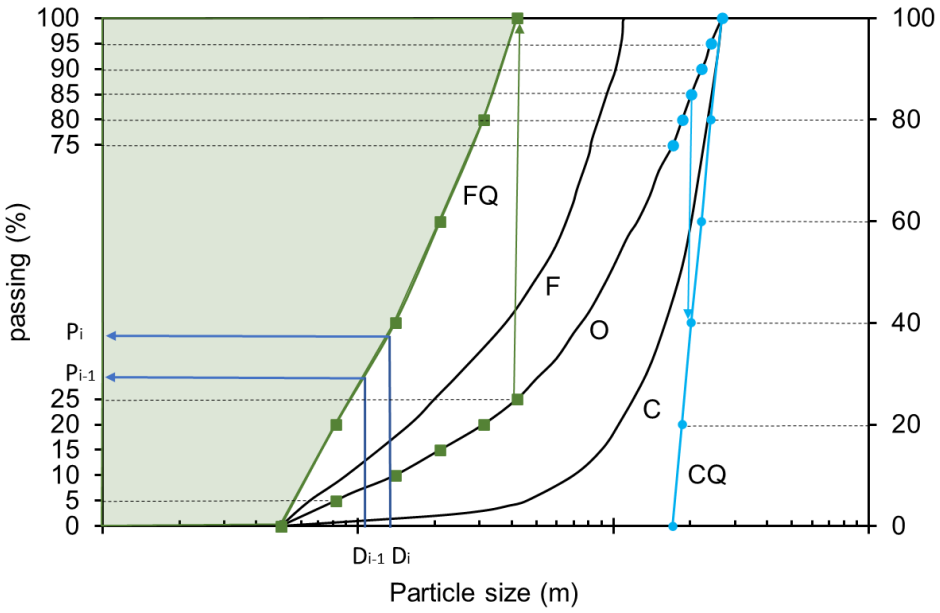

Figure 2.6: Segregated gradation curves. F and C represent the finest zone and coarsest zone (see Figure 2.7), which are segregated from the original gradation curve (curve O). Curves FQ and CQ represent the finest quartile and coarsest quartile, respectively. The green shaded area represents the logarithmic mean particle size of PSD curve FQ. (Adapted from Asmaei et al., 2018).

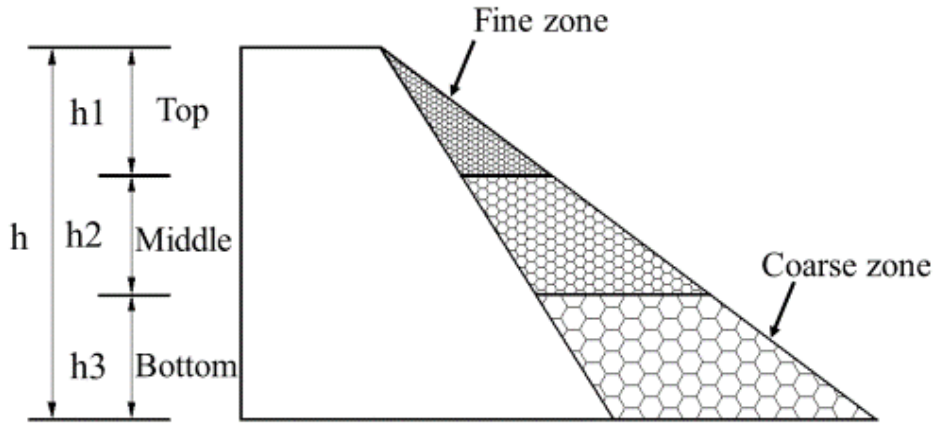

Figure 2.7: Conceptual illustration of the segregation characterization when the segregated waste rock is divided into top, middle and bottom sections. The fine and coarse zones are defined according to the research need (e.g., h1 = h2 = h3).

The relative segregation index (RSI; Milligan, 2003) can range from 0, indicating no segregation, to a theoretical upper limit of 1.0, indicating perfect segregation (only contain particles larger than D_{75} of the original material before segregation). RSI is considered applicable to characterize the segregation of the continuous graded material (Milligan, 2003; Sutherland, 2003). RSI has been applied to characterize the segregation of cohesionless soils (Asmaei et al., 2018). One limitation in RSI is that only the fine zone and coarse zone are used to characterize the segregation degree of the whole segregated material. The segregation state in other sections such as the middle section in Figure 2.7 cannot be considered.

Segregation degree from Sutherland (2003)

The relative segregation index (RSI; Kenney et al., 1993) has been developed by Sutherland (2003) to overcome the constraints on the minimum particle sizes that are difficult to accurately determined using image analysis. A new segregation index, coarsening index (CI), is proposed to distinguish from segregation index (SI) in Kenney et al. (1993). Coarsening index plays the same rule to SI, and can quantify the extend of the segregation in a soil mass.

The coarsening degree, also called segregation degree in this study, can be calculated according to the approach presented in Figure 2.8. The coarsening degree acts as the same rule to RSI

except that the finest quartile is replaced by the original material in coarsening degree (Sutherland et al., 2003). CI is found generally higher than RSI but the trend of CI and RSI is proved virtually the same (Sutherland, 2003). Coarsening degree only uses the segregated material in the coarse zone to characterize the segregation. Similar to RSI, CI can range from 0.0, indicating no segregation, to a theoretical upper limit of 1.0, indicating perfect segregation (only contain particles larger than D_{75} of the original material before segregation). CI is also applicable to characterize the segregation of the continuous graded material such as waste rock (Sutherland et al., 2003).

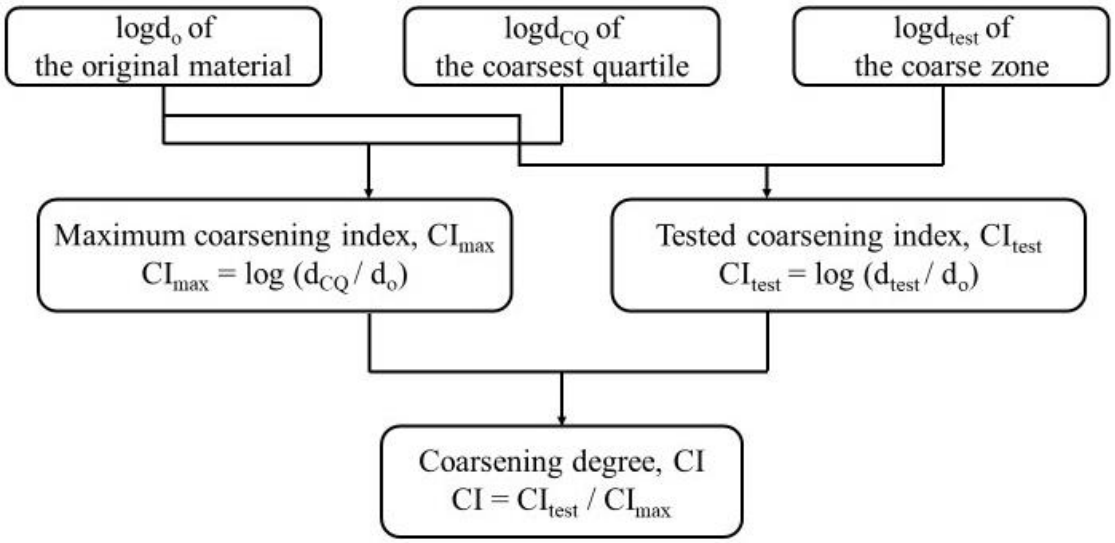

Figure 2.8: Steps to determine the coarsening degree of continuous graded soil. $Logd_0$, $logd_{CQ}$, and $logd_{test}$ can be calculated in the same way to Kenney (1993).

2.3.4 Segregation evaluation

2.3.4.1 Experiments

There is no recognized standard to evaluate granular material segregation using experiments, which are usually designed for different research purposes, such as segregation in chute flow tests (Zhang et al., 2004; Idelsohn et al., 2006; Bhattacharya et al., 2014), rotating drum tests (Ristow,

1994; Govender, 2016; Liao et al., 2021), silo / hopper tests (Ketterhagen et al., 2007; Engblom et al., 2012), flume tests (Asmaei et al., 2018; Cheng et al., 2019), and some self-designed segregation tests (Nichol, 1986; Combarros et al., 2014).

The rotating drum is used in different processes such as mixing in the pharmaceutical industry and wood debarking in the papermaking industry (Seiden et al., 2011). Silo and hopper tests involve filling of bulk solids into confined vessels, where the solids segregated under the effect of particle size, density and discharge rate (Zigan et al., 2008). Segregation in the drum test and silo / hopper tests develops in vessels, which is different to waste rock segregation that is developed in a manner of the free surface segregation (Drahun et al., 1983; Huang et al., 2021). But the segregation in the silo and hopper also involves percolation and rolling mechanisms (Engblom et al., 2012), and the relevant research is also expected to provide implications to analyze the mechanisms in waste rock segregation.

Both chute flows and flume tests are designed to allow continuous flows of granular material in inclined channels. The chute and flume flow mainly involves free surface flow (Dolgunin et al., 1995). These experiments mainly analyze influence factors such as particle size, shape, and density. Results indicate that the particle size is the most deterministic factor, while particle shape seems to have less influence on segregation (Combarros et al., 2014). The results from such studies can be applied to other systems such as rockfill and waste rock disposal on the inclined surface (Khakhar et al., 1999; Cheng et al., 2019).

Limited experiment has been conducted to investigate waste rock segregation during disposal. Experiments conducted by Nichol (1986) study the effect of construction methods (end-dumping and push-dumping method) and the slope length (1 m and 2 m) on waste rock segregation. The experiments are conducted with a maximum particle diameter of 19 mm. The results indicate waste rock disposal using end-dumping method creates similar segregation for the short and long slopes. However, these experiments are cownducted in small scales with limited amount of waste rock, which is far from the reality where every hundreds of tons of waste rock will be dumped with the maximum particle diameter reached 2 m (Zhang et al., 2017).

2.3.4.2 Numerical simulation

Numerical simulations can be an efficient way to overcome the limitations in experiments and extend to analyze the granular flow in large scales. Numerical simulations of granular flow mainly consist of two methods: continuum modelling methods (Gingold et al., 1977; Lucy, 1977; Idelsohn et al., 2004) and discrete element method (Cundall et al., 1979).

(1) Continuum modelling methods

Continuum modelling method simulates the granular material as a continuous media and the flow behaviour is predicted by fundamental laws of physics in terms of mass, momentum and energy (Larsson, 2019). A constitutive model is required to obtain the relationship between stress and strain. Continuum modelling methods mainly include smoothed particle hydrodynamics (SPH) method (Gingold et al., 1977; Lucy, 1977), material point method (MPM) (Sulsky et al., 1994), and particle finite element method (PFEM) (Idelsohn et al., 2004). The main feature of these methods is listed in Table 2.10.

SPH can simulate waste rock flow, and the information of each particle such as its motion, mass, velocity, and position can be monitored (Cao et al., 2021). Fei et al., (2017) indicates that MPM can well simulate the segregation in granular flow of binary material using 7200 material points with material parameters (e.g., E-modulus, friction coefficient) assigned for each particle. However, currently only limited numbers of particles can be simulated with SPH and MPM, and the calculation pressure is still a challenge when these methods are used to simulate waste rock at field scales. Although PFEM can well simulate multi-fluid flows such ass heterogeneous fluid flows, no literature indicates its possibility to simulate waste rock segregation (Idelsohn et al., 2006).

Table 2.10: Features of the main continuum modelling methods. SPH: smoothed particle hydrodynamics method; MPM: material point method; PFEM: particle finite element method.

Methods	Description	Advantage	Disadvantage	References
SPH	•Lagrangian mesh-free method •Computational domain is represented by particles •No direct connectivity between particles	•Well deal with the interface, free surface, and large deformation. •No mesh distortion.	•Tensile instability. •Difficulties to handle boundary conditions. •a homogeneous and smooth particle distribution is required to ensure stable and reliable results.	Gingold et al. (1977); Lucy (1977); Cao et al. (2021)
MPM	•Mesh-based particle method •Lagrangian-Eulerian description of motion. •The state variables are traced on Lagrangian material points	•Well model the column collapse of granular material and silo discharge. •Allow for mesh distortion and follow the evolution of free surfaces. •Handle large deformations in large-scale failure problems •Flexibility in tracking evolution of densities, velocities, and stress fields for different mechanical states of granular materials.	•Each particle has to be assigned a fixed mass, which requires the number of particles kept constant during the simulation. •The particle distribution may become irregular and limit the simulation accuracy.	Sulsky et al. (1994); Bandara et al. (2016); Fei et al. (2017)
PFEM	•Mesh-based method. •A Lagrangian motion is used for the nodes in a finite element mesh. •Particles define the computational domain •Nodes are considered as free particles, allowing particles to separate from the domain. •Particles are projected onto the mesh for calculation.	•Calculate fluid mechanics including heterogeneous flows •Particles have no fixed mass.	•Unclear application for rock mechanics. •Constitutive models dealing with hydromechanical coupling problems with large deformation are still needed.	Idelsohn et al. (2004); Idelsohn et al. (2006); Monforte et al. (2017); Cremonesi et al. (2020)

(2) Discrete element method

Discrete element method (DEM) simulates the motion of granular material as spheres or non-sphere particles by calculating the stress and deformation of contacts, which are generated when particles interact with each other or with boundary walls (Cundall et al., 1979; Zhu et al., 2008; Jiang et al., 2019). DEM has been widely used to simulate the flow behaviour of granular materials including rockfill (Jiang et al., 2018; Manso et al., 2018), soil-rock mixture (Xu et al., 2016) and waste rock (Thoeni et al., 2019; Zhu et al., 2019). The DEM model consists of bodies and contacts, and bodies consist of walls, balls, irregular shaped particles (e.g., clumps, rigid blocks). The details of bodies and contacts, and the main parameters for model calibration are discussed below.

- Wall

A wall is composed of facets and can move, translate and rotate with an assigned velocity, but do not obey the motion equations because no mass can be assigned to walls (Itasca, 2019). Walls are used to apply boundary conditions, interacting with particles (i.e., balls, clumps, and rigid blocks) to simulate supporting and functional structures (Potyondy, 2015). For example, walls can be used to simulate the haul trucks which contains waste rock particles for disposal. Also walls can simulate the shear box in direct shear tests (Xu et al., 2016).

- Ball / clump / rigid block

Balls, clumps and rigid blocks are the main entities to simulate solid particles (Figure 2.9). Balls are preferred to simulate granular material (e.g., waste rock, gravels and rockfill) because contacts between balls are easier to detect so that the simulation can be speeded up (Ding et al., 2013; Jiang et al., 2018). However, the bulk friction of balls is usually too low to simulate the friction properties of crushed rock (Coetzee, 2016). The main methods to increase the bulk friction include incorporating rolling resistance (Roessler et al., 2019) and using irregular particles (Zhang et al., 2020). Clumps and rigid blocks can also simulate the irregular particles of granular material. However, accurately modelling the irregular shapes is challenging because it is impractical to reproduce most real particles in practice (Annabattula et al., 2012). In addition, simulations suffer great calculation pressure when large amounts of waste rock at field scale are simulated using irregular shapes (Katterfeld et al., 2017). Some reports the simulation time using

clumps is 30 times of that using sphere particles when one second of hopper discharge is simulated (Coetzee, 2016).

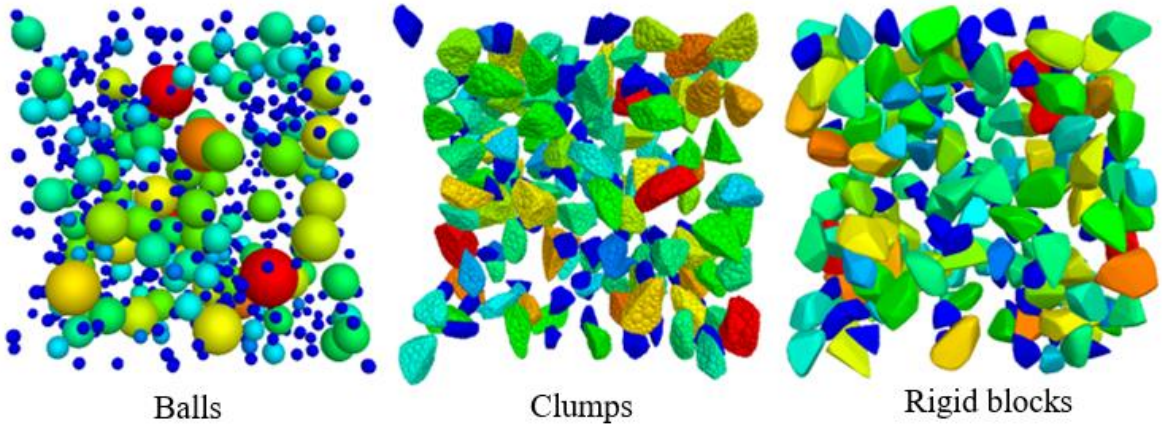

Figure 2.9: Basic entities in forms of balls, clumps and rigid blocks generated with PFC3D (Itasca, 2019). A ball is a rigid sphere with a specified radius. A clump is a rigid collection of rigid balls acting as one object. A rigid block can be generated with closed, convex and manifold polyhedral. Particles are colored according to their sizes (from blue with a diameter of 8 mm to red with a diameter of 38 mm).

- Contact models

Distinct particle interacts with other particles or walls at contact points, in which the particle interaction laws are embodied to calculate the force and deformation (Di Renzo et al., 2004; Shen et al., 2016b). The particle-interaction laws are referred to as contact models, and each contact can be assigned a single contact model (Itasca, 2019). The basic contact model in DEM is a linear contact model, and some different models such as rolling resistance linear model and Hertz-Mindlin model are widely developed to simulate the granular material.

Linear model

The contact force in linear model is composed of a linear force and a dashpot force that act in parallel (Figure 2.10). The linear force provides linear elastic frictional behaviour, while the dashpot force provides viscous behaviour (Itasca, 2019). The linear force is produced by linear

springs with normal and shear stiffnesses, k_n and k_s. Slip is accommodated by imposing a Coulomb limit on the shear force using the friction coefficient, μ. The dashpot force is produced by dashpots with viscosity given in terms of the normal and shear critical-damping ratios, β_n and β_s, which control the energy dissipation during particle collision. Linear model can simulate the flow of granular material, but the simulation generates too dispersive flow compared with experiments when sphere particles are modelled (Teufelsbauer et al., 2009). This is attributed to the disadvantage of the linear model that the relative rotation is not considered (Itasca, 2019). So a simple linear model cannot simulate the rolling effect in the flow of irregular material such as in waste rock disposal.

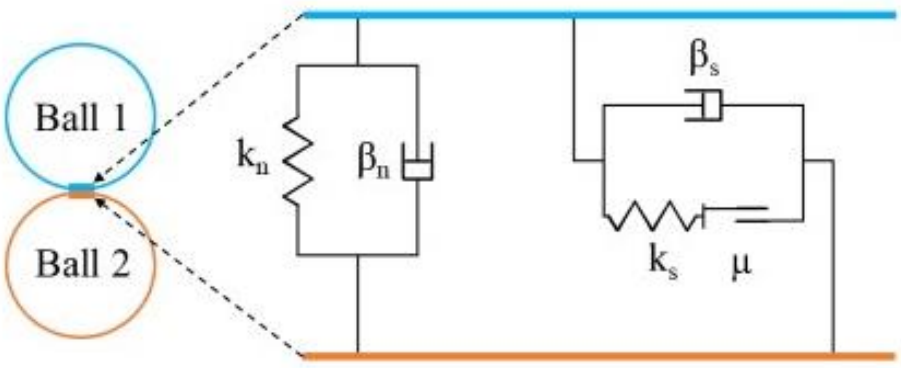

Figure 2.10: Conceptual contact model of the linear model. Linear model consists of two parts: linear spring (related to k_n, k_s, and μ) and dashpots (related to β_n and β_s). These parameters govern the development of force and deformation at the contact. (Adapted from Ai et al., 2011)

Rolling resistance linear (rrlinear) model

Rolling resistance linear model (Figure 2.11) can indirectly consider particle shape effect as the rolling resistance also arises from the effect of non-spherical particles (Jiang et al., 2005). Rolling resistance coefficient (μ_r) is then introduced to represent the resistance to the movement of particles rolling on a surface (Iwashita et al., 1998). The rolling resistance moment (M) will be first incremented in rolling resistance linear model with the accumulated relative rotation of the

contacting pieces at the contact point (Ai et al., 2011). The updated rolling resistance moment can be expressed as (Itasca, 2019):

$$M' = M - k_r \Delta\theta \tag{2.10}$$

Where M': the updated rolling resistance moment (N·m); $\Delta\theta$: the relative rotation increment (-); k_r: the rolling resistance stiffness (N·m), which can be calculated by:

$$k_r = k_s R^2 \tag{2.11}$$

Where: k_s: the shear stiffness of the spring at the contact (N/m). R: the effective radius at the contact (m).

The contact effective radius R can be calculated by the radii of contact balls:

$$\frac{1}{R} = \frac{1}{R1} + \frac{1}{R2} \tag{2.12}$$

Where R1 and R2: the radii of the two contacted balls (m). R2 = ∞ if ball 1 contacts with walls (facets).

Rolling slip then starts when the rolling resistance moment (M) exceeds the limiting torque and this rolling resistance moment can be expressed as (Ai et al., 2011):

$$M = \mu_r R F_n^l \tag{2.13}$$

Where μ_r: the rolling resistance coefficient (-); F_n^l: the normal linear force (N).

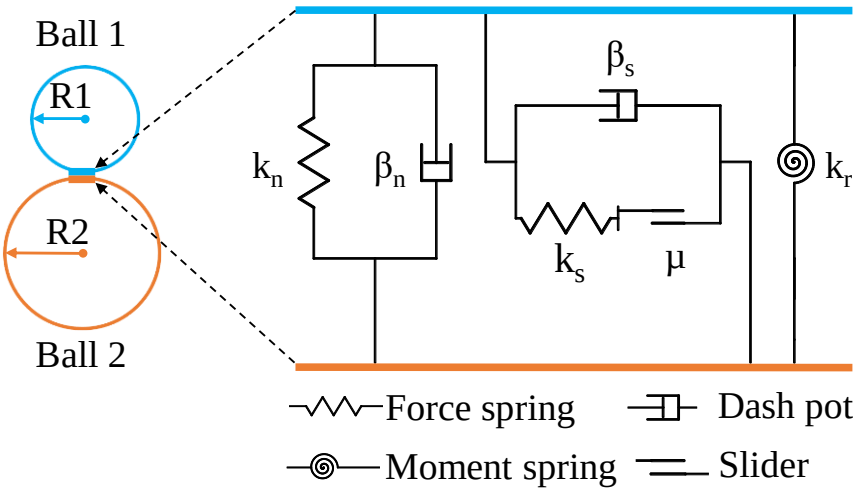

Figure 2.11: Interpretation of rolling resistance linear model. Normal and shear stiffness k_n and k_s, and friction coefficient μ control the linear force; normal and shear critical-damping ratios β_n and β_s control the dashpot force; rolling resistance stiffness k_r controls the rolling moment (see text for more details) (adapted from Ai et al., 2011).

Rolling resistance mechanism provides multi-functions that can indirectly account for shape effects, slipping, plastic deformation, viscous hysteresis, and surface adhesion (Ai et al., 2011). Rrlinear model provides the function governing the rolling effect of particles, and can be used to consider particle shape effect when sphere particles are used for granular simulations (Iwashita et al., 1998; Ai et al., 2011). Therefore, the contact mechanism of rrlinear model is particularly adapted to simulate waste rock disposal using spheres.

Hertz-mindlin model

Hertz-mindlin model consists of a non-linear formulation based on Hertz's theory in the normal direction and the Mindlin's no-slip model in the tangential direction (Tsuji et al., 1992). Hertz-mindlin model has been widely used to simulate the behaviour of granular material such as shear strength tests of rockfill (Landry et al., 2006) and the flow behaviour of rockfill (Jiang et al., 2019). However, this model is usually computationally expensive to simulate large amounts of particles (e.g., waste rock disposal, rockfill dam construction) because of the smaller time step

required as compared to the linear-spring-dashpot model such as linear model and rolling resistance linear model (Navarro et al., 2013; Coetzee, 2016). So, simulations of the field waste rock disposal may be very challenging when Hertz-mindlin model is used.

- Main parameters of rolling resistance linear model

These contact models govern the behaviour of particles by defining a set of input parameters that controls different mechanisms such as sliding, rolling, and viscosity (Di Renzo et al., 2004; Shen et al., 2016b). The main challenge to apply contact models for waste rock disposal simulations is the determination of input parameters (Paulick et al., 2015; Al-Hashemi et al., 2018). Different contact models may include different parameters, such as the rolling resistance coefficient in rrlinear model (Ai et al., 2011). Although the calibrated parameters might be model dependent, some parameters such as friction coefficient, rolling resistance coefficient, contact damp, and elastic modulus, are fundamental but important in governing the flow behaviour of simulated waste rock (Coetzee, 2016, 2020).

Friction coefficient and rolling resistance Coefficient

Friction coefficient (μ) describes the contact forces of two sliding surfaces and is calculated by the ratio of the tangential force to the normal force of the two contact surfaces (Just et al., 2013). Rolling resistance coefficient (μ_r) is usually used to consider the shape effect when spheres are used to simulate irregular particles (Iwashita et al., 1998; Coetzee, 2016; Roessler et al., 2019). μ and μ_r are considered the most critical parameters governing the flow behaviour of granular material such as waste rock and rockfill (Just et al., 2013; Santos et al., 2016a). Both μ and μ_r, with values ranged between 0 and 1, are usually calibrated synergistically using experimental tests such as repose angle tests, shear strength tests (Fu et al., 2011; Combarros et al., 2014). Repose angle tests and shear strength tests gave an indication of the material flowability and were directly related to the intrinsic properties (e.g., friction and rolling) of granular particles (Belheine et al., 2009; Al-Hashemi et al., 2018).

Contact damp

Particle flow code 3D (PFC3D, Itasca, 2019) provides two damp models for energy dissipation: local damp and viscous damp (Itasca, 2019). Viscous damping can be applied at the contacts through a viscous dashpot in the normal and the tangential direction by specifying the critical

damping ratio (β_n and β_s) (Mao et al., 2004). Viscous damp is more preferred for dynamic simulations (Besinger et al., 1995). Viscous dissipates a small amount of energy but reduces the timestep which is less than optimal for simulation. Local damp can be applied to the governing equation of motion at local level to establish equilibrium and it is efficient to simulate quasi-static deformation (Coetzee, 2016). A damping force is added to the motion equation when local damp is applied (Itasca, 2019):

$$F_d = -\alpha|F_t|\text{sign}(v) \tag{2.14}$$

Where F_d: the damping force vector applied to the particle (N), F_t: the generalized force acting on the particle, together including the action of gravity force (N), v: the particle velocity vector; α: local damp (-).

Drop tests are usually used to determine the contact damp of granular materials such as waste rock (Wang et al., 2015). Drop tests measure the rebound height of granular particles (waste rock, rockfill, gravels) when they freely fall down from a certain height (Chung et al., 2008; Barrios et al., 2013). Local damp usually ranges between 0.15 and 0.7 for different granular materials (Sadek et al., 2014; Simons et al., 2015; Yan et al., 2015).

Elastic modulus / stiffness

Elastic modulus between 10^6 and 10^{10} Pa is usually recommended for hard rock when the DEM model is used to simulate strength properties such as UCS test and shear strength tests (Landry et al., 2006; Coetzee et al., 2009). Increasing the effective modulus from 0.15 to 2 MPa can lead to a four-time increase of the shear stress contact force (Landry et al., 2006; Paulick et al., 2015). However, the repose angle changed by only 1° when the elastic modulus decreased from 10^{10} Pa to 10^5 Pa (Combarros et al., 2014). It was also reported that reducing the particle stiffness by a factor of 100 ~ 1000 from the measured value had no significant influence on the flow pattern (e.g., particle velocity, dispersion) (Xu et al., 2002; Chung et al., 2008).

2.4 Knowledge frontiers

In summary, waste rock disposal using end-dumping and push-dumping methods generally causes segregation and stratification, resulting in heterogeneous distribution of waste rock in terms of particle size distribution and compactness, and increasing risks for both geochemical and geotechnical instabilities (Morin et al., 1991; Herasymuik et al., 2006; Lahmira et al., 2016). End-dumping usually is considered to generates more segregation than push-dumping method, and a longer slope tends to produce more segregation (Nichol, 1986). However, the effect of construction method and bench height on segregation has not yet been investigated at field scale. One reason is that waste rock characterization at field scale is very challenging because access to the steep and loose slopes of waste rock piles can be dangerous and the determination of the sizes and mass of large irregular waste rock particles can be complicated (Williams et al., 2008; Zevgolis, 2018; Dwumfour et al., 2020). In this project, waste rock segregation at Canadian Malartic mine was firstly characterized in the field using image analysis. Discrete element method (DEM) was then used to reproduce waste rock flow behaviour during disposal (model calibration and validation) and to evaluate segregation under different operational factors such as construction method and bench height. The details of the methodological approaches used in this study were organized in chapter 3 and results are presented and discussed in chapters 4 to 7.

CHAPTER 3 METHODOLOGY

The effect of waste rock disposal on the heterogeneous properties of waste rock pile was characterized at various scales including field observation, experimental tests and discrete element simulations. The basic properties of waste rock were characterized in the laboratory. Waste rock segregation and lateral heterogeneity were characterized in the field by analyzing waste rock PSD along the slope of waste rock pile at Canadian Malartic mine using image analysis. Simulations were conducted using particle flow code 3D (PFC3D, Itasca, 2019) to investigate the effect of waste rock disposal on segregation.

3.1 Characterization of waste rock properties

The waste rock used in this study was sampled from Canadian Malartic mine and transported to the laboratory for testing. Canadian Malartic mine is an open-pit mine located within the Municipality of Malartic, approximately 25 km west of Val-d'Or and 80 km east of Rouyn-Noranda in Quebec, Canada. The latest mine production schedule plans to feed the mill from the open pits and stockpiles at a nominal rate of 57,000 tons per day (Lehouiller et al., 2020). An estimated total of 450 Mt of waste is placed on the waste rock pile, at an in-situ compacted density of 1.96 t/m^3, representing a storage volume of 230 Mm^3. The waste rock pile is constructed in 10 m benches with 11.5 m terraces between benches for an overall slope angle of 21.8°. The slope angle of each bench is around 37° (Gervais et al., 2014). The total height of the waste rock pile reaches 100 m in most sections (Lehouiller et al., 2020).

A field waste rock PSD curve (G0 in Figure 3.1) at Canadian Malartic mine was obtained by combining manual field measurements for large particles (> 90 mm), sieving analysis for intermediate particles (0.075 mm < D < 90 mm), and hydrometer tests for fine particles (< 0.075 mm) (Essayad, 2021). The maximum particle size (D_{max}) of this PSD curve was 254 mm, but blocks up to 2 m were observed in the field. The characterized C_U and C_C of PSD G0 were 39 and 1.8, respectively.

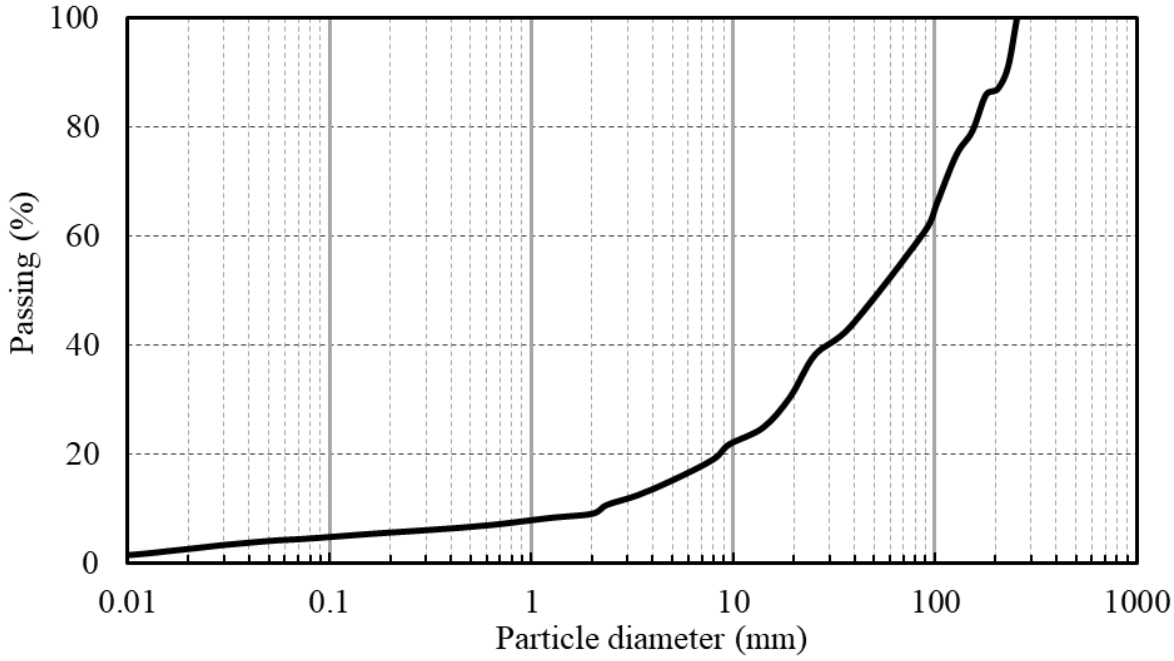

Figure 3.1: The field PSD curve characterized at Canadian Malartic mine.

3.1.1 Specific gravity

The specific gravity (G_S) of waste rock was measured using ASTM C127 (ASTM, 2015) for the fractions larger than 4.75 mm, and using water pycnometer method (ASTM, 2016a) for fractions larger than 4.75 mm. The specific gravity of waste rock smaller than 50 mm was tested in the laboratory. 3 waste rock specimens were prepared using scalping technique by removing waste rock particles larger than 50 mm from PSD curve G0 (Figure 3.1). Scalping technique is a widely used technique to prepare specimens of various fractions, which allows to change the particle size distribution of waste rock with different minimum and maximum particle diameters (Bagherzadeh-Khalkhali et al., 2009; Deiminiat et al., 2020).

The average G_S of the tested waste rock was 2.758 for the fractions ranged between 5 mm and 50 mm, and 2.755 for the fractions ranged between 0 and 5 mm (see details in Appendix A). The absorption of tested waste rock was 0.34%. These values ranged between the values in the literature (Gamache-Rochette, 2004; Essayad, 2021)

3.1.2 Characterization of waste rock shapes

The shapes of waste rock particles were described in terms of the circularity (= $4\pi A / P^2$) and elongation (= b / a) in the laboratory. P represents the perimeter of the projected area of the particle; A represents the projected particle area; Values a and b represent the long axis and medial axis. The details of the shape descriptors can be found in section 2.2.2.

Around 12.2 kg waste rock, containing 2224 particles with diameters ranged between 8 mm and 38 mm, were analyzed to characterize particle shapes using image analysis (Figure 3.2). Waste rock circularity mainly ranged between 0.6 and 0.8, with the maximum frequency of 0.4 for the circularity of 0.7. The elongation mainly ranged between 0.5 and 0.8, with the maximum frequency of 0.3 for the elongation of 0.7. The values of characterized circularity and elongation of waste rock are included in the ranges mentioned in the literature (Linero et al., 2017; Ovalle et al., 2020).

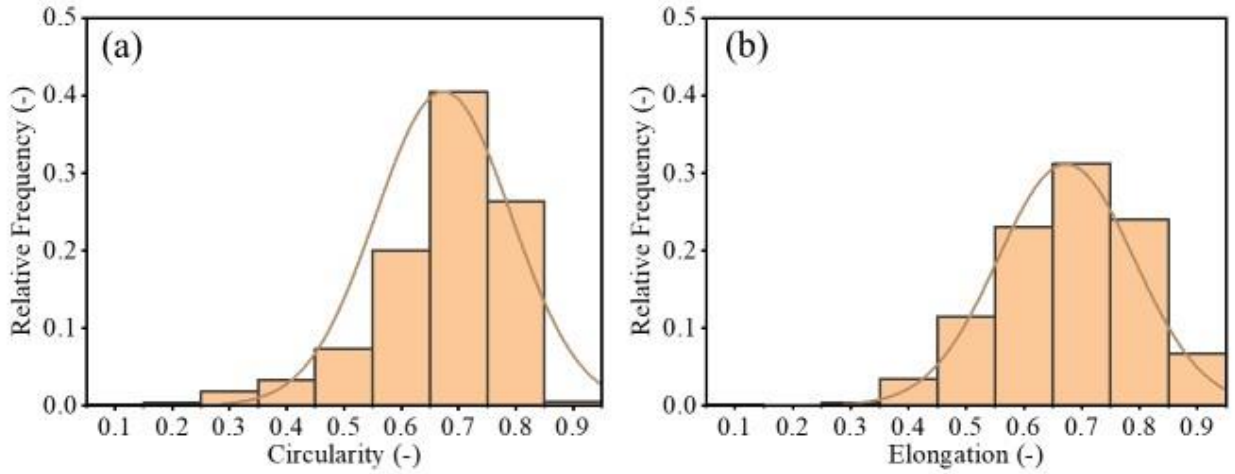

Figure 3.2: Characterization of waste rock shapes in the laboratory using (a) circularity and (b) elongation. The results were obtained using image analysis based on the 2224 particles between 8 mm and 38 mm diameter.

3.2 Evaluation of waste rock segregation

3.2.1 Sample preparation

Around one ton of waste rock, transported from Canadian Malartic mine, was air dried in the laboratory and then sieved between 0.075 mm and 100 mm (ASTM D6913). The sieved waste rock was stored within buckets by fractions. PSD curve Lab0 was scalped from PSD curve G0 (Figures 3.1 and 3.3) and used for repose angle and segregation tests. Particles smaller than 8 mm were removed to reduce the calculation time because the number of contacts will significantly increase when more smaller particles are generated in PFC3D (see details in chapter 5). Particles larger than 89 mm were also removed because of the operational limitations in the laboratory. The characterized C_U and C_C of PSD Lab0 were 3.5 and 0.9, respectively.

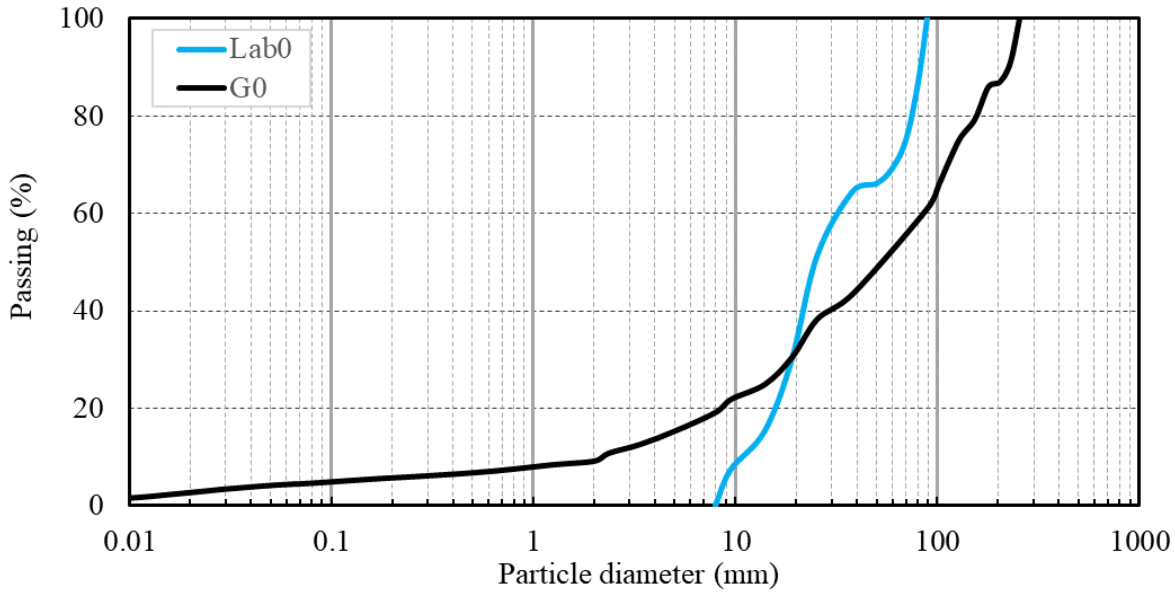

Figure 3.3: Particle size distribution curves of waste rock used for repose angle and segregation tests. G0 was the field PSD curve characterized at Canadian Malartic mine. PSD curve Lab0 was scalped from G0 and used for sample preparation in repose angle tests and segregation tests.

3.2.2 Laboratory repose angle tests

Repose angle tests were used to calibrate the PFC3D model. Around 75 kg of waste rock were sampled for each specimen in the laboratory according to Lab0 (Figure 3.3). Waste rock was then placed in a 60 cm high and 35 cm diameter bucket, which was placed on the ground (Figure 3.4a). The bucket was quickly (< 1 s) lifted vertically so the waste rock formed a conic pile on the ground (Figure 3.4a). The repose angle of the pile (θ, Figure 3.4a) was determined by measuring the pile radius (R) and the pile height (H) using a ruler with a precision of 0.1 cm. The radius was defined as the distance from the center to the edge of the pile where no particles overlapped (although some individual particles could have moved outside this radius). Four values of the radius (R1 – R4, Figure 3.4b) were measured in four directions and four repose angles were obtained for each test. The test was repeated 10 times to ensure the repeatability of the measurement. Repose angle tests results are presented in Chapter 5.

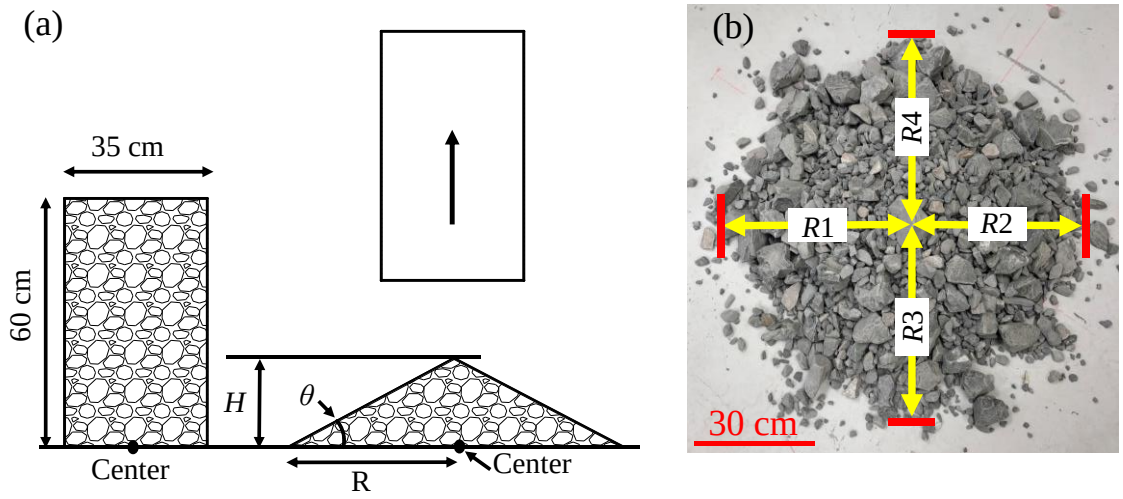

Figure 3.4: Laboratory repose angle tests. (a): Repose angle tests setup. R: radius of the cone in one direction, H: height of the pile, θ: repose angle (θ = arctan(H/R)). (b): Radii (R1 – R4) in four directions of the tested waste rock cone.

3.2.3 Laboratory segregation tests

Segregation tests were designed for this study to validate the calibrated model. Waste rock specimens were prepared according to the same PSD curve used for repose angle tests (PSD Lab0 in Figure 3.3). Around 20 kg of waste rock were filled in a 30 cm high and 27 cm diameter bucket. The bucket was lifted to the top of a 1 m high vertical wall and then inclined around 60° (Figure 3.5a). The bucket was inclined around 60° between the bucket and the horizontal direction so that it was easier to control waste rock dumping (Figure 3.5a). Waste rock then fell along the wall when the bottom cap was removed, and ten buckets of waste rock were dumped progressively. A semi-cone was finally created, and segregation was observed from the top to the bottom of the cone (Figure 3.5b). The cone was divided into 6 sections (Figure 3.5a) and the waste rock in each section was sieved using a large-scale sieving machine. The mass of each size fraction was measured with a precision of 1 g, and the PSD curve in each section was finally determined. In total, segregation tests were repeated five times. The characteristic diameters (e.g., D_{10}, D_{50}, D_{80}) and segregation degree of waste rock from the top to the bottom of the slope were compared. These results are presented in Chapter 5.

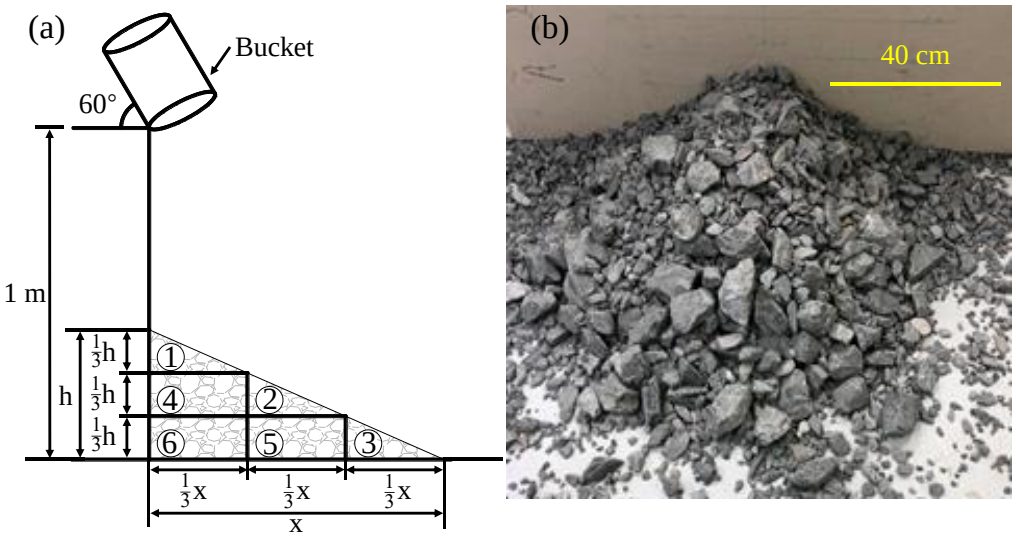

Figure 3.5: Laboratory segregation test setup. (a): Sectional characterization. The pile was equally divided into three horizontal sections and three vertical sections. (b): The segregation tests with ten buckets of waste rock dumped.

3.2.4 Field characterization of waste rock segregation using image analysis

3.2.4.1 Digital image acquisition

Image analysis was carried out on the waste rock pile of Canadian Malartic mine. A total of 87 imags were taken using a camera installed on a drone flying parallelly to the slope of the waste rock pile. The camera was oriented orthogonally to the slope to limit lateral distortion. A 1400 m long and 10 m high section slope was photographed with a resolution of 5280 × 2970 pixels for each image (one example is presented in Figure 3.6). The pixel conversion factor was 1.15 cm. Finally, a total of 42 independent photos (i.e., with no overlap) covering each around 30 m wide and 10 m high zone were selected for image analysis, considering the quality of the image in terms of the brightness and resolution.

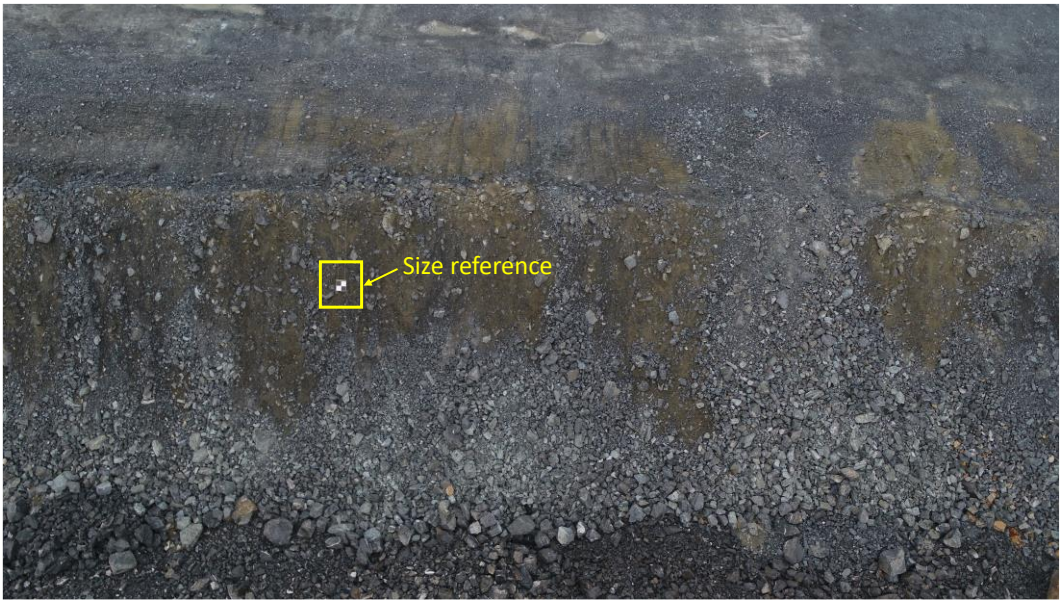

Figure 3.6: Original photo of the slope of waste rock pile at Canadian Malartic mine. The size reference (0.5 m × 0.5 m) was used for all the photos in the following image analysis.

3.2.4.2 Image processing

Selected images were analyzed using ImageJ to determine particle shapes and sizes. However, original images could not directly be processed because of the difficulty to differentiate particles and voids and therefore required to be processed using multiple sequential steps such as pre-processing (Figure 3.7a), binary conversion (Figure 3.7b), processes on binary image (Figure 3.7c), and particle analysis (Figure 3.7d). Figure 3.7 is used as an example to describe the different processing steps. The detailed processing steps are presented in Chapter 4.

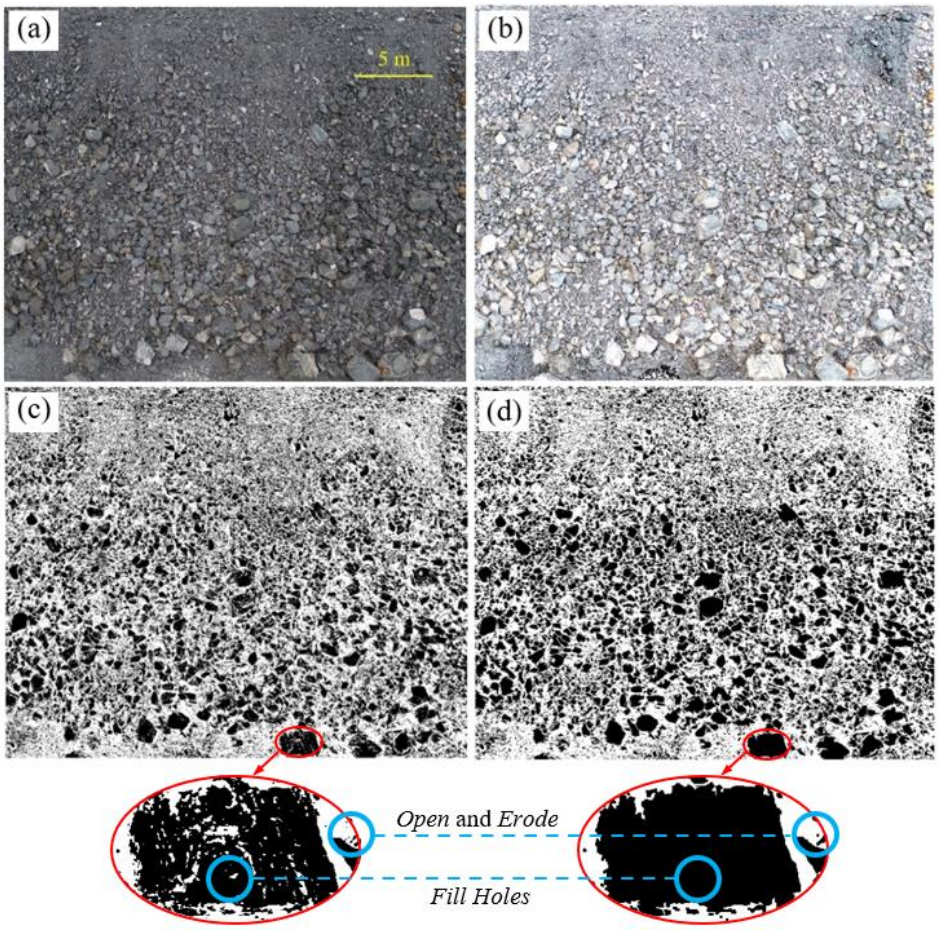

Figure 3.7: Processes of image analysis for waste rock. (a): Original waste rock on the slope surface. (b): Pre-processing to increase the brightness and contract of the image. (c): Binary conversion. Black colour represented waste rock particles. (d): Final image after processing with functions such as *Fill Holes* to improve the image quality (see text in chapter 4 for details).

3.2.4.3 Determination of particle shape factor and diameter

The ellipsoid shape model (see details in section 2.2.1) was applied to determine waste rock PSD curve based on particle shape and size. Particle volume was converted from the particle area in the binary image, which only displayed the long and medial axes. A calibrated shape factor λ ($\lambda = 0.53$) was introduced to determine the volumes of particles in the field image analysis. Particle diameter, in the sense of PSD analyses, typically corresponds to the size of the square sieve aperture and can be smaller than the medial axis. Therefore, an equivalent particle diameter (D_e) was introduced and determined based on the medial and short axes of waste rock. More details in determining the volume and diameter can be found in Chapter 4.

3.2.4.4 Waste rock segregation characterization in Canadian Malartic mine

Each of the 42 images was divided into 6 vertical sections (Figure 3.8) and PSD curves of each section were determined based on the ellipsoid model using a shape factor $\lambda = 0.53$ (details in section 4.2.3). The PSD curve of the original waste rock (before deposition and segregation) was determined from the image analysis of the entire slope in each image. The characteristic diameters such as D_{10}, D_{50}, and D_{95}, C_U and C_C of each PSD curve were then determined. Relative particle diameter D_{10} / D_{10}' (also D_{50} / D_{50}', D_{95} / D_{95}'), defined as the ratio of D_{10} in each section to D_{10}' of the original PSD curve in each image, was compared to investigate the segregation properties. The details about these segregation indices can be found in Chapter 4.

Statistical analysis was conducted using Gauss distribution model. The mean and standard deviation of the passing percentage were obtained for each section and for the whole slope. Then, the mean and median PSD curves, and PSD curves with passing percentage less than one standard deviation (σ) of the mean (68% of the data set), and two standard deviations of the mean (95% of the data set) were obtained for each section. The results are presented in Chapter 4.

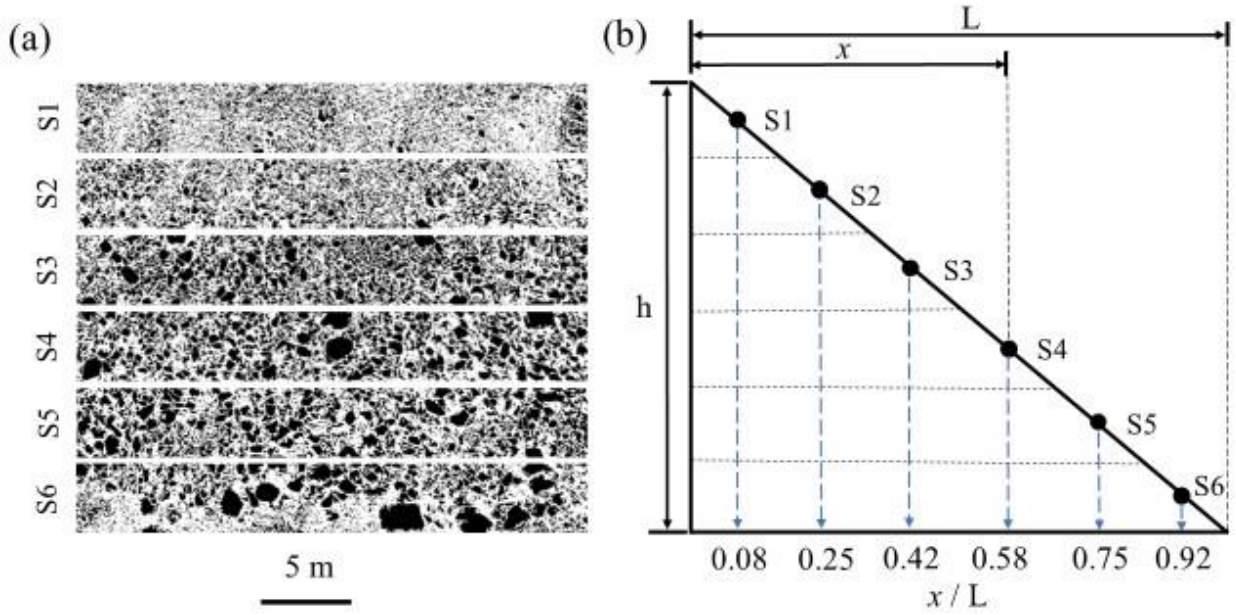

Figure 3.8: (a) Sectional binary images of waste rock with the slope divided into 6 sections (S1 – S6). (b) Characterization of the 6 sections along the slope. x / L [-]: the position of each section with x [L] the horizontal distance of the section center to the deposition point and L [L] the horizontal length of the slope. h [L]: bench height.

3.3 Simulations of waste rock disposal

The flow behaviour of waste rock during disposal was simulated using PFC3D. The main target of the discrete element simulations was to investigate waste rock segregation during disposal under various influence factors (e.g., construction methods, bench heights). The simulation models first required to be calibrated and validated to make sure simulations could provide reliable results for large-scale investigations.

3.3.1 Waste rock materials

Waste rock used for laboratory scale simulations was the same to laboratory tests (Lab0 in Figure 3.3). Field scale simulations were conducted based on the field conditions of Canadian Malartic mine and Quebrada Blanca mine (details are presented in Chapter 5). The original waste rock PSD curve of Canadian Malartic mine was obtained by field observations in this study (the

results are presented in Chapter 4). The original waste rock PSD curve of Quebrada Blanca mine was obtained from the literature (Zhang et al., 2017). Waste rock materials used for field scale simulations were then scalped from Canadian Malartic mine with diameters comprised between 0.1 m and 1.5 m (CM0 in Figure 3.9), and from Quebrada Blanca mine with diameters comprised between 0.1 m and 2.66 m (QB0 in Figure 3.9). The particle density was set to 2760 kg/m^3 (measured using ASTM C127, 2015) in this study.

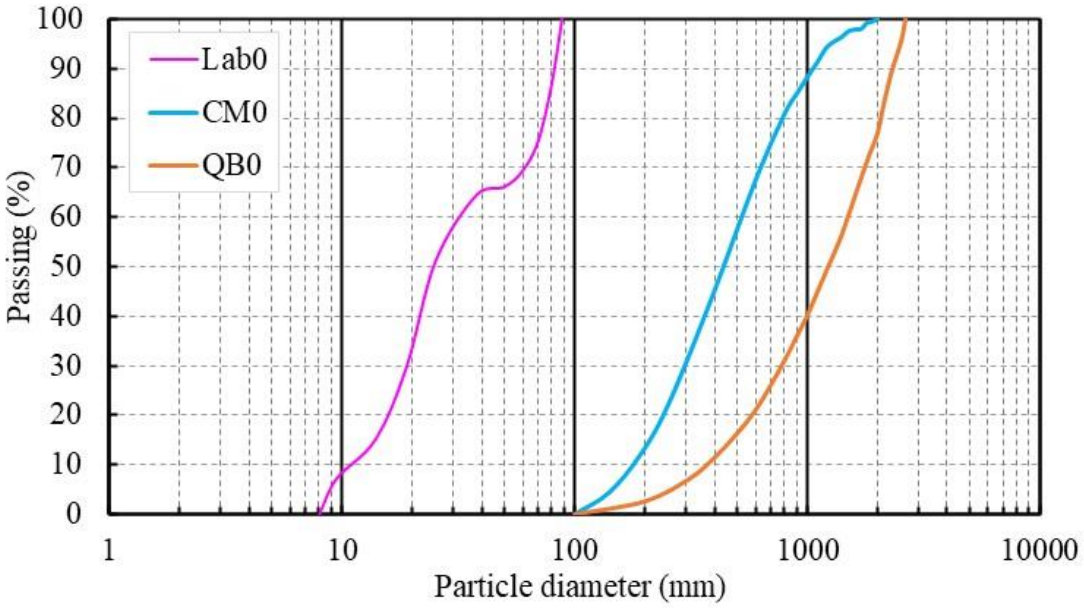

Figure 3.9: Waste rock PSD curves used for simulations. PSD curve Lab0 was used for laboratory scale simulations. PSD curves CM0 and QB0 represented PSD curves from Canadian Malartic mine and Quebrada Blanca mine, and were used for field scale simulations. These PSD curves were scalped based on their field PSD curves.

3.3.2 Calibration and validation of numerical simulations

Waste rock was simulated as spheres of various diameters with rolling resistance linear (rrlinear) model (model verification can be find in Appendix D). A rolling resistance coefficient was introduced in rrlinear model to indirectly account for the shape effect. The calibration mainly focused on the parameters including friction coefficient (μ) and rolling resistance coefficient (μ_r).

3.3.2.1 Laboratory scale calibration and validation

The same process was simulated to reproduce the repose angle tests (Figure 3.10). Input parameters such as friction coefficient (μ) and rolling resistance coefficient (μ_r) were calibrated with μ ranging between 0.1 and 0.4 and μ_r ranging between 0.1 and 0.4. Each pair of μ and μ_r was simulated 10 times with 10 different random seeds in PFC3D to account for PSD variability and evaluate model repeatability. The details of the simulation process are presented in Chapter 5.

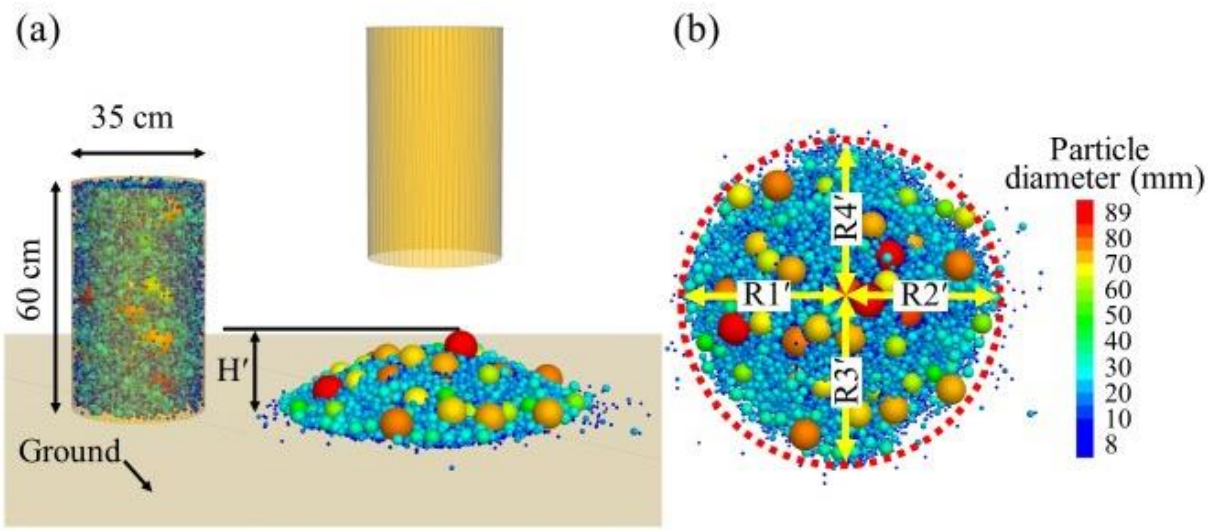

Figure 3.10: Simulated repose angle tests. (a): Simulated repose angle test in the same scale to the laboratory test. (b): The radii (R1′ – R4′) in four directions of the simulated waste rock cone. Particles were colored in the simulation according to their size (from blue with a diameter of 8 mm to red with a diameter of 89 mm).

Segregation tests were simulated with calibrated μ and μ_r to validate the simulation model (Figure 3.11). The simulations of segregation tests were conducted in the same way to laboratory segregation. Simulation results were compared with the laboratory results to check the effectiveness of the calibrated model. The detailed simulation procedures and results are presented in Chapter 5.

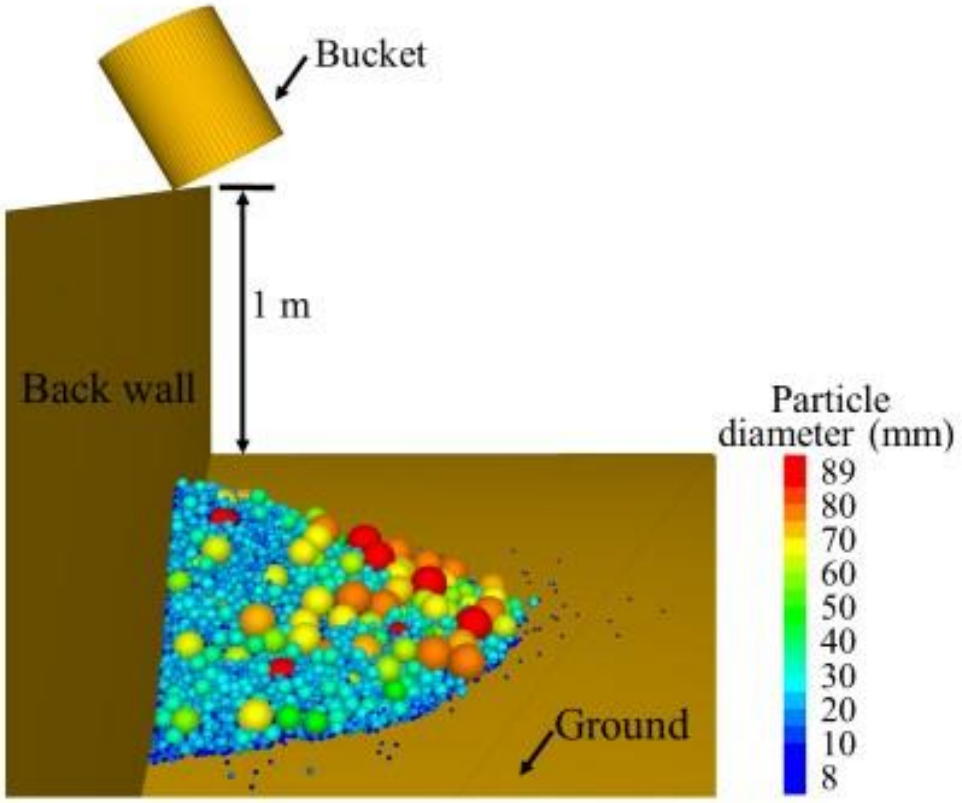

Figure 3.11: Simulation models of segregation tests. One vertical wall and one horizontal wall in yellow colour were built as back wall and ground. One cylinder wall was generated from one meter high with the same dimension of the laboratory bucket (Ø 0.27 m × 0.3 m).

3.3.2.2 Field scale calibration and validation

The results from laboratory calibration and validation indicated that the simulation models calibrated using repose angle tests can reproduce well waste rock segregation (See details in Chapter 5). So, this calibration method was also used to calibrate and validate the field scale models. Waste rock from two different mine sites (Canadian Malartic and Quebrada Blanca mines) were used to calibrate the model using the natural repose angles measured in the field.

- Case 1: waste rock pile in Canadian Malartic mine (CM0 in Figure 3.9) was characterized by an average repose angle of 37° in the field (Gervais et al., 2014).

- Case 2: waste rock pile in Quebrada Blanca mine (QB0 in Figure 3.9) was characterized by repose angles between 30° and 40°, with a reference repose angle of 37° for the model calibration in this study (Zhang et al., 2017).

Simulated field repose angle tests (Figure 3.12) were conducted following the similar approach to laboratory tests described above. A base layer covered with one-meter diameter fixed balls (grey balls in Figure 3.12) to simulate waste rock surface so that dumped waste rock could directly interact with the existing waste rock. These grey balls were assigned the same properties as the waste rock particles dumped at the surface of the model. Simulated waste rock particles were dumped from a larger cylinder (30 m high and 9 m diameter) in a similar way to laboratory scale repose angle test simulations. The friction coefficient (μ) and rolling resistance coefficient (μ_r) both ranging between 0.2 and 0.8 were mainly calibrated for the field model. Each pair of μ and μ_r was simulated five times with different random seeds.

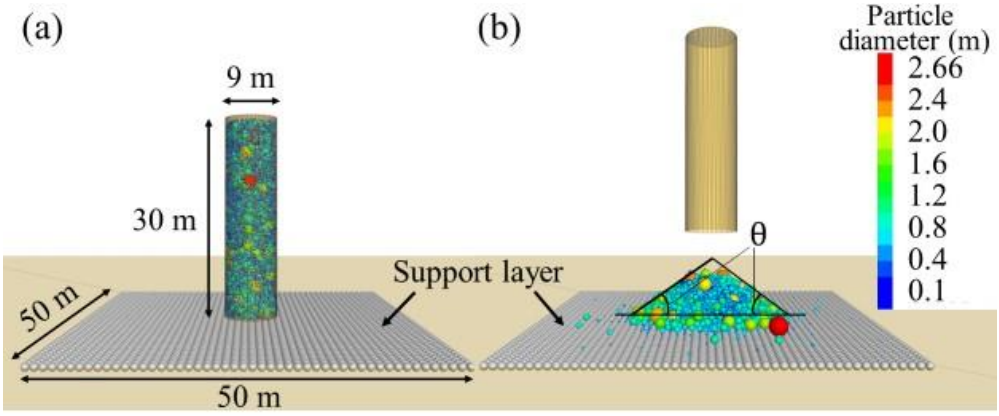

Figure 3.12: Field repose angle test simulations. (a): Simulated initial state of waste rock before lifting the cylinder. (b): Simulated waste rock cone. This simulation model for Quebrada Blanca mine was exhibited as an example. Particles are colored based on their radii. The same setup was set for Canadian Malartic mine except the original PSD CM0 was used for waste rock generation.

The calibrated models were validated by reproducing waste rock segregation at Canadian Malartic mine and Quebrada Blanca mine. A basic field-scale simulation model was built for waste rock disposal (Figure 3.13). The support walls (in yellow color in Figure 3.13) represented

the ground and physical boundaries of the models. An inclined wall was generated to represent an existing waste rock slope with a slope angle of 45°. The support walls were covered by a base layer made of fixed 1 m diameter balls (grey balls in Figure 3.13) to simulate waste rock surface so that dumped waste rock could directly interact with existing waste rock particles. Waste rock was dumped from the top edge of the bench slope. For model validations, the bench height (h in Figure 3.13) was 10 m for Canadian Malartic mine and 20 m for Quebrada Blanca mine. The simulated waste rock PSD curves from the top to the bottom of the slope were obtained and compared with the corresponding measured PSD curves. The details of model validations are presented in Chapter 5. This basic model setup was also used for the simulations in the next section (section 3.3.3).

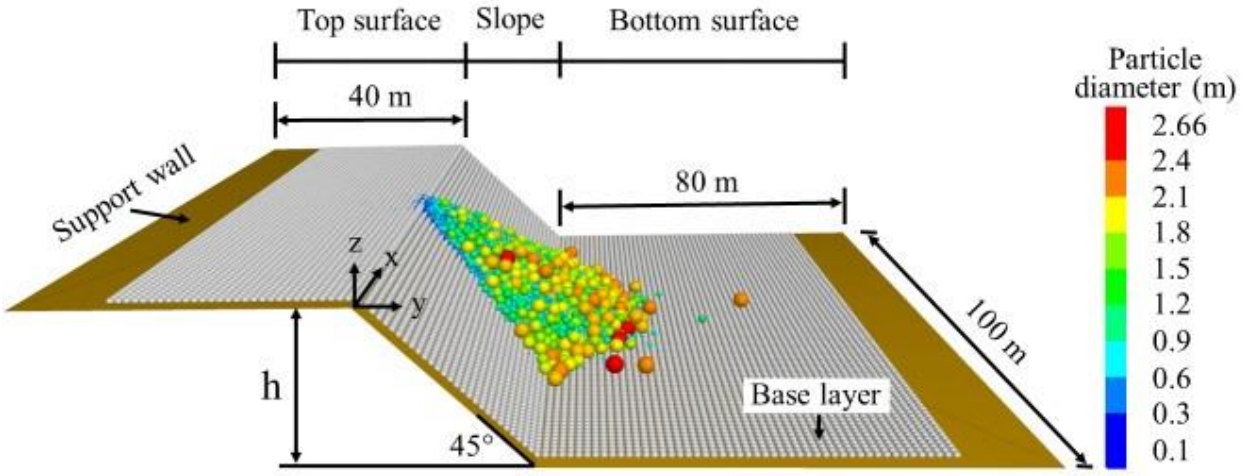

Figure 3.13: Simulation model for waste rock disposal. h [L]: bench height. Base layer was composed of 1 m diameter balls (in grey). Dumped waste rock particles were colored depending on their diameters (from 0.1 m in blue to 2.66 m in red).

3.3.3 Investigation of waste rock segregation under different influence factors

Numerical models were built to evaluate waste rock segregation and heterogeneity using end-dumping and push dumping methods. The effect of operational influence factors was analyzed

based on these two construction methods. Waste rock from Quebrada Blanca mine was mainly used for these simulations (Canadian Malartic waste rock was used only to investigate the effect of waste rock PSD).

(1) Simulation of end-dumping method

End-dumping method was simulated by dumping waste rock directly from the top of the bench (Figure 3.14a). The effect of bench height, mine truck payload, waste rock PSD and lateral disposal was investigated based on end-dumping method simulations.

Four different bench heights were simulated, i.e., 10 m (case A1), 15 m (case A2), 20 m (case A3), and 25 m (case A4) (Table 3.1). Waste rock was dumped until the slope was completely covered (along the y-axis), which represented a total of 4, 16, 30, and 66 dumps of waste rock for bench heights of 10 m, 15 m, 20 m and 25 m, respectively.

Another payload of 600 t of waste rock (case B1) was simulated to investigate the effect of mine truck payload on segregation. Every 600 t of waste rock was dumped from top of a 10 m high bench. Other settings were the same to case A1.

The effect of waste rock PSD was also investigated by dumping Canadian Malartic waste rock (case C1), with all the other parameters similar to case A1 (Table 3.1).

The effect of lateral disposal on waste rock segregation was investigated by dumping around 300 t of waste rock sequentially from three points on a 10 m high bench using end-dumping method (Figure 3.14b). The details of these settings are presented in Chapter 6.

(2) Simulation of push-dumping method

Push-dumping method was simulated by pushing waste rock on the top edge of the 10 m high bench (Figure 3.14c). At the beginning of the simulations, the front wall (green wall in Figure 3.14c) was deleted, and the box was moved toward the slope with a certain speed (between 0.1 m/s – case C1 and 0.6 m/s – case C6) to push the waste rock in the slope. The details are presented in Chapter 6.

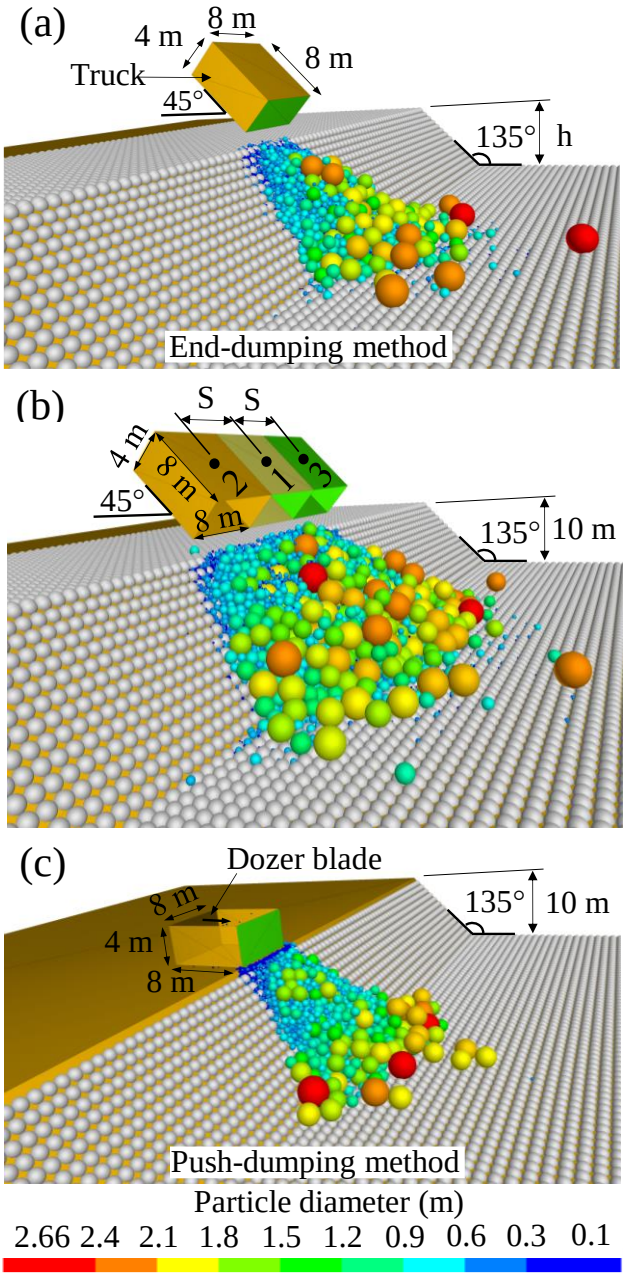

Figure 3.14: Simulations of waste rock disposal using (a) end-dumping method, (b) lateral disposal and (c) push-dumping method. (a) end-dumping and (c) push dumping methods dumped waste rock from one single point on the top of the slope. (b) Lateral disposal dumped waste rock sequentially from points 1, 2 and 3 with dump spacing (S) of 4 m, 8 m and 12 m. h [L] represents the bench height and varies between 10 and 25 m depending on the cases. Dumped waste rock particles are colored depending on their diameters (from 0.1 m in blue to 2.66 m in red).

Table 3.1: Summary of parametric simulation cases. QB0 and CM0: PSD of waste rock from Quebrada Blanca mine and Canadian Malartic mine, respectively. N/A: not applicable. Each case was simulated 5 times with various random seeds.

Case	Pile height (m)	PSD	Push velocity (m/s)	Payload (tonnes)	Construction method	Number of dumps
A1	10	QB0	N/A	300	End-dumping	4
A2	15					16
A3	20					30
A4	25					66
B1	10	QB0	N/A	600	End-dumping	4
C1	10	CM0	N/A	300	End-dumping	4
D1	10	QB0	0.1	300	Push-dumping	4
D2			0.2			
D3			0.3			
D4			0.4			
D5			0.5			
D6			0.6			

The methodological approach mainly included laboratory experiments, field observation and numerical simulations (Figure 3.15), and the details are presented in Chapter 4 to Chapter 6. The slopes in all the cases were equally divided into 6 sections in vertical direction. The PSD curve, typical characteristics diameters (D_{10}, D_{50}, and D_{90}) and segregation degree (χ) in each section were obtained and compared for segregation analysis. The results obtained from these parametric analyses are expected to investigate waste rock segregation and heterogeneity under various operational conditions and propose recommendations to better control segregation and improve mine waste disposal strategy.

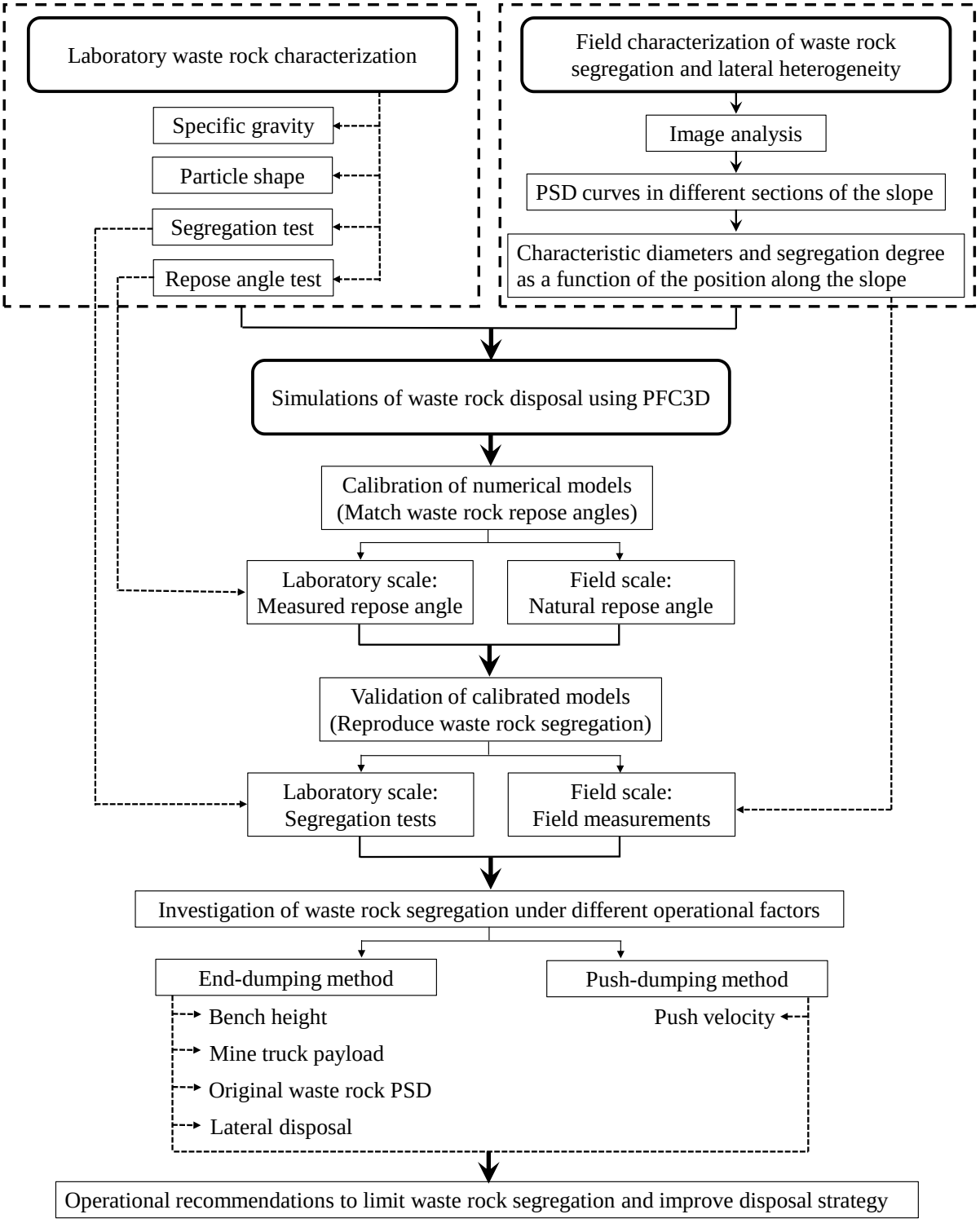

Figure 3.15: Summary of the research methodology.

CHAPTER 4 ARTICLE 1: CHARACTERIZATION OF PARTICLE SIZE SEGREGATION AND HETEROGENEITY ALONG THE SLOPES OF A WASTE ROCK PILE USING IMAGE ANALYSIS

Peiyong Qiu and Thomas Pabst

Department of civil, geological, and mining engineering, Polytechnique Montréal, Montréal, Québec, Canada

Research Institute on Mines and Environment (RIME), Québec, Canada

This article was submitted to Engineering Geology, Submitted on August 18, 2022

Abstract: Large amounts of waste rock are produced during mining operation and often disposed of in waste rock piles. Segregation usually occurs during waste rock disposal which can bring challenges to the safety of mining operations. However, segregation characterization is difficult because of the large dimensions of waste rock piles which can sometimes exceed hundreds of meters in height. In this study, images of waste rock pile were captured using a drone and analyzed using image analysis to characterize segregation along the slope of a waste rock pile. Images covered a 1400 m wide and 10 m high section of the pile. Ellipsoid model was used to characterize the irregular shapes of waste rock particles and a calibrated shape factor ($\lambda = 0.53$) was applied to determine the particle diameters. The particle size distribution (PSD) curves in different sections along the slope were obtained and the segregation degree and characteristic diameters (e.g., D_{10}, D_{50}, D_{80}, D_{95}) were quantitatively compared. Results showed that the increase of relative particle diameters and segregation degree indicated significant segregation along the vertical direction of waste rock pile. High variations of PSD curves along the lateral direction indicated significant lateral heterogeneity. Segregation and lateral heterogeneity could result in high variations (one to two orders of magnitude difference) of the saturated hydraulic conductivity of waste rock in the field.

Keywords: Waste rock segregation; Lateral heterogeneity; Image analysis

4.1 Introduction

Large amounts of waste rock are generated in mining operations and then disposed of in large piles that can exceed hundreds of metres in height and several square kilometers in area (Mclemore et al., 2009; Aubertin, 2013; Bar et al., 2020). The particle size distribution (PSD) of waste rock ranges from clayey particles to metre-sized blocks (Morin et al., 1991; James et al., 2013). Waste rock piles are usually constructed in benches which are typically between 10 m and 25 m high. Waste rock is repeatedly dumped down the slopes by haul trucks with either end-dumping method or push-dump method (Aubertin, 2013; Amos et al., 2015; Hajizadeh Namaghi et al., 2015).

These construction methods usually lead to significant segregation: larger (i.e., heavier with more momentum) particles tend to move down the slope and create a coarse zone at the base of the benches, while finer particles are more easily blocked and tend to remain closer to the crest and the deposition point (Herasymuik et al., 2006; Van Staden et al., 2018). Segregation is a complicated process involving different mechanisms such as inertial segregation (Goyal et al., 2006), sieving effect (Mosby et al., 1996) and percolation (Khola et al., 2016). Segregation is also affected by material properties such as the original PSD particle shape and roughness (Alizadeh et al.,2017). Continuous traffic of construction equipment can also create compacted layers of crushed material at the surface of the benches (Fala et al., 2005; Bao et al., 2020; Maknoon et al., 2021). Fine and coarse-grained inclined layers therefore alternate in the pile profile as the waste rock pile advances (Azam et al., 2007; Anterrieu et al., 2010).

Consequently, waste rock piles are highly heterogeneous structures (Anterrieu et al., 2010; Lahmira et al., 2016; Van Staden et al., 2019). These heterogeneities can directly affect the spatial distribution of geotechnical and hydrogeological properties (e.g., shear strength, hydraulic conductivity) and cause preferential flow, thus increasing the risk for both geochemical and geotechnical instabilities (Lahmira et al., 2016; Martin et al., 2019; Bréard Lanoix et al., 2020).

Much effort was therefore put to characterize particle size distribution of waste rock in piles but also rockfill in dams, both in the field (Essayad, 2021; Wilson et al., 2022) and in the laboratory (Shepherd, 1989; Ayres et al., 2006; Gupta, 2016). Most of the research, however, focused on small scales with particles usually smaller than 0.5 m (Cash, 2014; Barsi, 2017). Sieve analysis

(ASTM D6913) for the coarse fractions (> 0.075 mm), combined with wet sieving (ASTM C117) and hydrometer tests (ASTM D7928) for fine fractions (< 0.075 mm), are indeed traditionally the most used approaches to characterize the PSD of waste rock (and other mine wastes) (Bao et al., 2020; Hao and Pabst, 2022; Essayad, 2021).

Sieve analysis can be accurate to determine the PSD of samples, but limited sieve sizes and the practical difficulties to obtain and transport large samples may affect the representativeness of the samples, which may not reflect the whole particle sizes in field conditions (Hawley et al., 2017). Sampling and field characterization along the slope of a waste rock pile is also dangerous because of the large dimensions of the pile, the instability of the blocks and the steep slopes (Raymond et al., 2021). Characterizing segregation of waste rock at large scale therefore remains a challenge.

Recently, using a drone, combined with image analysis, was proposed to determine waste rock PSD in the field (Bhatia et al., 1990; Fernlund, 2005; Dipova, 2017). Image analysis is widely applied in different industries and research areas including particle mixing in rotary drums (Liu et al., 2015), soil crack analysis (An et al., 2020; Zhang et al., 2021; Meng et al., 2022), rock fragmentation (Andriani et al., 2002; Lawal, 2021) and mining engineering (Al-Thyabat et al., 2006; Ko et al, 2011). The approach usually consists in automatically extracting particle information such as particle shape, area and axis lengths, but the main challenge for applications to waste rock characterization is to determine 3D characteristics from 2D images (Fernlund et al., 2007; Lee et al., 2007; Zhang et al., 2012).

In this study, waste rock segregation was investigated using image analysis. A total of 87 drone images, covering a 1400 m wide and 10 m high bench, were taken on the waste rock pile of Canadian Malartic mine, a surface gold mine located in Quebec, Canada. 42 images were selected to analyze the waste rock in these images. Segregation of waste rock was characterized based on segregation degree and characteristic diameters including D_{10} to D_{95}. The lateral heterogeneity of waste rock was also investigated by analyzing the variability of the PSD curves and characteristic diameters (i.e., D_{10}, D_{50} and D_{95}) along the lateral direction of the slope.

4.2 Methodology

4.2.1 Digital image acquisition

The study was carried out on the waste rock pile of Canadian Malartic mine, a gold mine located in Abitibi-Témiscamingue, Quebec, Canada. The storage capacity of the waste rock pile is estimated to a total of 450 Mt corresponding to a volume of 230 Mm^3 (Lehouiller et al., 2020). The waste rock pile is constructed with 10 m benches for a total height of 100 m (Lehouiller et al., 2020). The waste rock pile is constructed in 10 m benches with 11.5 m terraces between benches for an overall slope angle of 21.8°. The slope angle of each bench is around 37° (Gervais et al., 2014). A total of 87 photos were taken using a camera installed on a drone flying parallelly to the slope of the pile. The camera was oriented orthogonally to the slope to avoid lateral distortion. The drone moved horizontally along the bench and with a constant elevation so that the images were taken with the same size scale. An accumulated around 4000 m long slope was photographed with a resolution of 5280 × 2970 pixels for each image. A 0.5 m × 0.5 m reference target was placed on the slope surface for size calibration. The pixel conversion factor was 1.2 cm. The top and bottom edges of each bench (i.e., compacted zones between benches) could be observed on each image and clearly delimited the investigated slope. Finally, a total of 42 independent photos (i.e., with no overlap) covering each around 30 m wide and 10 m high zone were selected for analysis based on the quality, brightness and resolutions of the images.

4.2.2 Image processing

Waste rock particles were analyzed using ImageJ, an open-source program for image processing (Abràmoff et al., 2004; Ferreira, et al., 2012). Original images (Figure 4.1a) could not directly be processed for particle size distribution because of the difficulty to differentiate particles and voids. Indeed, waste rock exhibited colour differences because of differences in mineral composition and shades. Images were therefore processed using multiple sequential steps including pre-processing, binary conversion, processes on binary image and particle analysis. These different steps are briefly presented and illustrated below.

Pre-processing: the original RGB colour images were first pre-processed using filtering, colour adjustment, brightness, and contrast adjustments to increase the brightness and enhance particle boundaries (Figure 4.1b).

Binary conversion: pre-processed images were converted to 8-bit grayscale images in which the gray level of the image ranged between 0 and 255 (0 representing black colour and 255 representing white colour). Thresholding was conducted to set lower and upper gray levels to distinguish particles from the background (Figure 4.1c). The black areas represented waste rock particles in binary images. The white areas represented voids between particles, as well as particles below 2 cm diameter which were not considered in the analysis (more details below).

Processes on binary image: Binary images usually exhibited different defects, such as grains from the background of the image, or blurry boundaries between particles (Figure 4.1d). Functional processes included in ImageJ, such as *Erode, Dilate, Open, Close, Fill Holes*, were used to remove this noise and make the transition between particles clearer. For example, two particles in contact might be detected as one particle in binary conversion process, so *Erode* function was used to remove pixels from the particle edges and separate the two particles. *Dilate* provided the opposite function to *Erode* by adding pixels so that the edge of the particles could be more precisely determined. *Open* function smoothed objects and removed isolated pixels which were smaller than 1.2 cm and not considered in this study. *Close*, followed by *Erode*, performed a dilation operation to smooth particles and fill small holes by adding pixels. *Fill Holes* was similar to function *Erode* and was used to fill small holes inside particles.

Particle analysis: Processed binary images were finally used to extract particle information including surface area, shape and axis lengths. The area of every individual particle was estimated from its pixels. The minimum detectable area in ImageJ was 25 cm^2 (corresponding approximately to a diameter of 2 cm) and smaller particles were ignored to reduce the influence of noise and resolution. Ellipses were used to fit particles in binary images and the primary and secondary axes of ellipses were obtained. ImageJ provided a list of each individual particle information including its area and primary and secondary axes lengths.

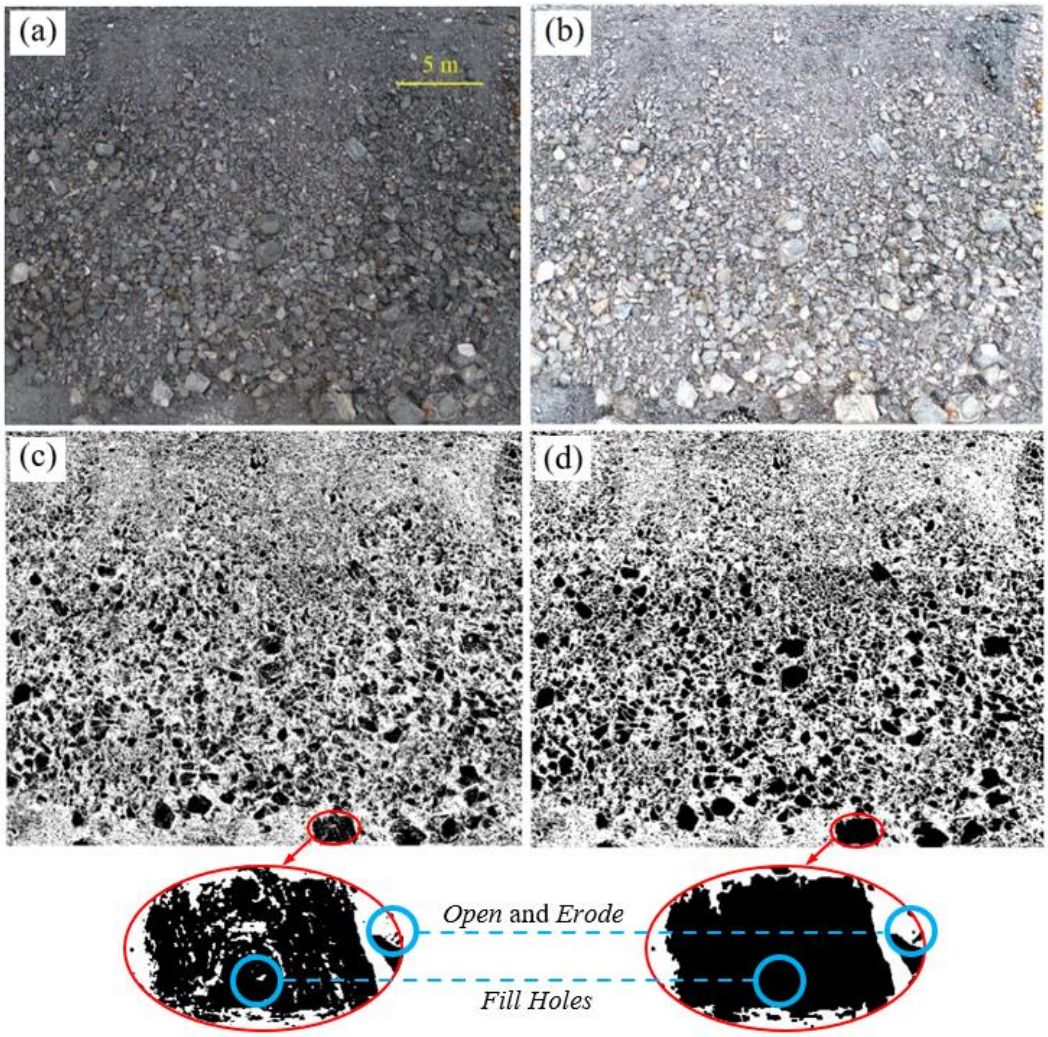

Figure 4.1: Processes of image analysis for waste rock along the slope. (a): Original waste rock on the slope surface of waste rock pile. (b): Pre-processing to increase the brightness and contract of the image. (c): Binary conversion. Black colour represented waste rock particles. (d): Final image after processing with functions such as *Open, Erode* and *Fill Holes* to improve the image quality (see text for details).

4.2.3 Particle shape and diameter

The mass and diameter of particles are the two main properties used to determine the PSD curve. The mass of each waste rock particle was calculated by estimating its volume multiplied by its specific gravity (Gs = 2760 kg/m^3 based on laboratory measurements following ASTM C127-15,

2015). However, particle volume can be difficult to estimate from 2D images and various shape models, such as the sphere model (Zhang, et al., 2017) and ellipsoid model (Podczeck, 1997), are therefore typically used to convert 2D areas to 3D volumes. Ellipsoid model was successfully used in previous studies to determine the PSD curve of coarse-grained materials using image analysis (Kumara, et al., 2012; Dipova, 2017), and was therefore also used in this study.

An ellipsoid particle is represented by a long (a; Figure 4.2a), a medial (b; Figure 4.2a and b) and a short axis (c; Figure 4.2b). The volume (V) of an ellipsoid is then calculated as (Kumara et al., 2012):

$$V = \frac{4\pi}{3} \times \frac{a}{2} \times \frac{b}{2} \times \frac{c}{2} \tag{4.1}$$

Particle diameter, in the sense of PSD analyses, typically corresponds to the size of the square sieve aperture (d in Figure 4.2b) and can be smaller than the medial axis (b in Figure 4.2). In other words, waste rock retained in a specific sieve is often slightly larger than its diameter (d). Therefore, an equivalent particle diameter (D_e = d) was introduced and was calculated based on the medial (b) and short axes (c) of waste rock in images (Kumara et al., 2011; Dipova, 2017). The detailed derivation process can be found in Ohm et al (2013). The equivalent particle diameter (D_e) can be expressed as:

$$\mathrm{D_e} = \sqrt{(\mathrm{b}^2 + \mathrm{c}^2)/2} \tag{4.2}$$

Where D_e: equivalent particle diameter (mm); b and c: medial and short axis (mm).

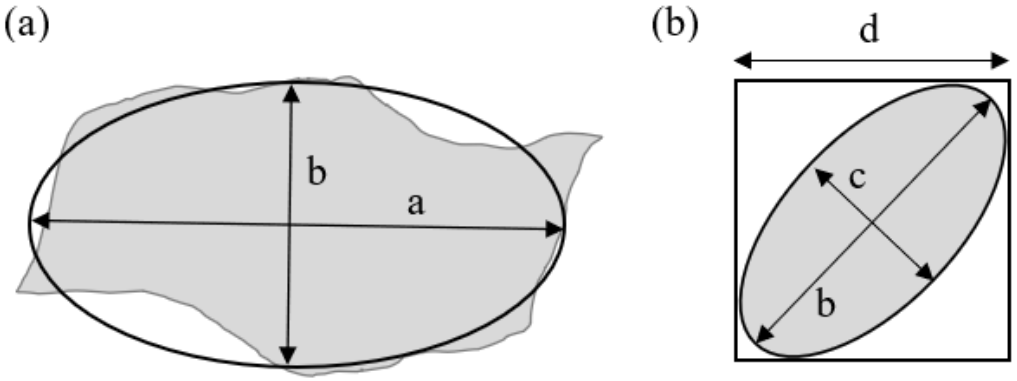

Figure 4.2: Dimensions of the ellipsoid model. (a): The projected area of a particle in image analysis; (b): Particle passing through a square sieve. Lengths a and b are the primary (long) and secondary (medial) axes of the ellipsoid determined in image analysis. Length c represents the short axis of the best fitted ellipsoid. Length d is the square sieve aperture in sieve analysis.

Lengths a and b were obtained directly from image analysis (see above), but length c was hidden in the out of plane dimension. A shape factor λ (= c / b) was introduced (Podczeck, 1997; Đuriš et al., 2016). Particles from the same source are considered to exhibit constant shape characteristics, i.e., λ is constant and independent of particle size (Mora et al., 1998; Dipova, et al., 2017).

The shape factor α for the investigated waste rock was therefore calibrated in the laboratory by comparing sieve analysis and image analysis conducted on samples collected from the same pile at Canadian Malartic mine. Sieve analysis was first conducted to determine the diameter and weight of various waste rock fractions (ASTM D6913). Five fractions ranging between 8 mm and 38 mm were prepared, spread on a black geotextile (no contacts) and photographed (Figure 4.3). Images were taken vertically at a distance of approximately 1 m and a 0.3 m long ruler was used for size calibration (pixel conversion factor was 0.17 mm). The projected area of each particle was analyzed, and the long (a) and medial (b) axis were determined with the best fitting ellipsoid model, following the same procedure as describe above for field image analysis.

The mass (M) of each waste rock fraction was first measured in the laboratory using a balance. The mass of every particle was calculated by multiplying its volume estimated using the ellipsoid model (equation 4.1) by its specific gravity. The short axis c in the ellipsoid model was expressed

as αb. The mass of each waste rock fraction was then estimated by summing the mass of all the particles, and as a function of the shape factor λ. Thus, λ in each fraction could be calculated using equation 4.3. The average shape factor of the five fractions was 0.53 (Figure 4.3), and was used to estimate the short axis c of waste rock particles in the field.

$$\lambda = \frac{M}{\beta \times \sum_{i=1}^{n} \frac{4\pi}{3} \times \frac{a_i}{2} \times \frac{b_i}{2} \times \frac{b_i}{2}} \quad (4.3)$$

Where M: the mass of one waste rock fraction measured using a balance in the laboratory (g); β: the density of waste rock particles (kg/m^3).

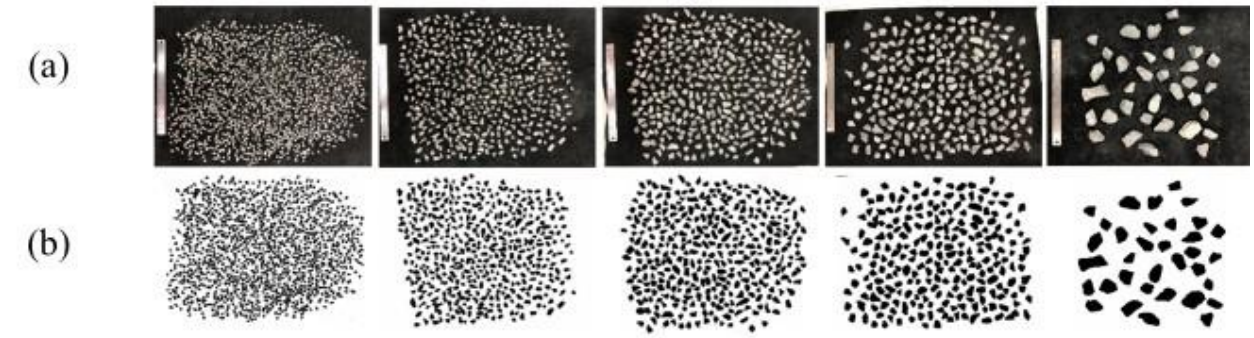

Fraction :	8 – 9.5 mm	9.5 – 14 mm	14 – 19 mm	19 – 25 mm	25 – 38 mm
Number (n) :	1169	435	349	236	34
Mass (M) :	1382 g	1504 g	2770 g	4038 g	2501 g
Shape factor (α) :	0.53	0.49	0.59	0.52	0.52

Figure 4.3: Determination of the shape factors with different size fractions. (a): Original images of waste rock with size reference (0.3 m long). (b): Binary images used for image analysis. The mass (M) of each fraction was measured using a balance in the laboratory.

4.2.4 Segregation characterization

Each of the 42 images was divided into 6 vertical sections (Figure 4.4a) and PSD curves of each section were determined based on the ellipsoid model using a shape factor $\alpha = 0.53$. The PSD curve of the original waste rock (before the deposition) was determined from the image analysis of the entire slope in each image. This so called original PSD curve was used to evaluate the waste rock segregation along the slope in each image. The characteristic diameters D_{10}, D_{15}, D_{30}, D_{50}, D_{60}, D_{80}, D_{95} (i.e., the particle diameters corresponding to 10%, 15%, 30%, 50%, 60%, 80%, 95% passing, respectively), the coefficient of uniformity C_U ($C_U = D_{60} / D_{10}$) and the coefficient of curvature C_C ($C_C = (D_{30})^2 / (D_{10} \times D_{60})$) of each PSD curve were determined.

Statistical analyses were conducted using Gauss distribution model. The mean and standard deviation of the passing percentage were obtained for each section and for the whole slope. The mean and median PSD curves, and the PSD curves with passing percentage less than one standard deviation (σ) of the mean (68% of the data set), and PSD curves with passing percentage less than two standard deviations of the mean (95% of the data set) were obtained for each section.

The segregation degree of waste rock (χ) in each section was determined as:

$$\chi = \frac{\log d_{tested} - \log d_0}{\log d_{CQ} - \log d_0} \tag{4.4}$$

Where $\log d_0$: the logarithmic mean particle size of the original material before disposal, d was in cm in this study; $\log d_{tested}$: the logarithmic mean particle size of waste rock in the local sections (i.e., sections 1 – 6); $\log d_{CQ}$: the logarithmic mean particle size of coarsest quartile. The coarsest quartile represented the fraction of particles larger than the diameter D_{75} of the original gradation (Westland, 1988; Kenney et al., 1993). Logarithmic mean particle size ($\log d$) is often considered a representative parameter for delineating the PSD curve, and is calculated as (Kenney et al., 1993):

$$\log d = \sum_{i=1}^{n}(P_i - P_{i-1}) \log \sqrt{D_i \cdot D_{i-1}} \quad (4.5)$$

Where D_i and D_{i-1} [L]: consecutive particle diameters corresponding to passing P_i and P_{i-1}.

Relative particle diameter D_{10} / D_{10}' (also D_{50} / D_{50}', D_{95} / D_{95}') was defined as the ratio between D_{10} in each section and D_{10}' in the original PSD curve in each image. Relative particle diameters and the segregation degree in the 6 sections were used to characterize the segregation along the waste rock slope. The center of each section along the slope was characterized in Figure 4.4b.

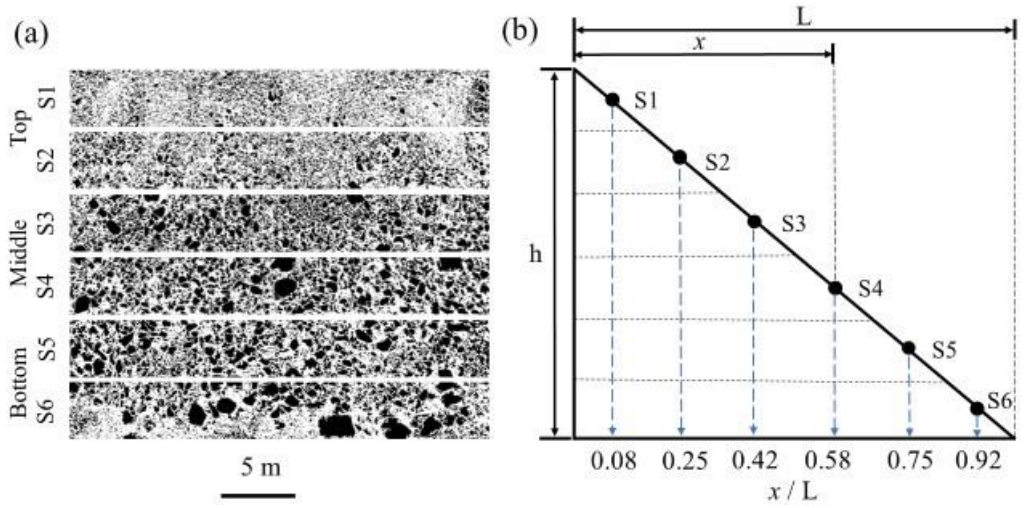

Figure 4.4: (a) Sectional binary images of waste rock with the slope divided into 6 sections (S1 – S6). (b) Characterization of the 6 sections along the slope. *x* / L [-] represents the position of each section with *x* [L] the horizontal distance of the section center to the deposition point and L [L] the horizontal length of the slope. h [L] represents the height of the bench.

4.3 Results

4.3.1 Segregation along the slope

A total of 42 original PSD curves were obtained from the 42 images. The maximum particle diameter was 180 cm among the 42 images. The original waste rock in each image was

characterized by D_{10}', D_{50}', D_{80}' and D_{95}' (Figure 4.5b). The maximum and minimum D_{95}' were 175 cm and 69 cm, with a mean and median of 123 cm and 126 cm. The maximum and minimum D_{10}' were 19 cm and 12 cm, with the same mean and median of 15 cm. The mean and median PSD curves were obtained from the 42 original PSD curves (Figure 4.5a). The median and mean PSD curves exhibited the same C_U (= 3.4) and C_C (= 1.04). Difference between mean and median PSD curves mainly concentrated around particles larger than 130 cm, which only accounted for 4% of the total waste rock. Particles larger than 100 cm accounted for 10% of the total waste rock and fractions between 19 cm and 80 cm accounted for around 68%. Waste rock with diameters ranging between $D_{40} - D_{80}$ exhibited the highest level of variability, with standard deviation around 10%, but otherwise results were similar (standard deviation < 8%).

Significant segregation was observed from the top to the bottom of the slope i.e., from section 1 to section 6 (Figure 4.5, c – f). For example, D_{10} / D_{10}' increased from 0.58 ± 0.13 in section 1 (top section, $x / L = 0.08$) to 1.66 ± 0.23 in section 6 (bottom section, $x / L = 0.92$), i.e., an increase by 186%. D_{50} / D_{50}' increased from 0.58 ± 0.18 in section 1 to 1.56 ± 0.23 in section 6, i.e., an increase by 168%. Similar trend was also observed from D_{80} / D_{80}' and D_{95} / D_{95}', which increased by about 149% and 95%, respectively, from section 1 to section 6. The increase rate of relative particle diameters decreased from 1.26 for D_{10} / D_{10}' to 0.55 for D_{95} / D_{95}', thus indicating that smaller particles were more sensitive to segregation (Figure 4.5, c – f).

Segregation degree (χ) of waste rock along the slope also indicated significant segregation. Segregation degree was -0.77 ± 0.39 in section 1 and increased to -0.29 ± 0.21 in section 4 ($x / L = 0.58$), indicating that waste rock in section 1 was significantly finer (+ 166%) than in section 4 (Figure 4.6). Also, the segregation degree was smaller than 0 when $x / L < 0.7$ thus confirming that waste rock was finer than the original PSD in the top two third of the slope. The segregation degree in section 6 was significantly greater and around $+ 0.4 \pm 0.14$ and waste rock in the bottom of the slope was coarser than the original waste rock, but also coarser than waste rock in sections 1 to 5. Finally, the standard deviation of the segregation degree decreased from 0.39 in section 1 to 0.14 in section 6. Waste rock in the top sections was, indeed, significantly finer than the original waste rock and a few additional or fewer large particles would therefore strongly affect the PSD curve.

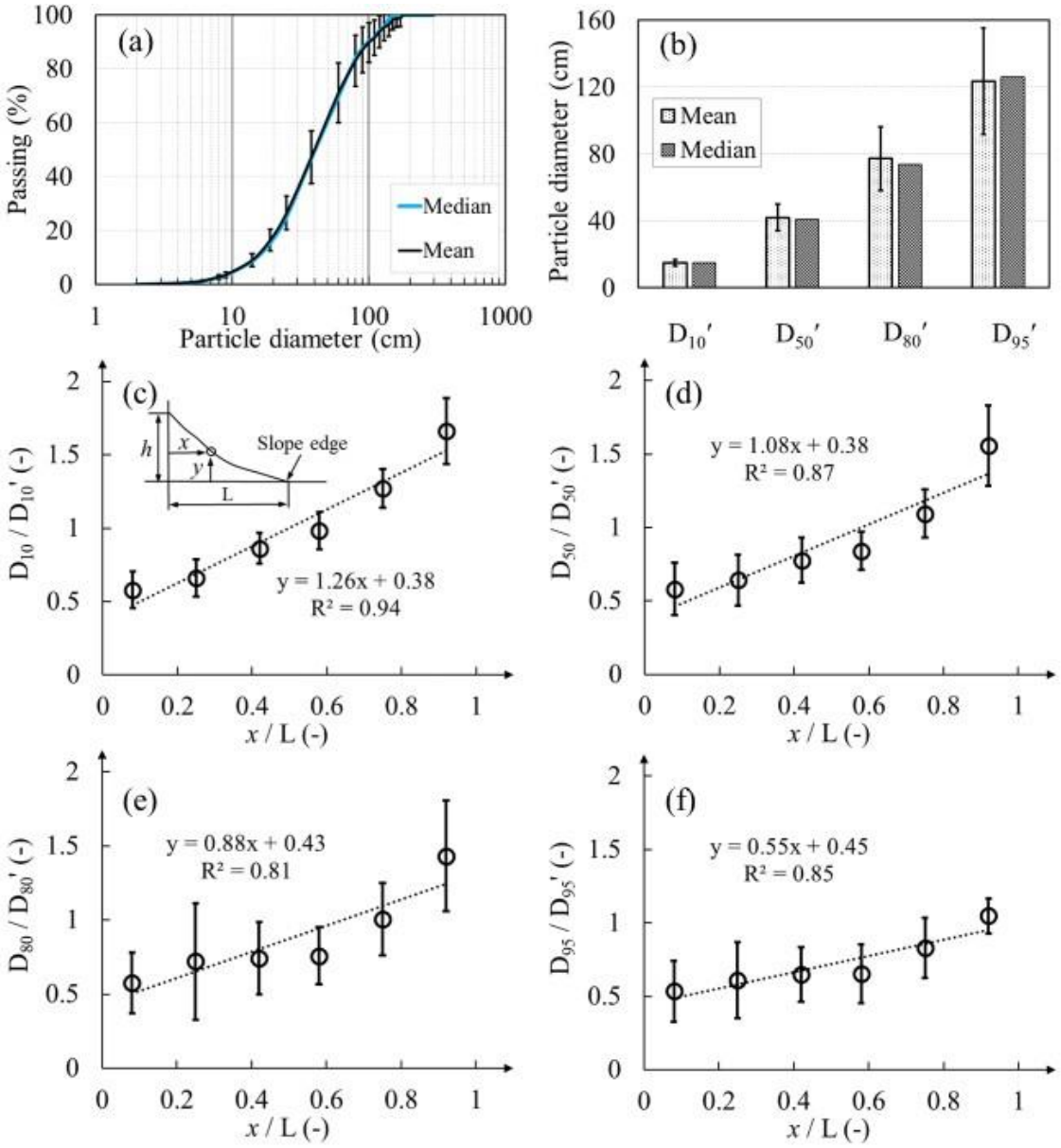

Figure 4.5: Segregation characteristics of waste rock in the 6 sections of the slope. (a): Measured median and mean PSD curves of the whole slope. (b): Measured characteristic diameters of the original PSD curves. The mean and median were obtained from the 42 PSDs. Measured (c) D_{10} / D_{10}', (d) D_{50} / D_{50}', (e) D_{80} / D_{80}' and (f) D_{95} / D_{95}' as functions of the section positions. Relative particle diameter D_{10} / D_{10}' (also D_{50} / D_{50}', D_{95} / D_{95}') was defined as the ratio between D_{10} in each section and D_{10}' of the original PSD curve in each image. x / L [-] represents the position of each section with x [L] the horizontal distance of the section center to the deposition point and L [L] the horizontal length of the slope. Error bars represent standard deviation.

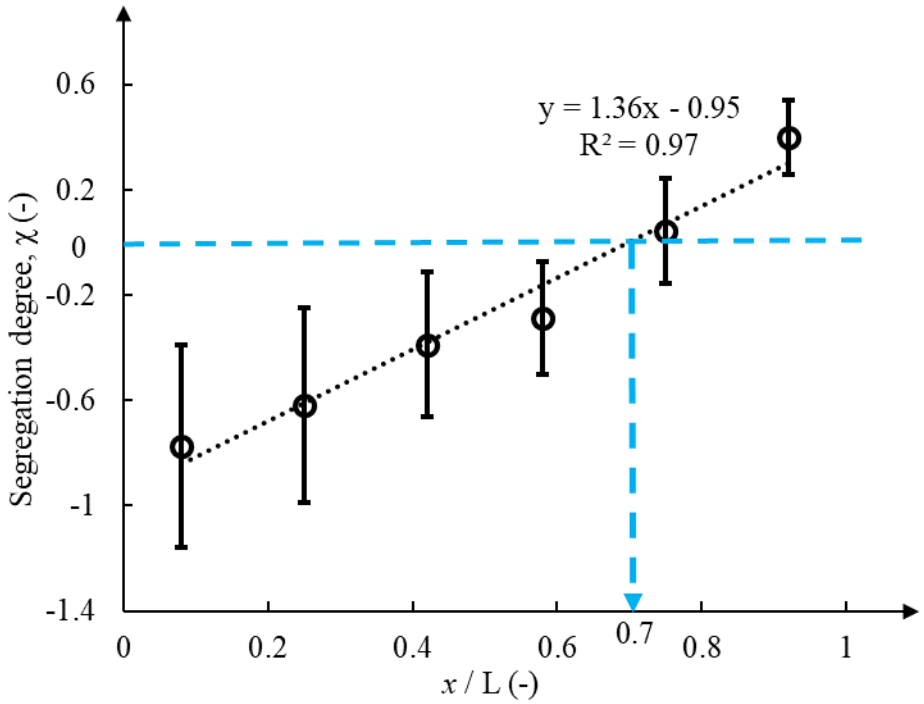

Figure 4.6: Segregation degree along the slope. Particles were finer than the original (i.e., X < 0; blue dashed line) when x / L < 0.7 and coarser than the original (i.e., X > 0) when x / L > 0.7. Error bars represent standard deviation.

4.3.2 Lateral heterogeneity

The 42 PSD curves analyzed above represented the PSD of waste rock along a lateral distance of 1400 m and along a same bench of the waste rock pile. As mentioned above, there was no overlap between the PSD curves so the data set was used to evaluate the lateral variability. It was assumed, based on information received from the mine, that the geology of the rock was sensibly similar and that the deposition method was the same (i.e., end dumping in that case).

PSD curves of waste rock exhibited high lateral variability, especially for sections 1 and 6. For example, the maximum standard deviation (σ) of the passing percentage was around 17% for a particle diameter of 40 cm in section 1 and 18% for a particle diameter of 80 cm in section 6. This indicated that in practice, particles ranging between 40 cm and 80 cm exhibited the highest

variability along the lateral direction and therefore brought uncertainties to the hydrogeotechnical properties (e.g., porosity, hydraulic conductivity) which are highly related to waste rock PSD. The highest variability in sections 2 – 5 occurred at particle diameters varied between 40 cm and 60 cm, with the maximum standard deviation (σ) of the passing percentage around 10%. The maximum diameter (D_{max}) in the top section varied between 30 cm and 130 cm (Figure 4.7a). Similar variations of D_{max} in sections 2 – 6 were also observed, ranging between 80 cm and 180 cm (Figure 4.7, b – f).

The distributions of D_{10}, D_{50} and D_{80} and C_U in each section were exhibited using the relative frequency (f) (Figures 4.8 and 4.9). The maximum frequency (f_m) decreased from D_{10} to D_{80}, indicating that the lateral variation increased with particle diameters. For example, diameter D_{10} in section 1 varied between 5 cm and 15 cm, with a maximum frequency $f_m = 0.8$ for a particle diameter of 8 cm. Diameter D_{50} was between 15 cm and 25 cm, with $f_m = 0.36$ for a particle diameter of 23 cm. Finally, diameter D_{80} distributed along a wider range comprised between 30 cm and 55 cm, with $f_m = 0.29$ for a particle diameter of 33 cm. C_U mainly varied between 2.4 and 5 in the 6 sections and exhibited higher C_U in section 1 with $f_m = 0.29$ for a C_U of 3 (Figure 4.9).

Similar results were also observed in other sections, both close to the top (finer zones) and the bottom (coarser zones) of the slope (Figures 4.8). For example, diameter D_{50} in section 1 was concentrated between 18 cm ($f = 0.31$) and 23 cm ($f = 0.36$), while D_{50} in section 6 was between 43 cm and 68 cm ($f = 0.45$). Diameter D_{80} in section 6 exhibited much higher variations than that in section 1 with a maximum frequency of $f_m = 0.1$, indicating that larger waste rock particles tended to distribute more variably at the bottom of the slope.

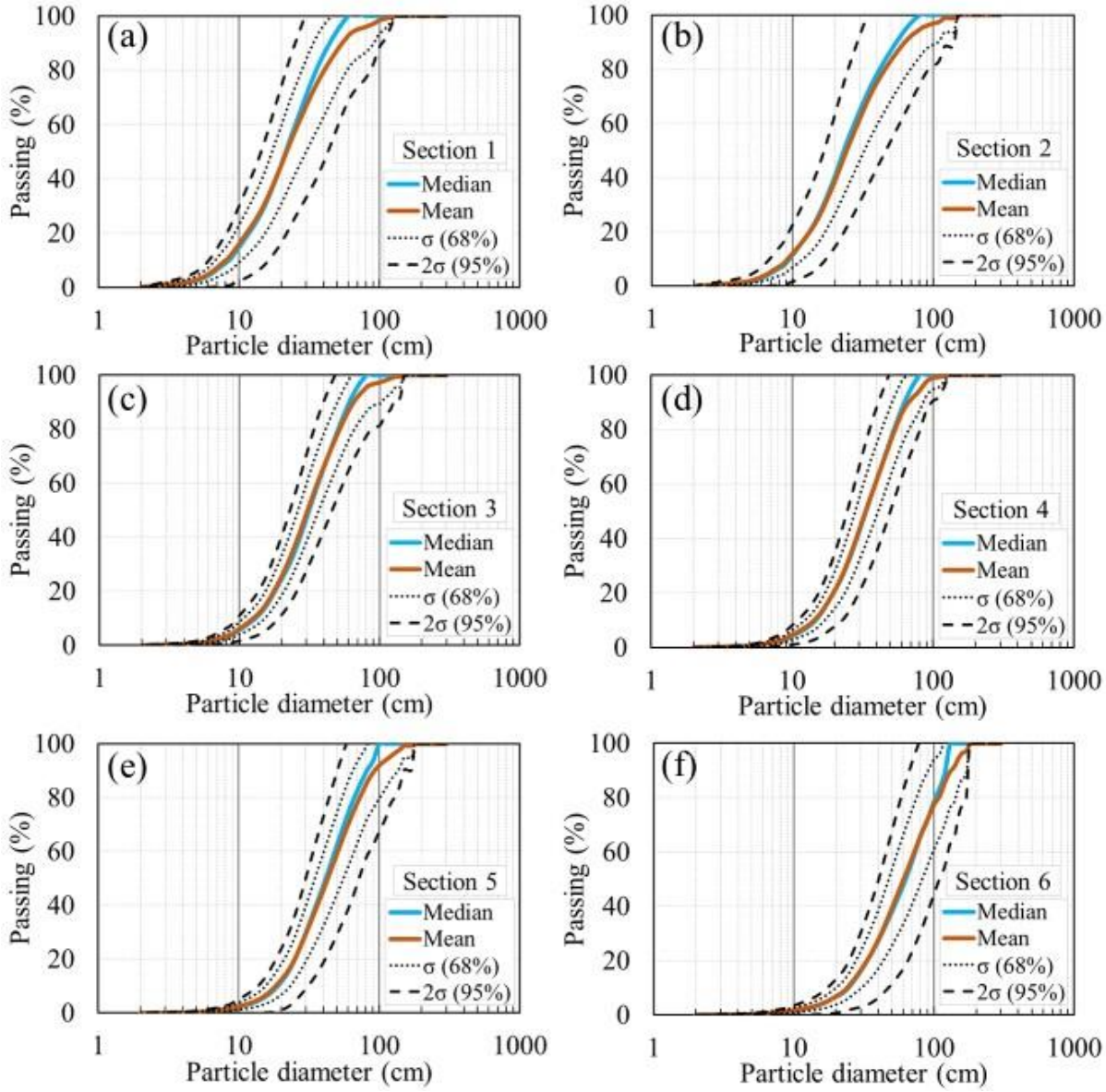

Figure 4.7: Lateral variabilities of waste rock PSD curves along the slope from (a) section 1 to (f) section 6. 68% envelope (dotted line) represented PSD curves with passing percentage less than one standard deviation (σ) around the mean. 95% envelope (dashed line) represented PSD curves with passing percentage less than two standard deviations of the mean.

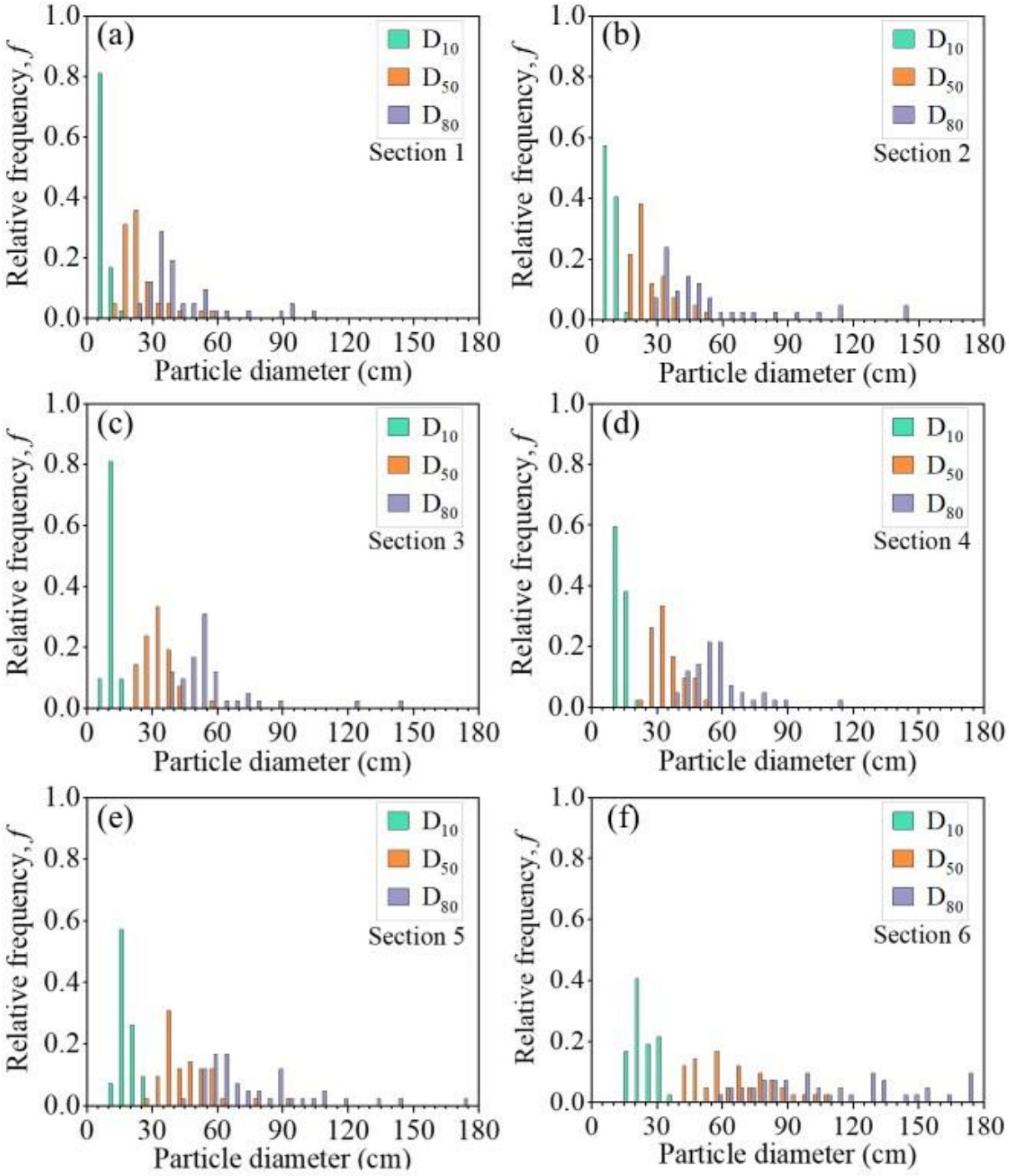

Figure 4.8: Lateral variabilities of characteristic diameters D_{10}, D_{50}, D_{80} along the slope from (a) section 1 to (f) section 6. The distributions of D_{10}, D_{50}, D_{80} were analyzed based on the 42 PSD curves which covered a horizontal length of 1400 m.

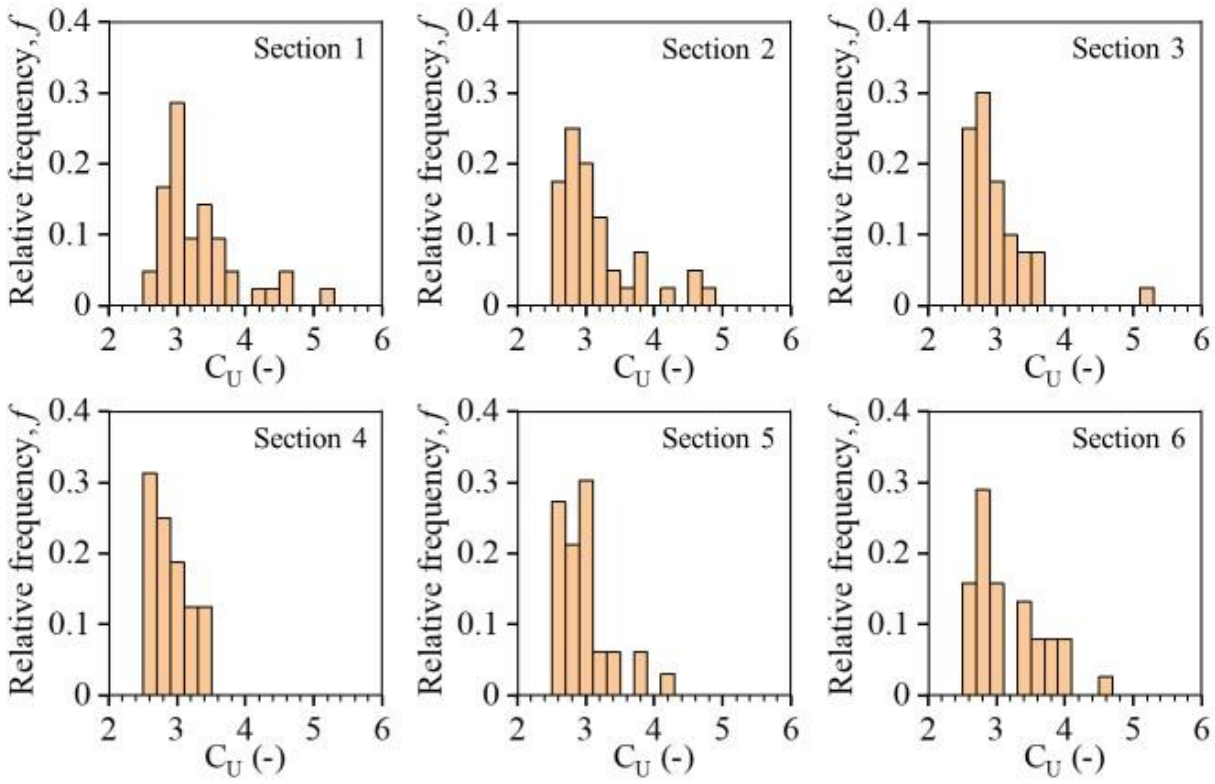

Figure 4.9: Lateral variabilities of C_U in the 6 sections. The distribution of C_U in each section was analyzed based on the 42 PSD curves which covered a horizontal length of 1400 m.

4.4 Result analysis and discussion

4.4.1 Segregation and lateral heterogeneity in a waste rock pile

The results of the waste rock pile image analysis presented above indicated a significant vertical segregation along the slope of the 10 m high bench, with a segregation degree increasing from − 0.77 ± 0.39 in section 1 (top) to + 0.4 ± 0.14 in section 6 (bottom). Maximum particle size and characteristic diameters also tended to increase from section 1 to section 6. For example, D_{50} increased from 24 cm ± 95 cm in section 1 to 66 cm ± 18 cm in section 6 (an increase by 168%). Similarly, other waste rock piles with different heights also exhibited segregation. For example, diameter D_{50} at 15 m high waste rock pile (Chi, 2010) increased from 21 cm in the top section to 41 cm in the bottom section, i.e., an increase by about 95%, Also, diameter D_{50} at an around 20 m

high waste rock pile (Zhang et al., 2017) was 40 cm in the top section and 143 cm in the bottom section, i.e., an increase by about 258%.

High variations of PSD curves and characteristic diameters of waste rock along the lateral direction indicated significant heterogeneity in the studied pile. For example, diameter D_{50} of the original material (before the deposition) varied between 33 cm and 63 cm along the 1400 m of the investigated bench, with a maximum frequency of only 0.24. Similar results were also observed from other waste rock piles. For example, diameter D_{50} of the original waste rock (before the deposition) varied between 6 cm and 36 cm along the lateral direction of the 15 m high waste rock pile at Diavik mine (Chi, 2010; Barsi, 2017). Such lateral heterogeneity is mainly attributed to lithological and mineralogical characteristics of the host rock, as well as blast pattern and energy which affect rock fragmentation degree (Raymond et al., 2021; Kinyua et al., 2022).

Vertical and lateral heterogeneity is therefore particularly critical when determining and simulating waste rock piles geotechnical, hydrogeological, and geochemical behaviour (St-Arnault et al., 2020; Vriens et al., 2019). For example, the difference of friction angle in different locations of a pile could exceed 14° because of spatial variations of particle sizes (Zevgolis, 2018; Rahmani et al., 2021) and local wetting front velocities can vary over four orders of magnitude (Nichol et al., 2005; Webb et al., 2008). The following sections therefore discuss various approaches to predict and account for segregation and heterogeneity in large-scale waste rock piles.

4.4.2 Prediction of segregation and segregation degree

The uniformity coefficient C_U (= D_{60} / D_{10}) is often considered a practical and easy-to-use criterion to estimate possible segregation of a coarse material, and a greater C_U (usually $C_U > 3$) is generally deemed to indicate a higher segregation risk (Langroudi et al., 2015). However, this study has shown that such criterion should be considered carefully and may sometimes underestimate the segregation risk. Indeed, C_U of the original waste rock in this study was sometimes as small as 2.8, but segregation was still significant with segregation degrees around – 1.53 in section 1 and 0.34 in section 6. One of the reasons for the poor fit of the C_U criterion is that particles coarser than D_{60} are more prone to segregate (Sherard et al., 1984). For example, waste rock particles larger than 150 cm (while D_{60} = 50 cm) were all accumulated in the bottom

section of the investigated waste rock pile. So, using D_{60} and D_{10} may be not always reliable to predict segregation in the field.

Predicting the segregation degree using greater characteristic diameters such as D_{90} was therefore considered, and a ratio D_{90} / D_{15} was proposed to better evaluate segregation (Burenkova,1993; Asmaei et al., 2018). In this study, D_{90} / D_{15} of the original waste rock was between 3.7 and 9.5, with an average of 6.7 ± 1.6. The segregation degree was fitted as a function of D_{90} / D_{15} with an intercept of 0 considering the reality that D_{90}/D_{15} is always a positive value (> 1) and waste rock tends to be homogenous when D_{90}/D_{15} closes to 1. The segregation degree in section 6 tended to indicate a linear relationship with D_{90} / D_{15} with a coefficient of determination (R^2) greater than 0.9 (Figure 4.10). The fitted trend indicated that the segregation degree in the coarse zone (e.g., Section 6) tended to linearly increase with D_{90} / D_{15}, and that waste rock tended to be finer in the top of the pile (Section 1) with increasing D_{90} / D_{15}. However, the relation between the segregation degree and the ratio D_{90} / D_{15} was less clear in the top section of the pile ($R^2 = 0.74$) than in the bottom ($R^2 = 0.92$), most probably because large particles can strongly affect the PSD curve in this area (similarly to what was observed in Figures 4.5 to 4.7 above). Other researchers (Asmaei et al., 2018) also reported that the segregation degree of the whole slope tended to increase with the ratio D_{90} / D_{15}. However, the slope of the fitted linear relation in their study was 0.29 ($R^2 = 0.99$), that is around 5 times greater than the fitted slope of 0.07 ($R^2 = 0.92$) in this study. A possible reason for this difference may be that D_{90} / D_{15} in the present study varied in a relatively smaller range (i.e., between 3.7 and 9.5) compared to their analysis (i.e., between 13 and 64). In other words, if the general trend between segregation and D_{90} / D_{15} was verified in several waste rock piles, the linear relation parameter may depend on waste rock properties.

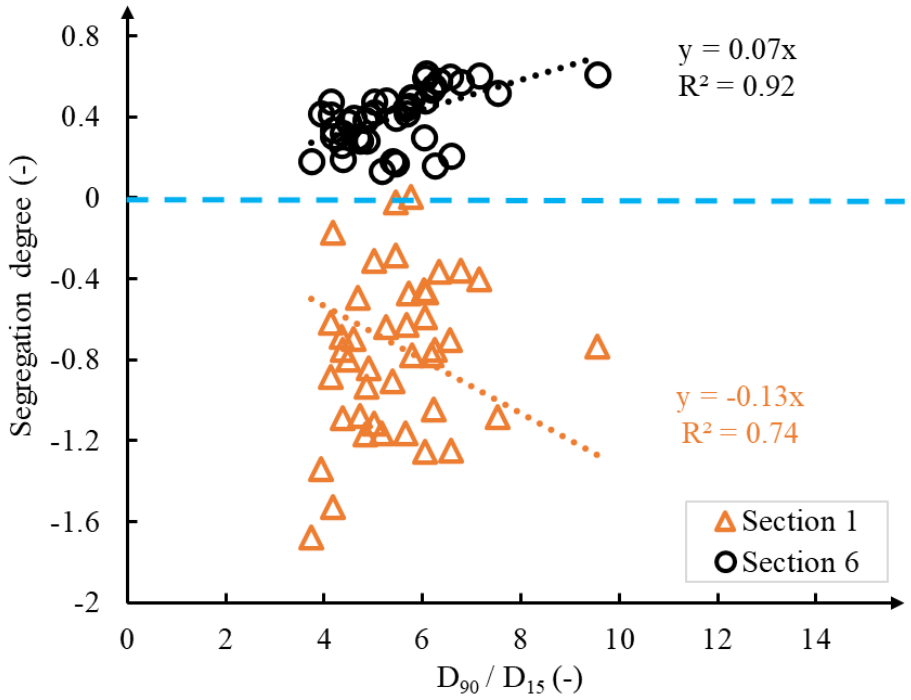

Figure 4.10: Segregation degree as a function of D_{90} / D_{15} of the original waste rock in section 1 and section 6. A segregation degree less than 0 indicates finer material than the original and a segregation degree greater than 0 indicates a coarser material than the original.

4.4.3 Correction of particle size distribution for fine particles

In this study, the uniformity coefficient C_U in the 42 waste rock slopes ranged between 2.8 and 4.1. Similar results were obtained using image analysis in a different mine waste rock pile where the C_U of the whole slope was around 4.8 (Zhang et al., 2017). However, in practice, waste rock C_U is typically around 20 or more (Aubertin, 2013). This difference was mainly attributed to the fact that particles smaller than 5 cm (i.e., corresponding to around 25 cm^2) were not detectable using image analysis. This is a general limitation to the technique and similar results were also reported for other waste rock piles where the minimum particle diameter that could be detected using image analysis was between 1 cm and 20 cm (Chi, 2011; Zhang et al., 2017).

Fine particles can, however, have a significant impact on hydrogeological (Bao et al., 2020; Essayad, 2021), geotechnical (Laverdière et al., 2022) and even geochemical (Neuner et al.,

2013) properties of waste rock. So, the PSD curve determined using image analysis should often be corrected using field and/or laboratory measured PSD curves. These are, however, also incomplete and rarely contain particles coarser than 50 cm (Cash, 2014; Barsi, 2017), but there is still a rather significant overlap (2 cm to 50 cm) between directly measured and image-based PSD curves so they can be combined.

In this study, around 1000 kg of waste rock were sampled at Canadian Malartic mine for PSD analysis (Essayad, 2021). Waste rock particles larger than 10 cm and up to 25.4 cm were directly and manually characterized in the field (particles coarser than 25.4 cm were not characterized for practical reasons) and waste rock smaller than 10 cm was transported to the laboratory for sieve analysis (diameter > 0.075 mm) and hydrometer tests (diameter < 0.075 mm).

The median PSD curve (Figure 4.5a and Figure 4.11) of the original waste rock obtained from image analysis was corrected and combined with measured PSD curve. In the corrected PSD curve, the passing percentages of fractions larger than 25.4 cm were kept the same to those in the median PSD curve from image analysis. The correction was mainly focused on size fractions smaller than 25.4 cm, which accounted for 25% of the median PSD curve of image analysis sample. The corrected passing percentage of fractions smaller than 25.4 cm were then calculated through multiplying the passing percentage of each diameter in measured PSD curve by 25%. These recalculated PSD fractions (smaller than 25.4 cm) were finally combined with the median PSD fractions larger than 25.4 cm. A similar correction approach was used to correct PSD curves by integrating measured and image analysis obtained PSD curves in other studies (Cash, 2014; Zhang et al., 2017). The resulting PSD curve covered particle diameters from 10^{-4} cm (measured in the laboratory) to a maximum diameter of 150 cm (estimated using image analysis). The corrected D_{10} (= 2.9 cm) was 1 / 5 of that in the original median PSD curve determined from image analysis only (Figure 4.11), resulting in a $C_U = 18$ (compared to $C_U = 3.4$ from image analysis). The correction of field PSD curve was made for the waste rock of the whole slope, and this corrected PSD curve was used to characterize waste rock in Canadian Malartic mine. Such correction can have a significant impact on the estimation of waste rock properties, but assumes that this correction process can be applied in segregated sections although fractions smaller than 25.4 cm in these segregated sections would be slightly different (see the next section below).

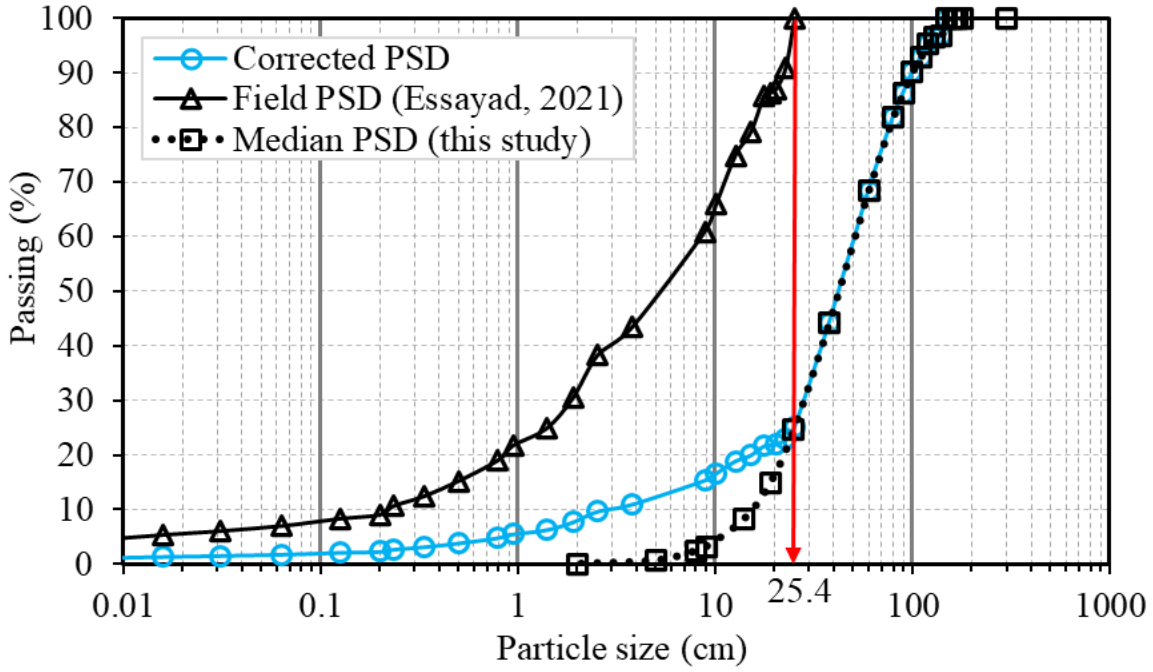

Figure 4.11: Correction of waste rock PSD curve at Canadian Malartic mine (in blue) by integrating field measured PSD (between 0 and 25.4 cm; black triangles) and image analysis (between 25.4 cm and 150 cm; black squares).

4.4.4 Effect of segregation and lateral heterogeneity on waste rock pile properties

4.4.4.1 Effect of segregation and lateral heterogeneity on the estimation of in situ saturated hydraulic conductivity

In practice, vertical segregation and lateral heterogeneity have a direct impact on waste rock hydrogeotechnical properties. For example, the variations of saturated hydraulic conductivity (k_{sat}) could affect the hydrogeotechnical properties and result in preferential flow within waste rock piles (Fala, et al., 2005, 2012). Sometimes, one or two orders of magnitude difference in the hydraulic conductivity can make water flow along irregular and diverted paths (Lahmira et al., 2016, 2017), thus challenging waste rock reclamation. In this study, the effect of segregation and lateral heterogeneity on waste rock hydrogeological behaviour was investigated using Kozeny-

Carman Modified (KCM) model (equation 4.6; Mbonimpa et al., 2002) and Taylor model (equation 4.7; Taylor, 1948), which are both regularly used to predict waste rock saturated hydraulic conductivity (Peregoedova et al., 2013; Bréard Lanoix et al., 2020; Essayad, 2021).

KCM model (Mbonimpa et al., 2002):

$$k_{sat}\left(\frac{cm}{s}\right) = C_G \frac{\gamma_w}{\mu_w} \frac{e^{(3+x)}}{(1+e)} C_U^{1/3} D_{10}^2 \quad (4.6)$$

Where C_G: a constant ($C_G = 0.1$ for granular material); γ_w: unit weight of water ($\gamma_w = 9.8$ kN/m^3); μ_w: dynamic viscosity of water ($\approx 10^{-3}$ N.s/m^2 at 20℃); e: void ratio [-]; x: tortuosity factor (x = 2 for granular material); C_U: uniformity coefficient [-]; D_{10}: particle diameter corresponding to 10% passing (cm).

Taylor model (Taylor, 1948):

$$k_{sat}\left(\frac{cm}{s}\right) = C_1 \frac{\gamma_w}{\mu_w} \frac{e^3}{(1+e)} D_{50}^{1.5} \quad (4.7)$$

Where C_1: a shape factor ($C_1 = 0.004$ is suggested for waste rock by Peregoedova et al. (2013)); γ_w: water unit weight (= 9.8 kN/m^3); μ_w: dynamic viscosity of water ($\approx 10^{-3}$ N.s/m^2 at 20℃); e: void ratio [-]; D_{50}: particle diameter corresponding to 50% passing (cm).

The ratio of waste rock saturated hydraulic conductivity in the bottom section divided by that in the top section, i.e., k_{sat} (bottom) / k_{sat} (top), varied between 1.4 and 25.5 with KCM model and between 0.9 and 14.3 with Taylor model (Figure 4.12). In other words, waste rock segregation during deposition could induce vertical variations of hydraulic conductivity by around one order of magnitude in Canadian Malartic waste rock pile. Similar trends were also observed in other waste rock piles where the permeability in the bottom section was 3 to 12 times greater than that in the top section (Zhang et al., 2017; Chi, 2011). This effect could even be more pronounced because of the crushing and compaction of waste rock at the surface of the pile because of the

frequent circulation of haul trucks (Fala et al., 2012; Maknoon et al., 2021; Raymond et al., 2021).

Lateral heterogeneity of waste rock particle sizes also indicated significant variations of saturated hydraulic conductivities. No clear trend was observed for the lateral distribution of ratios k_{sat} (bottom) / k_{sat} (top) which were randomly distributed and could exceed 16 (Figure 4.12). Such field results are scarce in the literature, but similar lateral variations (up to 25 times) were also observed for saturated hydraulic conductivity of waste rock samples measured in the laboratory (Cash, 2014).

These results tend to confirm the representativity of numerical simulations which consider heterogeneity by randomly distributing materials with different permeabilities (with one order of magnitude difference) within the whole waste rock pile (Lahmira et al., 2016, 2017). However, this study has also shown that waste rock sizes exhibited a strong vertical correlation, which could be considered to improve the way to simulate segregation in waste rock piles.

Here, the discussion was conducted in terms of saturated hydraulic conductivity, but the effect of segregation on waste rock shear strength (Kim et al., 2014; Zevgolis, 2018) and geochemical reactivity (St-Arnault et al., 2020; Seigneur et al., 2021) is expected to be similar.

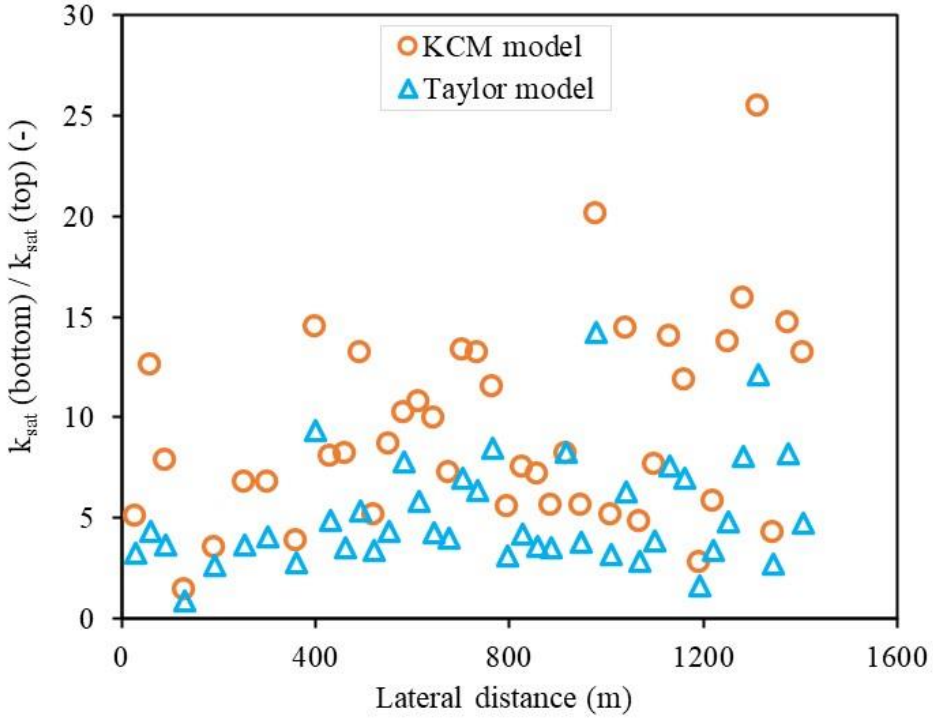

Figure 4.12: Variation of ratio k_{sat} (bottom) / k_{sat} (top) as a function of lateral heterogeneity. Waste rock saturated hydraulic conductivity k_{sat} was predicted using KCM (equation 4.6) and Taylor (equation 4.7) models.

4.4.4.2 Comparison of original non-segregated and segregated waste rock saturated hydraulic conductivity

The saturated hydraulic conductivity (k_{sat}) is usually determined by characterizing waste rock samples (before the deposition, i.e., non-segregated) in the laboratory and as the measured result is deemed representative of field waste rock (Abdelghani et al., 2015; Maknoon et al., 2021). However, the analyses above indicated that segregation could significantly affect in situ hydraulic conductivity. The saturated hydraulic conductivity was predicted using KCM (equation 4.6) and Taylor (equation 4.7) models, but this time based on the PSD curves of each section corrected using the approach proposed above and including fine particles (i.e., diameter < 5 cm). The void ratio e = 0.3 was determined from field measurements at Canadian Malartic mine (Essayad, 2021).

The ratio of waste rock saturated hydraulic conductivity (k_{sat}) in each section divided by the saturated hydraulic conductivity of original waste rock, i.e., k_{sat} / k_{sat}', was 0.06 in section 1 (x / L = 0.08, top of the slope) with KCM model and 0.3 with Taylor model (Figure 4.13). The ratio k_{sat} / k_{sat}' in section 6 (x / L = 0.92, bottom of the slope) was 38 with KCM model and 1.8 with Taylor model. The saturated hydraulic conductivity in the middle of the slope (x / L = 0.6 ~ 0.8) was similar to that of the original waste rock ($k_{sat} / k_{sat}' \approx 1$). In other words, the saturated hydraulic conductivity of the original unsegregated waste rock could be one order of magnitude greater than that in the top of the pile and one order of magnitude smaller than that in the bottom of the pile. The saturated hydraulic conductivity of the original waste rock is therefore not representative of the waste rock properties in the slope (as also suggest by Wilson et al., 2013 and Barsi, 2017) and can in practice vary by more than one order of magnitude for a 10 m high bench. In practice, the saturated hydraulic conductivity of waste rock tended to be overestimated in the top section and underestimated in the bottom section when this correction method was used to correct the waste rock from image analysis.

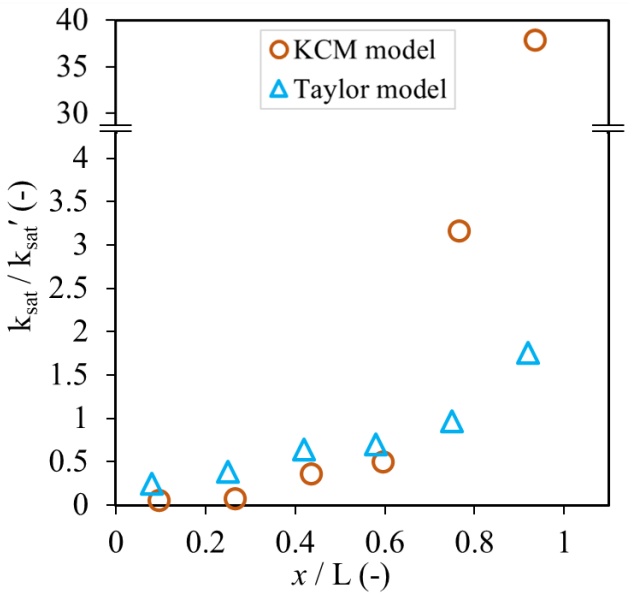

Figure 4.13: Variation of ratio k_{sat} / k_{sat}' as a function of vertical positions along the slope. Waste rock saturated hydraulic conductivity k_{sat} was predicted using KCM (equation 4.6) and Taylor (equation 4.7) models.

4.4.5 Particle shape effect

In this study, particle diameters and masses were determined using ellipsoid model, and the short axis of the particles was estimated using a shape factor, $\alpha = c / b = 0.53$. This shape factor was, however, measured in the laboratory and assumed constant and independent of the particle diameter, while in practice it may decrease with particle diameter (Linero et al., 2017). Even though the field shape factor could not be determined because of the lack of data, the influence of choosing a constant value was investigated by comparing the shape of around 10 000 particles in the field (using image analysis) with the results of the 2 200 particles analyzed in the laboratory (see methodology section).

The ratio b / a of waste rock varied between 0.5 and 0.8 in the laboratory and between 0.4 and 0.8 in the field (Figure 4.14). The ratio c / a ranged between 0.3 and 0.4 in the laboratory and between 0.2 and 0.4 in the field. Although waste rock generally exhibited similar shapes in the laboratory and in the field, the distribution of both b / a and c / a tended to be slightly wider in the field than in the laboratory. For example, the maximum frequency of b / a was 0.26 in the field, i.e., slightly less than the 0.31 measured in the laboratory. One reason for this discrepancy can be that significantly more particles were analyzed in the field, thus statistically covering a larger variety of shapes. Another reason could be that ratios b / a (Linero et al., 2017) and c / a (Ovalle, et al., 2020) both tended to increase with particle diameters.

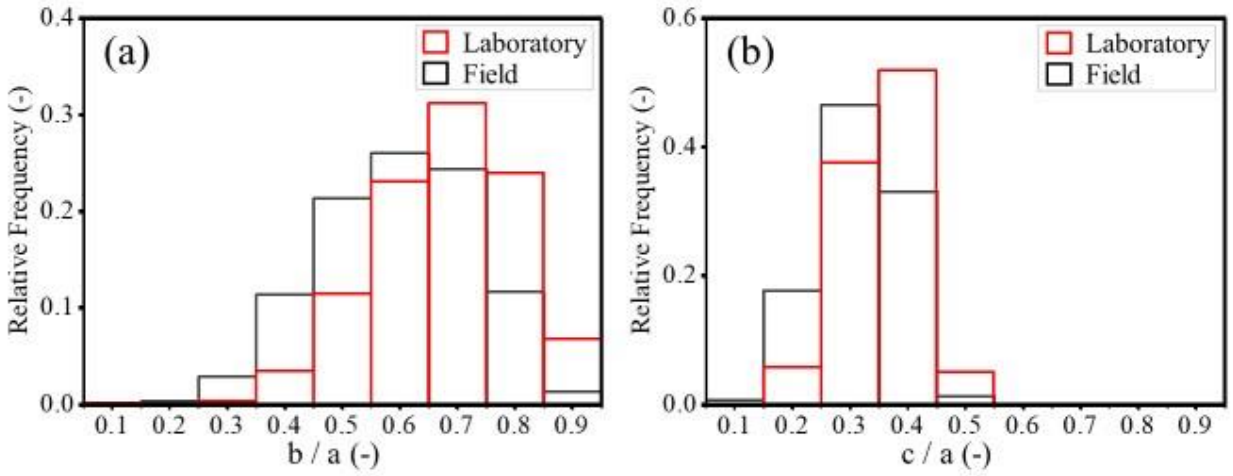

Figure 4.14: Waste rock particle shape ratios (a) b / a and (b) c / a in the laboratory (red) and in the field (black). a, b and c are the long, medial and short axis of waste rock particles. The comparison is based on the analysis of 2224 particles in the laboratory with diameters between 0.8 cm and 3.8 cm, and 10 000 particles in the field with diameters larger than 10 cm (assuming a constant shape factor c / b).

The ellipsoid model (Figure 4.2) is usually considered efficient to estimate the dimensions of granular particles, but, as mentioned above, the estimation of the short axis can be difficult. Other models such as sphere model and Feret's diameter model were therefore also used in this study to determine waste rock PSD. Sphere model (Figure 4.15a) is easy to apply when the specimen comprises a large number of particles (Shanthi et al., 2014; Zhang et al., 2017). Measured particle area (A) from image analysis is converted to an equivalent particle diameter (D_e, $D_e = 2 \times \sqrt{A / \pi}$), which is then used to calculate sphere volumes and determine their mass (Li et al., 2005). Feret's diameter model (Figure 4.15b) is also an ellipsoid-based shape model except that the long and medial axes are defined by maximum (F_{max}, the longest distance between any two points along the particle boundary) and minimum (F_{min}, the minimum caliper diameter of the particle) Feret's diameters (Ferreira et al., 2012; Hamzeloo et al., 2014). The equivalent particle diameter is then calculated as $D_e = F_{min} / \sqrt{2}$.

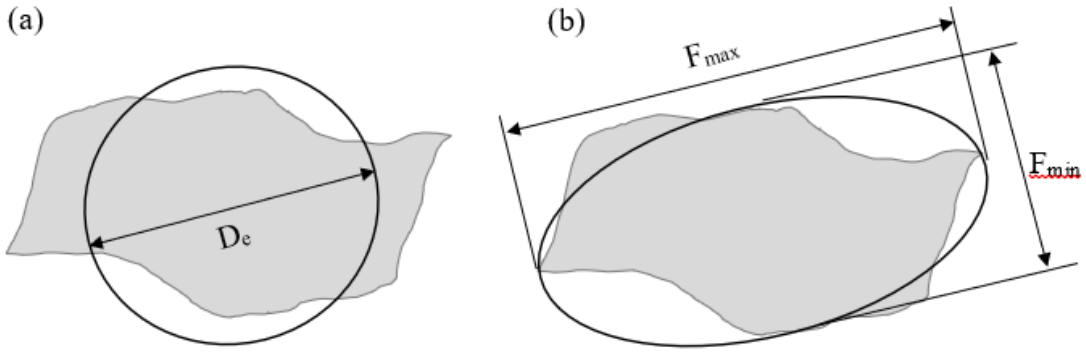

Figure 4.15: Shape characterization using (a) sphere model and (b) Feret's diameter model. D_e represents the equivalent particle diameter; F_{max} and F_{min} represent the maximum and minimum Feret's diameters.

Among these three models, the PSD curve obtained using the ellipsoid model was the closest to the PSD curve measured using sieve analysis in the laboratory (Figure 4.16a). At field scale (Figure 4.16b), Feret's diameter model results were similar to ellipsoid model. However, PSD obtained using sphere model was always coarser than that using ellipsoid model and Feret's diameter model both in the laboratory and in the field (Figure 4.16). The main reason is that waste rock particles are mostly elongated and using a sphere therefore tends to overestimate the diameter under the same equivalent projected area. From the comparison above, ellipsoid model is considered the best to estimate waste rock shapes in general, but Feret's diameter model can also give good results in the field.

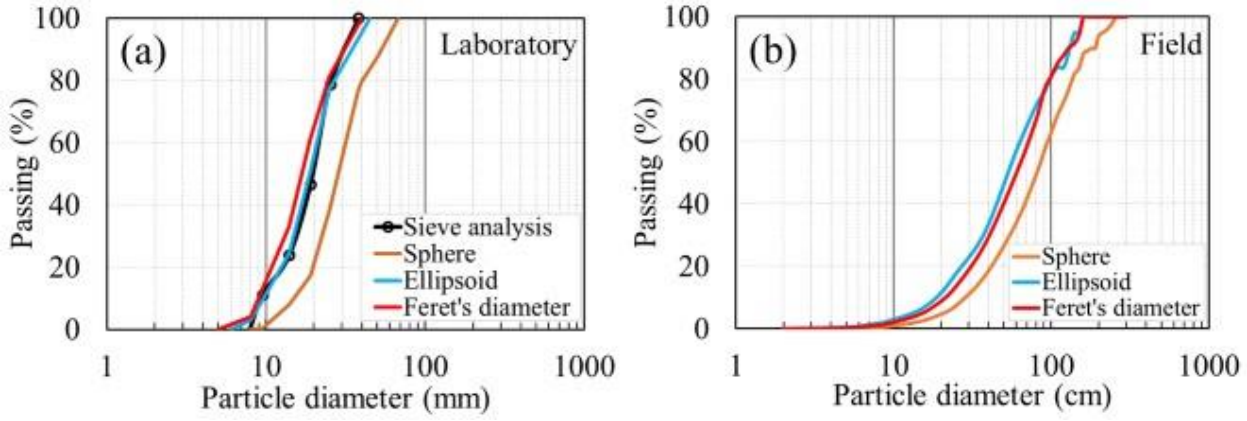

Figure 4.16: PSD curves of waste rock in the (a) laboratory and (b) field using sphere, ellipsoid and Feret's diameter models in image analysis. The PSD curve determined with sieve analysis in the laboratory was used for comparison.

4.4.6 Discussion

Image analysis was used in this study to quantify both segregation and lateral heterogeneity in a waste rock pile. Despite its numerous advantages (e.g., easy operation, low cost, high efficiency), image analysis also has a few limitations, and several assumptions were made to interpret the results. First, the boundary of every single particle was detected based on pixel intensity differences between the particles and the background. However, pixel intensity is sensitive to image brightness and resolution (Ferreira et al., 2012; Đuriš et al., 2016; Zhang et al., 2017), and detection of particle boundaries may be difficult if pixel intensity is not contrasted enough, resulting in an overestimation particle diameter. Secondly, different colours within the same particle (for example because of different mineral composition) or brightness (because of shades), may lead the image processing code to distinguish several smaller particles where there is just on (Azzali et al., 2011). Particle overlap would hide parts of the particles and also result in underestimation of these particle (Zhang, 2016). Also, the pixel conversion factor was 1.2 cm in this study, and particles smaller than 2 cm could not be detected, even though they represented (based on direct PSD measurement) about 8% of the entire PSD curve. Neglecting fine particles could have a significant impact on the estimation of waste rock hydrogeotechnical properties (Chapuis, 2012). Higher resolution cameras are therefore recommended to improve the precision

of particle detection. Today's cameras usually have a resolution between 0.7 and 10 cm / pixel (Chabot et al., 2016; Inzerillo et al., 2022), but some specific cameras such as infrared thermal cameras (which can be installed on a drone) can reach 0.27 cm / pixel (Westfeld et al., 2015; Di Felice et al., 2018). Other remote sensing techniques such as LiDAR could also be an alternative option with a resolution of around 3 cm / pixel (Collin et al., 2018; Li et al., 2020).

This study focused on the segregation and lateral heterogeneity on the surface of a waste rock pile. However, internal heterogeneity can also be significant because of the presence of the alternance of inclined fine and coarse-grained layers (Anterrieu et al., 2010; Bao et al., 2020). Such internal structure is, however, difficult to characterize using only image analysis and would require additional investigation methods such as geophysical methods (Anterrieu et al., 2010; Azzali et al., 2011; Dimech et al., 2019) and trench excavation (Stockwell et al., 2006; Boekhout et al., 2015). In addition, lateral heterogeneity was characterized along the slope of a field waste rock pile, but no clear trend could be observed along the lateral direction. More field observations are expected to investigate the possible prediction of lateral heterogeneity.

Finally, this study was carried out only for a 10 m bench of waste rock pile at Canadian Malartic mine which exhibits similar mineral composition. Even though comparison with literature has shown similar trends in other waste rock piles, segregation analyses on more waste rock piles are recommended to confirm the field observations and contribute to further understand heterogeneity of waste rock piles.

4.5 Conclusions

In this study, waste rock segregation and lateral heterogeneity were characterized using image analysis on drone pictures obtained from Canadian Malartic mine, a surface gold mine located in Quebec, Canada. A total of 42 drone images, covering an area with 1400 m wide and 10 m high (one bench), were analyzed. Ellipsoid model was used to represent the irregular shapes and a calibrated shape factor of 0.53 was applied to determine waste rock diameters and masses. The bench slope was divided into 6 sections in the vertical direction and the PSD curve in each section was determined. A total of 252 PSD curves were analyzed to quantify waste rock segregation and heterogeneity. The segregation degree and the characteristic diameters from the

top to the bottom section of the slope were obtained and quantitatively compared. Most important findings can be summarized as follows:

(1) The increase of relative particle diameters and segregation degree indicated significant segregation along the slope of waste rock pile. Segregation degree increased from -0.77 ± 0.39 in the top (finer zone) to $+0.4 \pm 0.14$ in the bottom (coarser zone). The strong vertical correlation of waste rock sizes characterized in this study could improve the way to simulate segregation in waste rock piles.

(2) Significant lateral heterogeneity was characterized by investigating the lateral distribution of waste rock particles. The maximum diameters varied between 30 cm and 130 cm in the top section and between 80 cm and 180 cm in the bottom section. The maximum frequency of characteristic diameters D_{50} and D_{80} were always smaller than 0.4.

(3) Segregation and lateral heterogeneity resulted in high variations (one to two orders of magnitude difference) of the saturated hydraulic conductivity and more generally of the geotechnical properties of waste rock in the field. The saturated hydraulic conductivity in the bottom section was up to 26 times than that in the top section.

(4) Image analysis with ellipsoid model is an efficient method to characterize waste rock segregation and lateral heterogeneity in large-scale waste rock piles. A calibrated constant shape factor $\alpha = 0.53$ can well estimate the short axis of waste rock particles in this study. The image resolution constrained particle detection precision, and fine particles (e.g. < 5 cm) were therefore underestimated in image analysis.

This research should provide a reference to quantitatively characterize waste rock segregation and lateral heterogeneity in the field and provide the basis to investigate segregation in numerical simulations in future works.

4.6 Acknowledgement

The authors would like to acknowledge the financial support from NSERC (grant number: RGPIN-2017-05725), FRQNT (grant number: 2017-MI-202116), the industrial partners of the Research Institute on Mines and the Environment (RIME) (http://rime.ca/). Special thanks to partners at Canadian Malartic mine for taking these photos with great efforts.

4.7 References

Abdelghani, F. B., Aubertin, M., Simon, R., & Therrien, R. (2015). Numerical simulations of water flow and contaminants transport near mining wastes disposed in a fractured rock mass. International Journal of Mining Science and Technology, 25(1), 37-45.

Abràmoff, M. D., Magalhães, P. J., & Ram, S. J. (2004). Image processing with ImageJ. Biophotonics international, 11(7), 36–42.

Al-Thyabat, S., & Miles, N. J. (2006). An improved estimation of size distribution from particle profile measurements. Powder Technology, 166(3), 152–160.

Amos, R.T., Blowes, D.W., Bailey, B.L., Sego, D.C., Smith, L. and Ritchie, A.I.M. (2015). Waste-rock hydrogeology and geochemistry. Applied Geochemistry, 57: 140–156.

An, N., Tang, C. S., Cheng, Q., Wang, D. Y., & Shi, B. (2020). Application of electrical resistivity method in the characterization of 2D desiccation cracking process of clayey soil. Engineering Geology, 265, 105416.

Aubertin, M. (2013). Waste rock disposal to improve the geotechnical and geochemical stability of piles. Proceedings of the world mining congress, Montreal, Quebec, Canada.

Alyamani, M. S., and Sen, Z. (1993). Determination of Hydraulic Conductivity from Grain-Size Distribution Curves. Ground Water, 31, 551–555.

Andriani, G. F., & Walsh, N. (2002). Physical properties and textural parameters of calcarenitic rocks: qualitative and quantitative evaluations. Engineering Geology, 67(1-2), 5-15.

Anterrieu, O., Chouteau, M. and Aubertin, M. (2010). Geophysical characterization of the large-scale internal structure of a waste rock pile from a hard rock mine. Bulletin of Engineering Geology and the Environment, 69(4), 533–548.

Appels, W. M., Ireson, A. M., & Barbour, S. L. (2018). Impact of bimodal textural heterogeneity and connectivity on flow and transport through unsaturated mine waste rock. Advances in water resources, 112, 254–265.

Asmaei, S., Shourijeh, P. T., Binesh, S. M., & Ghaedsharafi, M. H. (2018). An experimental parametric study of segregation in cohesionless soils of embankment dams. Geotechnical Testing Journal, 41(3), 473–493.

ASTM C117-17, (2017). Standard Test Method for Materials Finer than 75 μm (No. 200) Sieve in Mineral Aggregates by Washing. In. West Conshohocken, PA: ASTM International.

ASTM C127-15, (2015). Standard Test Method for Relative Density (Specific Gravity) and Absorption of Coarse Aggregate, ASTM International, West Conshohocken, PA.

ASTM D6913/D6913M-17, (2017). Standard Test Methods for Particle-Size Distribution (Gradation) of Soils Using Sieve Analysis. In. West Conshohocken, PA.

ASTM D7928-17, (2017) Standard Test Method for Particle-Size Distribution (Gradation) of Fine-Grained Soils Using the Sedimentation (Hydrometre) Analysis. In. West Conshohocken, PA: ASTM International.

Ayres, B., Landine, P., Adrian, L., Christensen, D., & O'Kane1, M. (2006). Cover and final landform design for the B-zone waste rock pile at Rabbit Lake Mine. Uranium in the Environment 739–749.

Azam, S., Wilson, G. W., Herasymuik, G., Nichol, C., & Barbour, L. S. (2007). Hydrogeological behaviour of an unsaturated waste rock pile: a case study at the Golden Sunlight Mine, Montana, USA. Bulletin of Engineering Geology and the Environment, 66(3), 259–268.

Azzali, E., Carbone, C., Marescotti, P., & Lucchetti, G. (2011). Relationships between soil colour and mineralogical composition: application for the study of waste-rock dumps in abandoned mines. Neues Jahrbuch fur Mineralogie-Abhandlungen, 188(1), 75.

Bao, Z., Blowes, D. W., Ptacek, C. J., Bain, J., Holland, S. P., Wilson, D., ... & MacKenzie, P. (2020). Faro Waste Rock Project: Characterizing variably saturated flow behavior through full‐scale waste‐rock dumps in the continental subarctic region of Northern Canada using field measurements and stable isotopes of water. Water Resources Research, 56(3), e2019WR026374.

Bar N, Semi J, Koek M, Owusu-Bempah G, Day A, Nicoll S, Bu J. (2020). Practical waste rock dump and stockpile management in high rainfall and seismic regions of Papua New Guinea. Mine Closure (2020), Australian Centre for Geomechanics, Perth, Australia, pp 117–128.

Barsi, D. (2017). Spatial variability of particles in waste rock piles. Master's thesis, University of Alberta.

Bhatia, S. K., & Soliman, A. F. (1990). Frequency distribution of void ratio of granular materials determined by an image analyzer. Soils and Foundations, 30(1), 1–16.

Boekhout, F., Gérard, M., Kanzari, A., Michel, A., Déjeant, A., Galoisy, L., ... & Descostes, M. (2015). Uranium migration and retention during weathering of a granitic waste rock pile. Applied Geochemistry, 58, 123-135.

Bréard Lanoix ML, Pabst T, Aubertin M. (2020). Field determination of the hydraulic conductivity of a compacted sand layer controlling water flow on an experimental mine waste rock pile. Hydrogeology Journal. 28(4):1503–15.

Cash, A. (2014). Structural and Hydrologic Characterization of Two Historic Waste Rock Piles. Master's thesis, University of Alberta.

Chabot, D., & Francis, C. M. (2016). Computer‐automated bird detection and counts in high‐resolution aerial images: A review. Journal of Field Ornithology, 87(4), 343–359.

Chapuis, R. P. (2012). Predicting the saturated hydraulic conductivity of soils: a review. Bulletin of engineering geology and the environment, 71(3), 401-434.

Chi, X. (2011). Characterizing low-sulfide instrumented waste-rock piles: image grain-size analysis and wind-induced gas transport (Master's thesis, University of Waterloo).

Collin, A., Ramambason, C., Pastol, Y., Casella, E., Rovere, A., Thiault, L., ... & Davies, N. (2018). Very high resolution mapping of coral reef state using airborne bathymetric LiDAR surface-intensity and drone imagery. International journal of remote sensing, 39(17), 5676-5688.

Di Felice, F., Mazzini, A., Di Stefano, G., & Romeo, G. (2018). Drone high resolution infrared imaging of the Lusi mud eruption. Marine and Petroleum Geology, 90, 38-51.

Dimech, A., Chouteau, M., Aubertin, M., Bussière, B., Martin, V., & Plante, B. (2019). Three‐dimensional time‐lapse geoelectrical monitoring of water infiltration in an experimental mine waste rock pile. Vadose Zone Journal, 18(1), 1-19.

Dipova, N. (2017). Determining the grain size distribution of granular soils using image analysis. Acta Geotechnica Slovenica, 14(1), 29–37.

Đuriš, M., Arsenijević, Z., Jaćimovski, D., & Radoičić, T. K. (2016). Optimal pixel resolution for sand particles size and shape analysis. Powder Technology, 302, 177–186.

Fala, O., Molson, J., Aubertin, M., and Bussière, B. (2005). Numerical Modelling of Flow and Capillary Barrier Effects in Unsaturated Waste Rock Piles. Mine Water and the Environment, 24(4): 172–185.

Fala, O., Molson, J., Aubertin, M., Dawood, I., Bussière, B., & Chapuis, R. P. (2012). A numerical modelling approach to assess long-term unsaturated flow and geochemical transport in a waste rock pile. International Journal of Mining, Reclamation and Environment, 27(1), 38-55. doi:10.1080/17480930.2011.644473

Fernlund, J. M. R. (2005). 3-D image analysis size and shape method applied to the evaluation of the Los Angeles test. Engineering geology, 77(1-2), 57–67.

Fernlund, J. M., Zimmerman, R. W., & Kragic, D. (2007). Influence of volume/mass on grain-size curves and conversion of image-analysis size to sieve size. Engineering geology, 90(3-4), 124-137.

Ferreira, T., & Rasband, W. (2012). ImageJ user guide. ImageJ/Fiji, 1.46r.

Goyal, R. K., & Tomassone, M. S. (2006). Power-law and exponential segregation in two-dimensional silos of granular mixtures. Physical Review E, 74(5), 051301.

Gupta, A. K. (2016). Effects of particle size and confining pressure on breakage factor of rockfill materials using medium triaxial test. Journal of Rock Mechanics and Geotechnical Engineering, 8(3), 378–388.

Hajizadeh Namaghi, H., Li, S. and Jiang, L. (2015). Numerical simulation of water flow in a large waste rock pile, Haizhou coal mine, China. Modeling Earth Systems and Environment, 1(1–2).

Hamzeloo, E., Massinaei, M., & Mehrshad, N. (2014). Estimation of particle size distribution on an industrial conveyor belt using image analysis and neural networks. Powder technology, 261, 185–190.

Hao, S., & Pabst, T. (2022). Experimental Investigation and Prediction of the Permanent Deformation of Crushed Waste Rock Using an Artificial Neural Network Model. International Journal of Geomechanics, 22(5), 04022032.

Hawley, M., & Cunning, J. (2017). Guidelines for mine waste dump and stockpile design. CSIRO Publishing.

Herasymuik G, Azam S, Wilson G.W., Barbour L.S., Nichol C. (2006). Hydrological characterization of an unsaturated waste rock dump. In: Proceedings of the 59th Canadian geotechnical conference, Vancouver, BC, Canada.

Inzerillo, L., Acuto, F., Di Mino, G., & Uddin, M. Z. (2022). Super-Resolution Images Methodology Applied to UAV Datasets to Road Pavement Monitoring. Drones, 6(7), 171.

James, M., Aubertin, M., and Bussière, B. (2013). On the use of waste rock inclusions to improve the performance of tailings impoundments. Proceedings of 18th International Conference on Soil Mechanics and Geotechnical Engineering, Paris, France, 735–738.

Essayad, K. (2021). Évaluation multi-échelle de l'instabilité interne et de la migration des résidus à travers les inclusions de roches stériles. Polytechnique Montreal.

Kenney, T.C. and Westland, J. (1993). Laboratory Study of Segregation of Granular Filter Materials," Filters In Geotechnical and Hydraulic Engineering: Proceedings of the First International Conference "Geo-Filter", Karlesruhe, Germany, pp. 313–319.

Khola, N., & Wassgren, C. (2016). Correlations for shear-induced percolation segregation in granular shear flows. Powder Technology, 288, 441–452.

Kim, D., & Ha, S. (2014). Effects of Particle Size on the Shear Behavior of Coarse Grained Soils Reinforced with Geogrid. Materials (Basel), 7(2), 963-979.

Kinyua, E. M., Jianhua, Z., Kasomo, R. M., Mauti, D., & Mwangangi, J. (2022). A review of the influence of blast fragmentation on downstream processing of metal ores. Minerals Engineering, 186, 107743.

Kumara, G. H. A. J. J., Hayano, K., & Ogiwara, K. (2011). Fundamental study on particle size distribution of coarse materials by image analysis. In First International Conference on Geotechnique, Construction Materials and Environment.

Kumara, G. H. A. J. J., Hayano, K., & Ogiwara, K. (2012). Image analysis techniques on evaluation of particle size distribution of gravel. GEOMATE Journal, 3(5), 290–297.

Ko, Y. D., & Shang, H. (2011). A neural network-based soft sensor for particle size distribution using image analysis. Powder Technology, 212(2), 359–366.

Kwan, A. K., Mora, C. F., & Chan, H. C. (1999). Particle shape analysis of coarse aggregate using digital image processing. Cement and Concrete Research, 29(9), 1403–1410.

Lahmira, B., Lefebvre, R., Aubertin, M. and Bussiere, B. (2016). Effect of heterogeneity and anisotropy related to the construction method on transfer processes in waste rock piles. Journal of Contaminant Hydrology, 184: 35–49.

Lahmira, B., Lefebvre, R., Aubertin, M. and Bussiere, B. (2017). Effect of material variability and compacted layers on transfer processes in heterogeneous waste rock piles. Journal of Contaminant Hydrology, 204: 66–78.

Laverdière, A., Hao, S., Pabst, T., & Courcelles, B. (2022). Effect of gradation, compaction and water content on crushed waste rocks strength. Road Materials and Pavement Design, 1–15.

Lawal, A. I. (2021). A new modification to the Kuz-Ram model using the fragment size predicted by image analysis. International Journal of Rock Mechanics and Mining Sciences, 138, 104595.

Lee, J. R. J., Smith, M. L., & Smith, L. N. (2007). A new approach to the three-dimensional quantification of angularity using image analysis of the size and form of coarse aggregates. Engineering Geology, 91(2-4), 254–264.

Lehouiller, P., Lampron, S., Gagnon, G., Houle, N., Bouchard, F. (2020). NI 43-101 Technical Report, Canadian Malartic Mine, Québec, Canada.

Li, L., Lan, H., & Peng, J. (2020). Loess erosion patterns on a cut-slope revealed by LiDAR scanning. Engineering Geology, 268, 105516.

Li, M., Wilkinson, D., & Patchigolla, K. (2005). Comparison of particle size distributions measured using different techniques. Particulate Science and Technology, 23(3), 265–284.

Linero, S., Fityus, S., Simmons, J., Lizcano, A., & Cassidy, J. (2017). Trends in the Evolution of Particle Morphology with Size in Colluvial DepositsOverlying Channel Iron Deposits. Paper presented at the EPJ Web of Conferences.

Liu, X., Zhang, C., & Zhan, J. (2015). Quantitative comparison of image analysis methods for particle mixing in rotary drums. Powder Technology, 282, 32–36.

Loth, E. (2008). Drag of non-spherical solid particles of regular and irregular shape, Powder Technology. 182,342–353.

Maknoon, M., & Aubertin, M. (2021). On the Use of Bench Construction to Improve the Stability of Unsaturated Waste Rock Piles. Geotechnical and Geological Engineering, 39(2), 1425–1449.

Martin, V., Pabst, T., Bussière, B., Plante, B., & Aubertin, M. (2019). A new approach to control contaminated mine drainage generation from waste rock piles: Lessons learned after 4 years of field monitoring. In Proceedings of the 18th Global Joint Seminar on Geo-Environmental Engineering.

McLemore, V.T., Fakhimi, A., van Zyl, D., et al. (2009). Literature review of other rock piles: Characterization, weathering, and stability. Report OF-517, Questa Rock Pile Weathering Stability Project. New Mexico Bureau of Geology and Mineral Resources.

Meng, Y., Wang, Q., Su, W., Ye, W., & Chen, Y. (2022). Effect of sample thickness on the self-sealing and hydration cracking of compacted bentonite. Engineering Geology, 106792.

Molson, J. W., Fala, O., Aubertin, M. and Bussiere, B. (2005). Numerical simulations of pyrite oxidation and acid mine drainage in unsaturated waste rock piles. Journal of Contaminant Hydrology, 78(4): 343–371.

Mora, C. F., Kwan, A. K. H., & Chan, H. C. (1998). Particle size distribution analysis of coarse aggregate using digital image processing. Cement and Concrete Research, 28(6), 921–932.

Mora, C. F., & Kwan, A. K. H. (2000). Sphericity, shape factor, and convexity measurement of coarse aggregate for concrete using digital image processing. Cement and concrete research, 30(3), 351–358.

Morin, K. A., Gerencher, E., Jones, C. E., and Konasewich, D. E. (1991). Critical literature review of acid drainage from waste rock. MEND Report 1.11.1. Ottawa.

Mosby, J., de Silva, S. R., & Enstad, G. G. (1996). Segregation of particulate materials–mechanisms and testers. KONA Powder and Particle Journal, 14, 31–43.

Neuner, M., Smith, L., Blowes, D. W., Sego, D. C., Smith, L. J., Fretz, N., & Gupton, M. (2013). The Diavik waste rock project: Water flow through mine waste rock in a permafrost terrain. Applied geochemistry, 36, 222–233.

Nichol, C., Smith, L., & Beckie, R. (2005). Field-scale experiments of unsaturated flow and solute transport in a heterogeneous porous medium. Water Resources Research, 41(5).

Nichol, R. S. (1986). Rock segregation in waste dumps. Proceedings of the international conference on flow-through rock drains.

Ohm, H. S., & Hryciw, R. D. (2013). Translucent segregation table test for sand and gravel particle size distribution. Geotechnical Testing Journal, 36(4), 592–605.

Ovalle, C., & Dano, C. (2020). Effects of particle size–strength and size–shape correlations on parallel grading scaling. Géotechnique Letters, 10(2), 191–197.

Pedretti, D., Mayer, K. U., & Beckie, R. D. (2017). Stochastic multicomponent reactive transport analysis of low quality drainage release from waste rock piles: Controls of the spatial distribution of acid generating and neutralizing minerals. Journal of Contaminant Hydrology, 201, 30–38.

Pedretti, D., Mayer, K.U. and Beckie, R.D. (2020). Controls of uncertainty in acid rock drainage predictions from waste rock piles examined through Monte-Carlo multicomponent reactive transport. Stochastic Environmental Research and Risk Assessment, 34: 219–233.

Podczeck, F. (1997). A shape factor to assess the shape of particles using image analysis. Powder technology, 93(1), 47–53.

Rahmani, H., & Panah, A. K. (2021). Influence of particle size on particle breakage and shear strength of weak rockfill. Bulletin of Engineering Geology and the Environment, 80(1), 473-489.

Raymond, K. E., Seigneur, N., Su, D., & Mayer, K. U. (2021). Investigating the Influence of Structure and Heterogeneity in Waste Rock Piles on Mass Loading Rates—A Reactive Transport Modeling Study. Frontiers in Water, 39.

Revil A, Karaoulis M, Johnson T et al. (2012). Some low-frequency electrical methods for subsurface characterization and monitoring in hydrogeology. Hydrogeololy Journal, 20(4):617–658

Seigneur, N., Vriens, B., Beckie, R. D., & Mayer, K. U. (2021). Reactive transport modelling to investigate multi-scale waste rock weathering processes. Journal of Contaminant Hydrology, 236, 103752.

Shanthi, C., Porpatham, R. K., & Pappa, N. (2014). Image analysis for particle size distribution. International Journal of Engineering and Technology, 6(3), 1340–1345.

Shepherd, R. G. (1989). Correlations of Permeability and Grain Size. Ground Water, 27(5), 633–638.

Sherard, J. L., Dunnigan, L. P., & Talbot, J. R. (1984). Basic properties of sand and gravel filters. Journal of Geotechnical Engineering, 110(6), 684–700.

Smith, L. J., Blowes, D. W., Jambor, J. L., Smith, L., Sego, D. C., & Neuner, M. (2013). The Diavik Waste Rock Project: Particle size distribution and sulfur characteristics of low-sulfide waste rock. Applied geochemistry, 36, 200–209.

St-Arnault, M., Vriens, B., Blaskovich, R., Aranda, C., Klein, B., Mayer, K. U., & Beckie, R. D. (2020). Geochemical and mineralogical assessment of reactivity in a full-scale heterogeneous waste-rock pile. Minerals Engineering, 145, 106089.

Stockwell, J., Smith, L., Jambor, J. L., & Beckie, R. (2006). The relationship between fluid flow and mineral weathering in heterogeneous unsaturated porous media: A physical and geochemical characterization of a waste-rock pile. Applied geochemistry, 21(8), 1347-1361.

Van Staden, P. J., & Petersen, J. (2018). The effects of simulated stacking phenomena on the percolation leaching of crushed ore, Part 1: Segregation. Minerals engineering, 128, 202–214.

Van Staden, P. J., & Petersen, J. (2019). The effects of simulated stacking phenomena on the percolation leaching of crushed ore, Part 2: Stratification. Minerals Engineering, 131, 216–229.

Vizcarra, J. C., Burlingame, E. A., Hug, C. B., Goltsev, Y., White, B. S., Tyson, D. R., & Sokolov, A. (2022). A community-based approach to image analysis of cells, tissues and tumors. Computerized Medical Imaging and Graphics, 95, 102013.

Vriens, B., Peterson, H., Laurenzi, L., Smith, L., Aranda, C., Mayer, K. U., & Beckie, R. D. (2019). Long-term monitoring of waste-rock weathering at the Antamina mine, Peru. Chemosphere, 215, 858-869.

Webb, G., Tyler, S. W., Collord, J., Van Zyl, D., Halihan, T., Turrentine, J., & Fenstemaker, T. (2008). Field‐scale analysis of flow mechanisms in highly heterogeneous mining media. Vadose Zone Journal, 7(3), 899-908.

Westfeld, P., Mader, D., & Maas, H. G. (2015). Generation of TIR-attributed 3D point clouds from UAV-based thermal imagery. Photogrammetrie-Fernerkundung-Geoinformation, 381-393.

Westland, J. (1988). A study of segregation in cohesionless soil. M.A.Sc. Thesis, Department of Civil Engineering, University of Toronto, Toronto, Canada.

Williams, J.C. (1976). The segregation of particulate materials: a review. Powder technology, 15, 245–251.

Wilson, D., Smith, L., Atherton, C., Smith, L. J., Amos, R. T., Barsi, D. R., ... & Blowes, D. W. (2022). Diavik Waste Rock Project: Geostatistical Analysis of Sulfur, Carbon, and Hydraulic Conductivity Distribution in a Large-Scale Experimental Waste Rock Pile. Minerals, 12(5), 577.

Wilson, J.A., Wilson, G.W., Fredlund, D.G. (2000). Numerical modeling of vertical and inclined waste rock layers. In: Proceeding of 5th International Conference Acid Rock Drainage, Society for Mining, Metallurgy and Exploration, Denver, 257–266.

Xie, W. Q., Zhang, X. P., Yang, X. M., Liu, Q. S., Tang, S. H., & Tu, X. B. (2020). 3D size and shape characterization of natural sand particles using 2D image analysis. Engineering Geology, 279, 105915.

Zevgolis, I. E. (2018). Geotechnical characterization of mining rock waste dumps in central Evia, Greece. Environmental Earth Sciences, 77(16), 1-18.

Zhang, J. M., Luo, Y., Zhou, Z., Chong, L., Victor, C., & Zhang, Y. F. (2021). Effects of preferential flow induced by desiccation cracks on slope stability. Engineering Geology, 288, 106164.

Zhang, S., & Liu, W. (2017). Application of aerial image analysis for assessing particle size segregation in dump leaching. Hydrometallurgy, 171, 99–105.

Zhang, Z. (2016). Particle overlapping error correction for coal size distribution estimation by image analysis. International Journal of Mineral Processing, 155, 136-139.

Zhang, Z., Yang, J., Ding, L., & Zhao, Y. (2012). An improved estimation of coal particle mass using image analysis. Powder Technology, 229, 178–184.

CHAPTER 5 ARTICLE 2: WASTE ROCK SEGREGATION DURING DISPOSAL: CALIBRATION AND UPSCALING OF DISCRETE ELEMENT SIMULATIONS

Peiyong Qiu and Thomas Pabst

Department of Civil, Geological, and Mining Engineering, Polytechnique Montréal, Montréal, Québec, Canada

Research Institute on Mines and Environment (RIME), Québec, Canada

This article has been published in Powder Technology online on 10 October 2022.

Abstract: Large volumes of waste rock are produced during mining operations and are often disposed of in large piles on the surface. Segregation caused by particle sizes and deposition methods usually leads to heterogenous internal structures, increasing the risk for hydrogeotechnical and geochemical instabilities. Disposal optimization could improve the geotechnical stability of piles but are difficult to test at field scale. Discrete element methods are therefore used to investigate waste rock flow behaviour. The main challenge is, however, their calibration and extrapolation to field scale. A new calibration process was proposed and tested in this study based on laboratory repose angle tests and field natural repose angles. Calibrated models were then used to reproduce waste rock segregation, which was compared with laboratory and field measurements. Results indicated that numerical models calibrated using repose angle tests were able to reproduce waste rock segregation, and friction and rolling resistance coefficients were scale dependent.

Keywords: Waste rock segregation; Discrete element method (DEM); Model calibration; Model upscaling.

5.1 Introduction

Large volumes of waste rock are produced during mining activities, and are commonly disposed of in large piles that can exceed hundreds of meters in height and several square kilometers in area (Blight, 2010; McLemore et al., 2009; Aubertin, 2013; Bar et al., 2020). The particle size distribution (PSD) of waste rock is widely graded ranging from clayey particles to cobbles, boulders and meter-sized blocks (Morin et al., 1991; James et al., 2013). This widely ranged gradation usually leads to complex internal structure within waste rock piles during disposal (Molson et al., 2005; Anterrieu et al., 2010; Lahmira et al., 2016).

Waste rock piles are usually constructed with different methods mainly including end-dumping method, push-dumping method, free dumping method and drag-line spoiling method, which are selected depending on the topography, cost and transportation equipment (McLemore et al., 2009; Morin et al., 1991). End-dumping and push-dumping methods are mostly used because of their lower cost and higher efficiency compared to other methods (Burnley, 1993; Maknoon, 2016; Hawley, 2017).

Deposition of waste rock using end-dumping or push-dumping methods generally causes segregation: coarse blocks tend to move downward to the toe of the pile while fine particles remain closer to the deposition point and the crest of the pile (Nichol, 1986; Herasymuik et al., 2006). There are several mechanisms controlling segregation, such as rolling, sieving, percolation, and repose angle effects (Mosby et al., 1996; Jain et al., 2013). These mechanisms and their mutual influence mainly depend on the construction method and particle sizes (Jain et al., 2013; Džiugys et al., 2009; Zhou et al., 2016). In a waste rock pile, segregation is mainly related to rolling and sieving effects (Iverson, 1997; Cheng et al., 2019). Fine particles can indeed move through the voids between larger particles and sink down to the lower layer, while larger particles move faster and further in the upper layer with relatively higher velocity driven by gravity and fluid dynamics (Cheng et al., 2019; Dolgunin et al., 1995). The spatial variations of waste rock properties within piles can therefore present a high degree of heterogeneity. Consequently, the hydraulic conductivity may vary by several orders of magnitude, resulting in high degree variabilities of the water flow and water retention capacity within waste rock piles (Lahmira et al., 2017; Raymond et al., 2021; Maknoon et al., 2021). Large water fluxes favored

by the high permeability of waste rock may contribute to a rapid transport of contaminated water to the environment, bringing risks to the geochemical stability of waste rock piles in terms of acid mine drainage (AMD) (Broda et al., 2014; St-Arnault et al., 2020). But the heterogeneous structure of waste rock pile is complex to characterize in the field because of the difficulty to investigate large particles in steep slopes (Aubertin, 2013; Bar et al., 2020; Amos et al., 2015).

Discrete element method (DEM) provides an efficient way to overcome such limitations and to quantify the segregation of granular material by simulating simultaneously different mechanisms including rolling, sieving and percolation (Cheng et al., 2019; Su et al., 2019; Combarros et al., 2014; Cundall et al., 1979). DEM has been widely used to simulate granular behaviour subjected to large deformations and free boundaries in simulating granular material including rockfill (Jiang et al., 2018), soil-rock mixture (Fan et al., 2014; Xu et al., 2016) and waste rock (Thoeni et al., 2019; Zhu et al., 2019). The main challenges for the field application of DEM include the heavy calculation pressure, the representativity of simulated particles and the determination of input parameters (Ai et al., 2011; Roessler et al., 2019; Coetzee, 2016; Coetzee, 2020). The heavy calculation pressure is induced by the extremely large number of contacts, which significantly increase with the number of particles (Ferellec et al., 2008; Saeed et al., 2019). In practice, accounting for every particle involved and in particular for fine particles is computationally impractical (Thakur et al., 2016). An efficient way to maintain the representative of the model and speed up the calculation is therefore to remove the small particles in DEM simulations (Crosta et al., 2007; Utili et al., 2015). Using spheres to represent individual particles is also efficient to decrease the number of contacts, thus accelerating the calculations compared to irregular shapes (Su et al., 2019; Grima et al., 2011). But the representativeness of spheres to simulate irregular particles (such as waste rock blocks) is uncertain because spheres usually provide lower friction when compared to real granular material (Coetzee, 2016; Li et al., 2013). Incorporating a rolling resistance coefficient in DEM model can provide rolling effect so that the shape effect can indirectly be considered during particle flow (Ai et al., 2011; Iwashita et al., 1998). The input parameters in the DEM model, such as the friction coefficient and rolling resistance coefficient, need therefore to be calibrated using laboratory experiments or field tests so that the model can provide reliable results.

Different experimental approaches are used to calibrate numerical simulations such as rotating cylinders (Escotet-Espinoza et al., 2018), shear flows (Guo et al., 2012), repose angle tests (Frankowski et al., 2013) and self-designed experiments (Combarros et al., 2014). These calibration methods are mostly conducted at the laboratory scale with limited particle sizes and volumes (Roessler et al., 2019; Rackl et al., 2017). However, the representativeness of the calibration on laboratory experiments for field applications remains controversial considering the extremely large-scale difference and the particle volumes and sizes in the field. Although scaling down the system size or scaling up the size of particles can be used to somewhat overcome the scale effect (Feng et al., 2007; Bierwisch et al., 2009; Mio et al., 2009), the input parameters for large-scale simulations still need to be reinvestigated to make sure simulations provide reliable results, especially for the simulation of segregation during waste rock disposal in the field.

The objective of this study is therefore to propose, test and validate an easy and efficient method to calibrate numerical models to reliably simulate waste rock flow behaviour and characterize segregation during deposition. This new approach is based on the measurement of the repose angle, either in the laboratory using repose angle tests developed specifically for this purpose, and in the field using the natural repose angle measured on waste rock piles. Calibrated models are then used to reproduce waste rock segregation by comparing simulated segregation properties (e.g., characteristic diameters, segregation degree) with laboratory and field measurements. The sensitivity of the repose angle and segregation to input parameters is also assessed.

5.2 Methodology

5.2.1 Numerical simulation model

In this study, the flow behaviour of waste rock was simulated using Particle Flow Code 3D (PFC3D; Itasca, 2019). Waste rock was simulated as spheres of various diameters and using the rolling resistance linear (rrlinear) model which could account for the shape effect (Ai et al., 2011; Iwashita et al., 1998). Rolling resistance linear (often abbreviated as rrlinear) model (Figure 5.1) is a linear-based model except that the internal moment is implemented (Iwashita et al., 1998). The contact force in rrlinear model is composed of a linear force and a dashpot force that act in parallel and interact with one another (Ai et al., 2011).

The linear force, controlling linear elastic (no-tension) frictional behavior, is represented by linear springs with normal and shear stiffnesses, k_n and k_s (Itasca, 2019). The shear slider (slip) is accommodated by imposing a Coulomb limit on the shear force using the friction coefficient, μ. This friction coefficient describes the contact forces of two sliding surfaces and is calculated from the ratio of the tangential force to the normal force at contact surface (Just et al., 2013).

The dashpot force, controlling viscous behavior, is represented by dashpots with viscosity given in terms of the normal and shear critical-damping ratios, β_n and β_s (Itasca, 2019). No viscous behaviour was considered in this study (a typical simplification for waste rock, which is often considered cohesionless) and the dashpot force was therefore also neglected (i.e., $\beta_n = \beta_s = 0$).

Rolling resistance linear model (Figure 5.1) can indirectly consider particle shape effect as the rolling resistance also arises from the effect of non-spherical particles (Jiang et al., 2005). Rolling resistance coefficient (μ_r) is then introduced to represent the resistance to the movement of particles rolling on a surface (Iwashita et al., 1998). The rolling resistance moment (M) will be first incremented in rrlinear model with the accumulated relative rotation of the contacting pieces at the contact point (Ai et al., 2011). The updated rolling resistance moment can be expressed as (Itasca, 2019):

$$M' = M - k_r \Delta\theta \tag{5.1}$$

Where M': the updated rolling resistance moment (N·m); $\Delta\theta$: the relative rotation increment (-); k_r: the rolling resistance stiffness (N·m), which can be calculated by:

$$k_r = k_s R^2 \tag{5.2}$$

Where: k_s: the shear stiffness of the spring at the contact (N/m). R: the effective radius at the contact (m).

The contact effective radius R can be calculated by the radii of contact balls:

$$\frac{1}{R}=\frac{1}{R1}+\frac{1}{R2} \tag{5.3}$$

Where R1 and R2: the radii of the two contacted balls (m). R2 = ∞ if ball 1 contacts with walls (facets).

Rolling slip then starts when the rolling resistance moment (M) exceeds the limiting torque and this rolling resistance moment can be expressed as (Ai et al., 2011):

$$M = \mu_r R F_n^l \tag{5.4}$$

Where μ_r: the rolling resistance coefficient (-); F_n^l: the normal linear force (N).

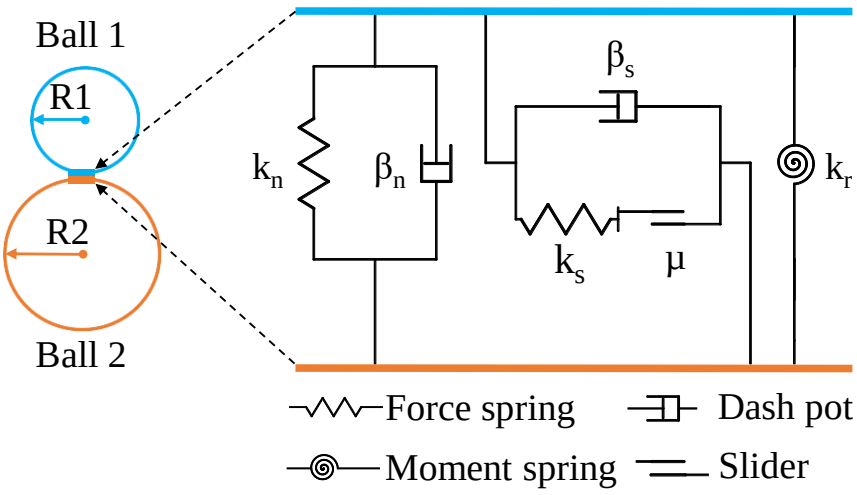

Figure 5.1: Interpretation of rolling resistance linear model. Normal and shear stiffness k_n and k_s, and friction coefficient μ control the linear force; normal and shear critical-damping ratios β_n and β_s control the dashpot force; rolling resistance stiffness k_r controls the rolling moment (see text for more details) (adapted from (Ai et al., 2011)).

Local damp (α) was applied to account for energy dissipation following particle impacts. Drop tests were conducted in the laboratory, where waste rock particles with a diameter of 0.1 m were dropped from an elevation of one meter. The test was repeated 20 times and the rebound height of waste rock (recorded using a camera) varied between 0.05 m and 0.2 m, with an average of around 0.1 m. The drop tests were then simulated using PFC3D and a local damp $\alpha = 0.4$ was found the most suitable to match the measured rebound height and was applied in the rest of the simulations presented below.

The effective modulus (E) was set to 1×10^6 Pa to maintain the system within the rigid limit while optimizing the calculation speed (Itasca, 2019); also see "Results analysis and discussion" section). The timestep (Δt) was determined automatically in PFC3D using the critical timestep, which was calculated based on the stiffnesses and masses of particles in the model (Itasca, 2019). The stiffness ratio $k^*(= k_n / k_s)$ was set to 2.5 as recommended by others (Itasca, 2019; Li et al., 2019). The friction coefficient (μ) and rolling resistance coefficient (μ_r) were considered the main parameters governing the flow behaviour of waste rock (Just et al., 2013; Santos et al., 2016) and were calibrated based on laboratory-scale and field measurements (see below). The main input parameters for model calibration were summarized in Table 5.1.

Table 5.1: Input parameters used for model calibrations.

Parameters	Laboratory model	Field model
Particle density, β (kg/m^3)	2760	2760
Particle number, N	30 000	135 000
Timestep, Δt (s)	[5 ×10 $^{-5}$; 1 × 10^{-3}]	[5 ×10 $^{-5}$; 1 × 10^{-3}]
Friction coefficient, μ	[0.1 ; 0.4]	[0.2 ; 0.8]
Rolling resistance coefficient, μ_r	[0.1 ; 0.4]	[0.2 ; 0.8]
Local damp, α	0.4	0.4
Effective modulus, E (Pa)	1 × 10^6	1 × 10^6
Stiffness ratio, k*	2.5	2.5
Normal critical damping ratio, β_n	0	0
Shear critical damping ratio, β_s	0	0

5.2.2 Calibration and validation of numerical models at laboratory scale

5.2.2.1 Sample preparation

Waste rock (around 1 t) was sampled from Canadian Malartic mine, an open-pit mine located in Abitibi-Témiscamingue, Quebec, Canada. The storage capacity of the waste rock pile is estimated to a total of 450 Mt corresponding to a volume of 230 Mm^3 (Lehouiller et al., 2020). The waste rock pile in Canadian Malartic mine was constructed with 10 m benches for a total height of around 100 m (Lehouiller et al., 2020).

Sampled waste rock was sent to the laboratory in barrels, where it was sieved (ASTM C136, 2019), homogenized (ASTM D6323-19, 2019) and characterized. Particles smaller than 8 mm were removed to reduce the calculation time because the number of contacts will significantly increase when more smaller particles are generated in PFC3D. Particles larger than 89 mm were also removed because of the operational limitations in the laboratory. The resulting PSD curve

(Lab0 in Figure 5.2) ranged from 8 mm to 89 mm and was considered the original gradation for repose angle and segregation tests (Figure 5.2). A total of 10 laboratory segregation tests were conducted and showed a good reproducibility (standard deviation < 4%). The coefficient of uniformity C_U (= D_{60} / D_{10}) and the coefficient of curvature C_C (= $(D_{30})^2$ / (D_{10} × D_{60})) were 3.5 and 0.9, respectively (D_x corresponding to x% passing). The specific gravity of the tested waste rock was around 2760 kg/m^3 (ASTM C127, 2015).

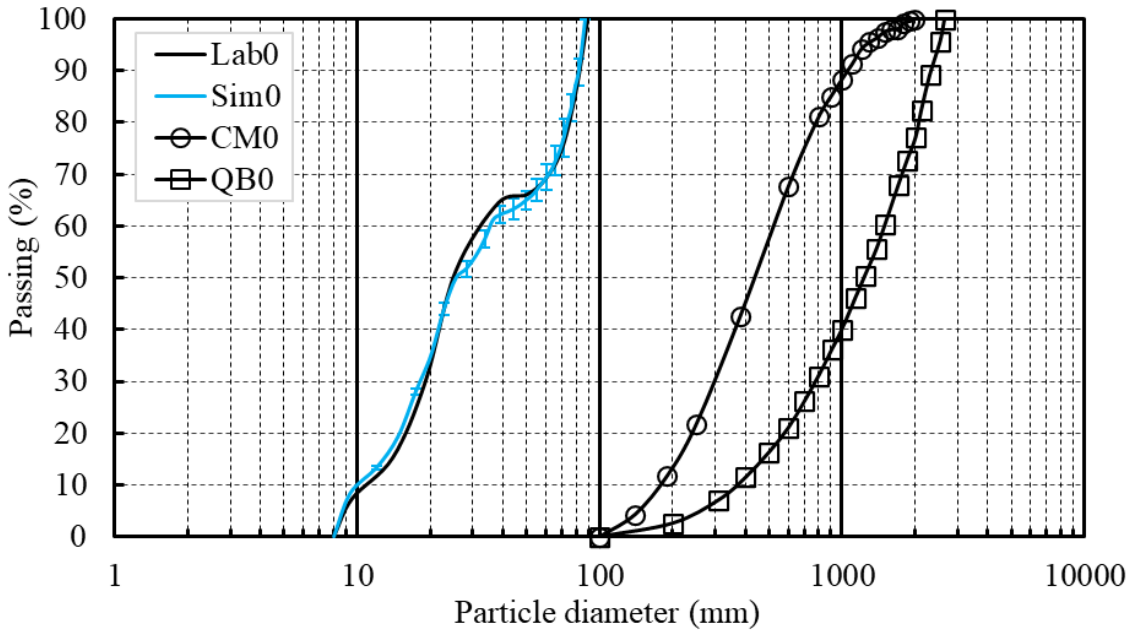

Figure 5.2: PSD curves for waste rocks used in laboratory tests (Lab0) and simulations (Sim0). Error bars indicate standard deviation. CM0 and QB0 were used for field simulations and correspond to Canadian Malartic and Quebrada Blanca mine sites, respectively.

5.2.2.2 Laboratory calibration - repose angle tests

Repose angle test is an easy and quick method with good repeatability (Frankowski et al., 2013; Richter et al., 2020) which can give an indication of the material flowability and is directly related to the intrinsic properties of particles such as the friction and rolling properties (Roessler et al., 2019; Al-Hashemi et al., 2018). Even though these tests do not reproduce exactly the way

waste rock is disposed of in the field (especially because of the limited waste rock amount and initial energy), they allow to back calculate material intrinsic properties (Zhou et al., 2022; Coetzee et al., 2010).

Around 75 kg of waste rock were placed in a 60 cm high and 35 cm diameter bucket, which was placed on the ground (Figure 5.3a). The bucket was quickly (< 1 s) lifted vertically so the waste rock formed a conic pile on the ground (Figure 5.3a). The repose angle of the pile (θ, Figure 5.3a) was determined by measuring the pile radius (R) and the pile height (H) using a ruler with a precision of 0.1 cm. The radius was defined as the distance from the center to the edge of the pile where no particles overlapped (although some individual particles could have moved outside this radius). Four values of the radius (R1 – R4, Figure 5.3b) were measured in four directions and four repose angles were obtained for each test. The test was repeated 10 times to ensure the repeatability of the measurement.

Numerical models were built to precisely simulate the repose angle tests (Figure 5.3, c and d). The same bucket dimension (Ø 35 cm × 60 cm) was built in PFC3D using wall elements. The same mass of waste rock as in the laboratory tests were generated using sphere particles. The target PSD curve was first input in PFC3D by defining the passing percentage of each size fraction in PSD curve Lab0 (Figure 5.2). The total target mass of waste rock particles was then obtained in the specified volume (i.e., bucket) by automatically generating particles with specified diameters representing each size fraction according to its mass proportion in the PSD curve. The simulated bucket was lifted with a velocity of 0.5 m/s (similar to that in the laboratory) and the simulations were stopped when all the particles stopped moving. The maximum height (H′, Figure 5.3c) of the simulated pile was estimated. Four radii (R1′ – R4′, Figure 5.3d) were determined in the four directions of the simulated pile in the same way as in the laboratory. Four simulated repose angles were obtained for each simulation, and the simulations were repeated 10 times.

Preliminary simulations showed that laboratory repose angles were more sensitive to friction and rolling resistance coefficients than field repose angles. For example, increasing μ from 0.4 to 0.6 increased the field repose angle by around 2° and the laboratory repose angle by around 4°. Consequently, an interval of 0.2 was chosen for field calibration and a smaller interval of 0.1 was selected for laboratory calibration. Friction coefficient (μ) and rolling resistance coefficient (μ_r)

were then calibrated with μ ranging between 0.1 – 0.4 and μ_r ranging between 0.1 – 0.4, with an interval of 0.1. Each pair of μ and μ_r was simulated 10 times with 10 different random seeds to account for PSD variability and evaluate model repeatability. Each simulation case was assigned a specified random seed ranging from 10001 to 10010. Different random seeds could change the initial relative positions of particles in a specific volume (i.e., different initial particles packing states) without significantly changing the accuracy of waste rock PSD (Itasca, 2019). The PSD curves of the generated waste rock with the ten random seeds were verified each time and the average PSD Sim0 (Figure 5.2) of the simulated waste rock indicated a good agreement with the laboratory PSD (Lab0 in Figure 5.2).

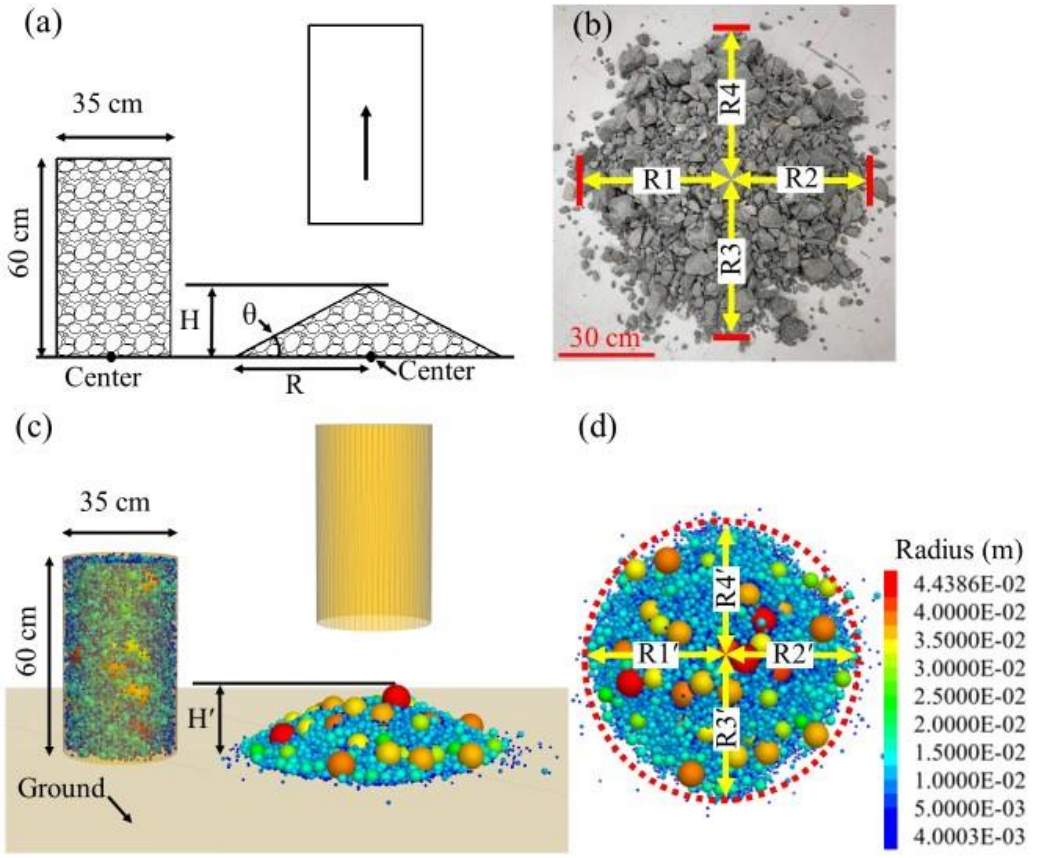

Figure 5.3: Repose angle tests for (a – b) experiments and (c – d) simulations. Particles in the simulations are colored based on their radii (smaller particles in blue and coarser particles in red).

5.2.2.3 Laboratory validation - segregation tests

Segregation tests were designed in this study to validate the calibrated model. Waste rock specimens were prepared according to the same PSD curve as used for repose angle tests (Lab0 in Figure 5.2). Around 20 kg of waste rock were filled in a 30 cm high and 27 cm diameter bucket. The bucket was lifted to the top of a 1 m high vertical wall and then inclined around 60° (Figure 5.4a). Ten buckets of waste rock were dumped sequentially. A semi-cone was formed, and segregation could be observed (Figure 5.4a). The cone was divided into 6 sections (Figure 5.4a) and the PSD curves of each section were measured using sieve analysis (ASTM C136, 2019). Segregation tests were repeated five times.

Segregation was evaluated by estimating the variation of the characteristic diameters (i.e., D_{10}, D_{50} and D_{80}), and determining the segregation degree (χ) in each section (Sutherland et al., 2003):

$$\chi = \frac{\log d_{tested} - \log d_0}{\log d_{CQ} - \log d_0} \tag{5.5}$$

Where $\log d_0$: the logarithmic mean particle size of the original waste rock before disposal, d was in mm in this study; $\log d_{tested}$: the logarithmic mean particle size of waste rock in the local section, and $\log d_{CQ}$ the logarithmic mean particle size of the coarsest quartile. The coarsest quartile represents the fraction of particles larger than the diameter D_{75} of the original gradation (Westland, 1988). The logarithmic mean particle size is often considered a representative parameter for delineating the PSD curve, and can be calculated as (Kenney et al., 1993):

$$\log d = \sum_{i=1}^{n} (P_i - P_{i-1}) \log \sqrt{D_i \cdot D_{i-1}} \tag{5.6}$$

Where D_I and D_{i-1} [L]: consecutive particle diameters corresponding to passing P_i and P_{i-1}.

Simulated segregation tests (Figure 5.4b) were conducted using friction and rolling resistance coefficients calibrated on repose angle tests (see previous section). Vertical and horizontal walls were simulated as supporting structures representing back wall and ground surface in laboratory

segregation tests. A cylinder shape was generated in the model with the same dimensions as the laboratory bucket (Ø 0.27 m × 0.3 m). The same waste rock mass (around 20 kg) was generated within the cylinder using spherical particles and the same PSD as waste rock in the laboratory. The bottom wall of the cylinder was removed at the beginning of the simulations so that waste rock could fall along the vertical wall, similarly to what was observed in the laboratory. The next bucket of waste rock was dumped when the previous waste rock particles stopped moving and a total of ten buckets of waste rock were dumped in one simulation. Simulations were repeated five times with different random seeds. The characteristic diameters (e.g., D_{10}, D_{50}, D_{80}) and segregation degree of the simulated waste rock from the top to the bottom sections (Figure 5.4a) were compared with the laboratory results.

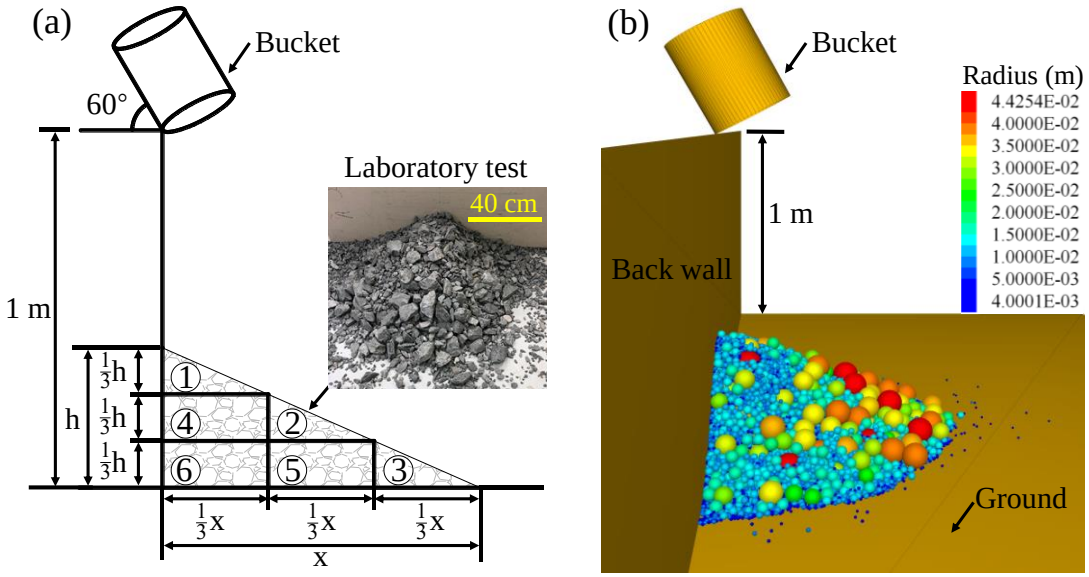

Figure 5.4: Segregation test in the (a) laboratory and (b) simulation. The pile was equally divided into three horizontal and three vertical sections.

5.2.3 Calibration and validation of numerical models at field scale

5.2.3.1 Field calibration – Repose angle tests

The same calibration approach, using repose angle, was also applied for simulating segregation in waste rock piles at field scale. Two waste rock piles were considered: Case 1: waste rock pile in Canadian Malartic mine was characterized by a repose angle of 37° ± 3° (Gervais et al., 2014); Case 2: waste rock pile in Quebrada Blanca mine was characterized by repose angles between 30° and 40°, with a reference repose angle of 37° ± 3° for the model calibration (Zhang et al., 2017).

The maximum particle diameter was 1.5 m at Canadian Malartic mine and 2.66 m in Quebrada Blanca mine (Figure 5.2). Particles smaller than 0.1 m accounted for less than 4.5% of the field PSD curves and were assumed to have a negligible effect on the flow behaviour in this study, so they were removed to decrease the particle number generated in PFC3D model and accelerate calculation speed. PSD curves QB0 and CM0 (Figure 5.2) were used to generate particles in simulations and used as original gradations for segregation degree calculation.

Simulated field repose angle tests (Figure 5.5) were conducted following a similar approach to laboratory tests described above. A wall was first generated as support structure and boundary to the model, and covered with one-meter diameter fixed balls (grey balls in Figure 5.5) to simulate waste rock surface so that dumped waste rock could directly interact with the existing waste rock. These grey balls were assigned the same properties (including contact model parameters; Table 5.1) as the waste rock particles dumped at the surface of the model. A larger cylinder (30 m high and 9 m diameter) was generated, filled with around 2500 t of waste rock, and placed on the base layer (Figure 5.5a). The cylinder was then rapidly lifted up, and a conic pile was formed. The repose angle was obtained by measuring the cone slope (Figure 5.5b).

The friction coefficient (μ) and rolling resistance coefficient (μ_r), both ranging between 0.2 and 0.8 with an interval of 0.2 for each parameter, were then calibrated to match the repose angle measured in the field for both Canadian Malartic and Quebrada Blanca mines. Other parameters, such as local damp, specific gravity, and effective modulus, were the same as in the laboratory model for Canadian Malartic mine. Considering their limited effect on segregation (Coetzee,

2020), these parameters were set the same for Quebrada Blanca mine. Simulations were repeated 5 times for each pair of μ and μ_r.

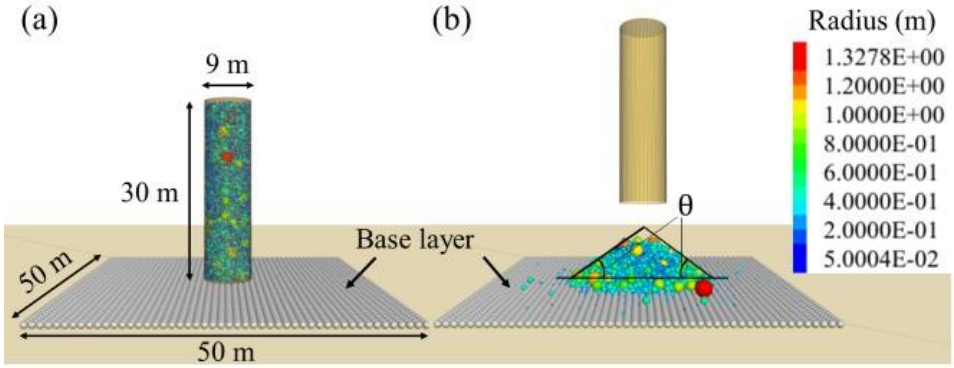

Figure 5.5: Field repose angle test simulations. Simulated (a) initial state and (b) waste rock cone after lifting the cylinder. Particles are colored based on their radii.

5.2.3.2 Field validation – Segregation investigation

Field segregation simulations were conducted following field disposal conditions with bench height of 10 m for Canadian Malartic mine and 20 m for Quebrada Blanca mine. However, despite the simplifications mentioned above (e.g., using balls instead of real shape particles or removing particles smaller than 0.1 m), simulations still contained 7×10^4 balls (with 3×10^5 contacts) and could take a very long time (up to several days). Simulating a whole waste rock pile was therefore not realistically feasible, and the following approach was proposed to simulate a simple yet realistic and flexible initial condition for field scale waste rock piles. An inclined wall was initially generated to simulate an already existing waste rock slope (from previous dumps) and reduce calculation time. The initial slope angle was slightly greater than the repose angle to prevent any influence on the results. This initial slope did not significantly affect the final result but contributed to decrease the number of dumps (and therefore the time required for the simulations) to reach this final state observed in the field. Similar to the function of the base layer in field repose angle test, a base layer was created with one-meter fixed balls (grey balls in

Figure 5.6) on the surface of the slope and the ground. The base layer was large enough to make sure all the waste rock particles finally stopped on it.

Waste rock was dumped from the top of the slope using end-dumping method. The end-dumping method was simulated in the models by dumping waste rock from an 8 m (width) × 8 m (length) × 4 m (height) box inclined by an angle of 45° to match the maximum lifting angle of haul trucks in practice. The vertical distance between the bottom of the box (i.e., haul truck) and the waste rock pile surface was 1.5 m, that is very similar to the 1 to 2 m observed in practice (Gervais et al., 2014). Around 300 t of waste rock were generated within the cubic box and dumped by deleting the bottom wall of the box (green wall in Figure 5.6). Waste rock could then fall out of the box and move along the slope, creating a new slope. The same dumping process was repeated for the next dump (after waste rock particles in the previous dump stopped moving). A total of 3 dumps (for Canadian Malartic mine) and 30 dumps (for Quebrada Blanca mine) were simulated and simulations were repeated five times for each case with different random seeds.

The simulated PSD curves, grading characteristic diameters (e.g., D_{10}, D_{50}, and D_{80}) and segregation degree (χ) were then determined for each section of the slope and compared with field measurements. These sections were set in the same way to the field measurements. The field observation results of Canadian Malartic mine in chapter 4 were used for comparison. The slope of a 10 m high bench was vertically divided into 3 sections (i.e., top, middle and bottom sections) for Canadian Malartic mine. The 20 m high pile at Quebrada Blanca mine was divided into 9 sections in the literature (Zhang et al., 2017), but five sections were selected for comparison in this study: sections 1 to 5 corresponded to distances of 6 m, 14 m, 22 m, 30 m, and 34 m to the pile top along the slope.

In summary, the proposed calibration method consists in material characterization, model calibration and validation by reproducing waste rock repose angle and segregation (Figure 5.7). The main calibrated parameters are the friction coefficient (μ) and the rolling friction coefficient (μ_r) which are adjusted to match the measured repose angle (either from repose angle tests in the laboratory or natural repose angle in the field). Several pairs of μ and μ_r can provide the target repose angle but taking μ equal to μ_r is recommended to well reproduce waste rock flow behaviour. Calibrated models can then be used to simulate waste rock segregation at both laboratory and field scales. This calibration method is only valid for material with a given PSD.

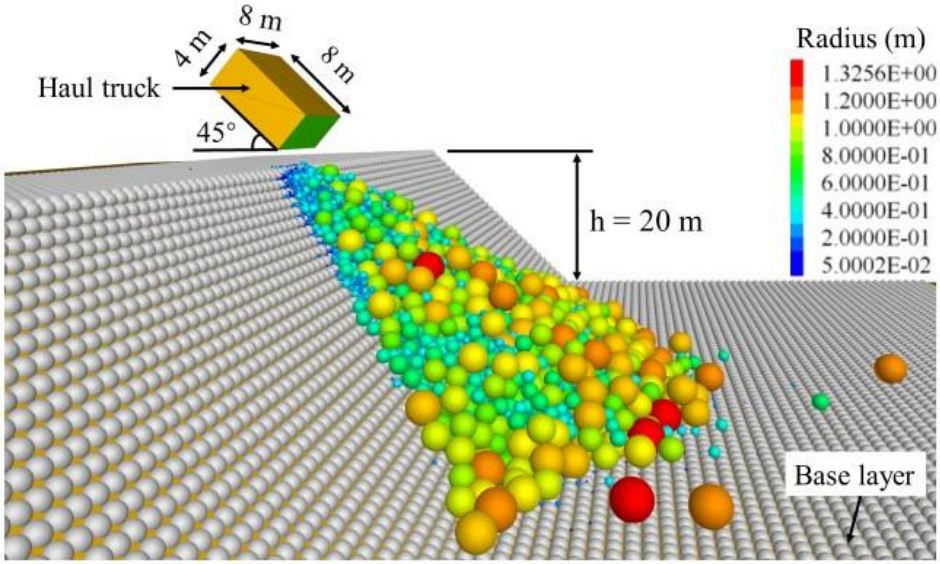

Figure 5.6: Simulation of waste rock disposal for Quebrada Blanca mine using end-dumping method. The same conditions were used for Canadian Malartic mine except the bench height was 10 m.

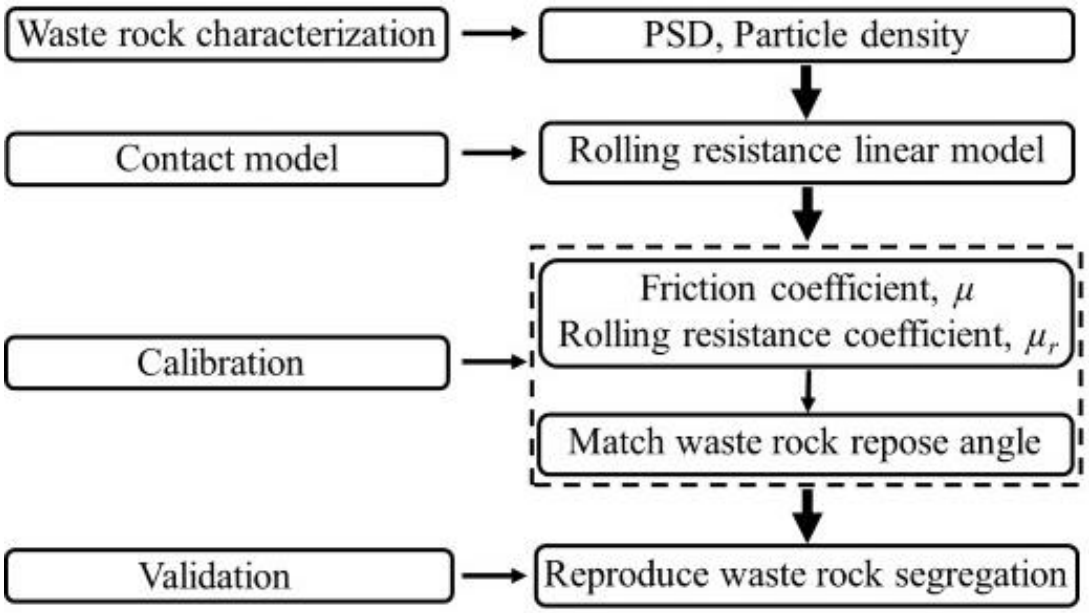

Figure 5.7: Approach proposed to calibrate numerical simulations.

5.3 Results

5.3.1 Repose angle and segregation of waste rock at laboratory scale

5.3.1.1 Measured and simulated repose angle at laboratory scale

Ten repose angle tests were carried out in the laboratory using waste rock from Canadian Malartic mine with a maximum particle diameter of 89 mm (Figure 5.2). The repose angle was measured 4 times for each test with a precision of 0.1°. Measured minimum and maximum repose angles were 23.8° and 28°, respectively, with an average of 25.4° ± 1.5° (see details in Appendix B).

The repose angle of tested waste rock was simulated using PFC3D for various friction coefficients (μ) and rolling resistance coefficients (μ_r) and compared with laboratory results. Each simulation was repeated ten times with various random seeds (see above for details), but simulated repose angles were usually very close with a standard deviation of 1.3° in average and which never exceeded 2.1°. Simulated repose angle was very sensitive to the choice of friction and rolling resistance coefficients. However, several pairs of parameters could lead to the same repose angle, so a contour map was developed, based on 160 simulations carried out for 16 pairs of friction and rolling resistance coefficients varying between 0.1 and 0.4 (Figure 5.8). The repose angle from each pair was an average of 10 values and the rest of the map was obtained by linear interpolation.

Previous research has shown that taking μ equal to μ_r was usually giving a good approximation of real flow behaviour of cohesionless material (Aela et al., 2022; Roessler et al., 2018). The same approach was therefore used in this study to determine $\mu = \mu_r = 0.2$ and calibrate the model on the repose angle test results. Simulations with calibrated friction and rolling resistance coefficients were repeated ten times with different random seeds and the average simulated repose angle was 25.2° ± 1.5°, which was very close to the average measured repose angle of 25.4° ± 1.5° (green line in Figure 5.8). The repose angle of 25.4° measured in the laboratory test was shown in green colour. Calibrated model therefore provided good agreement with laboratory results, despite the natural variability of waste rock particle sizes.

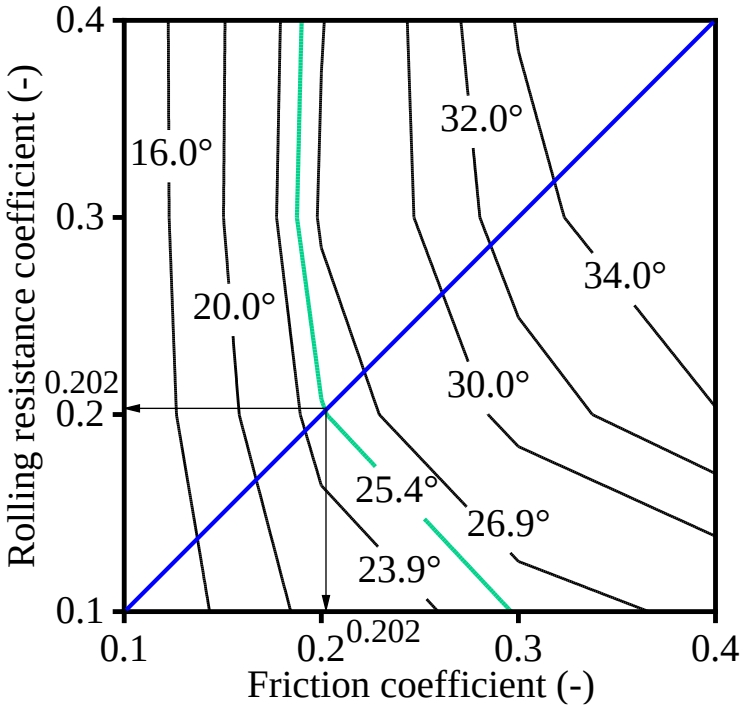

Figure 5.8: Contour of repose angles as a function of friction coefficient (μ) and rolling resistance coefficient μ_r for waste rock in the laboratory. The green line indicates the pairs of μ and μ_r matching the measured repose angle of 25.4°. The blue line indicates the 1:1 line (i.e., $\mu = \mu_r$).

5.3.1.2 Measured and simulated segregation at laboratory scale

Segregation at laboratory scale was evaluated by comparing the PSD curves in the top (section 1 in Figure 5.4a), middle (section 2) and bottom (section 3) of the small-scale waste rock pile. The segregation test was repeated 5 times and the resulting PSD curves for each section were very close, thus indicating good repeatability (see details in Appendix C). Standard deviation of passing percentage was smaller than 5% in the middle and bottom sections (Figure 5.9, b – c), but was slightly greater (up to 9%) in the top section (Figure 5.9a). Apparent particle segregation was observed during laboratory tests, with a large number of coarse particles moving down to the bottom section of the slope, while finer particles tended to accumulate closer to the top. As a consequence, the proportion of particles with diameters smaller than a given value tended to increase from the top to the bottom of the slope (Figures 5.9 and 5.10). For example, measured D_{50} increased from 26.3 mm ± 4 mm in the top section to 59 mm ± 4.1 mm in the bottom section,

increasing by about 125% (Figure 5.10). Measured D_{10} also increased from 12 mm ± 1 mm in the top section to 15.2 mm ± 1.1 mm in the bottom section, increasing by about 27%.

Segregation degree (equation 5.5) was − 0.02 in the top section (indicating that the material was finer than the original waste rock), 0.18 in the middle section and 0.35 in the bottom section (i.e., material in the bottom section was significantly coarser than original waste rock) (Figure 5.10d). The standard deviation of the segregation degree was smaller than 0.07 in the middle and bottom sections, but was slightly greater (i.e., 0.14) in the top section.

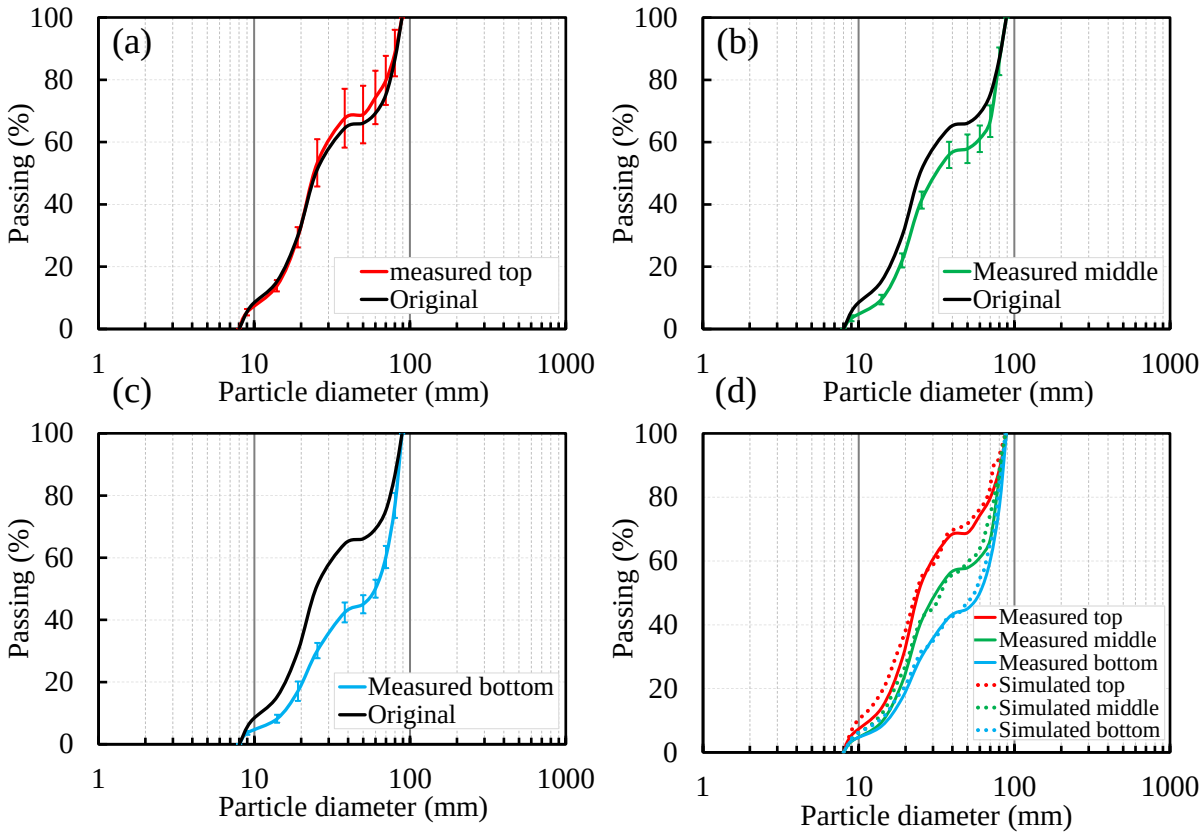

Figure 5.9: PSD curves of (a) top section, (b) middle section, and (c) bottom section measured in laboratory segregation tests. (d): Simulated and measured mean PSD curves for each section. The original PSD curve (black line) is shown for comparison. Error bars indicate standard deviation.

Segregation tests in the laboratory were simulated using PFC3D. The simulated PSD curves in the top, middle and bottom of the slope generally matched well the measured PSD curves (Figure 5.9d). As a reminder, material properties (and in particular friction and rolling resistance coefficients) were directly obtained from the calibration of repose angle tests, and applied to the segregation test models. The simulated characteristic diameters increased from the top to the bottom section, in a similar manner than laboratory results (Figure 5.10, a – c). For example, the simulated D_{50} was 55.4 mm ± 5.9 mm in the bottom section, which was very close to the measured 59 mm ± 4.1 mm. In general, the difference between simulated and measured D_{50} was smaller than 3.7 mm in the three sections. The difference between simulated and measured D_{10} was always smaller than 1.9 mm in the three sections. The simulated segregation degree in the top section was − 0.07 ± 0.06, which was relatively close to the value obtained in the laboratory (− 0.02 ± 0.14) and also indicated that the material in the top section was finer than the original waste rock (Figure 5.10d). Simulated segregation degree in the middle and bottom sections was 0.16 ± 0.08 and 0.33 ± 0.04, respectively, both showing very good agreement (i.e., less than 0.05 difference) with the laboratory tested results (0.18 ± 0.07 and 0.35 ± 0.06, respectively).

Overall, simulated segregation tests with parameters calibrated on repose angle tests showed a good agreement with the experimental segregation results, indicating that repose angle tests could be used to calibrate the simulation models for field waste rock segregation investigation, at least at laboratory scale.

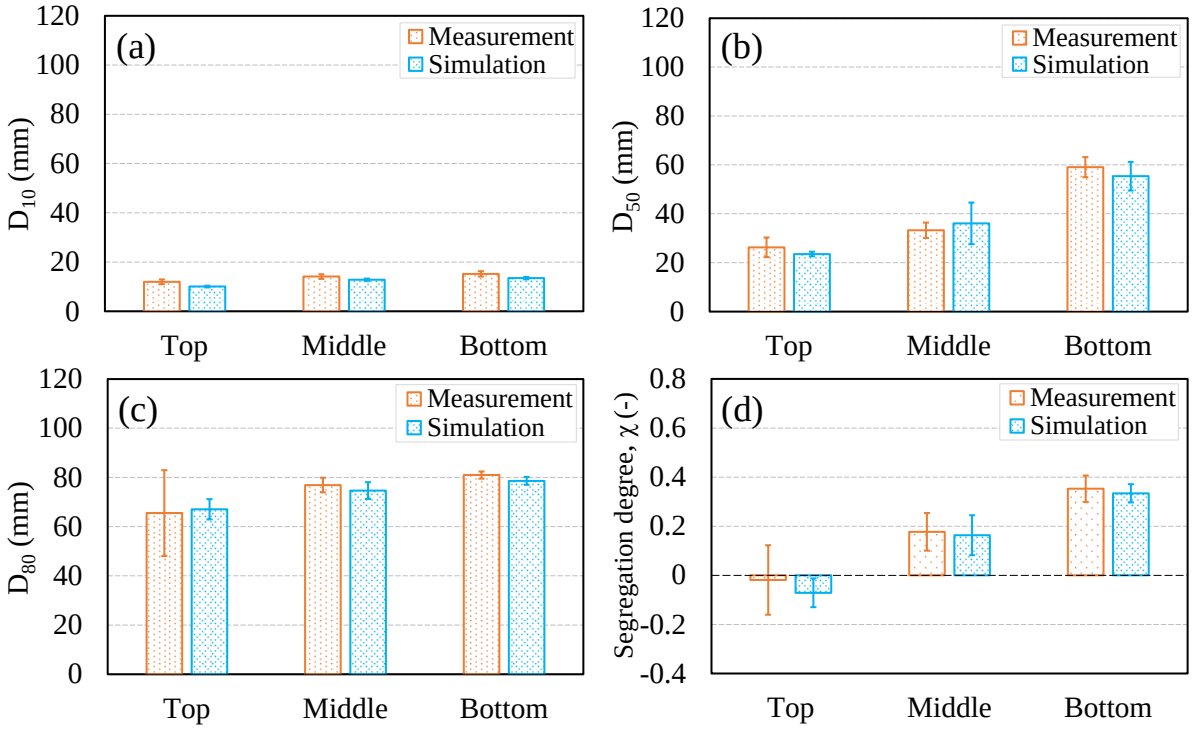

Figure 5.10: Measured and simulated (a – c) characteristic diameters (D_{10}, D_{50}, D_{80}) and (d) segregation degree in the top, middle and bottom sections of waste rock slope from laboratory segregation tests. Error bars indicate the standard deviation.

5.3.2 Field repose angle and segregation simulations

5.3.2.1 Repose angles in the field

Waste rock natural repose angles measured in the field were used to calibrate models for Canadian Malartic mine and Quebrada Blanca mine. Friction coefficients (μ) and rolling resistance coefficients (μ_r) were varied between 0.2 – 0.8 (Figure 5.11). Each simulation was repeated five times with various random seeds.

Simulated repose angles were usually very close with a standard deviation that never exceeded 2.7°. Similar to laboratory repose angle tests, several pairs of parameters could match the reference natural repose angle (i.e., 37° ± 3°, green line in Figure 5.11) and it was assumed that μ = μ_r. The natural repose angle of 37° measured in the field was shown in green colour.

Calibration indicated that $\mu = \mu_r = 0.44$ for Canadian Malartic waste rock and $\mu = \mu_r = 0.47$ for Quebrada Blanca waste rock. Calibrated repose angle simulations were then repeated ten times for each case to validate the precision of the calibration. The average simulated repose angle was $37.4° \pm 1.6°$ for Canadian Malartic mine and $37.3° \pm 1.2°$ for Quebrada Blanca mine. The difference between simulated repose angles and reference natural repose angle being smaller than 0.4°, i.e., less than 1%, calibrated models were deemed to reproduce well repose angle observed in the field.

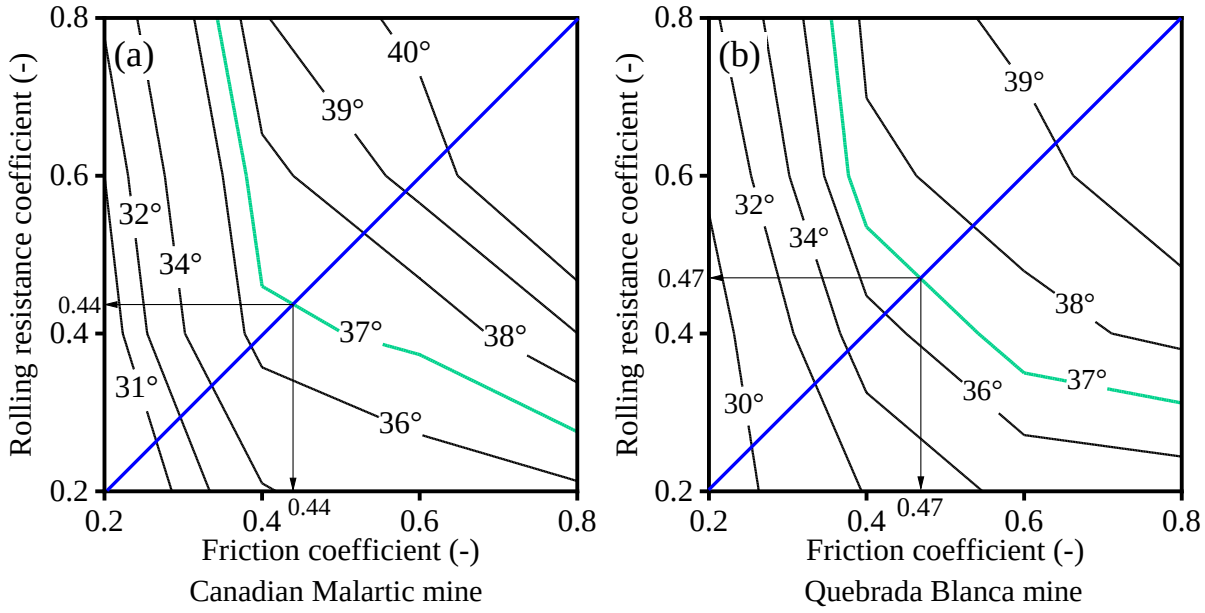

Figure 5.11: Contour of repose angles as a function of μ and μ_r for waste rock in the field. The green line indicates the pairs of μ and μ_r matching the field natural repose angle of 37°. The blue line indicates the 1:1 line (i.e., $\mu = \mu_r$).

5.3.2.2 Segregation of waste rock in the field

The segregation along the slope of a waste rock pile at Canadian Malartic mine was characterized by analyzing waste rock PSD curves from 42 images using image analysis. The increase of characteristic diameters (i.e., D_{10}, D_{50}, D_{80}) and segregation degree indicated significant segregation along the slope (Figure 5.13). For example, the measured segregation degree was

-0.58 ± 0.27 in the top section, -0.26 ± 0.17 in the middle section and 0.27 ± 0.12 in the bottom section. Also, the measured D_{50} increased from $0.26\,m \pm 0.09\,m$ in the top section to $0.56\,m \pm 0.14\,m$ in the bottom section, increasing by about 113%.

The simulated PSD curves in each section indicated good repeatability, and the maximum standard deviation of the passing percentage was less than 2.9% (Figure 5.12). The simulated PSD curve generally matched well the measured PSD curve in each section (Figure 5.12), thus showing similar apparent particle segregation from the top to the bottom of the pile (Figure 5.13, a – c). For example, the simulated D_{50} increased from $0.3\,m \pm 0.01\,m$ in the top section to $0.58\,m \pm 0.01\,m$ in the bottom section, i.e., an increase by about 96%. The difference between simulated and measured D_{50} was therefore smaller than $0.03\,m$ in the three sections (Figure 5.13b). The difference between simulated and measured D_{10} was always smaller than $0.03\,m$ (Figure 5.13a). The simulated segregation degree in the top section was -0.43 ± 0.04, and slightly greater than the measured -0.58 ± 0.27 (Figure 5.13d), showing that the simulations somewhat underestimated the quantity of fines close to the crest. The segregation degree in the middle and bottom sections were -0.31 ± 0.04 and 0.31 ± 0.02, respectively, showing good agreements (i.e., less than 0.05 difference) with the field measurements (-0.26 ± 0.17 and 0.27 ± 0.12, respectively)

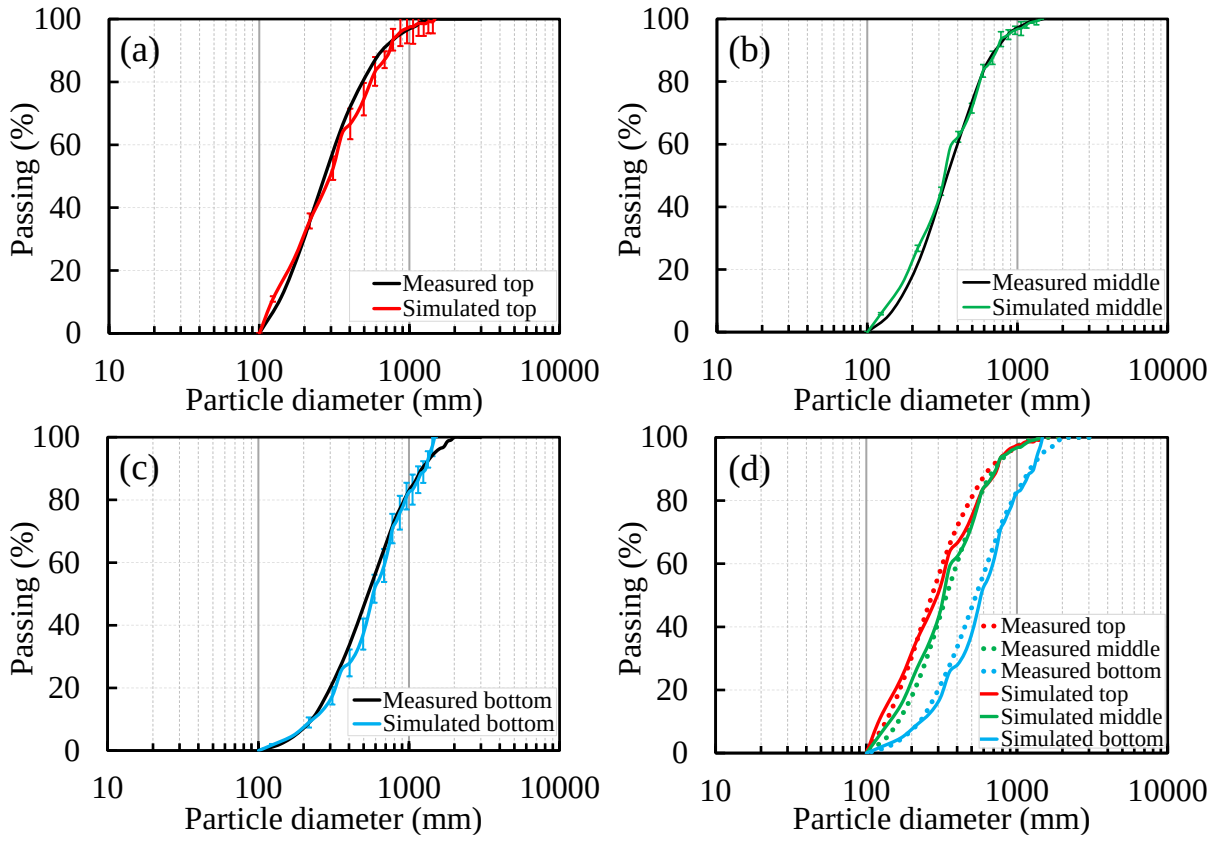

Figure 5.12: Simulated and measured PSD curves of (a) top section, (b) middle section, (c) bottom section, and (d) simulated and measured PSD mean curves for each section in Canadian Malartic mine waste rock pile. Error bars indicate standard deviation.

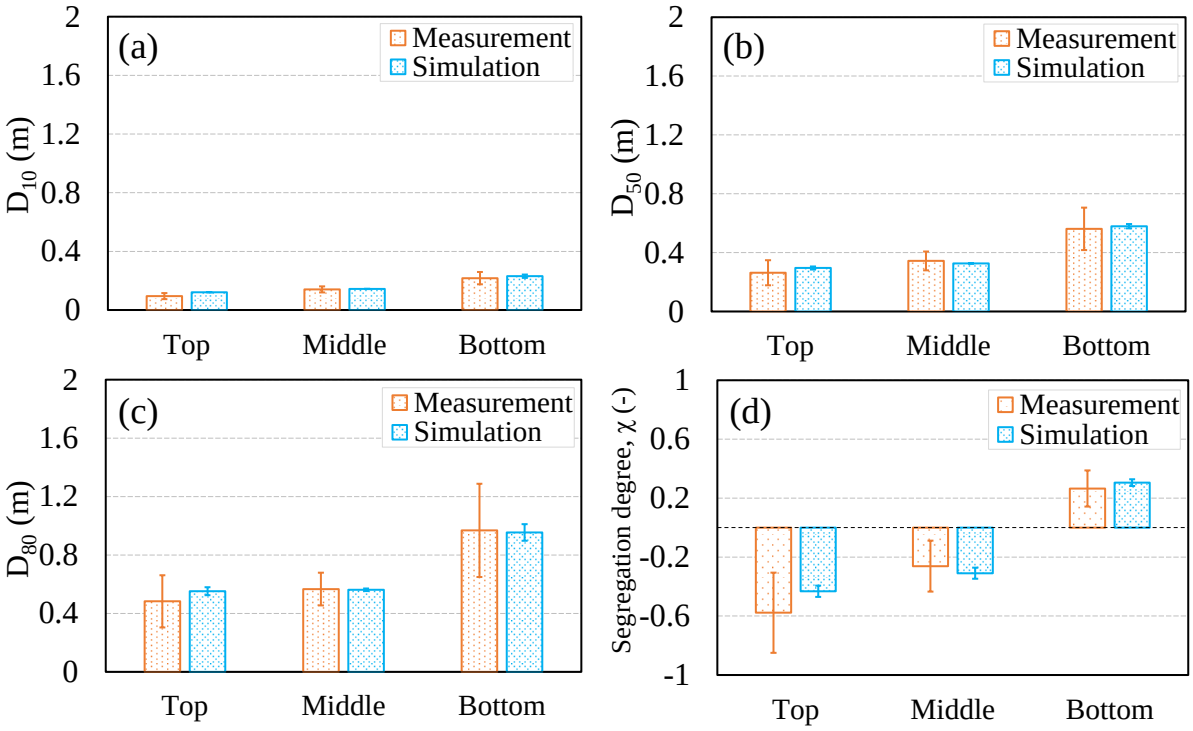

Figure 5.13: Measured and simulated (a – c) characteristic diameters (D_{10}, D_{50}, D_{80}), and (d) segregation degree in the top, middle and bottom sections of the slope of a waste rock pile at Canadian Malartic mine. Error bars indicate standard deviation.

The segregation along the pile slope at Quebrada Blanca mine was characterized by analyzing waste rock PSD curves from 10 images using image analysis. Significant segregation was also observed along the slope (Figure 5.14). For example, measured D_{50} increased from 0.72 m ± 0.14 m in the top section to 1.43 m ± 0.41 m in the bottom section, increasing by about 99%. Measured D_{80} increased from 1.29 m ± 0.14 m in the top section to 2.3 m ± 0.39 m in the bottom section, increasing by about 78%.

The simulated PSD curves generally showed good agreement with the measured PSD curves (Figure 5.14, a – e). The simulated characteristic diameters increased from the top (section 1) to the bottom (section 5) of the pile, in a similar manner than the field measurements. For example, the simulated D_{50} slightly increased from 1.05 m ± 0.27 m in section 1 to 1.8 m ± 0.05 m in section 5. In general, the difference between simulated and measured D_{50} was smaller than 0.37 m for all the five sections. The difference between simulated and measured D_{80} was always

smaller than 0.19 m (10%) in sections 2 – 4, but slightly greater (up to 0.5 m) in section 1 (top). Similar results were obtained for D_{10}.

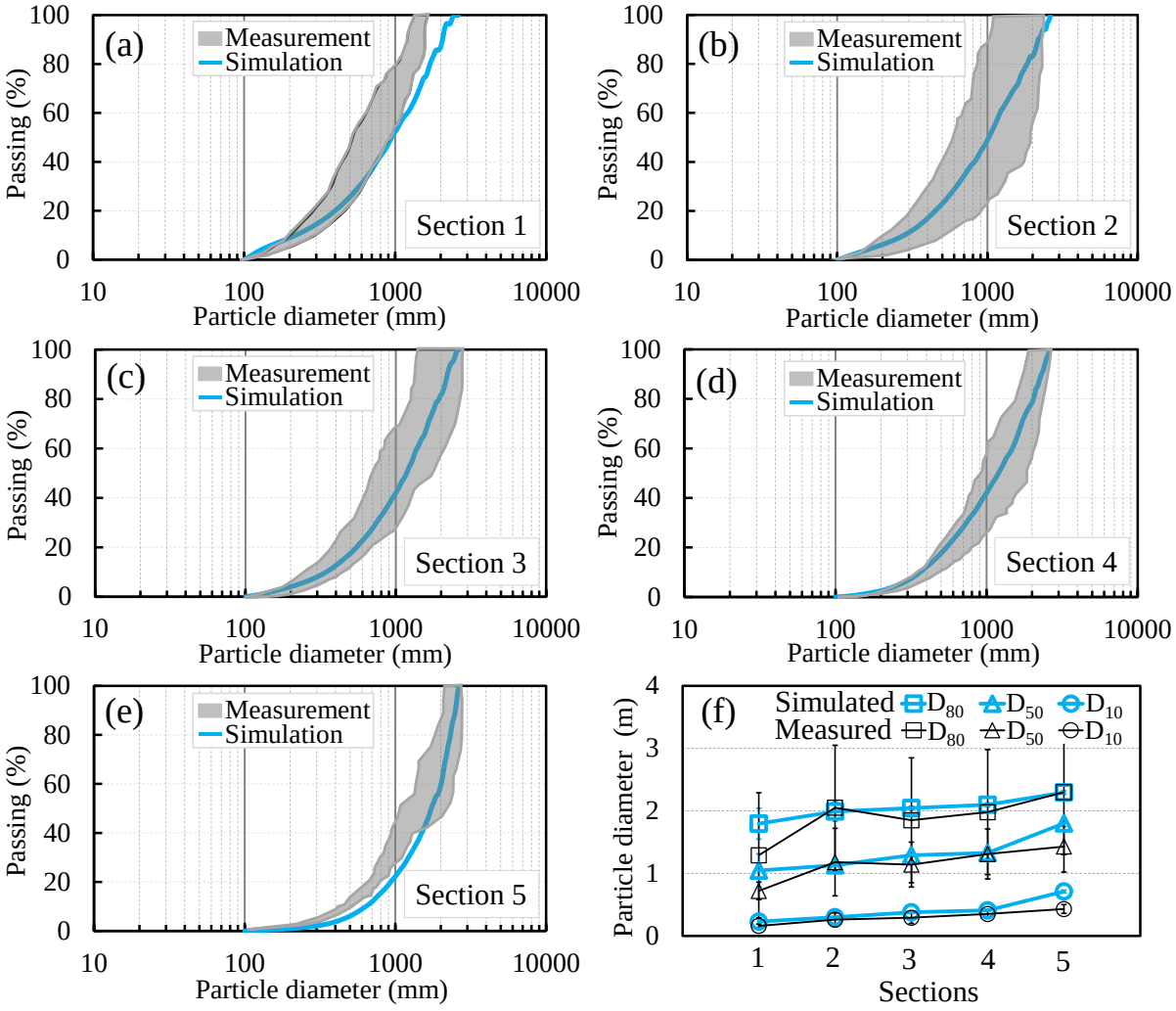

Figure 5.14: Gradation characterization of waste rock along the slope in Quebrada Blanca mine. (a – e): The PSD curves from section 1 (top) to section 5 (bottom). (f): Simulated (in blue) and measured (in black) D_{80}, D_{50} and D_{10} in the 5 sections. Error bars indicate standard deviation.

5.4 Results analysis and discussion

A new calibration method was proposed and tested to simulate the flow behaviour of waste rock using PFC3D. Usually, calibrating discrete element models to simulate waste rock (or more generally rockfill material) can be difficult because of the large volumes considered and the material irregular shapes (Coetzee, 2020). In this study, however, models were calibrated to reproduce repose angle measured in the laboratory and in the field by adjusting both friction coefficient (μ) and rolling resistance coefficient (μ_r). Calibrated parameters were then used to simulate segregation and models showed very good agreement with laboratory and field measurements. The method was also verified for two relatively different types of waste rocks.

This new calibration approach is relatively simple because it only requires measuring the natural repose angle. Also, only two parameters were adjusted during the calibration process, namely the friction coefficient (μ) and the rolling resistance coefficient (μ_r), which limits the number of parameters to test. Results showed, however, that these two coefficients varied with the PSD and in particular with the maximum particle diameter (as the repose angle does). In other words, laboratory tests cannot be used to determine the friction and rolling resistance coefficient for field applications, and they need to be calibrated specifically for each case. Nevertheless, laboratory and field simulations have shown that the proposed calibration method was applicable both at small and large scales.

However, the calibration approach proposed here also implied some hypotheses regarding the choice of μ, μ_r, local damp and effective modulus, and their effect on the repose angle and segregation are discussed in more details below.

5.4.1 Effect of friction coefficient and rolling resistance coefficient

Calibration mainly focused on the determination of friction coefficient (μ) and rolling resistance coefficient (μ_r), which are considered the main parameters governing the flow behaviour of simulated waste rock (and coarse particles in general; (Ucgul et al., 2014). These two parameters could contribute to give sphere particles a similar behaviour to elongated particles (Coetzee, 2020), which would otherwise be too demanding to simulate in terms of calculation time (Katterfeld et al., 2017). However, calibrating one measurement (repose angle) using two

parameters (friction and rolling resistance coefficients) results in an infinity of solutions (). The approach proposed in this study suggested to choose two coefficients that were equal, as also recommended by Roessler et al. (Roessler et al., 2018). In fact, the friction coefficient and rolling resistance coefficient are not completely independent (Derakhshani et al., 2015). For example, choosing a low friction coefficient (e.g., $\mu < 0.2$) significantly constrains the model which can become more or less independent of the rolling resistance coefficient. However, under a higher friction coefficient around 0.3 to 0.4, the repose angle significantly increased by 7° when rolling resistance coefficient increased from 0.1 to 0.4. Previous research showed similar results, and in particular that the repose angle was insensitive to the change of the rolling resistance coefficient when the friction coefficient was smaller than the rolling resistance coefficient (i.e., $\mu < \mu_r$) (Wensrich et al., 2012; Yan et al., 2015). Such observations may indicate that the calibration process could be reduced to the determination of only one parameter. However, this may be unrealistic because DEM simulations are controlled by different parameters that account for different mechanisms such as rolling resistance coefficient for rolling effect, especially when spheres are used to simulate irregular particles (Coetzee, 2016; Rackl et al., 2017; Cleary et al., 2002). This study therefore proposed to choose $\mu = \mu_r$ which corresponds more or less to the range of values where the models are the most sensitive to the input parameters.

Parameters $\mu = \mu_r = 0.2$ were calibrated for waste rock with a maximum particle diameter of 89 mm in the laboratory, and $\mu = \mu_r = 0.44$ for waste rock with a maximum particle diameter of 1.5 m in the field, although the waste rock was from the same mine (Canadian Malartic mine). In other words, calibrated parameters are scale dependent and cannot be directly extrapolated. This could be explained by the fact that increasing rolling resistance coefficient can increase resistance force to the rotational motion of spheres, which can then consume more kinetic energy and stop the rotation faster, resulting in a higher pile with steeper slopes (Katterfeld et al., 2017; Yan et al., 2015), and that this phenomenon is not linearly linked with particle maximum diameter. Similarly, friction coefficient governs the translational motion of particles, and a higher friction coefficient can tolerate more elastic deformation in the tangential direction and increase contact stability (Cleary et al., 2002). As a consequence, greater particle sizes induce a decrease of the total sliding friction force and rolling torque and therefore a decrease of the repose angle (Ucgul et al., 2014; Yan et al., 2015). In other words, larger particle sizes require higher friction

coefficient and rolling resistance coefficient to maintain a steeper slope angle. Based on the results presented in this study, a relationship between the friction coefficient (μ), the rolling resistance coefficient (μ_r) and the maximum particle size (D_{max}) was investigated. However, it was not possible to determine if the relation was linear or exponential because of the significant gap between maximum particle diameter in the laboratory (D_{max} = 89 mm) and in the field (D_{max} > 1 m). More studies on materials with intermediate particle size are therefore recommended to propose a predictive function for the friction and rolling resistance coefficients.

Another typical risk of model calibration is to over-constrain the simulations which then always provide the same results, independently of the input parameters (Crouzal et al., 2021). This was investigated by testing the effect of other friction and rolling resistance coefficients on segregation simulation results. These simulations were conducted using a maximum rolling resistance coefficient of 0.4 (case L1) for the laboratory and 0.8 (case F1) for the field, and a maximum friction coefficient of 0.3 (case L2) for the laboratory and 0.8 (case F2) for the field (Figure 5.15). Although cases L1 and L2 matched the measured repose angle (i.e., 25.4°), the segregation didn't match well the segregations measured in the laboratory (Figure 5.15a). For example, the segregation degree with a high rolling resistance coefficient 0.4 (L1) was 0.29 in the middle section of the pile, which was 62% greater than the measured value of 0.18. Also, the segregation degree with a high friction coefficient 0.3 (L2) in the middle section was 75% smaller than the measurement. In other words, segregation simulations at laboratory scale were highly sensitive to friction and rolling resistance coefficients. However, for the field cases, a high rolling resistance coefficient (= 0.8; case F1) or a high friction coefficient (= 0.8; case F2) resulting in a repose angle of 37° still produced similar results to the segregation observed in the field (Figure 5.15b). For example, for the two cases F1 and F2, the maximum difference between the simulated and measured segregation degree was 0.1 (about 17%), which was smaller than one standard deviation. These results indicated that field segregation simulations were not very sensitive to friction coefficient and rolling resistance coefficients as long as the repose angle was correctly simulated. They also confirmed that the friction and rolling resistance coefficients calibrated at laboratory scale could not be directly applied to field-scale models.

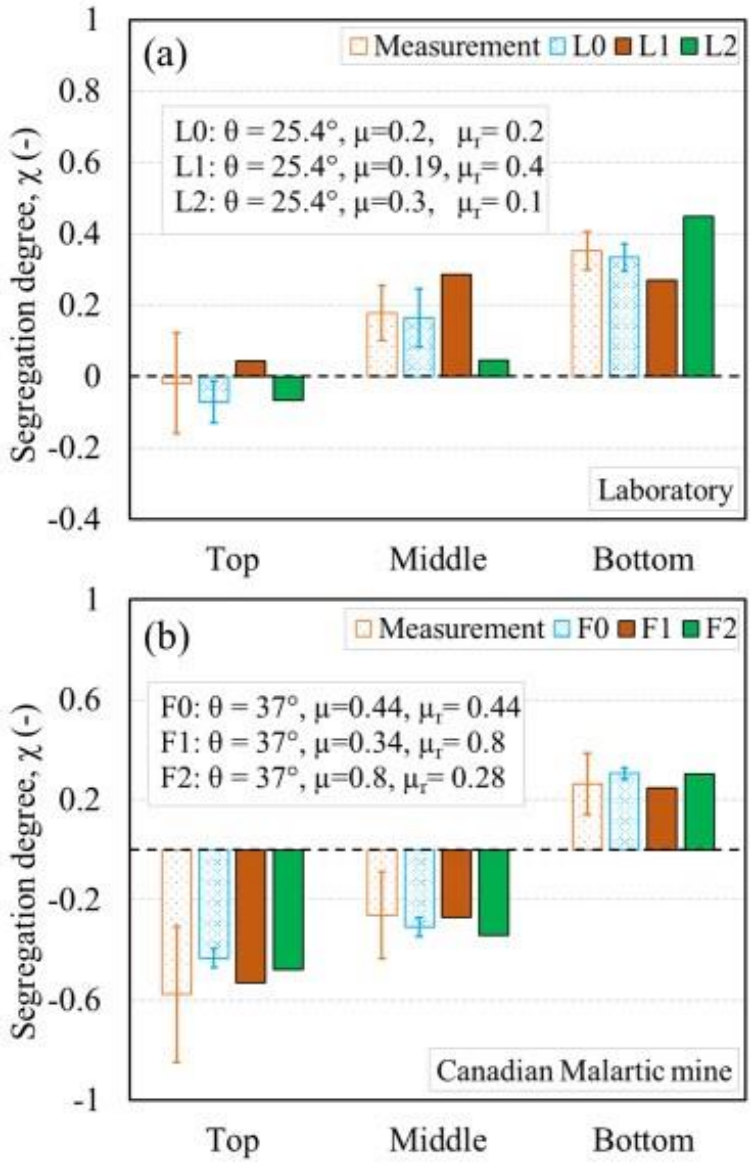

Figure 5.15: Segregation degree with different pairs of μ and μ_r in (a) laboratory and (b) field models for Canadian Malartic mine. θ indicates the repose angle. Error bars indicate standard deviation.

5.4.2 Effect of local damp

The local damp (α = 0.4) in this study was calibrated using laboratory drop tests (see above). Its value is generally comprised between 0.15 and 0.7 (Yan et al., 2015; Sadek et al., 2014; Simons

et al., 2015). However, laboratory calibration was based on only small diameter waste rock particles, so the effect of local damp was investigated for 10 m high bench by varying its value between 0.2 and 0.8. The simulations were conducted using the calibrated friction and rolling resistance coefficients ($\mu = \mu_r = 0.44$), with all the other parameters remaining the same as in the models presented above. The resulting repose angles ranged between 36.6° and 37.8° with a maximum standard deviation of 3.2° (Figure 5.16a), indicating little effect of local damp on repose angles. In fact, previous research also indicated that local damp ($\alpha = [0.1 ; 0.8]$) had little effect on the repose angle of granular material (Kashizadeh et al., 2020).

A local damp 0.2 produced similar segregation (i.e., -0.59 ± 0.03) in the top section than measurements but significantly less segregation in the bottom section where the segregation degree was 44% smaller than the measured value of 0.27 ± 0.12 (Figure 5.16b). However, local damp between 0.4 and 0.8 produced similar segregation degree along the entire slope, and no significant differences were observed in the top nor the bottom sections. For example, segregation degrees were around 0.3 in the bottom section for all simulations, independently on the local damp value. These results indicated that a local damp smaller than 0.2 could lead to an underestimation of segregation, while local damp greater than 0.4 and 0.8 have limited effect on the simulations in this study. Although no similar research on the effect of local damp on segregation was reported in the literature, some indicated that local damp had little effect on the flow behaviour of coarse materials (Just et al., 2013; Santos et al., 2016).

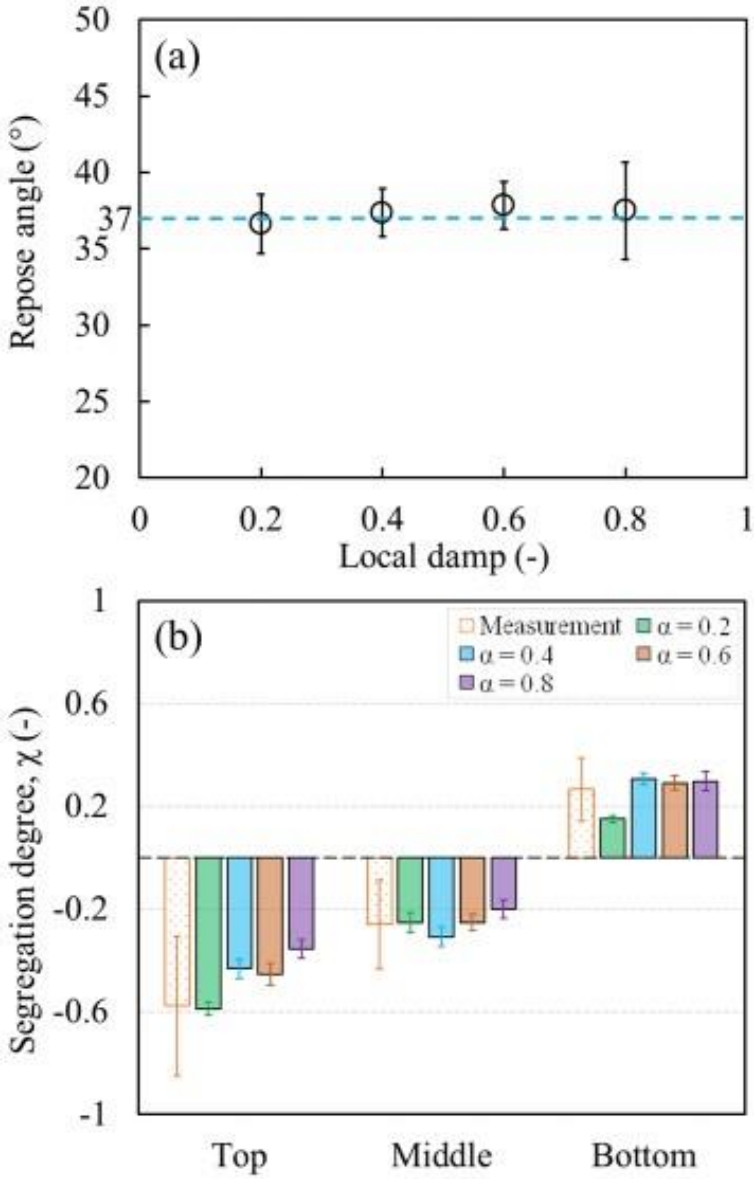

Figure 5.16: Effect of local damp on (a) repose angle and (b) segregation degree of waste rock at Canadian Malartic mine. Each case was repeated 5 times with different random seeds. Error bars indicate standard deviation.

5.4.3 Effect of Young's modulus

DEM simulations are particularly demanding in terms of calculation power, and some of the simulations presented above took over 200 hours to converge. One of the reasons for that, is that

numerical time steps are inversely proportional to the square root of the material Young's modulus (Chen et al., 2017). Young's modulus of 10^8 to 10^{10} Pa is usually recommended to represent hard rock particles when the DEM model is used to simulate strength properties such as UCS test and shear strength tests (Landry et al., 2006; Coetzee et al., 2009) and a value of 1×10^6 Pa was chosen in this study. However, Young's modulus seems to have little effect on the simulated repose angle which changes by only 1° when it decreases from 10^{10} Pa to 10^5 Pa (Combarros et al., 2014; Zhou et al., 2001). It was also reported that reducing the particle stiffness by a factor 100 to 1000 from the measured value had no significant influence on the flow patterns (Chung et al., 2008; Xu et al., 2002). Decreasing stiffness by one order of magnitude could therefore accelerate calculation time by 3 to 10 times without significantly altering the results (Tsuji et al., 1993; Renzo et al., 2004), but this was not further investigated in this study.

5.4.4 Discussion

Using spheres is an operational way for field scale simulation by introducing a rolling resistance coefficient to consider the shape effect. It was also demonstrated in this study that spheres can be efficiently used for repose angle test and segregation test simulations. Previous research also indicated that sphere particles could simulate size segregation in granular flows (Zhou et al., 2016). However, although the overall collision characteristics of waste rock can be reproduced by spheres with acceptable accuracy using a well calibrated local damp (Plassiard et al., 2010; Calvetti et al., 2005), field waste rock exhibits complicated collisions which are affected by different factors such as irregular shape, particle size and falling height (Bourrier et al., 2008; Plassiard et al., 2010). These factors are difficult to evaluate and compare in a system containing large amounts of particles, and further investigation on the collision of unique particle on existing slope is recommended (Bourrier et al., 2008; Effeindzourou et al., 2017). Using irregular shapes (either by using clumps or rigid blocks (Itasca, 2019)) is another alternative to simulate more accurately collision and contacts between waste rock particles, but the calculation time would significantly increase (up to 30 times; (Coetzee, 2016)) and simulations of large waste rock piles could become unrealistic (Favier et al., 1999; Windows-Yule et al., 2016; Coetzee, 2017).

Using spheres and removing particles smaller than 5 mm at laboratory scale and 0.1 m at field scale were used in this study, which are also widely used methods to efficiently reduce the calculation pressure and overcome the limitation of DEM program calculation capacity (Crosta et al., 2007; Grima et al., 2011). The calculation time could then be reduced to 35 hours for a 20 m high bench when the simulation was run using an 8-core CPU. However, the program ran slowly (slower than 1 cycle/s) when the particle number was greater than 0.3 million, and could not run by itself when the particle number reached around 1 million. Developing algorithms in software and improving PC calculation capacity are expected to optimize the calculation so that much more particles can be simulated with reasonable calculation pressure.

The interactions between friction coefficient and rolling resistance coefficient strongly affected waste rock flow behaviour in this study. Other parameter interactions may also have had an effect, based on previous research (Yan et al., 2015). For example, the repose angle increases with increasing the coefficient of restitution (i.e., contact damp) for low friction coefficients, but it slightly decreases with increasing the coefficient of restitution for higher sliding friction coefficients (Yan et al., 2015). These interactions between parameters were, however, out of the scope of this study and were therefore not deeply analyzed. A more comprehensive parameter analysis using sensitivity analysis methods such as principal component analysis (PCA) may contribute to identify most significant parameter interactions and evaluate their interaction degree (Yan et al., 2015; Wold et al., 1987).

Also, in practice, waste rock is usually dumped using multiple methods including end-dumping method and push-dumping method (Aubertin, 2013; Morin et al., 1991; Tomaschitz et al., 2018). Only end-dumping method was simulated in this study and the effect of push-dumping method on waste rock segregation should therefore be further investigated. Similarly, waste rock was dumped from one fixed point in this study, while in practice dumping progresses laterally as the pile is constructed (Lehouiller et al., 2020; Mahmood et al., 2017). Lateral construction was not considered in this study but should be included in further application of the approach proposed in this research.

5.5 Conclusion

In this study, a new calibration method was proposed and tested with PFC3D to simulate the flow behaviour of waste rock during disposal. Repose angle tests were conducted in the laboratory to calibrate the model with maximum particle size of 89 mm, and field models were calibrated based on the natural repose angle. Calibrated models were then used to investigate segregation properties (e.g., characteristic diameters, segregation degree) of waste rock and compared with laboratory and field measurements to check the representative of the simulation model. The following statements can be made based on the results of this study:

(1) The main input parameters (i.e., friction coefficient and rolling resistance coefficient) calibrated using repose angle tests were able to reproduce well waste rock segregation at both laboratory and field scales.

(2) This simple calibration method was considered applicable to calibrate granular materials such as waste rock and rockfill for segregation simulations.

(3) Friction coefficient (μ) and rolling resistance coefficient (μ_r) ($\mu = \mu_r = 0.2$) were calibrated for waste rock with a maximum particle diameter of 89 mm in the laboratory, and $\mu = \mu_r = 0.44$ for waste rock with a maximum particle diameter of 1.5 m in the field, indicating that calibrated parameters are scale dependent and cannot be directly extrapolated.

This research should provide the basis to investigate segregation during waste rock disposal in the field under different practical influence factors such as construction methods and bench heights, to optimize deposition strategies and minimize heterogeneities within the waste rock piles.

5.6 Acknowledgements

The authors would like to acknowledge the financial support from NSERC, FRQNT, and the industrial partners of the Research Institute on Mines and the Environment (RIME) (http://irme.ca/).

5.7 References

Aela, P., Zong, L., Esmaeili, M., Siahkouhi, M., & Jing, G. (2022). Angle of repose in the numerical modeling of ballast particles focusing on particle-dependent specifications: Parametric study. Particuology, 65, 39-50.

Ai, J., Chen, J. F., Rotter, J. M., & Ooi, J. Y. (2011). Assessment of rolling resistance models in discrete element simulations. Powder Technology, 206(3), 269-282.

Al-Hashemi, H. M. B., & Al-Amoudi, O. S. B. (2018). A review on the angle of repose of granular materials. Powder technology, 330, 397-417.

Amos, R. T., Blowes, D. W., Bailey, B. L., Sego, D. C., Smith, L., & Ritchie, A. I. M. (2015). Waste-rock hydrogeology and geochemistry. Applied Geochemistry, 57, 140-156.

Anterrieu, O., Chouteau, M., & Aubertin, M. (2010). Geophysical characterization of the large-scale internal structure of a waste rock pile from a hard rock mine. Bulletin of engineering geology and the environment, 69(4), 533-548.

ASTM C127-15, (2015). Standard Test Method for Relative Density (Specific Gravity) and Absorption of Coarse Aggregate, ASTM International, West Conshohocken, PA.

ASTM C136 / C136M-19, (2019). Standard Test Method for Sieve Analysis of Fine and Coarse Aggregates, ASTM International, West Conshohocken, PA.

ASTM D6323-19, (2019). Standard Guide for Laboratory Subsampling of Media Related to Waste Management Activities, ASTM International, West Conshohocken, PA.

Aubertin, M. (2013). Waste rock disposal to improve the geotechnical and geochemical stability of piles. Proceedings of the world mining congress, Montreal, Quebec, Canada.

Bar, N., Semi, J., Koek, M., Owusu-Bempah, G., Day, A., Nicoll, S., & Bu, J. (2020). Practical waste rock dump and stockpile management in high rainfall and seismic regions of Papua New Guinea. Slope Stability, 117-128.

Bierwisch, C., Kraft, T., Riedel, H., & Moseler, M. (2009). Three-dimensional discrete element models for the granular statics and dynamics of powders in cavity filling. Journal of the Mechanics and Physics of Solids, 57(1), 10-31.

Blight, G. E. (2009). Geotechnical engineering for mine waste storage facilities. CRC Press.

Bourrier, F., Nicot, F., & Darve, F. (2008). Physical processes within a 2D granular layer during an impact. Granular Matter, 10(6), 415-437.

Broda, S., Aubertin, M., Blessent, D., Hirthe, E., & Graf, T. (2014). Improving control of contamination from waste rock piles. Environmental Geotechnics, 4(4), 274-283.

Burnley, R. B. (1993). Mine reclamation and waste dump stability. University of Nevada, Reno.

Calvetti, F., Di Prisco, C. G., & Vecchiotti, M. (2005). Experimental and numerical study of rock-fall impacts on granular soils" Rivista Italiana di Geotecnica.

Chen, H., Xiao, Y. G., Liu, Y. L., & Shi, Y. S. (2017). Effect of Young's modulus on DEM results regarding transverse mixing of particles within a rotating drum. Powder technology, 318, 507-517.

Cheng, Y. M., Fung, W. H. I., Li, L., & Li, N. (2019). Laboratory and field tests and distinct element analysis of dry granular flows and segregation processes. Natural Hazards and Earth System Sciences, 19(1), 181-199.

Chung, Y. C., & Ooi, J. Y. (2008). A study of influence of gravity on bulk behaviour of particulate solid. Particuology, 6(6), 467-474.

Cleary, P. W., & Sawley, M. L. (2002). DEM modelling of industrial granular flows: 3D case studies and the effect of particle shape on hopper discharge. Applied Mathematical Modelling, 26(2), 89-111.

Combarros, M., Feise, H. J., Zetzener, H., & Kwade, A. (2014). Segregation of particulate solids: Experiments and DEM simulations. Particuology, 12, 25-32.

Coetzee, C. J. (2016). Calibration of the discrete element method and the effect of particle shape. Powder Technology, 297, 50-70.

Coetzee, C. J. (2017). Calibration of the discrete element method. Powder Technology, 310, 104-142.

Coetzee, C. J. (2020). Calibration of the discrete element method: Strategies for spherical and non-spherical particles. Powder Technology, 364, 851-878.

Coetzee, C. J., & Els, D. N. J. (2009). Calibration of granular material parameters for DEM modelling and numerical verification by blade–granular material interaction. Journal of Terramechanics, 46(1), 15-26.

Coetzee, C. J., Els, D. N. J., & Dymond, G. F. (2010). Discrete element parameter calibration and the modelling of dragline bucket filling. Journal of Terramechanics, 47(1), 33-44.

Crosta, G. B., Frattini, P., & Fusi, N. (2007). Fragmentation in the Val Pola rock avalanche, Italian alps. Journal of Geophysical Research: Earth Surface, 112(F1).

Crouzal, T., & Pabst, T. (2021). A black-box automated approach to calibrate numerical simulations and optimize cover design: Application to a flow control layer constructed on an experimental waste rock pile. Vadose Zone Journal, 20(3), e20130.

Cundall, P. A., & Strack, O. D. (1979). A discrete numerical model for granular assemblies. geotechnique, 29(1), 47-65.

Džiugys, A., & Navakas, R. (2009). The role of friction in mixing and segregation of granular material. Granular Matter, 11(6), 403-416.

Derakhshani, S. M., Schott, D. L., & Lodewijks, G. (2015). Micro–macro properties of quartz sand: experimental investigation and DEM simulation. Powder Technology, 269, 127-138.

Di Renzo, A., & Di Maio, F. P. (2004). Comparison of contact-force models for the simulation of collisions in DEM-based granular flow codes. Chemical engineering science, 59(3), 525-541.

Dolgunin, V. N., & Ukolov, A. A. (1995). Segregation modeling of particle rapid gravity flow. Powder technology, 83(2), 95-103.

Effeindzourou, A., Giacomini, A., Thoeni, K., & Sloan, S. W. (2017). Numerical investigation of rockfall impacts on muckpiles for underground portals. Rock Mechanics and Rock Engineering, 50(6), 1569-1583.

Escotet-Espinoza, M. S., Foster, C. J., & Ierapetritou, M. (2018). Discrete Element Modeling (DEM) for mixing of cohesive solids in rotating cylinders. Powder Technology, 335, 124-136.

Fan, Y., Schlick, C. P., Umbanhowar, P. B., Ottino, J. M., & Lueptow, R. M. (2014). Modelling size segregation of granular materials: the roles of segregation, advection and diffusion. Journal of fluid mechanics, 741, 252-279.

Favier, J. F., Abbaspour-Fard, M. H., Kremmer, M., & Raji, A. O. (1999). Shape representation of axi-symmetrical, non-spherical particles in discrete element simulation using multi-element model particles. Engineering computations.

Feng, Y., Han, K., Owen, D. R. J., & Loughran, J. (2007). Upscaling of discrete element models for particle systems.

Ferellec, J. F., & McDowell, G. R. (2008). A simple method to create complex particle shapes for DEM. Geomechanics and Geoengineering: An International Journal, 3(3), 211-216.

Frankowski, P., & Morgeneyer, M. (2013, June). Calibration and validation of DEM rolling and sliding friction coefficients in angle of repose and shear measurements. In AIP conference proceedings (Vol. 1542, No. 1, pp. 851-854). American Institute of Physics.

Gervais, D., Roy. C., Thibault, A., Pednault, C., Doucet, D. (2014). Technical Report on the mineral resource and mineral reserve estimates for the Canadian Malartic Property.

Grima, A. P., & Wypych, P. W. (2011). Development and validation of calibration methods for discrete element modelling. Granular Matter, 13(2), 127-132.

Guo, Y., Wassgren, C., Ketterhagen, W., Hancock, B., James, B., & Curtis, J. (2012). A numerical study of granular shear flows of rod-like particles using the discrete element method. Journal of fluid Mechanics, 713, 1-26.

Hawley, M., & Cunning, J. (2017). Guidelines for mine waste dump and stockpile design. CSIRO Publishing.

Herasymuik, G., Azam, S., Wilson, G. W., Barbour, L. S., Nichol, C. (2006). Hydrological characterization of an unsaturated waste rock dump. In: Proceedings of the 59th Canadian geotechnical conference, Vancouver, BC, Canada.

Itasca Consulting Group, Inc. (2020). PFC — particle flow code in 2 and 3 dimensions. Version 6.0, Documentation set of version 6.00.15. Minneapolis, Minnesota, USA.

Iverson, R. M. (1997). The physics of debris flows. Reviews of geophysics, 35(3), 245-296.

Iwashita, K., & Oda, M. (1998). Rolling resistance at contacts in simulation of shear band development by DEM. Journal of engineering mechanics, 124(3), 285-292.

Jain, A., Metzger, M. J., & Glasser, B. J. (2013). Effect of particle size distribution on segregation in vibrated systems. Powder technology, 237, 543-553.

James, M., Aubertin, M., & Bussière, B. (2013). On the use of waste rock inclusions to improve the performance of tailings impoundments. In Proceedings of the 18th International Conference Soil Mechanics and Geotechnical Engineering, Paris, France.

Jiang, M. J., Yu, H. S., & Harris, D. (2005). A novel discrete model for granular material incorporating rolling resistance. Computers and Geotechnics, 32(5), 340-357.

Jiang, Y. J., Fan, X. Y., Li, T. H., & Xiao, S. Y. (2018). Influence of particle-size segregation on the impact of dry granular flow. Powder Technology, 340, 39-51.

Just, S., Toschkoff, G., Funke, A., Djuric, D., Scharrer, G., Khinast, J., ... & Kleinebudde, P. (2013). Experimental analysis of tablet properties for discrete element modeling of an active coating process. AAPS PharmSciTech, 14(1), 402-411.

Kashizadeh, E., Mukherjee, A., & Tordesillas, A. (2020). Experimental and numerical investigation on heap formation of granular soil sparsely cemented by bacterial calcification. Powder Technology, 360, 253-263.

Katterfeld, A., & Wensrich, C. (2017). Understanding granular media: from fundamentals and simulations to industrial application. Granular Matter, 19(4), 1-4.

Kenney, T. C., Westland, J. (1993) . Laboratory Study of Segregation of Granular Filter Materials," Filters In Geotechnical and Hydraulic Engineering: Proceedings of the First International Conference "Geo-Filter", Karlesruhe, Germany, 313–319.

Lahmira, B., Lefebvre, R., Aubertin, M., & Bussière, B. (2016). Effect of heterogeneity and anisotropy related to the construction method on transfer processes in waste rock piles. Journal of Contaminant Hydrology, 184, 35-49.

Lahmira, B., Lefebvre, R., Aubertin, M., & Bussière, B. (2017). Effect of material variability and compacted layers on transfer processes in heterogeneous waste rock piles. Journal of contaminant hydrology, 204, 66-78.

Landry, H., Lague, C., & Roberge, M. (2006). Discrete element representation of manure products. Computers and electronics in agriculture, 51(1-2), 17-34.

Lehouiller, P., Lampron, S., Gagnon, G., Houle, N., Bouchard, F. (2020). NI 43-101 Technical report, Canadian Malartic mine, Quebec, Canada.

Li, Q., Feng, M., & Zou, Z. (2013). Validation and calibration approach for discrete element simulation of burden charging in pre-reduction shaft furnace of COREX process. ISIJ international, 53(8), 1365-1371.

Li, X., Wang, D., Li, C., & Liu, Z. (2019). Numerical simulation of surface subsidence and backfill material movement induced by underground mining. Advances in Civil Engineering, 2019.

Mahmood, F. N., Barbour, S. L., Kennedy, C., & Hendry, M. J. (2017). Nitrate release from waste rock dumps in the Elk Valley, British Columbia, Canada. Science of the Total Environment, 605, 915-928.

Maknoon, M. (2016). Slope stability analyses of waste rock piles under unsaturated conditions following large precipitations. Ecole Polytechnique, Montreal (Canada).

Maknoon, M., & Aubertin, M. (2021). On the Use of Bench Construction to Improve the Stability of Unsaturated Waste Rock Piles. Geotechnical and Geological Engineering, 39(2), 1425-1449.

McLemore, V. T., Fakhimi, A., van Zyl, D., Ayakwah, G. F., Anim, K., Boakye, K., ... & Viterbo, V. C. (2009). Literature review of other rock piles: characterization, weathering, and stability. Questa Rock Pile Weathering Stability Project. New Mexico Bureau of Geology and Mineral Resources. New Mexico Tech, USA.

Mio, H., Akashi, M., Shimosaka, A., Shirakawa, Y., Hidaka, J., & Matsuzaki, S. (2009). Speed-up of computing time for numerical analysis of particle charging process by using discrete element method. Chemical Engineering Science, 64(5), 1019-1026.

Molson, J. W., Fala, O., Aubertin, M., & Bussière, B. (2005). Numerical simulations of pyrite oxidation and acid mine drainage in unsaturated waste rock piles. Journal of Contaminant Hydrology, 78(4), 343-371.

Morin, K. A., Gerencher, E., Jones, C. E., Konasewich, D. E. (1991). Critical literature review of acid drainage from waste rock. MEND Report 1.11.1. Ottawa.

Mosby, J., de Silva, S. R., & Enstad, G. G. (1996). Segregation of particulate materials–mechanisms and testers. KONA Powder and Particle Journal, 14, 31-43.

Nichol, R. S. (1986). Rock segregation in waste dumps. Proceedings of the international conference on flow-through rock drains.

Plassiard, J. P., & Donzé, F. V. (2010). Optimizing the design of rockfall embankments with a discrete element method. Engineering structures, 32(11), 3817-3826.

Rackl, M., & Hanley, K. J. (2017). A methodical calibration procedure for discrete element models. Powder technology, 307, 73-83.

Raymond, K. E., Seigneur, N., Su, D., & Mayer, K. U. (2021). Investigating the Influence of Structure and Heterogeneity in Waste Rock Piles on Mass Loading Rates—A Reactive Transport Modeling Study. Frontiers in Water, 39.

Richter, C., Roessler, T., Kunze, G., Katterfeld, A., & Will, F. (2020). Development of a standard calibration procedure for the DEM parameters of cohesionless bulk materials–Part II: Efficient optimization-based calibration. Powder Technology, 360, 967-976.

Roessler, T., & Katterfeld, A. (2018). Scaling of the angle of repose test and its influence on the calibration of DEM parameters using upscaled particles. Powder technology, 330, 58-66.

Roessler, T., Richter, C., Katterfeld, A., & Will, F. (2019). Development of a standard calibration procedure for the DEM parameters of cohesionless bulk materials–part I: Solving the problem of ambiguous parameter combinations. Powder Technology, 343, 803-812.

Sadek, M. A., & Chen, Y. (2014). Microproperties calibration of discrete element models for soil-tool interaction. In 2014 Montreal, Quebec Canada July 13–July 16, 2014 (p. 1). American Society of Agricultural and Biological Engineers.

Saeed, M. K., & Siraj, M. S. (2019). Mixing study of non-spherical particles using DEM. Powder Technology, 344, 617-627.

Santos, D. A., Barrozo, M. A., Duarte, C. R., Weigler, F., & Mellmann, J. (2016). Investigation of particle dynamics in a rotary drum by means of experiments and numerical simulations using DEM. Advanced Powder Technology, 27(2), 692-703.

Simons, T. A., Weiler, R., Strege, S., Bensmann, S., Schilling, M., & Kwade, A. (2015). A ring shear tester as calibration experiment for DEM simulations in agitated mixers–a sensitivity study. Procedia engineering, 102, 741-748.

St-Arnault, M., Vriens, B., Blaskovich, R., Aranda, C., Klein, B., Mayer, K. U., & Beckie, R. D. (2020). Geochemical and mineralogical assessment of reactivity in a full-scale heterogeneous waste-rock pile. Minerals Engineering, 145, 106089.

Su, H., Fu, Z., Gao, A., & Wen, Z. (2019). Numerical simulation of soil levee slope instability using particle-flow code method. Natural Hazards Review, 20(2), 04019001.

Sutherland, K., & Grabinsky, M. (2003). Evaluating segregation in granular filters for earth dams.

Thakur, S. C., Ooi, J. Y., & Ahmadian, H. (2016). Scaling of discrete element model parameters for cohesionless and cohesive solid. Powder Technology, 293, 130-137.

Thoeni, K., Servin, M., Sloan, S. W., & Giacomini, A. (2019). Designing waste rock barriers by advanced numerical modelling. Journal of Rock Mechanics and Geotechnical Engineering, 11(3), 659-675.

Tomaschitz, J. D. O. P., Mannich, M., & Ota, J. J. (2018). Experimental results for guidance and design criteria of horizontal end-dumping type river closure. RBRH, 23.

Tsuji, Y., Kawaguchi, T., & Tanaka, T. (1993). Discrete particle simulation of two-dimensional fluidized bed. Powder technology, 77(1), 79-87.

Ucgul, M., Fielke, J. M., & Saunders, C. (2014). Three-dimensional discrete element modelling of tillage: Determination of a suitable contact model and parameters for a cohesionless soil. Biosystems Engineering, 121, 105-117.

Utili, S., Zhao, T., & Houlsby, G. T. (2015). 3D DEM investigation of granular column collapse: evaluation of debris motion and its destructive power. Engineering geology, 186, 3-16.

Wensrich, C. M., & Katterfeld, A. (2012). Rolling friction as a technique for modelling particle shape in DEM. Powder Technology, 217, 409-417.

Westland, J. (1988). A study of segregation in cohesionless soil. M.A.Sc. Thesis, Department of Civil Engineering, University of Toronto, Toronto, Canada.

Windows-Yule, C. R. K., Tunuguntla, D. R., & Parker, D. J. (2016). Numerical modelling of granular flows: a reality check. Computational particle mechanics, 3(3), 311-332.

Wold, S., Esbensen, K., & Geladi, P. (1987). Principal component analysis. Chemometrics and intelligent laboratory systems, 2(1-3), 37-52.

Xu, W. J., Wang, S., Zhang, H. Y., & Zhang, Z. L. (2016). Discrete element modelling of a soil-rock mixture used in an embankment dam. International Journal of Rock Mechanics and Mining Sciences, 86, 141-156.

Xu, Y., Kafui, K. D., Thornton, C., & Lian, G. (2002). Effects of material properties on granular flow in a silo using DEM simulation. Particulate Science and Technology, 20(2), 109-124.

Yan, Z., Wilkinson, S. K., Stitt, E. H., & Marigo, M. J. C. P. M. (2015). Discrete element modelling (DEM) input parameters: understanding their impact on model predictions using statistical analysis. Computational Particle Mechanics, 2(3), 283-299.

Zhang, S., & Liu, W. (2017). Application of aerial image analysis for assessing particle size segregation in dump leaching. Hydrometallurgy, 171, 99-105.

Zhou, W., Lai, Z., Ma, G., Yang, L., & Chen, Y. (2016). Effect of base roughness on size segregation in dry granular flows. Granular Matter, 18(4), 1-14.

Zhou, Y. C., Xu, B. H., Yu, A. B., & Zulli, P. (2001). Numerical investigation of the angle of repose of monosized spheres. Physical Review E, 64(2), 021301.

Zhou, Y. C., Xu, B. H., Yu, A. B., & Zulli, P. (2002). An experimental and numerical study of the angle of repose of coarse spheres. Powder technology, 125(1), 45-54.

Zhu, D., Tu, S., Ma, H., Wei, H., Li, H., & Wang, C. (2019). Modeling and calculating for the compaction characteristics of waste rock masses. International Journal for Numerical and Analytical Methods in Geomechanics, 43(1), 257-271.

CHAPTER 6 ARTICLE 3: INFLUENCE OF CONSTRUCTION METHOD AND BENCH HEIGHT ON WASTE ROCK SEGREGATION

Peiyong Qiu and Thomas Pabst

Department of civil, geological, and mining engineering, Polytechnique Montréal, Montréal, Québec, Canada

Research Institute on Mines and Environment (RIME), Québec, Canada

This article was submitted to Canadian Geotechnical Journal, Submitted on November 16, 2022

Abstract: Waste rock segregation and heterogeneity can contribute to increase hydrogeotechnical and geochemical instability of waste rock piles, but testing and characterizing segregation quantitatively in the field is difficult because of the large dimensions of these structures. In this study, a discrete element code (PFC3D) was calibrated on two real cases and used to simulate the flow behaviour of waste rock during disposal. The effect of the construction method and the bench height on particle segregation was investigated, together with the influence of various additional factors such as mine truck payloads and push velocities. Segregation degree and relative particle diameters of waste rock at different locations in the pile were compared to propose practical solutions to reduce segregation and heterogeneity during deposition. Results indicated that simulated bench heights and mine truck payloads had limited effect on segregation A smaller proportion of large particles in the original waste rock can increase segregation. Lateral disposal and increasing the push velocity tended to reduce segregation.

Keywords: Waste rock disposal; Segregation; Discrete element simulation; Construction method; Bench height.

6.1 Introduction

Large amounts of waste rock are generated by mining operations (Hudson-Edwards et al., 2011; Vriens et al., 2020) and generally stored on the surface in piles or dumps (Anterrieu et al., 2010; Aubertin, 2013). Waste rock piles are typically built up by repeatedly dumping waste rock along the slope with different construction methods such as end-dumping and push-dumping methods (Bishwal et al., 2019; Raymond et al., 2021). Construction methods are selected depending on economic and environmental concerns (Bian et al., 2010), topography (Ramani,2012), and haul truck fleet (Lucas et al., 2014).

Waste rock segregation usually leads to complicated heterogeneous structures in waste rock piles with significant variations of particle size distribution (Pedretti et al., 2020). The heterogeneous distribution of waste rock strongly affects waste rock friction angle, and therefore pile's geotechnical stability (Barton, 1982; Gupta, 2016; Zevgolis, 2018). Segregation can also induce significant variations in hydraulic conductivity (sometimes by several orders of magnitude; Cash, 2014), resulting in the formation of preferential flow paths within waste rock piles (Appels et al., 2018; Raymond et al., 2021). The presence of such preferential flow path can contribute to enhance oxygen and water flux in waste rock piles, therefore accelerating the oxidation of reactive minerals and the generation of acid mine drainage (AMD) (Akcil et al., 2006; Bréard Lanoix et al., 2017). Large water fluxes favored by the presence of preferential flow paths can also increase the transport of contaminated water to the environment, and impact significantly the performance of reclamation (Pedretti et al., 2020; St-Arnault et al., 2020). Controlling segregation is therefore critical to improve the hydro-geotechnical and geochemical stability of waste rock piles.

Construction method is often considered one of the main causes for waste rock segregation (Raymond, et al., 2021). End-dumping method consists in directly dumping waste rock from the top of the waste rock pile which then falls along the slope (Raymond et al., 2021). Push-dumping method consists in dumping waste rock on the surface of the pile and then push it to the edge using dozers (Burnley, 1993; Hawley et al., 2017). Both methods lead to the accumulation of coarser particles at the bottom of the pile, while smaller particles tend to remain near the top of the slope (Nichol, 1986; Maknoon, 2016). Some field observations have shown that the bottom of

the slope can contain around 40% of the total maximum particles when push-dumping method is used, and up to 75% with end-dumping method (Nichol, 1986). However, the effect of the construction methods on waste rock segregation is complex to quantitatively investigate because of various influence factors and natural heterogeneity of waste rock. For example, mine truck payloads, which typically range between 150 t and 380 t (Kumar et al., 2014; Soofastaei et al., 2016) and the speed at which dozers push waste rock may also affect segregation (Tang et al., 2004).

Another factor which can strongly influence segregation is the bench height (Tang et al., 2004). Some observations report that the higher the pile size, the more significant the segregation (Tang et al., 2004; Aubertin et al. 2013). Bench height vary a lot depending on the operational constraints such as terrain, topology and geology (Hawley et al., 2017) but also environmental concerns (Cepa, 2007). Quantitatively evaluating the effect of the bench height on waste rock segregation is also challenging because of the difficulty to access, sample and characterize large and highly heterogenous waste rock piles (Raymond et al., 2021).

The objective of this research was therefore to investigate the effect of construction method and bench height, among other influence factors such as waste rock particle size distribution, payload and push velocities, on waste rock segregation. Discrete element simulations, using particle flow code 3D (PFC3D; Itasca, 2019) were calibrated on real cases and sensitivity analyses were conducted. Waste rock segregation along the slope was evaluated based on segregation degree and relative particle diameters. Finally, numerical simulation results were used to propose recommendations to limit segregation during waste rock disposal.

6.2 Methodology

6.2.1 Waste rock materials

Two types of waste rock were considered in this study: waste rock from Quebrada Blanca mine (Zhang et al., 2017b) and waste rock from Canadian Malartic mine (Qiu and Pabst, 2022a).

Quebrada Blanca mine is located in Tarapacá region in Chile. The operation produces copper cathodes using dump leaching, solvent extraction, and electrowinning (Zhang et al., 2017). The material itself is not exactly waste rock because it is concentrated enough to produce copper.

However, the material properties and the deposition method used to build the heap leach pads are very similar to typical waste rock materials and dumps. Also, the ore will become a waste after extraction will have been completed. By commodity, material from Quebrada Blanca mine will therefore be referred to as waste rock in the following. The dump leach pad is constructed with end-dumping method using mine trucks. The dump leach pad is developed in the same way as a waste rock pile. The height of the pile is around 20 m with slope angles between 30° and 40° (Zhang et al., 2017b). Waste rock from Quebrada Blanca mine is characterized by minimum and maximum diameters of 0.1 m and 2.66 m, respectively, with a coefficient of uniformity $C_U = 4.1$ and a coefficient of curvature $C_C = 1.1$ (Figure 6.1). The specific gravity of waste rock in Quebrada Blanca mine is not reported and a specific gravity of 2.76 was assumed in this study.

Canadian Malartic mine is an open-pit mine located at Abitibi-Témiscamingue, Quebec, Canada. The waste rock pile is constructed in 10 m benches with 11.5 m terraces between benches for an overall slope angle of 21.8°. The slope angle of each bench is around 37° (Gervais et al., 2014). The total height of the waste rock piles reaches 100 m in most sections (Lehouiller et al., 2020). Waste rock from Canadian Malartic mine is characterized by a minimum and a maximum diameter of 0.1 m and 1.5 m, respectively, with a coefficient of uniformity $C_U = 2.9$ and a coefficient of curvature $C_C = 0.9$ (Figure 6.1). The specific gravity of waste rock in Canadian Malartic mine is around 2.76 (measured by the authors, using ASTM C127, 2015).

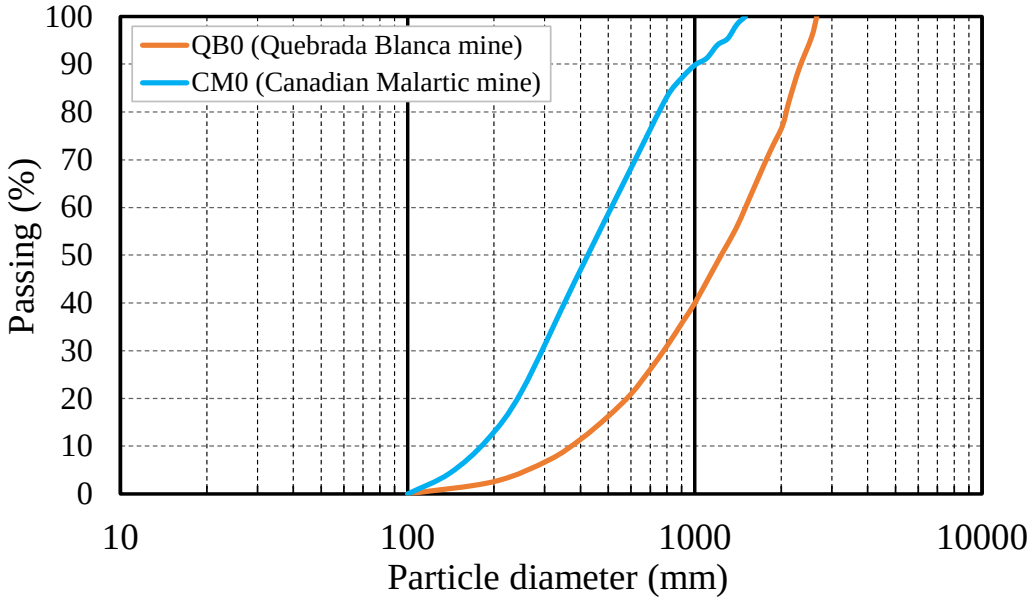

Figure 6.1: Waste rock PSD curves of Quebrada Blanca mine (QB0) and Canadian Malartic mine (CM0). These PSD curves were scalped based on their measured PSD curves in the field.

6.2.2 Calibration of numerical model

Discrete element method (DEM; Cundall et al., 1979) is efficient to simulate the flow behaviour of granular material and therefore provide a useful alternative to overcome field challenges (Combarros et al., 2014; Cheng et al., 2019; Qiu and Pabst, 2022b). DEM can simulate the motion of waste rock particles by calculating the stress and deformation of contacts generated when particles interact with each other or with boundary walls (Cundall et al, 1979; Jiang et al., 2020). In DEM models, distinct particles move independently from one another and interact at contact points based on assigned contact models (Thakur et al., 2014; Coetzee, 2020).

In this study, waste rock particles were simulated using spheres. Shape effect was indirectly simulated using rolling resistance linear (rrlinear) model (Iwashita et al., 1998; Ai et al., 2011). Friction coefficient (μ) and rolling resistance coefficient (μ_r) were calibrated and validated using repose angle tests and segregation tests (more details in Qiu and Pabst, 2022b). Waste rock was considered cohesionless granular material so no viscous behaviour was considered and normal and shear critical damping ratios were set to 0 ($\beta_n = \beta_s = 0$). Local damp ($\alpha = 0.4$), calibrated

using drop tests in the laboratory, was applied to simulate energy dissipation. The effective modulus $E = 1\times10^6$ Pa was used to maintain the system within the rigid limit while optimizing the calculation speed (Itasca, 2019). Calibrated friction coefficient and rolling resistance coefficient were $\mu = \mu_r = 0.47$ for Quebrada Blanca mine, resulting in a repose angle of $37.3° \pm 1.2°$ (similar to 35° to 40° measured in the field; Zhang et al., 2017b), and calibrated friction and rolling resistance coefficients were $\mu = \mu_r = 0.44$ for Canadian Malartic mine, resulting in a repose angle of $37.4° \pm 1.6°$ (similar to 37° measured in the field; Gervais et al., 2014). Parameters used for simulations are summarized in Table 6.1.

Table 6.1: Main parameters used in PFC3D to simulate waste rock segregation during disposal. Particle density (β) and local damp (α) were measured in the laboratory. Other parameters were determined by model calibration (Qiu and Pabst, 2022b; see text for details).

Parameters	Quebrada Blanca mine	Canadian Malartic mine
Particle density, β (kg/m^3)	2760	2760
Friction coefficient, μ	0.47	0.44
Rolling resistance coefficient, μ_r	0.47	0.44
Local damp, α	0.4	0.4
Effective modulus, E (Pa)	1×10^6	1×10^6
Stiffness ratio, k^*	2.5	2.5
Normal critical damping ratio, β_n	0	0
Shear critical damping ratio, β_s	0	0

6.2.3 Simulations of waste rock segregation during field disposal

6.2.3.1 General simulation approach

Field-scale simulation models were built to investigate waste rock segregation during waste rock disposal (Figure 6.2). The support walls (in yellow color in Figure 6.2) represented the ground and physical boundaries of the models. The length of the support walls in x-axis direction was 100 m. The length of the support walls in y-axis direction was 40 m for the top surface and 80 m for the bottom surface. An inclined wall was generated to represent an existing waste rock slope with a slope angle of 45°.This initial slope had no effect on the final results (its angle was greater than the natural repose angle of tested waste rock) but contributed to decrease the number of dumps and therefore the calculation time required to form a stable slope. The bench height (h in Figure 6.2) was adjusted depending on the simulated cases (see next section for more details). The support walls were covered by a base layer made of fixed 1 m diameter balls (grey balls in Figure 6.2) to simulate waste rock surface so that dumped waste rock could directly interact with existing waste rock particles. Waste rock was dumped from the top edge of the bench slope.

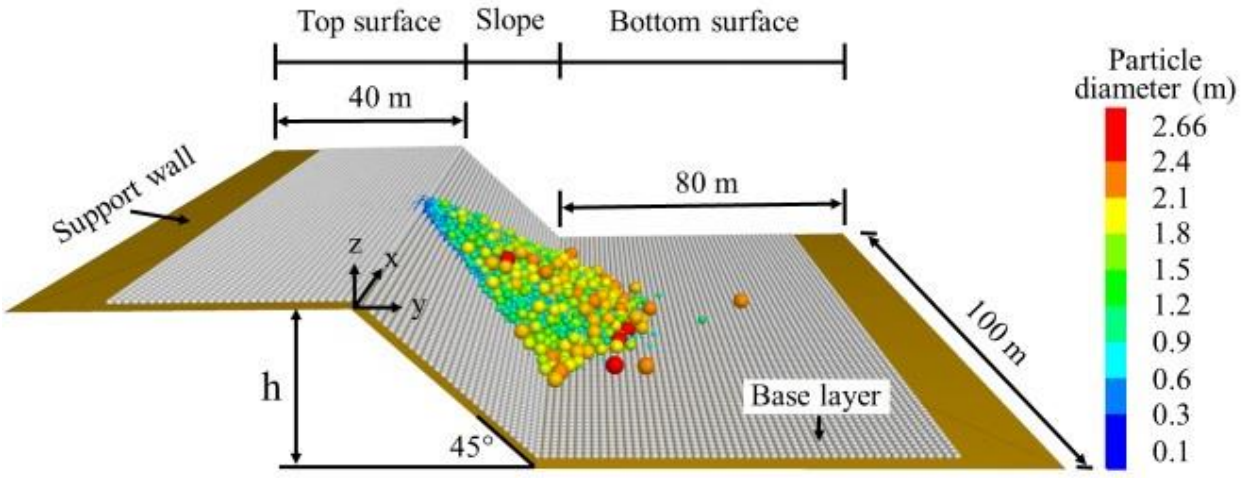

Figure 6.2: Simulation model for waste rock disposal. h [L] represents the bench height and varies between 10 and 25 m depending on the cases. Base layer is composed of 1 m diameter balls (in grey; see text for details). Dumped waste rock particles are colored depending on their diameters (from 0.1 m in blue to 2.66 m in red).

6.2.3.2 Simulations of end-dumping method

End-dumping method was simulated by dumping waste rock directly from the top of the bench (Figure 6.3a). An 8 m (width) × 8 m (length) × 4 m (height) box simulated the mine truck and was inclined at 45° to represent the maximum lifting angle of common mine trucks (e.g., CAT 794AC model; Caterpillar Inc., 2019). The vertical distance between the bottom of the mine truck (i.e., the box in Figure 6.3a) and the top of the bench was 1.5 m, which corresponded to the dump height of large mine trucks (typically between 1 m and 2 m for CAT 794AC model; Caterpillar Inc., 2019). Each waste rock dump (around 300 t) was generated within the simulated box and was disposed of by deleting the bottom wall of the box (green wall in Figure 6.3a) so that the waste rock could fall and move along the slope.

Four different bench heights were simulated, i.e., 10 m (case A1), 15 m (case A2), 20 m (case A3), and 25 m (case A4) (Table 6.2). Waste rock was dumped until the slope was completely covered (along the y-axis), which represented a total of 4, 16, 30, and 66 dumps of waste rock for bench heights of 10 m, 15 m, 20 m and 25 m, respectively. In practice, more dumps are expected to form a parallel layer with similar segregation as the surface layer in the model.

A 600 t payload (Case B1) was simulated using the same box as described above but with a lower initial porosity of 0.4. This porosity was smaller than the initial porosity of 0.65 used in cases A1 to A4. The initial porosity is used only for particle generation and has no effect on the real porosity of the material.

The effect of waste rock PSD was also investigated by dumping Canadian Malartic waste rock (case C1), with all the other parameters similar to case A1 (Table 6.2).

6.2.3.3 Simulation of push-dumping method

Push-dumping method was simulated by pushing waste rock on the top edge of the 10 m high bench (Figure 6.3b). An 8 m (width)×8 m (length)×4 m (height) box simulated on the surface of the bench represented a dozer with an 8 m wide blade (close to CAT D11CD model dozer; Caterpillar Inc., 2019). Around 300 t of waste rock were generated for each dump. At the

beginning of the simulations, the front wall (green wall in Figure 6.3b) was deleted, and back wall was moved toward the slope with a certain speed (between 0.1 m/s – case C1 and 0.6 m/s – case C6) to push the waste rock in the slope. The same process was repeated for each dump.

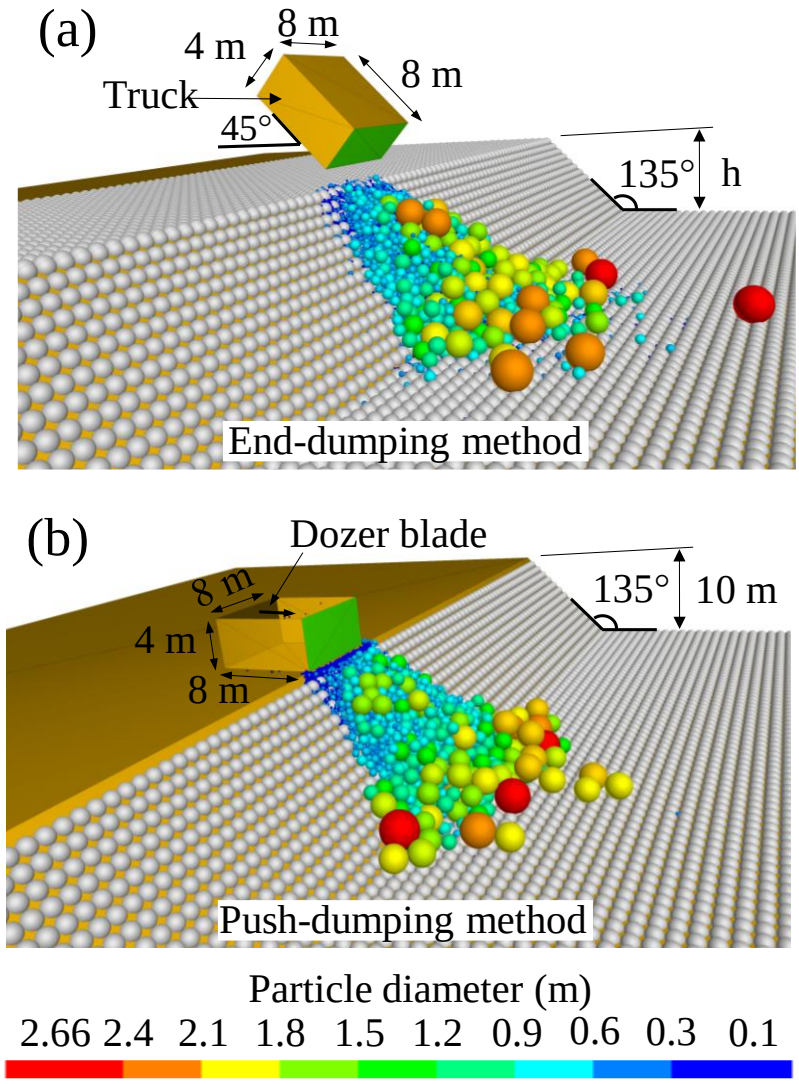

Figure 6.3: Simulation of waste rock disposal using (a) end-dumping method and (b) push-dumping method. h [L] represents the bench height and varies between 10 and 25 m depending on the cases. Dumped waste rock particles are colored depending on their diameters (from 0.1 m in blue to 2.66 m in red). The generated PSD curves in PFC3D are presented in Appendix E.

Table 6.2: Summary of parametric simulation cases. QB0 and CM0: PSD of waste rock from Quebrada Blanca mine and Canadian Malartic mine, respectively. N/A: not applicable. Each case was simulated 5 times with various random seeds.

Case	Pile height (m)	Payload (tonnes)	PSD	Push velocity (m/s)	Construction method	Number of dumps
A1	10	300	QB0	N/A	End-dumping	4
A2	15					16
A3	20					30
A4	25					66
B1	10	600	QB0	N/A	End-dumping	4
C1	10	300	CM0	N/A	End-dumping	4
D1	10	300	QB0	0.1	Push-dumping	4
D2				0.2		
D3				0.3		
D4				0.4		
D5				0.5		
D6				0.6		

6.2.3.4 Quantification of segregation

Each simulation used in this study was repeated five times with five different random seeds (e.g., 10001 to 10005) to check the repeatability of the simulations. Different random seeds can alter the initial relative positions of particles in a specific volume (i.e., different initial particles packing states) without affecting the PSD of the simulated waste rock (Itasca, 2019). Results presented in the following are average values calculated from these five simulations.

Segregation is usually evaluated by segregation indices such as the relative particle diameter (Blight, 2010), coarsening index (Sutherland et al., 2003; Qiu and Pabst, 2022b), relative segregation index (Kenney et al., 1993) and modified segregation index (Asmaei., et al., 2018). In this study, relative particle diameters (D_{10} / D_{10}', D_{50} / D_{50}', D_{95} / D_{95}') and segregation degree (χ)

(Qiu and Pabst, 2022b) were used to characterize waste rock segregation. Relative particle diameters were defined as the ratios D_{10} / D_{10}' (also D_{50} / D_{50}', D_{95} / D_{95}') where D_{10} and corresponds to 10% passing of the PSD in the slope (after deposition and segregation), and D_{10}' corresponds to 10% passing of the original PSD. A negative segregation degree indicates that waste rock was finer than the original material and a positive value indicates waste rock was coarser than the original material.

The segregation degree (χ) of waste rock in each section was determined as:

$$\chi = \frac{log\, d_{tested} - log\, d_0}{log\, d_{CQ} - log\, d_0} \tag{6.1}$$

Where $\log d_0$: the logarithmic mean particle size of the original waste rock before disposal, d was in mm in this study; $\log d_{tested}$: the logarithmic mean particle size of waste rock in the local section, and $\log d_{CQ}$ the logarithmic mean particle size of the coarsest quartile. The coarsest quartile represents the fraction of particles larger than the diameter D_{75} of the original gradation (Westland, 1988). The logarithmic mean particle size is often considered a representative parameter for delineating the PSD curve, and can be calculated as (Kenney et al., 1993):

$$log\, d = \sum_{i=1}^{n} (P_i - P_{i-1})\, log \sqrt{D_i \cdot D_{i-1}} \tag{6.2}$$

Where D_I and D_{i-1} [L]: consecutive particle diameters corresponding to passing P_i and P_{i-1}.

The slopes in all the cases (and independently of their height and length) were equally divided into 6 sections in the vertical direction (Figure 6.4). The PSD curve, relative particle diameters and segregation degree in each section were determined from simulation results.

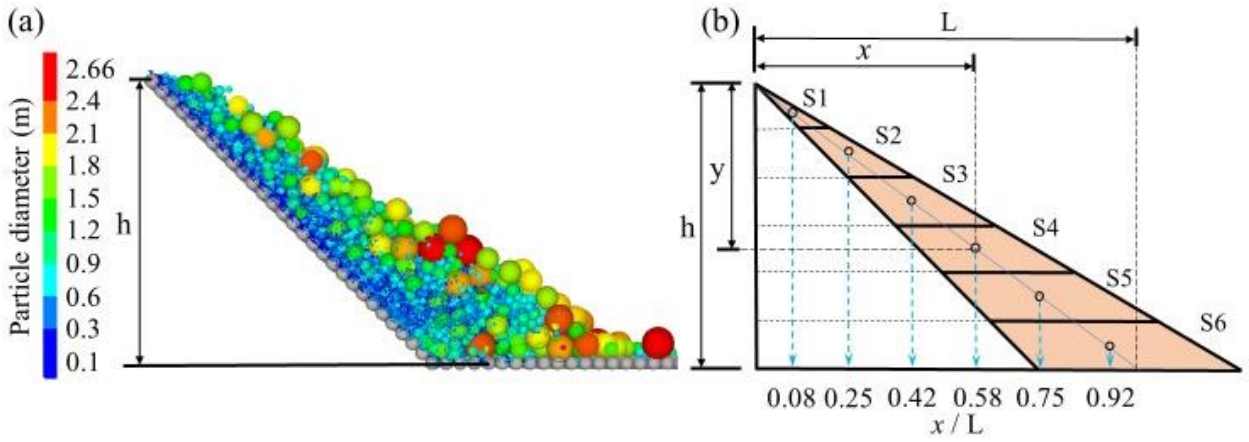

Figure 6.4(a): Cross section of simulated waste rock slope (typical example) and (b) location characterization of the 6 sections along the slope. x / L [-]: relative location of each section with x [L] the horizontal distance of the section center to the deposition point and L [L] the horizontal length of the slope. h [L]: bench height. y [L]: vertical distance to dump point. Dumped waste rock particles are colored depending on their diameters (from 0.1 m in blue to 2.66 m in red).

6.3 Results

6.3.1 Effect of bench height

Four different bench heights (i.e., 10 m, 15 m, 20 m, 25 m) were simulated in this study using end-dumping method. All cases showed significant waste rock segregation along the slope, with an increase of finer particles (compared to the original material) at the top of the bench and an accumulation of coarse particles at the bottom (Figure 6.5). For all cases, segregation degree was negative and smaller than − 0.58 at the top of the slope (x / L = 0.08) and was positive and greater than 0.35 at the bottom of the slope (x / L = 0.92) (Figure 6.5 a and b). Also, relative particle diameters (D_{10} / D_{10}', D_{50} / D_{50}', D_{90} / D_{90}') were all smaller than 0.98 (< 1) at the top of the slope and larger than 1.05 (> 1) at the bottom of the slope (Figure 6.5, d – f). More generally, waste rock was coarser than the original material for x / L > 0.7, for all the bench heights (Figure 6.5, a and b). However, bench height affected differently the material PSD at the top and bottom of the slope.

Bench height did not have a clear effect on waste rock segregation at the top of the slope. For example, segregation degree at the top of the slope (x / L = 0.08) was between − 1.04 (10 m bench) and − 0.58 (20 m bench) (Figure 6.5c). High variations of segregation degree and relative particle diameters were observed at the top of the slope. The minimum and maximum standard deviation of segregation degree for the simulated bench heights (10 to 25 m) were 0.22 and 0.48, respectively. The standard deviation of the ratio D_{90} / D_{90}' at the top of the slope was also relatively high and up to 0.18 (25 m bench) (Figure 6.5f). The reason for this variability was that the top of the slope contained a limited number of coarse particles therefore bringing uncertainties when calculating the segregation degree. For example, a single 150 cm diameter block can lead to 0.15 difference in the segregation degree at the top of the slope. Also, the investigated volume (S1 in Figure 6.4b) was smaller at the top than at the bottom of the slope, therefore increasing the variability of particle distribution. For example, for a 10 m high slope, the average mass of waste rock was around 32 t at the top of the slope, which was much smaller than that (around 375 t) at the bottom.

Bench height had a limited effect on waste rock segregation at the bottom of the slope. For example, segregation degree at the bottom of the slope was comprised between 0.26 and 0.38 (Figure 6.5c), and D_{50} / D_{50}' between 1.19 and 1.31 for all the cases (Figure 6.5d), indicating that bench height had insignificant effect on these values. Relatively low variations of the segregation degree and relative particle diameters were observed at the bottom of the slope. The maximum standard deviation of the segregation degree was only 0.09. The maximum standard deviation of D_{90} / D_{90}' at the bottom of the slope was also very small and did not exceed 0.04 (Figure 6.5f). The maximum standard deviation of D_{10} / D_{10}' was 0.11 at the bottom of the slope, which was slightly greater than that (i.e., 0.09) at the top of the slope (Figure 6.5e). The fact that the variability is significantly smaller at the bottom of the pile can be explained by the abundance of large particles (D > 1.5 m) which accounted for around 40% of the total simulated particles.

In this study only bench heights smaller than 25 m were tested because of recommendations for geotechnical stability (Aubertin, 2013) and numerical constraints (Coetzee, 2016). However, in the specific cases where higher benches are considered (e.g., in pit backfilling; MEND, 2015), it is recommended to carry out additional simulations to confirm the trends observed in this study.

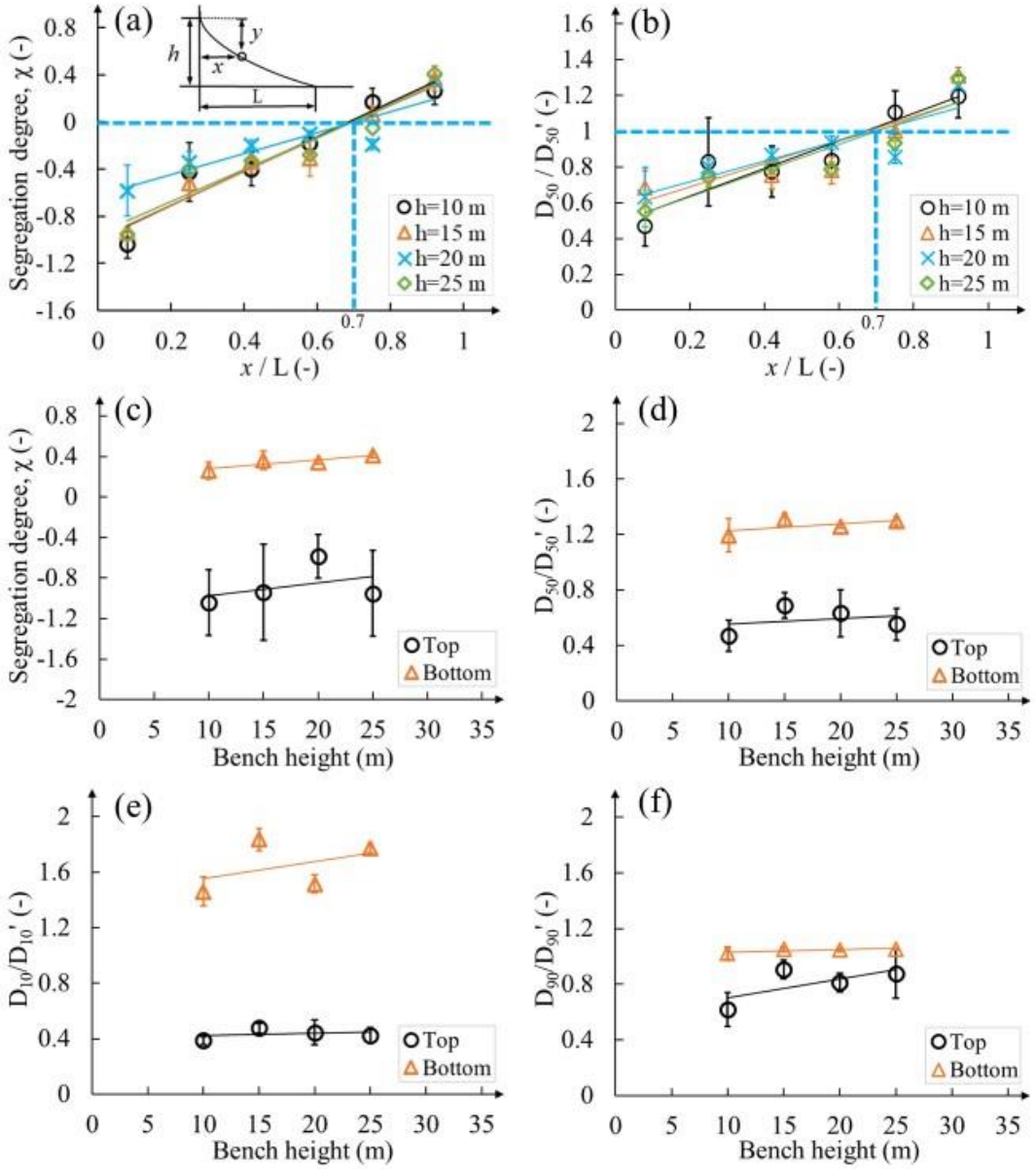

Figure 6.5: Characterization of waste rock segregation simulated for different bench heights using end-dumping method. Variation of (a) segregation degree and (b) D_{50} / D_{50}' with the relative location x / L. (c) Segregation degree, (d) D_{50} / D_{50}', (e) D_{10} / D_{10}' and (f) D_{90} / D_{90}' as functions of the bench height, and at the top (black circle, x / L = 0.08) and bottom (orange triangles, x / L = 0.92) of the slope. x [L]: horizontal distance to the deposition point. y [L]: vertical distance to dump point. L [L]: total horizontal length of the slope. h [L]: bench height. Error bars represent standard deviation.

6.3.2 Effect of waste rock PSD

The effect of waste rock PSD on segregation was investigated by comparing simulations of 4 dumps of waste rock from Quebrada Blanca mine (QB0; previous results) and Canadian Malartic mine (CM0 in Figure 6.1), for a 10 m high bench using end-dumping method. The simulated waste rock segregation for Canadian Malartic mine matched well the field observations (Qiu and Pabst, 2022a). For example, the difference of simulated and measured D_{50} / D_{50}' was smaller than 0.1 for the six sections along the slope (S1 to S6 in Figure 6.4b).

The difference of waste rock segregation for the two types of waste rock mainly focused on the bottom of the slope. For example, the difference of D_{50} / D_{50}' between the two types of waste rock was smaller than 0.16 in the top and middle sections (x / L ≤ 0.75) but was 0.4 at the bottom of the slope (x / L = 0.92) (Figure 6.6). In other words, segregation was more marked with waste rock from Canadian Malartic mine than from Quebrada Blanca mine. The reason for such difference was caused by material PSDs (before the deposition). Large particles (> 1 m) of the original waste rock accounted for only 10% of the total particle mass for Canadian Malartic but 60% for Quebrada Blanca mine. However, the percentage of large particles at the bottom of the slope (x / L = 0.92) was significantly greater for Canadian Malartic mine (70%) than for Quebrada Blanca mine (40%). In practice, reducing the quantity of the largest particles and homogenizing particle sizes could therefore contribute to limit segregation.

In practice, controlling waste rock particle sizes can be difficult and is mainly determined by blasting which depends on different basting parameters such as rock mass factors and explosive factors (Ouchterlony et al., 2019; Kinyua et al., 2022). Powder factor, i.e., the quantity of explosives (in kg) consumed per tonne of blasted rock, directly affects original waste rock sizes (greater powder factors result in finer waste rock; Singh et al., 2016). The powder factor for blasting in Canadian Malartic mine was between 0.28 and 0.34 kg/t (Lehouiller et al., 2021), but more generally, it is between 0.24 and 0.66 kg/t in hard rock mine (Kinyua et al., 2022). The mean particle size of blasted rock is sensitive to the powder factor and can decrease by 20% when the powder factor increases from 0.3 to 0.47 kg/t (Singh et al., 2016). A higher powder factor is therefore recommended to reduce the amount of large particles in the waste rock and thus contribute to limit segregation. However, further research is required to investigate the relation

between the safety range of the powder factors and the original waste rock sizes. Alternatively, crushing the largest waste rock particles before disposal (Li et al., 2019) could also be beneficial, but more studies are required to find a balance with increased costs for such operations.

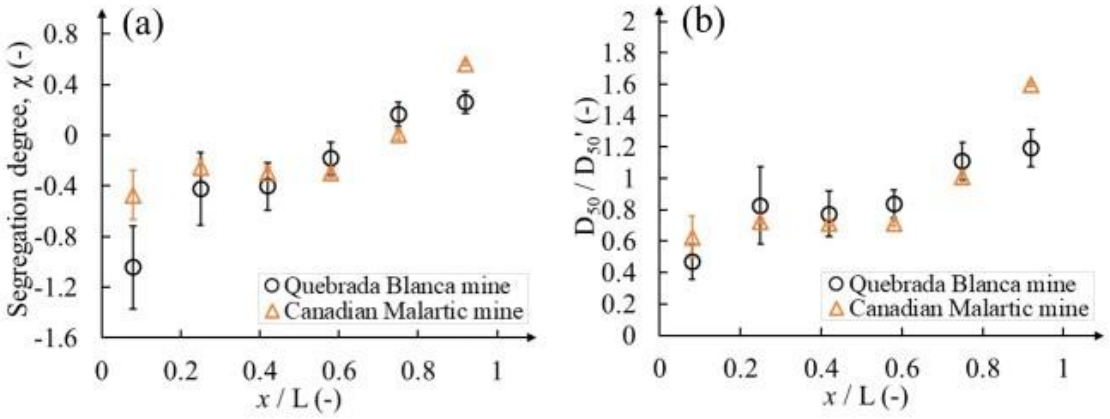

Figure 6.6: Simulated (a) segregation degree and (b) D_{50} / D_{50}' as functions of the relative location x / L for waste rock from Quebrada Blanca mine (black circles) and Canadian Malartic mine (orange triangles) using end-dumping method. Error bars represent the standard deviation.

6.3.3 Effect of mine truck payloads

The effect of the mine truck payload on waste rock segregation was investigated by dumping 4 dumps of waste rock using payloads of 300 t and 600 t (cases A1 and B1 in Table 6.2) from the top of a 10 m high bench using end-dumping method. Simulations showed that increasing mine truck payload tended to slightly reduce waste rock segregation during disposal, especially close to the top of the slope. In the finer sections (x / L $\leq$ 0.58), the segregation degree for a 600 t payload was generally greater than that for a 300 t payload with a maximum difference of 0.28. For example, the segregation degree at the top of the slope was -1.04 ± 0.33 for a 300 t payload and -0.76 ± 0.35 for a 600 t payload (Figure 6.7a). D_{50} / D_{50}' for a 600 t payload was 30% greater than that for a 300 t payload at the top of the slope.

The effect of the payload was less marked at the bottom than at the top of the slope. For example, in coarser sections (x / L $\geq$ 0.75), the difference of segregation degree for 300 t and 600 t

payloads was smaller than 0.04. Similarly, D_{50} / D_{50}' for a 600 t payload was almost the same as that for a 300 t payload (with difference smaller than 4%) at the bottom of the slope (Figure 6.7b). Despite these differences, trends were very similar, and payload therefore seemed to have a very limited effect on segregation, at least under the tested conditions. Results seem to indicate that a greater payload resulting in a larger quantity of smaller particles (e.g., D < 0.2m) moving together and contribute to restrain the movement of coarser particles, thus decreasing segregation in a similar manner to agglomeration effect for fine particles (Sutherland, 2002; Tang et al., 2004).

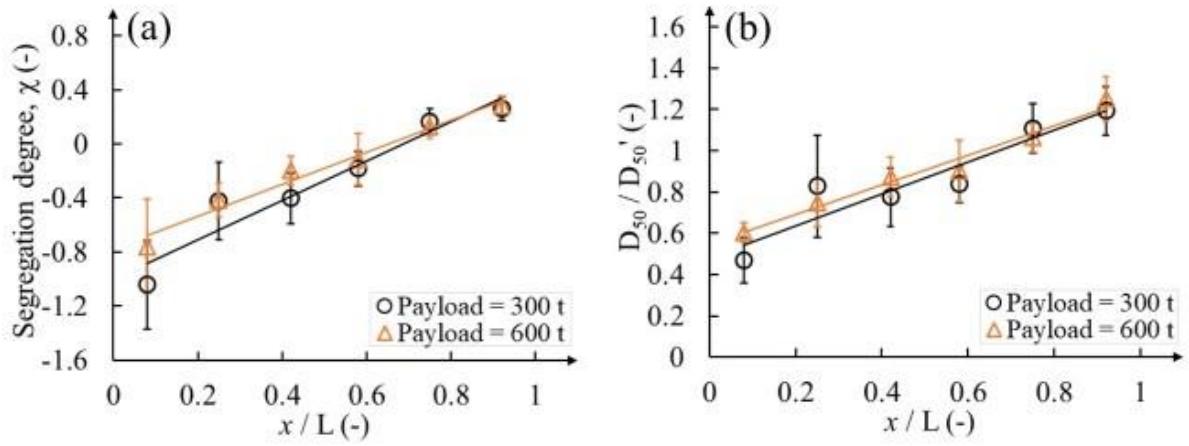

Figure 6.7: Simulated (a) segregation degree and (b) D_{50} / D_{50}' as a function of the relative location x / L with payloads of 300 t (black circles) and 600 t (orange triangles) using end-dumping method. Error bars represent standard deviation. Solid lines represent the fitted trendlines.

6.3.4 Segregation with push-dumping method

The effect of push-dumping and end-dumping methods on segregation was compared by dumping a total of 1200 t waste rock (i.e., 4 dumps) on a 10 m high bench using both methods. The relative location where segregation degree $\chi = 0$ was around x / L = 0.68 for both end-dumping and push-dumping methods. Push-dumping method tended to generate more

segregation than end-dumping method in this study (Figure 6.8). For example, the segregation degree at the top of the slope (x / L = 0.08) was -1.04 ± 0.33 for end-dumping method and -1.21 ± 0.27 (-16%) for push-dumping method (Figure 6.8a). The segregation degree at the bottom of the slope (x / L = 0.92) was 0.26 ± 0.09 for end-dumping method and 0.46 ± 0.03 ($+77\%$) for push-dumping method (Figure 6.8a). Similar trends were also observed from the distribution of D_{50} / D_{50}' along the slope. For example, D_{50} / D_{50}' for push-dumping method was 21% smaller (0.37 ± 0.11) at the top of the slope and 16% greater (1.39 ± 0.05) at the bottom than that for end-dumping method (Figure 6.8b). The main reason for the difference caused by construction method is that end-dumping method generated greater initial velocities, which, in turn, contributed to reduce waste rock segregation. However, this effect was also observed because of the limited bench height simulated and because of that, energy accumulation had less effect on segregation than initial energy.

Waste rock showed higher degree of heterogeneity along the slope with end-dumping method than with push-dumping method. For example, the maximum standard deviation of D_{50} / D_{50}' was 0.25 for end-dumping method and 0.14 for push-dumping method. End-dumping method therefore seemed to bring higher variability to the velocities of particles because of the significant collision on the slope after dumping the mine trucks, which resulted in greater collisions and energy loss. In push-dumping method, particles were less disturbed by collision and moved more homogeneously along the slope.

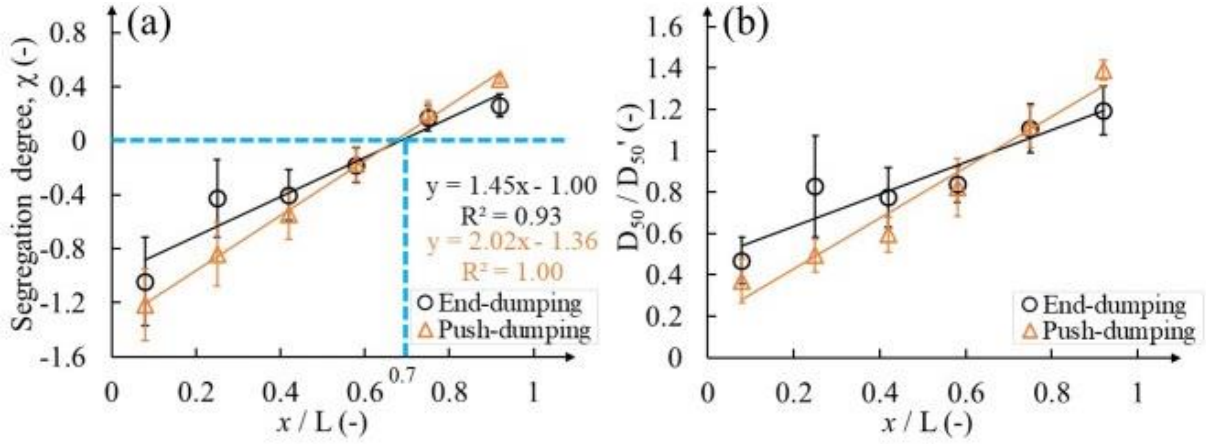

Figure 6.8: Simulated (a) segregation degree and (b) D_{50} / D_{50}' as functions of the relative location x / L when using end-dumping method (black circles) and push-dumping method (orange triangles). The push velocity was 0.2 m/s in these simulations. Error bars represent standard deviation. Solid lines represent the fitted trendlines.

The effect of push velocity on segregation was investigated by dumping 300 t waste rock on the 10 m high bench using push velocities comprised between 0.1 m/s and 0.6 m/s. Results showed that the segregation degree and relative particle diameters at the top of the slope tended to linearly increase with the push velocity (Figure 6.9). In other words, segregation decreased with push velocity, i.e., waste rock at the top of the slope was coarser as the push velocity increased, but still remained finer than the original waste rock. For example, the segregation degree at the top of the slope was − 1.23 for a push velocity of 0.1 m/s and − 0.89 (+ 28%) for a push velocity of 0.6 m/s (Figure 6.9a). D_{50} / D_{50}' at the top of the slope was 0.36 for a push velocity of 0.1 m/s and 0.51 (+ 43%) for a push velocity of 0.6 m/s (Figure 6.9c). Similar segregation in the heap formed by filling multi-sized particles though a hopper also indicates that increasing the feeding rate (i.e., increasing the initial velocity) would decrease particle segregation (Shinohara et al., 2002; Zhang et al., 2017a).

However, push velocity had limited effect on waste rock distribution at the bottom of the slope. Segregation degree and relative particle diameters at the bottom of the slope were almost the same for all the push velocities. The segregation degree at the bottom of the slope was comprised between 0.46 and 0.53 and D_{50} / D_{50}' between 1.36 and 1.46 for the investigated push velocities

(Figure 6.9 a and c). The main reason was that the effect of push velocities on coarse particles movement to the bottom of the slope was limited compared with their accumulated velocities induced by gravity. For example, the initial falling velocities of particles were almost the same (around 1 m/s) for different push velocities (Figure 6.10). The velocities of these coarse particles significantly developed to 3 to 4 m/s under gravity when they flowed to the middle of the slope.

Waste rock heterogeneity at the top of the slope tended to increase with push velocity. For example, the standard deviation of the segregation degree at the top of the slope was 0.27 for a push velocity of 0.1 m/s and was 0.39 for a push velocity of 0.5 m/s. The standard deviation of D_{50} / D_{50}' at the top of the slope was 0.08 for a push velocity of 0.1 m/s and was 0.23 for a push velocity of 0.5 m/s. However, push velocity had limited effect on waste rock heterogeneity at the bottom of the slope. For example, the standard deviations of both segregation degree and D_{50} / D_{50}' were smaller than 0.06 at the bottom of the slope for all investigated push velocities. The effect of push velocity was therefore significantly smaller than the particle energy accumulated during its movement.

In practice, although the velocity of dozers may vary depending on the operators, recommendations are based on the drawbar pull of the dozers (Klanfar et al., 2014). A higher drawbar pull generally requires a lower push velocity with 0 to 0.6 m/s for a 6 m wide blade with a drawbar pull of 100 to 150 t (Caterpillar Inc., 2019). Maximizing push velocities can therefore contribute to reduce waste rock segregation, following usual recommendations based on the drawbar pull of the dozers for security reasons.

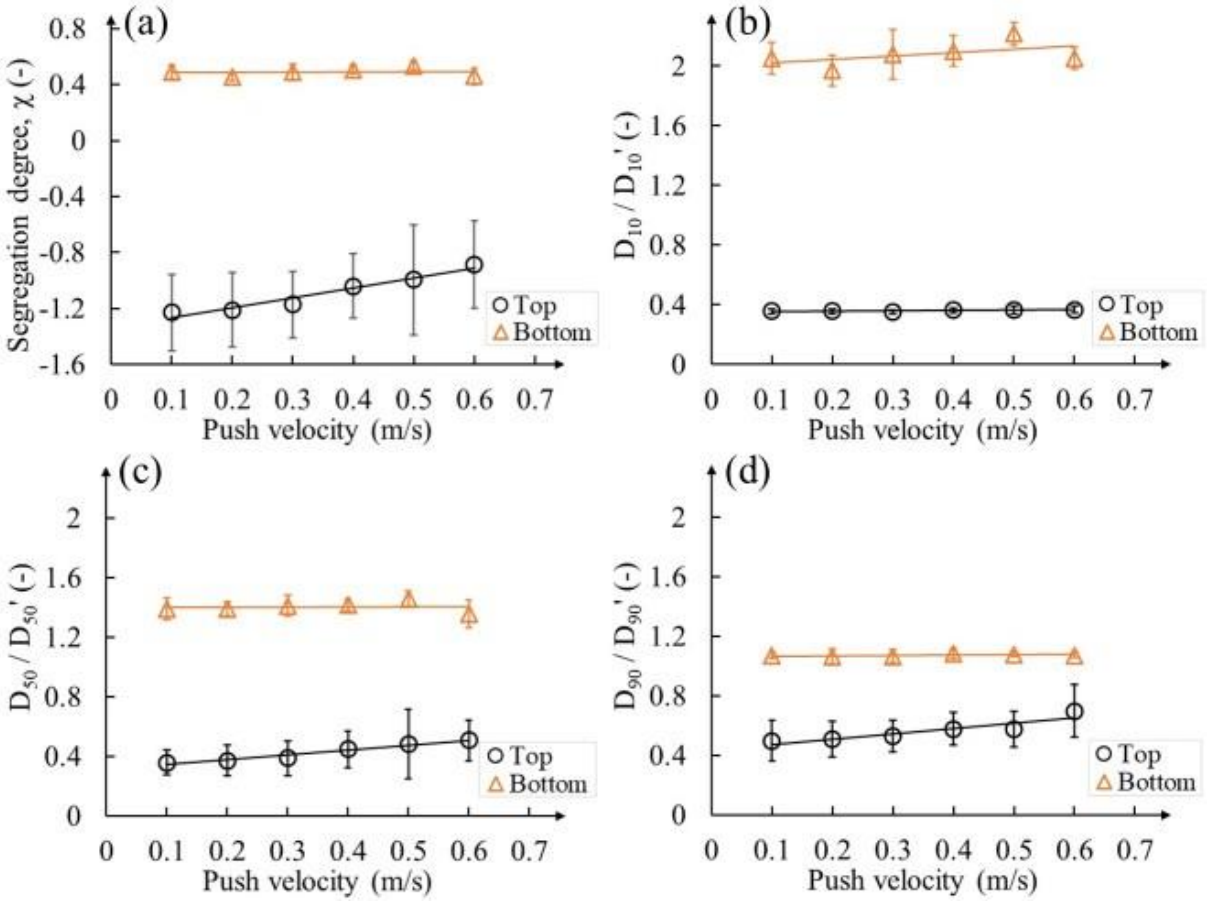

Figure 6.9: Simulated (a) segregation degree, (b) D_{10} / D_{10}', (c) D_{50} / D_{50}', and (d) D_{90} / D_{90}' as functions of the push velocity at the top (black circles, $x / L = 0.08$) and bottom (orange triangles, $x / L = 0.92$) of the slope. Error bars represent the standard deviation. Solid lines represent the fitted trendlines.

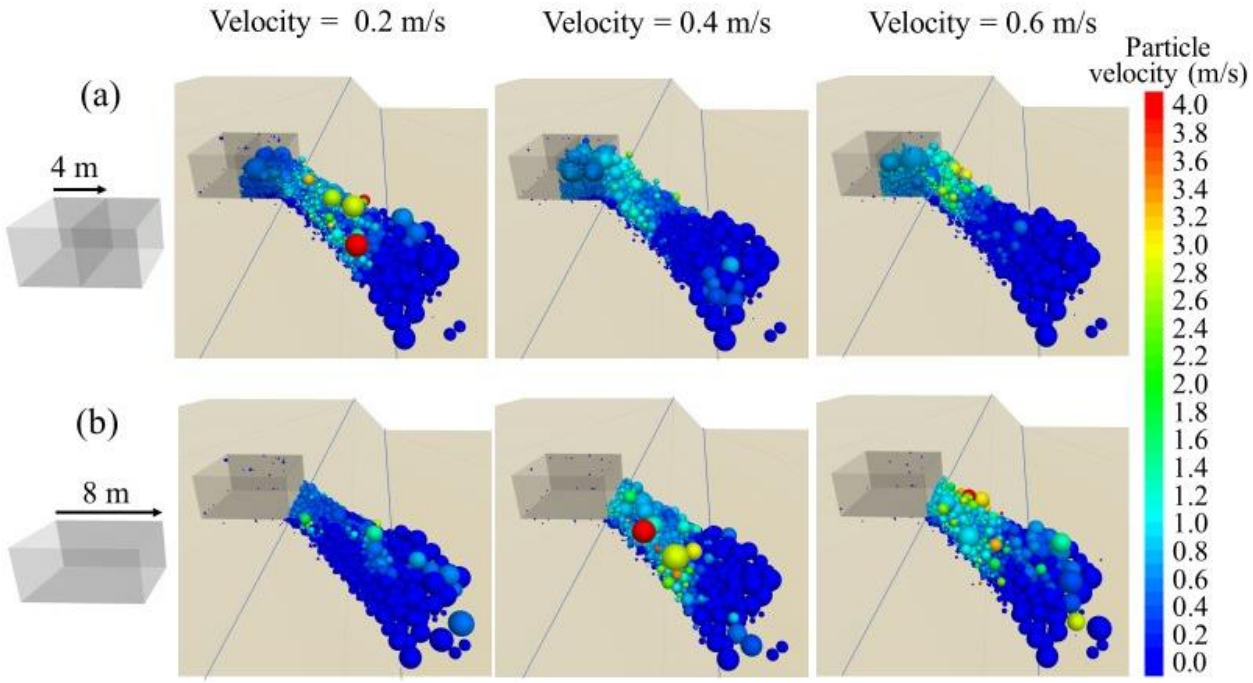

Figure 6.10: Waste rock velocities at push distances of (a) 4 m and (b) 8 m for push velocities ranging between 0.2 m/s and 0.6 m/s. The fourth dump moving on a 10 m bench was tracked. The color gradients represent particle velocities (from 0 m/s in blue to 4 m/s in red).

6.4 Result analysis and discussion

6.4.1 Practical considerations for waste rock disposal in piles

An optimal deposition of waste rock aims to reduce segregation. Controlling segregation can reduce the risk for geotechnical and geochemical instabilities in waste rock piles (Vriens et al., 2020; Raymond et al., 2021). Based on this study, the following approaches are therefore recommended:

- Bench height did not exhibit a clear effect on waste rock segregation at the top of the slope with segregation degree between − 1.04 and − 0.58 for bench heights of 10 to 25 m. Bench height had a limited effect on waste rock segregation at the bottom of the slope.
- Waste rock from the two investigated mine sites mainly affected the accumulation of large particles at the bottom of the slope. A smaller proportion of large particles in the original

waste rock can increase segregation. In practice, reducing the quantity of the largest particles and homogenizing particle sizes could therefore contribute to limit segregation.

- Increasing mine truck payloads tended to slightly reduce waste rock segregation at the top of the slope but had little effect on waste rock distribution at the bottom of the slope.
- Increasing push velocity tended to increase waste rock particle size at the top of the slope and can therefore contribute to reduce segregation.
- Construction methods had a strong impact on waste rock segregation during disposal. Push method tended to create more segregation than end-dumping method under the investigated bench height.

6.4.2 Effect of lateral disposal on waste rock segregation and heterogeneity

The effect of the studied influence factors on segregation was mainly investigated by dumping waste rock from one single point at the top of the slope. However, in practice, waste rock is commonly disposed of laterally, either sequentially or in parallel, i.e., almost concomitantly (Mclemore et al., 2009; Aubertin, 2013; Bar et al., 2020). Lateral disposal could result in high variations of waste rock sizes along the lateral direction (Chi, 2010; Barsi, 2017). In this study, the effect of lateral disposal on waste rock segregation was investigated by dumping around 300 t of waste rock sequentially from three points on a 10 m high bench using end-dumping method (Figure 6.11). Waste rock was first dumped at point 1, the second dump started at point 2 when waste rock in the previous dump stopped moving, and a third dump was simulated from point 3. A new disposal cycle started again with new dumps simulated at point 1, then point 2, and finally point 3. The dumping process continued until a total of 12 dumps were simulated, i.e., 4 dumps from each point. The total mass of waste rock dumped for lateral disposal was 3600 t in each case. The effect of the dump spacing between two sequential dumps was also investigated (4 m, 8 m and 12 m distance). Waste rock slopes were equally divided into 6 sections in the vertical direction (similarly to previous cases, see Figure 6.4). Segregation degree and D_{50} / D_{50}' in each section were obtained for each case and results were compared with base case A1 (1-point disposal in Figure 6.12).

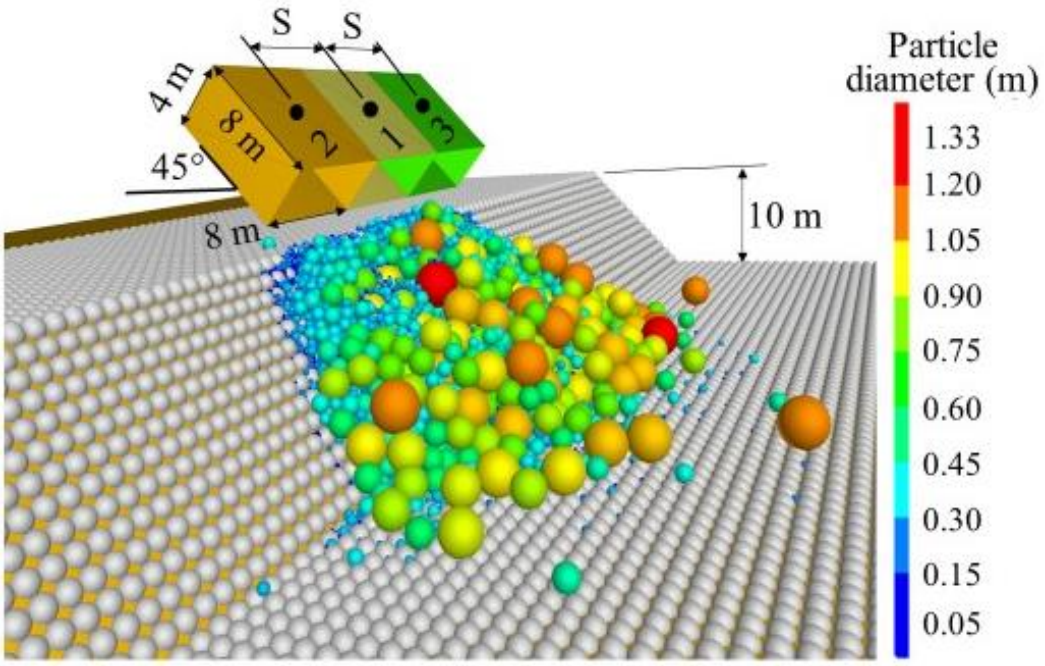

Figure 6.11: Model for lateral disposal on a 10 m high bench using end-dumping method. A total of 12 dumps were disposed sequentially and repeatedly from points 1 to 3 (4 dumps of 300 t waste rock per deposition point). S [L]: spacing between two sequential dumps (S = 4 m, 8 m and 12 m in this study). Dumped waste rock particles are colored depending on their diameters (from 0.1 m in blue to 2.66 m in red).

Significant segregation was observed for all the cases with lateral sequential disposal. The segregation degree was generally smaller than − 0.32 at the top (x / L = 0.08) of the slope and greater than 0.27 at the bottom (x / L = 0.92), and D_{50} / D_{50}' was smaller than 0.78 at the top of the slope, and greater than 1.2 at the bottom (Figure 6.13b).

Simulations showed that lateral disposal tended to limit waste rock segregation compared to deposition from a single point. For example, the segregation degree at the top of the slope was − 0.32 ± 0.19 for lateral disposal, i.e., 70% greater than that for 1-point disposal. Lateral disposal therefore tended to constrain waste rock movement in the lateral direction, but this effect tended to decrease with the spacing between lateral dumps. For example, waste rock dumped from

point 1 covered a width of around 23 m at the bottom of the slope with a single point dumping, 19 m with a lateral dumping with 4 m spacing, and 15 m with a lateral dumping with 8 m and 12 m spacing (Figure 6.12). Lateral disposal therefore resulted in a greater accumulation of particles at the top of the slope, including some coarse particles (e.g., > 1.5 m), therefore decreasing segregation compared to a 1-point disposal. Increasing dump spacing had limited effect on waste rock segregation. For example, the difference of segregation degree (also D_{50} / D_{50}') was smaller than 0.14 for each section of the slope, independently of the dump spacing (Figure 6.13). Lateral disposal with a dump spacing small enough to make sure dumps interact with each other, can therefore contribute to decrease segregation and homogenize waste rock along the slope. Increasing spacing too much would, however, result in the same results as for a single point dumping when lateral dumps do not interact anymore.

Lateral heterogeneity under lateral disposal tended to be less pronounced than with a single point disposal (1-pint disposal in Figures 6.12). For example, the maximum difference of segregation degree at the top of the slope was 0.55 for lateral disposal and 0.76 (38%) for single point disposal. The standard deviations of segregation degree and D_{50} / D_{50}' also were generally greater for single point disposal than for lateral disposal (Figure 6.13). For example, the standard deviations of segregation degree at different sections were generally smaller than 0.1 for lateral disposal, but were always greater than 0.1 and up to 0.33 for single point disposal (Figure 6.13a). There was, however, no clear relationship between heterogeneity and the relative location along the slope.

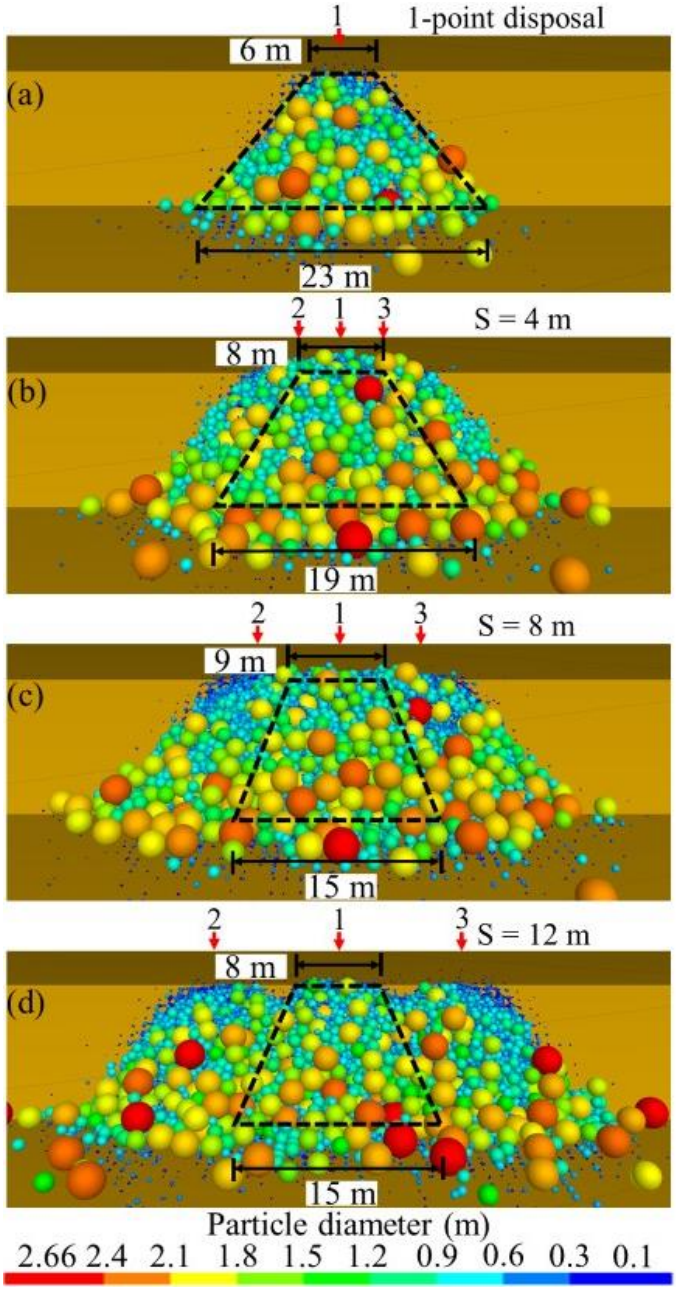

Figure 6.12: Waste rock distribution for (a) 1-point disposal and lateral disposal with dump spacing of (b) 4 m, (c) 8 m and (d) 12 m on a 10 m high bench using end-dumping method. (a): A total of 4 dumps were simulated from point 1. (b – d): A total of 12 dumps were simulated sequentially and repeatedly from points 1, 2 and 3 (4 dumps per point). Black dash lines cover the areas for waste rock that was dumped from point 1. S [L]: dump spacing between two sequential dumps. Dumped waste rock particles are colored depending on their diameters (from 0.1 m in blue to 2.66 m in red).

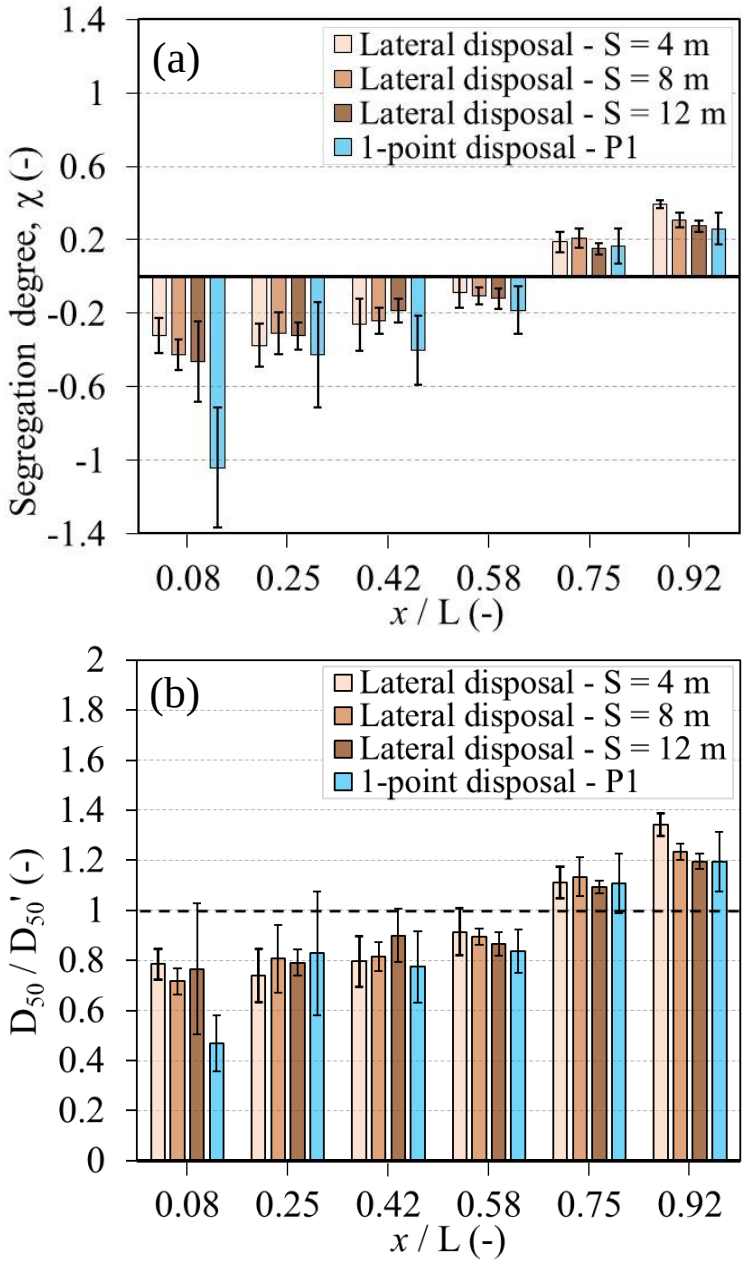

Figure 6.13: Simulated (a) segregation degree and (b) D_{50} / D_{50}' as a function of the relative location x / L both for lateral disposal and 1-point disposal using end-dumping method on a 10 m high bench. S [L]: spacing between two sequential dumps. Error bars represent the standard deviation (simulations were repeated five times).

6.4.3 Discussion

Waste rock disposal simulations in this study indicated that bench height and payload had limited effect on segregation, and lateral disposal and increasing push velocity limited segregation. Despite these encouraging trends which may be useful to give operators practical recommendations to reduce segregation in the field, numerical simulations carried out were based on a few assumptions that could somewhat affect these conclusions.

First, the minimum particle diameter simulated was 0.1 m, to increase the quantity of simulated waste rock without unrealistically increasing calculation time. For example, the number of particles was 9200 (with 1.8×10^5 contacts) for a 10 m bench and 1.5×10^5 (with 5.4×10^5 contacts) for a 25 m bench. The computational time reached 138 h for a 25 m bench, i.e., 55 times longer than for a 10 m bench. Actually, 100 kg waste rock with diameters between 0.5 cm and 1 cm would have generated 1.5×10^5 additional particles in PFC3D models. Simulating smaller particles with current computing ability for field scale simulations was thus practically impossible. Some techniques such as particle scale-up (e.g., Coarse-Graining technique; Nasato et al., 2015) have been developed to replace real particles by representative particles, substantially reducing the required number of particles and computational time (Roessler at al., 2018). However, the main limitation of these techniques is the determination of upscaling factors which determine the representativity of a simulated process (Xie et al., 2016). Because of the particle diameter limitation, the ratio of the bench height to the maximum particle diameter (e.g., 2.66 m in Quebrada Blanca mine) was only 3.8 for a 10 high bench, which was relatively small compared to typical values in the field (usually around 7).

In push-dumping simulations, waste rock was pushed to the edge of the slope from a short distance, which is different from the practice where waste rock is sometimes dumped on the pile surface and pushed over several dozens of meters to the slope edge. Further research on push-dumping method with a longer push distance was suggested to evaluate particle mixture state during pushing.

In this study, waste rock was dumped on an existing initial slope with the objective to reduce calculation time. This pre-existing slope was inclined with an angle of 45°, which was slightly greater than the natural slope angle ranging between 37° and 40° for the studied waste rock piles

(Zhang et al., 2017b; Lehouiller et al., 2020). This rather large angle was chosen specifically to reduce its potential impacts on the results. Additional simulations (not shown here) confirmed that smaller slope angles down to 37°had no significant effect on the simulated segregation, which indicates that it may be possible to accelerate calculation time by using even small initial slope angle. In addition, a base layer was built with homogeneous 1m-diameter balls. Heterogeneous base layer was then set with 1 m balls and 0.5 m balls. Heterogeneous base layer created similar repose angle to homogeneous base layer (difference smaller than 2°). The segregation degree with heterogeneous base layer was generally fall within the reasonable range of homogeneous base layer (See details in Appendix F).

The recommendations regarding waste rock disposal (see above) were given with the objective of reducing segregation. The geotechnical stability of waste rock pile is, however, also affected by waste rock disposal but was not considered in this study. Segregation and heterogeneity usually create negative effect on the geotechnical properties, but sometimes also bring positive effect on pile's stability. For example, although segregation and heterogeneity can bring risks to water flow along irregular and diverted paths within waste rock piles (Lahmira et al., 2016; Raymond et al., 2021), the presence of internal fine-grained layers (e.g., compacted layers during construction) sometimes also increase the factors of safety, resulting in positive effects on the geotechnical stability of waste rock piles (Maknoon et al., 2021). More investigations on waste rock disposal are thus necessary to comprehensively control waste rock segregation with considering both hydrogeological and geotechnical stability.

6.5 Conclusion

PFC3D was used to simulate the flow behaviour of waste rock disposal and evaluate the effect of construction methods (i.e., push-dumping and end-dumping method) and bench heights (10 to 25 m) on waste rock segregation. Segregation degree (χ) and relative particle diameters (D_{10} / D_{10}', D_{50} / D_{50}', D_{95} / D_{95}') from the top to the bottom of the slope were compared to quantify segregation. Various influence factors, including mine truck payloads (300 t and 600 t), push velocities (0.1 to 0.6 m/s), lateral disposal, and waste rock PSD were investigated. The following conclusions were made based on the results of this study:

- In general, waste rock segregation was significant for all the different investigated factors. Segregation degree was always negative and smaller than − 0.5 at the top of the slope, and positive and greater than 0.3 at the bottom, indicating waste rock was finer at the top and coarser at the bottom of the slope than the original waste rock (before disposal). Diameter D_{50} at the bottom of the slope was always 2 to 4 times greater than that at the top of the slope for all the simulated cases in this study.
- Simulated bench heights (10 m to 25 m) and mine truck payloads (300 t to 600 t) had limited effect on waste rock segregation.
- Waste rock containing a smaller proportion of large particles were more prone to segregation. A greater powder factor (yet respecting safety range) and crushing the largest particles is therefore suggested to homogenize waste rock and reduce segregation during disposal.
- Increasing the push velocity in push-dumping method (from 0.1 m/s to 0.6 m/s) tended to reduce segregation at the top of the slope but had limited effect on waste rock distribution at the bottom. Maximizing push velocities can therefore contribute to reduce waste rock segregation, following usual recommendations based on the drawbar pull of the dozers for security reasons.
- Push method tended to create more segregation than end-dumping method because end-dumping method generated greater initial velocities, which contributed to reduce waste rock segregation. However, this effect was also observed because of the limited bench height simulated and because of that, energy accumulation had less effect on segregation than initial energy.
- Lateral disposal tended to limit waste rock segregation compared to deposition from a single point. Lateral disposal with a suitable dumping spacing (i.e., small enough to make sure the sequential dumps interact with each other) was beneficial to homogenize waste rock along the slope. Sequential dumps with a small dump spacing were recommended to reduce waste rock segregation in practice.

These recommendations should contribute to improve the deposition plan of waste rock on operating and future mine sites. However, this research focused on a few key operational

influence factors and only for limited bench heights (mainly for numerical constraints), so further investigations taking into account the effect on the hydro-geotechnical and geochemical properties are recommended to improve segregation control and optimize waste rock disposal.

6.6 Acknowledgement

The authors would like to acknowledge the financial support from NSERC (grant number: RGPIN-2017-05725), FRQNT (grant number: 2017-MI-202116), the industrial partners of the Research Institute of Mines and Environment (RIME) (http://irme.ca/).

6.7 References

Ai, J., Chen, J.F., Rotter, J.M. and Ooi, J.Y. (2011). Assessment of rolling resistance models in discrete element simulations. Powder Technology, 206(3): 269-282.

Akcil, A., & Koldas, S. (2006). Acid Mine Drainage (AMD): causes, treatment and case studies. Journal of cleaner production, 14(12-13), 1139-1145.

Amos, R.T., Blowes, D.W., Bailey, B.L., Sego, D.C., Smith, L. and Ritchie, A.I.M. (2015). Waste-rock hydrogeology and geochemistry. Applied Geochemistry, 57: 140-156.

Anterrieu, O., Chouteau, M. and Aubertin, M. (2010). Geophysical characterization of the large-scale internal structure of a waste rock pile from a hard rock mine. Bulletin of Engineering Geology and the Environment, 69(4): 533-548.

Appels, W. M., Ireson, A. M., & Barbour, S. L. (2018). Impact of bimodal textural heterogeneity and connectivity on flow and transport through unsaturated mine waste rock. Advances in Water Resources, 112, 254-265. doi:10.1016/j.advwatres.2017.12.008

Asachi, M., Hassanpour, A., Ghadiri, M., & Bayly, A. (2018). Experimental evaluation of the effect of particle properties on the segregation of ternary powder mixtures. Powder technology, 336, 240-254.

Asmaei, S., Shourijeh, P.T., Binesh, S.M., & Ghaedsharafi, M.H. (2018). An experimental parametric study of segregation in cohesionless soils of embankment dams. Geotechnical Testing Journal, 41(3), 473-493.

Aubertin, M. (2013). Waste rock disposal to improve the geotechnical and geochemical stability of piles. Proceedings of the world mining congress, Montreal, Quebec, Canada.

Bar, N., Semi, J., Koek, M., Owusu-Bempah, G., Day, A., Nicoll, S. and Bu, J. (2020). Practical waste rock dump and stockpile management in high rainfall and seismic regions of Papua New Guinea, Proceedings of the (2020) International Symposium on Slope Stability in Open Pit Mining and Civil Engineering, Australian Centre for Geomechanics, Perth, pp. 117-128

Barsi, D. (2017). Spatial variability of particles in waste rock piles. Master's thesis, University of Alberta.

Barton, N. (1982). Shear strength investigations for surface mining. Paper presented at the Proceedings of the 23rd US Rock Mechanics Symposium.

Bian, Z., Inyang, H.I., Daniels, J.L., Otto, F., Struthers, S. (2010). Environmental issues from coal mining and their solutions. Mining Science and Technology (China), 20(2):215-223

Bishwal, R. M., Sen, P., & Jawed, M. (2019). Improving Stability of Overburden Dump Through Volume Minimization by Co-Deposition of Materials Based on Size and Material Type Distribution. In Waste Management and Resource Efficiency (pp. 483-493). Springer, Singapore.

Blight, G. E. (2010). Geotechnical engineering for mine waste storage facilities. CRC Press.

Bréard Lanoix, M.L., Pabst, T., & Aubertin, M. (2017). Characterization of the Hydrogeological Properties of a Sand Layer Placed on an Experimental Waste Rock Pile. In GeoOttawa 2017-70th Canadian Geotechnical Conference.

Burnley, R.B. (1993). Mine reclamation and waste dump stability. M. Sc. Thesis, University of Nevada, Reno, Reno, United States

Cash, A. (2014). Structural and Hydrologic Characterization of Two Historic Waste Rock Piles. Master's thesis, University of Alberta.

Caterpillar Inc., (2019). Caterpillar performance handbook. Edition 49. https://www.williamadams.com.au/media/3275/caterpillar-performance-handbook-49-william-adams-compressed.pdf

Cepa, C. E. P. A. (2007). Canadian soil quality guidelines for the protection of environmental and human health. Quebec, Canada: National Guidelines and Standards Office.

Cheng, Y.M., Fung, W.H.I., Li, L., and Li, N. (2019). Laboratory and field tests and distinct element analysis of dry granular flows and segregation processes. Natural Hazards and Earth System Sciences, 19: 181-199.

Chi, X. (2011). Characterizing low-sulfide instrumented waste-rock piles: image grain-size analysis and wind-induced gas transport (Master's thesis, University of Waterloo).

Cundall P.A. and Strack O.D.L. (1979). A discrete numerical model for granular assemblies. Géotechnique, 29(1): 47-65.

Coetzee C.J. (2020). Calibration of the discrete element method: Strategies for spherical and non-spherical particles. Powder Technology, 364: 851-878.

Coetzee, C.J. (2016). Calibration of the discrete element method and the effect of particle shape. Powder Technology, 297: 50-70.

Combarros, M., Feise, H.J., Zetzener, H. and Kwade A. (2014). Segregation of particulate solids: Experiments and DEM simulations. Particuology, 12: 25-32.

Chapuis, R. P. (2012). Predicting the saturated hydraulic conductivity of soils: a review. Bulletin of engineering geology and the environment, 71(3), 401-434.

Deiminiat, A., & Li, L. (2022). Experimental study on the reliability of scaling down techniques used in direct shear tests to determine the shear strength of rockfill and waste rocks. CivilEng, 3(1), 35-50.

Gervais, D., Roy, C., Thibault, A., Pednault, C., Doucet, D. (2014). Technical report on the mineral resource and mineral reserve estimates for the Canadian Malartic properties, Québec, Canada.

Gupta, A. K. (2016). Effects of particle size and confining pressure on breakage factor of rockfill materials using medium triaxial test. Journal of Rock Mechanics and Geotechnical Engineering, 8(3), 378-388.

Hawley M. and Cunning J. (2017). Guidelines for Mine Waste Dump and Stockpile Design, CSIRO Publishing, 2017. ProQuest Ebook Central

Hudson-Edwards, K. A., Jamieson, H. E., & Lottermoser, B. G. (2011). Mine wastes: past, present, future. Elements, 7(6), 375-380.

Itasca Consulting Group, Inc. (2019). PFC — particle flow code in 2 and 3 dimensions. Version 6.0, Documentation set of version 6.00.15. Minneapolis, Minnesota, USA.

Iwashita, K., and Oda, M. (1998). Rolling Resistance at Contacts in Simulation of Shear Band Development by DEM. Journal of Engineering Mechanics ASCE, 124: 285-292.

Jiang, Y., Wang, L., Wu, Q., Sun, Z., Elmo, D. and Zheng, L. (2020). An improved shear stress monitoring method in numerical direct shear tests by particle flow code, Journal of Testing and Evaluation (in press).

Kenney, T.C. and Westland, J. (1993). Laboratory Study of Segregation of Granular Filter Materials," Filters In Geotechnical and Hydraulic Engineering: Proceedings of the First International Conference "Geo-Filter", Karlesruhe, Germany, pp. 313-319.

Klanfar, M., Kujundžić, T., & Vrkljan, D. (2014). Calculation analysis of bulldozer's productivity in gravitational transport on open pits. Tehnički vjesnik, 21(3), 517-523.

Kumar, S. (2004). Vibration in operating heavy haul trucks in overburden mining. Applied Ergonomics, 35(6), 509-520.

Lahmira, B., Lefebvre, R., Aubertin, M. and Bussiere, B. (2016). Effect of heterogeneity and anisotropy related to the construction method on transfer processes in waste rock piles. Journal of Contaminant Hydrology, 184: 35-49.

Langroudi, M.F., Soroush, A., Shourijeh, P.T. (2015). A comparison of micromechanical assessments with internal stability/instability criteria for soils. Powder Technology, 276: 66-79.

Lehouiller, P., Lampron, S., Gagnon, G., Houle, N., Bouchard, F. (2020). NI 43-101 Technical Report, Canadian Malartic Mine, Québec, Canada.

Li, M., Zhang, J., Song, W., & Germain, D. M. (2019). Recycling of crushed waste rock as backfilling material in coal mine: effects of particle size on compaction behaviours. Environmental Science and Pollution Research, 26(9), 8789-8797.

Lucas, R & Kizil,M.S. (2014). Optimisation of Waste-Dump Lift Heights for Pre-strip Operations, in Naj Aziz and Bob Kininmonth (eds.), Proceedings of the (2014) Coal Operators' Conference, Mining Engineering, University of Wollongong. https://ro.uow.edu.au/coal/539

Molson, J.W., Fala, O., Aubertin, M. and Bussiere, B. (2005). Numerical simulations of pyrite oxidation and acid mine drainage in unsaturated waste rock piles. Journal of Contaminant Hydrology, 78(4): 343-371.

Maknoon M. (2016). Slope stability analyses of waste rock piles under unsaturated conditions following large precipitations. Ph.D. thesis, Ecole Polytechnique Montreal, Montreal, QC, Canada.

McLemore, V.T., Fakhimi, A., van Zyl, D., et al. (2009). Literature review of other rock piles: Characterization, weathering, and stability. Report OF–517, Questa Rock Pile Weathering Stability Project. New Mexico Bureau of Geology and Mineral Resources.

Maknoon, M. and Aubertin, M. (2021). On the Use of Bench Construction to Improve the Stability of Unsaturated Waste Rock Piles. Geotechnical and Geological Engineering, 39(2): 1425-1449.

MEND. (2015). MEND Report 2.36.1 In-Pit Disposal of Reactive Mine Wastes: Approaches, Update and Case Study Results. Retrieved from 555 Booth St Ottawa.

Nasato, D. S., Goniva, C., Pirker, S., & Kloss, C. (2015). Coarse graining for large-scale DEM simulations of particle flow–an investigation on contact and cohesion models. Procedia engineering, 102, 1484-1490.

Nichols, R.S. (1986). Rock segregation in waste dumps. Proceedings of the international conference on flow-through rock drains.

Ouchterlony, F., Sanchidrián, J.A., (2019). A review of development of better prediction equations for blast fragmentation. J. Rock Mech. Geotech. Eng. 11, 1094–1109.

Peacock, H. M. (1938). The design or adaptation of storage bunkers to prevent size segregation of solids. J. Instit. Fuel 11: 230–239.

Pedretti, D., Mayer, K.U. and Beckie, R.D. (2020). Controls of uncertainty in acid rock drainage predictions from waste rock piles examined through Monte-Carlo multicomponent reactive transport. Stochastic Environmental Research and Risk Assessment, 34: 219–233.

Qiu, P. and Pabst, T. (2022a). Characterization of particle size segregation and heterogeneity along the slopes of a waste rock pile using image analysis. Under review.

Qiu, P., and Pabst, T. (2022b). Waste rock segregation during disposal: Calibration and upscaling of discrete element simulations. Powder Technology, 117981.

Ramani, R.V. (2012). Surface mining technology: progress and prospects. Procedia Engineering, 46, 9-21.

Raymond, K. E., Seigneur, N., Su, D., & Mayer, K. U. (2021). Investigating the Influence of Structure and Heterogeneity in Waste Rock Piles on Mass Loading Rates—A Reactive Transport Modeling Study. Frontiers in Water, 39.

Roessler, T., & Katterfeld, A. (2018). Scaling of the angle of repose test and its influence on the calibration of DEM parameters using upscaled particles. Powder technology, 330, 58-66.

Sherard, J. L., Dunnigan, L. P., & Talbot, J. R. (1984). Basic properties of sand and gravel filters. Journal of Geotechnical Engineering, 110(6), 684–700.

Shimosaka, A., Nousou, I., Shirakawa, Y., & Hidaka, J. (2013). Effect of particle shape on size segregation of particles. Chemical Engineering Transactions, 32, 2143-2148.

Shinohara, K., & Golman, B. (2002). Segregation indices of multi-sized particle mixtures during the filling of a two-dimensional hopper. Advanced Powder Technology, 13(1), 93-107.

Singh, P. K., Roy, M. P., Paswan, R. K., Sarim, M. D., Kumar, S., & Jha, R. R. (2016). Rock fragmentation control in opencast blasting. Journal of Rock Mechanics and Geotechnical Engineering, 8(2), 225-237.

Smith, L. J., Bailey, B. L., Blowes, D. W., Jambor, J. L., Smith, L., & Sego, D. C. (2013). The Diavik Waste Rock Project: Initial geochemical response from a low sulfide waste rock pile. Applied geochemistry, 36, 210-221.

Soofastaei, A., Aminossadati, S. M., Kizil, M. S., & Knights, P. (2016). The influence of rolling resistance on haul truck fuel consumption in surface mines. Tribology International Journal, 2(1), 215-228.

St-Arnault, M., Vriens, B., Blaskovich, R., Aranda, C., Klein, B., Ulrich Mayer, K., & Beckie, R. D. (2020). Geochemical and mineralogical assessment of reactivity in a full-scale heterogeneous waste-rock pile. Minerals Engineering, 145.

Sutherland, K.J. (2002). Quantifying and Controlling Segregation in Earth Dam Construction, M.S. thesis, University of Toronto, Toronto, Canada.

Sutherland, K. and Grabinsky, M. (2003). Evaluating Segregation in Granular Filters for Earth Dams, the 56th Canadian Geotechnical Conference, Winnipeg, Canada, pp. 58–63.

Tang, P., & Puri, V. M. (2004). Methods for minimizing segregation: a review. Particulate Science and Technology, 22(4), 321-337.

Thakur, S.C., Morrissey J.P., Sun, J., Chen, J.F., Ooi, J.Y. (2014). Micromechanical analysis of cohesive granular materials using the discrete element method with an adhesive elasto-plastic contact model, Granular Matter, 16: 383-400.

Vriens, B., Plante, B., Seigneur, N., & Jamieson, H. (2020). Mine waste rock: Insights for sustainable hydrogeochemical management. Minerals, 10(9), 728.

Westland, J. (1988). A study of segregation in cohesionless soil. M.A.Sc. Thesis, Department of Civil Engineering, University of Toronto, Toronto, Canada.

Williams, D., & Rohde, T. (2008). Rainfall infiltration into and seepage from rock dumps—a review. Paper presented at the Rock Dumps (2008): Proceedings of the First International Seminar on the Management of Rock Dumps, Stockpiles and Heap Leach Pads.

Xie, L., Zhong, W., Zhang, H., Yu, A., Qian, Y., & Situ, Y. (2016). Wear process during granular flow transportation in conveyor transfer. Powder technology, 288, 65-75.

Xu, W., Xu, Q., & Hu, R. (2011). Study on the shear strength of soil–rock mixture by large scale direct shear test. International Journal of Rock Mechanics and Mining Sciences, 48(8), 1235-1247. doi:10.1016/j.ijrmms.2011.09.018

Zevgolis, I. E. (2018). Geotechnical characterization of mining rock waste dumps in central Evia, Greece. Environmental Earth Sciences, 77(16), 1-18

Zhang, D., Zhou, Z., & Pinson, D. (2017a). DEM simulation of particle stratification and segregation in stockpile formation. In EPJ Web of Conferences (Vol. 140, p. 15018). EDP Sciences.

Zhang, S., & Liu, W. (2017b). Application of aerial image analysis for assessing particle size segregation in dump leaching. Hydrometallurgy, 171, 99-105.

CHAPTER 7 SUMMARY, DISCUSSION, CONCLUSION AND RECOMMENDATIONS

7.1 Summary

Large amounts of waste rock are generated by mining operations and generally disposed of on the surface, close to the production sites (Anterrieu et al., 2010; Aubertin, 2013). Waste rock disposal usually causes segregation, creating complicated heterogeneous structures in waste rock piles (Nichols, 1986). These heterogeneities bring high degree of uncertainties to the spatial distribution of geotechnical and hydrogeological properties (e.g., shear strength, hydraulic conductivity), thus increasing the risk for both geochemical and geotechnical instabilities (Lahmira et al., 2016). Segregation characterization and evaluation at field scale considering the effect of construction method and bench height is, however, extremely challenging because of the large dimensions of the piles, the instability of the steep slopes and the difficulty to determine the mass and size of large and irregular particles (Dwumfour et al., 2020; Raymond et al., 2021).

The main objective of this project was therefore to assess the impact of waste rock disposal on waste rock segregation and heterogeneity in waste rock piles and to propose recommendations to reduce segregation and improve disposal strategy. This research also included secondary objectives which aimed to characterize waste rock segregation and heterogeneity in piles, and to evaluate segregation under various operational conditions during disposal. To achieve these objectives, waste rock segregation and heterogeneity were characterized and evaluated using field observations, experimental tests in the laboratory and discrete element simulations. Experimental and field results provided the basis to investigate waste rock segregation under various influence factors such as construction method and bench height by using discrete element simulations.

Field evaluation of waste rock segregation and heterogeneity was conducted using photos covering a 1400 m long slope of a waste rock pile, and analyzed with software ImageJ for the determination of particle mass and size. Waste rock segregation degree and characteristic diameters were characterized as a function of the relative location along the slope.

Waste rock used for tests and simulations at laboratory scale was obtained from Canadian Malartic mine, a partner mine site, and the material was scalped at diameters comprised between 8 mm and 89 mm.

Waste rock flow behaviour was simulated using rolling resistance linear model in PFC3D (Itasca, 2019), which could efficiently simulate contact interactions of granular media in three dimensions. A new model calibration method was proposed to reliably simulate waste rock segregation at both laboratory and field scales, and to provide the basis to evaluate the impact of waste rock disposal on segregation. This method included model calibration using repose angle tests and validation using segregation tests for laboratory scale models, and was then upscaled for field models.

Repose angle can give an indication of the material flowability and is directly related to the intrinsic properties of particles such as the friction and rolling. Waste rock repose angles were measured in the laboratory (repose angle tests) or in the field. Repose angle tests consisted in lifting a bucket filled with waste rock (around 75 kg) so it formed a conic pile on the ground. Field repose angles were determined by measuring slope angles of waste rock piles at two mine sites, namely Canadian Malartic and Quebrada Blanca mines. Friction and rolling resistance coefficients were then adjusted to match the measured angle formed by the waste rock.

Calibrated models were validated by simulating waste rock segregation behaviour measured in the laboratory (segregation tests) and observed in the field (image analysis – see above – or literature results). Laboratory segregation tests were conducted by dumping 10 buckets of waste rock (i.e., a total of around 200 kg) sequentially from the top edge of a 1 m high vertical wall to form a semi cone slope. The characteristic diameters and segregation degree of waste rock from the top to the bottom of the slope were measured and compared with simulation results at both laboratory and field scales.

Numerical models were then used to evaluate waste rock segregation and heterogeneity under various influence factors including construction methods (end-dumping and push-dumping methods), bench heights (10 to 25 m), waste rock PSD, mine truck payloads (300 t and 600 t), push velocities (0.1 to 0.6 m/s), and lateral disposal. Recommendations to control segregation and improve disposal strategy were proposed based on these results.

Waste rock characterization in the field indicated significant segregation and heterogeneity in waste rock piles. Characteristic diameters (e.g., D_{10}, D_{50}, D_{90}) and segregation degree significantly increased from the top to the bottom of the slope. Results also showed that segregation and lateral heterogeneity could result in high variability (one to two orders of magnitude difference) of the saturated hydraulic conductivity and more generally of the geotechnical properties of waste rock in the field.

The calibration approach proposed in this research proved easy to use and efficient to simulate waste rock segregation at various scales, as proven by laboratory and field validation. These encouraging results confirmed PFC3D models could be used to extrapolate these preliminary observations to larger scales and to evaluate and compare different construction methods depending on various operational constraints.

Simulations results tended to show that bench height did not have a clear effect on waste rock segregation along the slope (at least for the investigated bench heights).

Waste rock particle size distribution strongly affected the accumulation of large particles (e.g., >1 m) at the bottom of the slope. A smaller proportion of large particles in the original waste rock (i.e., before the deposition) tended to increase segregation. In practice, homogenizing particle sizes in the waste rock could therefore contribute to limit segregation. Using a greater powder factor or crushing the largest waste rock particles was therefore recommended to homogenize waste rock (before the deposition) and thus contribute to limit waste rock segregation.

Increasing mine truck payload tended to slightly reduce waste rock segregation at the top of the slope but had limited effect at the bottom. Despite these differences, rwaste rock distribution along the slope was very similar for simulated payloads of 300 t and 600 t, and truck sizes did therefore not seem to have a critical effect on segregation.

Waste rock segregation also tended to decrease with push velocity. The effect was especially noticeable close to the top of the slope where segregation degree and relative particle diameters tended to linearly increase with the push velocity while push velocity had little effect at the bottom of the slope. Maximizing push velocities can therefore contribute to reduce waste rock segregation, following usual recommendations based on the drawbar pull of the dozers for security reasons.

Results in this study indicated push-dumping method tended to create more segregation than end-dumping method because end-dumping method generated greater initial velocities, which, in turn, contributed to reduce waste rock segregation. The reason was the relatively limited height of the benches which should be smaller than 25 m to reduce geotechnical instabilities and simulation time. In these conditions, the energy accumulation during particle flow had less effect on segregation than the initial energy.

Finally, simulations showed that lateral disposal tended to limit waste rock segregation compared to deposition from a single point. Increasing dump spacing had limited effect on waste rock segregation. Increasing spacing too much would, however, result in the same results as for a single point disposal when lateral dumps do not interact anymore. Lateral disposal with a dump spacing small enough to make sure dumps interact with each other, can therefore contribute to homogenize waste rock and decrease segregation.

The results obtained from this study could be useful to investigate waste rock segregation and heterogeneity under various operational conditions, and to control segregation and improve mine waste disposal strategy.

7.2 Discussion

The results presented in this thesis are expected to contribute to improve waste rock disposal and reduce segregation. However, some assumptions and simplifications were necessary to conduct this research and may somewhat limit the extrapolability of the results.

First, waste rock characterization at field scale focused on the surface of a waste rock pile and internal waste rock could not be characterized using drone pictures. However, internal heterogeneity can be significant because of the presence of the alternance of inclined fine and coarse-grained layers (Anterrieu et al., 2010; Bao et al., 2020) and it is therefore recommended to regularly survey the waste rock pile slopes to monitor and document internal variability. Also, because of the limited resolution of the camera embarked on the drone (1.2 cm/pixel), only particles which diameters were greater than 2 cm could be detected. They usually represent over 80% of the waste rock mass (with maximum particle diameter of 25 cm) (Essayad, 2021), which means the precision of the measurement is acceptable, but the fine content can vary significantly

between mines (Gamache-Rochette, 2004; Corazao Gallegos, 2007; Blackmore, 2015). Ignoring or underestimating the fine fraction can have critical consequences in terms of geotechnical (Mclemore et al., 2009), hydrogeological (Chapuis, 2012; Raymond et al., 2021) and geochemical (Benarchid et al., 2019) analyses. Using cameras with better resolution, taking pictures from closer or completing image analysis with sampling is therefore recommended if the fine fraction is significant and/or has a strong impact on the measured behaviours.

Waste rock characterization in the field is also affected by pixel intensity differences (Ferreira et al., 2012), which is sensitive to image brightness and resolution (Đuriš et al., 2016; Zhang et al., 2017), and detection of particle boundaries may be not precisive if pixel intensity is not contrasted enough, resulting in an overestimation particle diameter. The loss of pixel intensity would be more significant for smaller particles, and waste rock diameters at the top of the slope (with most smaller particles) were therefore overestimated, resulting in underestimation of waste rock segregation. Secondly, different colours within the same particle may lead the image processing code to distinguish several smaller particles where there is just one, resulting in an underestimation of the particle diameter (Azzali et al., 2011). Thirdly, particle overlap would hide parts of the particles and also result in underestimation of these particles (Zhang, 2016). Such colour difference and particle overlap would bring high variability to particle mass and size determination. Choosing a cloudy day to reduce shades and conducting more field measurements could be good ways to correct the small size fractions (Cash, 2014).

Laboratory tests such as repose angle tests and segregation tests were conducted using limited amount of waste rock (i.e., around 75 kg) with a maximum diameter of 89 mm because of limitations of the available material and laboratory space. More experiments would be required to increase the result representativity by testing larger volumes of waste rock with larger diameters such as 40 cm or more (Ye et al., 2022). In addition, the model calibration method (i.e., with repose angle tests or measurements) proved efficient but was validated for a limited number of waste rock types. Other parameters such as particle size distribution (Jain et al., 2013), particle shape and roughness (Zhou et al., 2016; Alizadeh et al., 2017) and material density (Tripathi et al., 2013), but also external factors such as rainfall (Sutherland, 2002) may also affect the waste rock flow behaviours but was not investigated here. Research on more mine sites with different waste rock types is therefore recommended to further validate the proposed calibration method.

Accounting for every waste rock particle in DEM simulations is also computationally impractical because of the heavy calculation pressure induced by a large number of contacts between particles (Thakur et al., 2016; Saeed et al., 2019). Simplifications had to be made to speed up the calculation with ensuring simulation reliability. First, particles smaller than 10 cm were not simulated in field models to significantly reduce contact numbers. Secondly, using spheres to simulate waste rock particles also contributed to decrease the contact number and thus accelerated the calculation time (Grima et al., 2011; Su et al., 2019). However, although the overall collision characteristics of waste rock can be reproduced by spheres with acceptable accuracy using a well calibrated local damp (Calvetti et al., 2005; Plassiard et al., 2010), field waste rock exhibits complicated collisions during disposal which are affected by different factors such as irregular shape, particle size and falling height (Bourrier et al., 2008; Plassiard et al., 2010). More research on the collisions of larger particles with irregular shapes could help increase the representativity of numerical models (Thoeni, et al., 2019; Zhu et al., 2021).

Only bench up to 25 m high was investigated, while in practice it may be up to 100 m (Hawley et al., 2017). However, this choice was made because of current good practices which recommend to not exceed 25 m for improving geotechnical stability and calculation efficiency (Aubertin, 2013; Coetzee, 2016; Lehouiller et al., 2020). However, in the specific cases where higher benches are considered (e.g., in pit backfilling; MEND, 2015), it is recommended to carry out additional simulations to confirm the trends observed in this study. This would, however, be complex because of the large number of particles and contacts, and the simplifications and approaches proposed in this research may be even more critical.

Finally, the recommendations regarding waste rock disposal were given with the objective of reducing segregation. Segregation and heterogeneity usually create negative effect on the geotechnical properties, but sometimes also bring positive effect on pile's stability. For example, although segregation and heterogeneity can bring risks to water flow along irregular and diverted paths within waste rock piles (Lahmira et al., 2016; Raymond et al., 2021), the presence of internal fine-grained layers (e.g., compacted layers during construction) sometimes also increase the factors of safety, resulting in positive effects on the geotechnical stability of waste rock piles (Maknoon et al., 2021). The effect of disposal and segregation on geotechnical stability should be

further evaluated by coupling several methods such as FEM-DEM simulations (Latham et al., 2008; Guo et al., 2014).

7.3 Conclusion

The objective of this research was to assess the impact of waste rock disposal on waste rock segregation and heterogeneity in waste rock piles and to propose recommendations to reduce segregation and improve disposal strategy. To do so, waste rock segregation and heterogeneity were first characterized and evaluated by analyzing particle size distribution along the slope of a waste rock pile using image analysis. Discrete element simulations were then conducted to investigate waste rock segregation under various influence factors such as construction methods and bench heights, mine truck payloads, push velocities, waste rock PSD, and lateral disposal. The main conclusions of this research are summarized below.

A new method to calibrate discrete element models was proposed to simulate waste rock flow behaviour. This method was proposed to calibrate friction and rolling resistance coefficients by simulating repose angle (either from laboratory repose angle tests or natural repose angle measured in the field). The technique was validated using segregation tests in the laboratory scale models, and real segregation measurements in the field. The proposed method is efficient to simulate waste rock segregation during disposal under various practical conditions, including different particle sizes, waste rock quantities and construction methods.

Waste rock segregation degree and characteristic diameters were characterized as a function of the relative location along the slope of waste rock pile. The increase of characteristic diameters and segregation degree from the top to the bottom of the slope indicated significant segregation. Results also showed that segregation and lateral heterogeneity could result in high variability (one to two orders of magnitude difference) of the saturated hydraulic conductivity and more generally of the geotechnical properties of waste rock in the field. Controlling and limiting segregation seemed therefore beneficial to improve pile stability.

Simulated bench heights (10 m to 25 m) and mine truck payloads (300 t to 600 t) had limited effect on waste rock segregation in this study.

Optimizing waste rock PSD (before the deposition) and controlling push velocity could be efficient to limit waste rock segregation. A smaller proportion of large particles in the original

waste rock can increase segregation, so using a greater powder factor or crushing the largest waste rock particles is therefore recommended to homogenize waste rock and contribute to limit waste rock segregation. Also, results showed that increasing push velocity can reduce segregation at the top of the slope with limited effect on waste rock distribution at the bottom.

Construction methods had a strong impact on waste rock segregation during disposal. Push-dumping method tended to create more segregation than end-dumping method because end-dumping method generated greater initial velocities, which contributed to reduce segregation. However, this effect was also observed because of the limited bench height simulated and because of that, energy accumulation had less effect on segregation than initial energy.

Lateral disposal appeared to have a strong impact on segregation and significantly reduced segregation compared with single point disposal. Dump spacing had limited effect on waste rock segregation, as long as it remained small enough to ensure the interactions between each dump. Lateral and sequential disposal is therefore recommended to decrease segregation for waste rock disposal in the field.

7.4 Recommendations

This research has mainly focused on characterizing waste rock segregation and heterogeneity and investigating the effect of various influence factors on segregation. The following recommendations are proposed to overcome the limitations discussed above and to further improve waste rock disposal strategy in operating mines.

- Segregation analyses on more waste rock piles are recommended to confirm the field observations and contribute to further understand the heterogeneity of waste rock piles. In addition, complementary field measurement methods such as geophysical methods (Anterrieu et al., 2010; Dimech et al., 2019) and trench excavation (Stockwell et al., 2006; Boekhout et al., 2015) are recommended to investigate the effect of fine content and internal waste rock heterogeneity.
- Higher resolution cameras are recommended to improve the precision of particle detection when using image analysis. Other remote sensing techniques such as photogrammetric

techniques (Maas et al., 2006), LiDAR (Collin et al., 2018; Li et al., 2020) could also be alternative options to identify waste rock particles more precisely.

- More experiments by testing larger volumes of waste rock with larger diameters would be suggested to increase the result representativity for model calibration (Ye et al., 2022). Research on more mine sites with different waste rock types is recommended to further validate the proposed calibration method.
- Using irregular particle shapes is recommended to simulate waste rock particles so that particle shape effect and collision characteristics can be better considered in future research. In addition, techniques such as particle scale-up (e.g., Coarse-Graining technique; Nasato et al., 2015) could be used to replace real small particles by representative particles, substantially reducing the required number of particles and computational time (Roessler at al., 2018).
- Further investigations considering waste rock segregation, geotechnical and geochemical stability, and economic issues are recommended to comprehensively optimize waste rock disposal.

REFERENCES

Abrosimova, N., Gaskova, O., Loshkareva, A., Edelev, A., & Bortnikova, S. (2015). Assessment of the acid mine drainage potential of waste rocks at the Ak-Sug porphyry Cu–Mo deposit. Journal of Geochemical Exploration, 157, 1-14. doi:10.1016/j.gexplo.2015.05.009

Adams, R., Ahlfeld, D., & Sengupta, A. (2007). Investigating the potential for ongoing pollution from an abandoned pyrite mine. Mine Water and the Environment, 26(1), 2-13.

Ai, J., Chen, J.-F., Rotter, J. M., & Ooi, J. Y. (2011). Assessment of rolling resistance models in discrete element simulations. Powder Technology, 206(3), 269-282.

Akcil, A., & Koldas, S. (2006). Acid Mine Drainage (AMD): causes, treatment and case studies. Journal of Cleaner Production, 14(12-13), 1139-1145. doi:10.1016/j.jclepro.2004.09.006

Al-Hashemi, H. M. B., & Al-Amoudi, O. S. B. (2018). A review on the angle of repose of granular materials. Powder Technology, 330, 397-417. doi:10.1016/j.powtec.2018.02.003

Alias, R., Kasa, A., & Taha, M. R. (2014). Particle size effect on shear strength of granular materials in direct shear test. International Journal of Civil, Structural, Construction and Architectural Engineering, 8(11), 733-736.

Alizadeh, M., Hassanpour, A., Pasha, M., Ghadiri, M., & Bayly, A. (2017). The effect of particle shape on predicted segregation in binary powder mixtures. Powder Technology, 319, 313-322. doi:10.1016/j.powtec.2017.06.059

Amos, R. T., Blowes, D. W., Bailey, B. L., Sego, D. C., Smith, L., & Ritchie, A. I. M. (2015). Waste-rock hydrogeology and geochemistry. Applied Geochemistry, 57, 140-156. doi:10.1016/j.apgeochem.2014.06.020

Andjelkovic, V., Pavlovic, N., Lazarevic, Z., & Radovanovic, S. (2018). Modelling of shear strength of rockfills used for the construction of rockfill dams. Soils and Foundations, 58(4), 881-893.

Annabattula, R. K., Gan, Y., & Kamlah, M. (2012). Mechanics of binary and polydisperse spherical pebble assembly. Fusion Engineering Design, 87(5-6), 853-858.

Anterrieu, O., Chouteau, M., & Aubertin, M. (2010). Geophysical characterization of the large-scale internal structure of a waste rock pile from a hard rock mine. Bulletin of Engineering Geology and the Environment, 69(4), 533-548. doi:10.1007/s10064-010-0264-4

Appels, W. M., Ireson, A. M., & Barbour, S. L. (2018). Impact of bimodal textural heterogeneity and connectivity on flow and transport through unsaturated mine waste rock. Advances in Water Resources, 112, 254-265. doi:10.1016/j.advwatres.2017.12.008

Asachi, M., Hassanpour, A., Ghadiri, M., & Bayly, A. (2018). Experimental evaluation of the effect of particle properties on the segregation of ternary powder mixtures. Powder Technology, 336, 240-254. doi:10.1016/j.powtec.2018.05.017

Asadzadeh, M., & Soroush, A. (2009). Direct shear testing on a rockfill material. Arabian journal for science engineering, 34(2), 379.

Asmaei, S., Shourijeh, P. T., Binesh, S. M., & Ghaedsharafi, M.-H. (2018). An Experimental Parametric Study of Segregation in Cohesionless Soils of Embankment Dams. Geotechnical Testing Journal, 41(3). doi:10.1520/gtj20160325

ASTM. (2006). ASTM D2434 Standard Test Method for Permeability of Granular Soils (Constant Head). In. West Conshohocken, PA: ASTM International.

ASTM. (2007). ASTM D 5856 Standard Test Method for Measurement of Hydraulic Conductivity of Porous Material Using a Rigid-Wall, Compaction-Mold Permeameter. In. West Conshohocken, PA: ASTM International.

ASTM. (2011a). ASTM D3080/D3080M-11 Standard Test Method for Direct Shear Test of Soils Under Consolidated Drained Conditions. In. West Conshohocken, PA.

ASTM. (2011b). ASTM D4767-11 Standard Test Method for Consolidated Undrained Triaxial Compression Test for Cohesive Soils. In. West Conshohocken, PA.

ASTM. (2011c). ASTM D7181-11 Method for Consolidated Drained Triaxial Compression Test for Soils. In. West Conshohocken, PA.

ASTM. (2015). ASTM C127-15 Standard Test Method for Relative Density (Specific Gravity) and Absorption of Coarse Aggregate. West Conshohocken. In. PA; ASTM International.

ASTM. (2016a). ASTM D854-14 Standard Test Methods for Specific Gravity of Soil Solids by Water Pycnometer. In. West Conshohocken, PA: ASTM international.

ASTM. (2016b). ASTM D5084-16a Standard Test Methods for Measurement of Hydraulic Conductivity of Saturated Porous Materials Using a Flexible Wall Permeameter. In. West Conshohocken, PA.

Aubertin. (2013). Waste rock disposal to improve the geotechnical and geochemical stability of piles. Paper presented at the In Proceedings of the world mining congress, Montreal.

Aubertin, M., Fala, O., Molson, J., Chouteau, M., Anterrieu, O., Hernandez, M., . . . Lefebvre, R. (2008). Caractérisation du comportement hydrogéologique et géochimique des haldes à stériles. Paper presented at the Symposium 2008 sur l'environnement et les mines, Rouyn-Noranda, QC, Canada.

Ayres, B., Dobchuk, B., Christensen, D., O'Kane, M., & Fawcett, M. (2006). Incorporation of Natural Slope Features into the Design of Final Landforms for Waste Rock Stockpiles. Paper presented at the Presented at the 7th International Conference on Acid Rock Drainage (ICARD).

Azam, S., Wilson, G. W., Fredlund, D. G., & Zyl, D. V. (2009). Geotechnical characterization of mine waste rock. Paper presented at the Proceedings of the Seventh International Conference Soil Mechanics and Geotechnical Engineering.

Azam, S., Wilson, G. W., Herasymuik, G., Nichol, C., & Barbour, L. S. (2006). Hydrogeological behaviour of an unsaturated waste rock pile: a case study at the Golden Sunlight Mine, Montana, USA. Bulletin of Engineering Geology and the Environment, 66(3), 259-268. doi:10.1007/s10064-006-0077-7

Azam, S., Wilson, G. W., Herasymuik, G., Nichol, C., & Barbour, L. S. (2007). Hydrogeological behaviour of an unsaturated waste rock pile: a case study at the Golden Sunlight Mine, Montana, USA. Bulletin of Engineering Geology and the Environment, 66(3), 259-268. doi:10.1007/s10064-006-0077-7

Azema, E., & Radjai, F. (2010). Stress-strain behavior and geometrical properties of packings of elongated particles. Phys Rev E Stat Nonlin Soft Matter Phys, 81(5 Pt 1), 051304. doi:10.1103/PhysRevE.81.051304

Azzali, E., Carbone, C., Marescotti, P., & Lucchetti, G. (2011). Relationships between soil colour and mineralogical composition: application for the study of waste-rock dumps in abandoned mines. Neues Jahrbuch für Mineralogie - Abhandlungen, 188(1), 75-85. doi:10.1127/0077-7757/2011/0195

Bagheri, G., Bonadonna, C., Manzella, I., & Vonlanthen, P. (2015). On the characterization of size and shape of irregular particles. Powder Technology, 270, 141-153.

Bagherzadeh-Khalkhali, A., & Mirghasemi, A. A. (2009). Numerical and experimental direct shear tests for coarse-grained soils. Particuology, 7(1), 83-91.

Bandara, S., Ferrari, A., & Laloui, L. (2016). Modelling landslides in unsaturated slopes subjected to rainfall infiltration using material point method. International Journal for Numerical and Analytical Methods in Geomechanics, 40(9), 1358-1380. doi:10.1002/nag.2499

Bao, Z., Blowes, D. W., Ptacek, C. J., Bain, J., Holland, S. P., Wilson, D., . . . MacKenzie, P. (2020). Faro Waste Rock Project: Characterizing Variably Saturated Flow Behavior Through Full ‐ Scale Waste ‐ Rock Dumps in the Continental Subarctic Region of Northern Canada Using Field Measurements and Stable Isotopes of Water. Water Resources Research, 56(3). doi:10.1029/2019wr026374

Bar, N., Semi, J.,, Koek, M., Owusu-Bempah, G., Day, A., & Nicoll, S., & Bu, J. . (2020). Practical waste rock dump and stockpile management in high rainfall and seismic regions of Papua New Guinea. Paper presented at the the 2020 International Symposium on Slope Stability in Open Pit Mining and Civil Engineering Australian Centre for Geomechanics.

Bard, E., Anabalón, M. E., & Campaña, J. J. M. g. (2011). Waste rock behavior at high pressures: dimensioning high waste rock dumps. 83-112.

Bareither, C. A., Benson, C. H., & Edil, T. B. (2008). Comparison of shear strength of sand backfills measured in small-scale and large-scale direct shear tests. Canadian Geotechnical Journal, 45(9), 1224-1236. doi:10.1139/t08-058

Barfoud, L., Pabst, T., Zagury, G. J., & Plante, B. (2019). Effect of dissolved oxygen on the oxidation of saturated mine tailings. Geo-Environmental Engineering, 30-31.

Barrios, G. K. P., de Carvalho, R. M., Kwade, A., & Tavares, L. M. (2013). Contact parameter estimation for DEM simulation of iron ore pellet handling. Powder Technology, 248, 84-93. doi:10.1016/j.powtec.2013.01.063

Barton, N. (1982). Shear strength investigations for surface mining. Paper presented at the Proceedings of the 23rd US Rock Mechanics Symposium.

Bay, D. S. (2009). Hydrological and hydrogeochemical characteristics of neutral drainage from a waste rock test pile. University of British Columbia,

Béket Dalcé, J., Li, L., & Yang, P. (2019). Experimental Study of Uniaxial Compressive Strength (UCS) Distribution of Hydraulic Backfill Associated with Segregation. Minerals, 9(3). doi:10.3390/min9030147

Belem, T., & Benzaazoua, M. (2008). Design and application of underground mine paste backfill technology. Geotechnical Geological Engineering, 26(2), 147-174.

Belheine, N., Plassiard, J. P., Donzé, F. V., Darve, F., & Seridi, A. (2009). Numerical simulation of drained triaxial test using 3D discrete element modeling. Computers and Geotechnics, 36(1-2), 320-331. doi:10.1016/j.compgeo.2008.02.003

Benarchid, Y., Taha, Y., Argane, R., Tagnit-Hamou, A., & Benzaazoua, M. (2019). Concrete containing low-sulphide waste rocks as fine and coarse aggregates: Preliminary assessment of materials. Journal of Cleaner Production, 221, 419-429. doi:10.1016/j.jclepro.2019.02.227

Benito, J. G., Uñac, R. O., Vidales, A. M., & Ippolito, I. (2014). Influence of geometry on stratification and segregation phenomena in bidimensional piles. Physica A: Statistical Mechanics and its Applications, 396, 19-28. doi:10.1016/j.physa.2013.11.028

Benson, C. H., Sawangsuriya, A., Trzebiatowski, B., & Albright, W. H. (2007). Postconstruction Changes in the Hydraulic Properties of Water Balance Cover Soils. Journal of Geotechnical and Geoenvironmental Engineering, 133(4), 349-359. doi:10.1061/(asce)1090-0241(2007)133:4(349)

Besinger, F., Cebon, D., & Cole, D. (1995). Damper models for heavy vehicle ride dynamics. Vehicle System Dynamics, 24(1), 35-64.

Bhatia, S. K., & Soliman, A. F. (1990). Frequency Distribution of Void Ratio of Granular Materials Determined by an Image Analyzer. Soils and Foundations, 30(1), 1-16. doi:10.3208/sandf1972.30.1

Bhattacharya, T., & McCarthy, J. (2014). Chute flow as a means of segregation characterization. Powder Technology, 256, 126-139.

Blackmore, S. (2015). The role of hydrology, geochemistry and microbiology in flow and solute transport through highly heterogeneous, unsaturated waste rock at various test scales University of British Columbia,

Blight, G. E. (2010). Geotechnical engineering for mine waste storage facilities. London, UK: Taylor & Francis Group.

Blott, S. J., & Pye, K. (2008). Particle shape: a review and new methods of characterization and classification. Vadose Zone Journal, 55(1), 31-63.

Boakye, K. (2008). Large in situ direct shear tests on rock piles at the Qusta Mine,Taos County,New Mexico. (M.S. M.S. thesis), New Mexico Institute of Mining and Technology, Socorro NM.

Boekhout, F., Gerard, M., Kanzari, A., Michel, A., Dejeant, A., Galoisy, L., . . . Descostes, M. (2015). Uranium migration and retention during weathering of a granitic waste rock pile. Applied Geochemistry, 58, 123-135. doi:10.1016/j.apgeochem.2015.02.012

Broda, S., Aubertin, M., Blessent, D., Hirthe, E., & Graf, T. (2017). Improving control of contamination from waste rock piles. Environmental Geotechnics, 4(4), 274-283. doi:10.1680/envgeo.14.00023

Burenkova, V. (1993). Assessment of suffusion in non-cohesive and graded soils. Paper presented at the Proceedings of the First International Conference “Geo-Filter”, Karlesruhe, Germany.

Burnley, R. B. (1993). Mine reclamation and waste dump stability: University of Nevada, Reno.

Bussière, B. (2007). Hydrogeotechnical properties of hard rock tailings from metal mines and emerging geo-environmental disposal approaches. Canadian Geotechnical Journal, 44(9), 1019-1052.

Bussière, B., & Guittonny, M. (2020). Hard rock mine reclamation: from prediction to management of acid mine drainage: CRC press.

Cao, C.-h., Feng, J.-l., & Tao, Z.-g. (2021). Triggering mechanism and dynamic process of water-rock flow in Nanfen waste dump in 2010. Journal of Mountain Science, 18(10), 2565-2579.

Carrasco, S., Cantor, D., & Ovalle, C. (2022). Effects of particle size ‐ shape correlations on steady shear strength of granular materials: The case of particle elongation. International Journal for Numerical Analytical Methods in Geomechanics, 46(5), 979-1000.

Cash, A. (2014). Structural and Hydrologic Characterization of Two Historic Waste Rock Piles. (Master), University of Alberta,

Chabot, D., & Francis, C. M. (2016). Computer-automated bird detection and counts in high-resolution aerial images: a review. Journal of Field Ornithology, 87(4), 343-359. doi:10.1111/jofo.12171

Chapuis, R. P. (2004). Predicting the saturated hydraulic conductivity of sand and gravel using effective diameter and void ratio. Canadian Geotechnical Journal, 41(5), 787-795. doi:10.1139/T04-022

Chapuis, R. P., & Aubertin, M. (2003). On the use of the Kozeny– Carman equation to predict the hydraulic conductivity of soils. Canadian Geotechnical Journal, 40(3), 616-628. doi:10.1139/t03-013

Charles, J., & Watts, K. (1980). The influence of confining pressure on the shear strength of compacted rockfill. Géotechnique, 30(4), 353-367.

Cheng, Y. M., Fung, W. H. I., Li, L., & Li, N. (2019). Laboratory and field tests and distinct element analysis of dry granular flows and segregation processes. Natural Hazards and Earth System Sciences, 19(1), 181-199. doi:10.5194/nhess-19-181-2019

Chi, X. (2011). Characterizing low-sulfide instrumented waste-rock piles: image grain-size analysis and wind-induced gas transport. University of Waterloo,

Cho, G.-C., Dodds, J., & Santamarina, J. C. (2006). Particle shape effects on packing density, stiffness, and strength: natural and crushed sands. Journal of geotechnical geoenvironmental engineering, 132(5), 591-602.

Chung, Y.-C., & Ooi, J. Y. (2008). A study of influence of gravity on bulk behaviour of particulate solid. Particuology, 6(6), 467-474. doi:10.1016/j.partic.2008.07.017

Coetzee, C. J. (2016). Calibration of the discrete element method and the effect of particle shape. Powder Technology, 297, 50-70.

Coetzee, C. J. (2020). Calibration of the discrete element method: Strategies for spherical and non-spherical particles. Powder Technology, 364, 851-878.

Coetzee, C. J., & Els, D. N. J. (2009). Calibration of discrete element parameters and the modelling of silo discharge and bucket filling. Computers and Electronics in Agriculture, 65(2), 198-212. doi:10.1016/j.compag.2008.10.002

Coli, N., Berry, P., & Boldini, D. (2011). In situ non-conventional shear tests for the mechanical characterisation of a bimrock. International Journal of Rock Mechanics Mining Sciences, 48(1), 95-102.

Collin, A., Ramambason, C., Pastol, Y., Casella, E., Rovere, A., Thiault, L., . . . Davies, N. (2018). Very high resolution mapping of coral reef state using airborne bathymetric LiDAR surface-intensity and drone imagery. International Journal of Remote Sensing, 39(17), 5676-5688. doi:10.1080/01431161.2018.1500072

Combarros, M., Feise, H. J., Zetzener, H., & Kwade, A. (2014). Segregation of particulate solids: Experiments and DEM simulations. Particuology, 12, 25-32. doi:10.1016/j.partic.2013.04.005

Corazao Gallegos, J. C. (2007). The design, construction, instrumentation and initial response of a field-scale waste rock test pile. University of British Columbia,

Cox, E. (1927). A method of assigning numerical and percentage values to the degree of roundness of sand grains. Journal of Paleontology, 1(3), 179-183.

Cremonesi, M., Franci, A., Idelsohn, S., & Oñate, E. (2020). A state of the art review of the particle finite element method (PFEM). Archives of Computational Methods in Engineering, 27(5), 1709-1735.

Cundall, P. A., & Strack, O. D. (1979). A discrete numerical model for granular assemblies. Géotechnique, 29(1), 47-65.

Dawood, I., & Aubertin, M. (2013). Effect of Dense Material Layers on Unsaturated Water Flow Inside a Large Waste Rock Pile: A Numerical Investigation. Mine Water and the Environment, 33(1), 24-38. doi:10.1007/s10230-013-0251-7

De Mello, V. F. (1977). Reflections on design decisions of practical significance to embankment dams. Géotechnique, 27(3), 281-355.

de Silva, S. R., Dyrøy, A., & Enstad, G. G. (2000). Segregation mechanisms and their quantification using segregation testers. Paper presented at the IUTAM Symposium on Segregation in Granular Flows.

Deiminiat, A., Li, L., & Zeng, F. (2022). Experimental study on the minimum required specimen width to maximum particle size ratio in direct shear tests. CivilEng, 3(1), 66-84.

Deiminiat, A., Li, L., Zeng, F., Pabst, T., Chiasson, P., & Chapuis, R. (2020). Determination of the shear strength of rockfill from small-scale laboratory shear tests: A critical review. Advances in Civil Engineering, 2020.

Demers, I., & Pabst, T. (2021). Alternative and innovative integrated mine waste management approaches. In Hard Rock Mine Reclamation: From Prediction to Management of Acid Mine Drainage (pp. 321-342): CRC Press.

Di Felice, F., Mazzini, A., Di Stefano, G., & Romeo, G. (2018). Drone high resolution infrared imaging of the Lusi mud eruption. Marine and Petroleum Geology, 90, 38-51. doi:10.1016/j.marpetgeo.2017.10.025

Di Renzo, A., & Di Maio, F. P. (2004). Comparison of contact-force models for the simulation of collisions in DEM-based granular flow codes. Chemical Engineering Science, 59(3), 525-541.

Dimech, A., Cheng, L., Chouteau, M., Chambers, J., Uhlemann, S., Wilkinson, P., . . . Isabelle, A. (2022). A Review on Applications of Time-Lapse Electrical Resistivity Tomography Over the Last 30 Years : Perspectives for Mining Waste Monitoring. Surv Geophys, 43(6), 1699-1759. doi:10.1007/s10712-022-09731-2

Dimech, A., Chouteau, M., Aubertin, M., Bussière, B., Martin, V., & Plante, B. (2019). Three‐dimensional time‐lapse geoelectrical monitoring of water infiltration in an experimental mine waste rock pile. Vadose Zone Journal, 18(1), 1-19.

Ding, X., Zhang, L., Zhu, H., & Zhang, Q. (2013). Effect of Model Scale and Particle Size Distribution on PFC3D Simulation Results. Rock Mechanics and Rock Engineering, 47(6), 2139-2156. doi:10.1007/s00603-013-0533-1

Dipova, N. (2017). Determining the grain size distribution of granular soils using image analysis. Acta geotechnica Slovenica, 14(1), 29-37.

Dolgunin, V., & Ukolov, A. (1995). Segregation modeling of particle rapid gravity flow. Powder Technology, 83(2), 95-103.

Drahun, J. A., & Bridgwater, J. (1983). The mechanisms of free surface segregation. Powder Technology, 36(1), 39-53. doi:10.1016/0032-5910(83)80007-2

Đuriš, M., Arsenijević, Z., Jaćimovski, D., & Radoičić, T. K. (2016). Optimal pixel resolution for sand particles size and shape analysis. Powder Technology, 302, 177-186.

Dwumfour, D., Dixon, J., & Mylvaganam, J. (2020). Waste rock characterisation and stability assessments for feasibility level studies. Paper presented at the Slope Stability 2020: Proceedings of the 2020 International Symposium on Slope Stability in Open Pit Mining and Civil Engineering.

Engblom, N., Saxén, H., Zevenhoven, R., Nylander, H., & Enstad, G. (2012). Segregation of construction materials in silos. Part 2: Identification of relevant segregation mechanisms. Particulate Science Technology, 30(2), 161-178.

Essayad, K. (2021). Évaluation multi-échelle de l'instabilité interne et de la migration des résidus à travers les inclusions de roches stériles. (Philosophiae Doctor), Polytechnique Montreal, Montreal, Quebec, Canada.

Fakhimi, A., & Hosseinpour, H. (2011). Experimental and numerical study of the effect of an oversize particle on the shear strength of mined-rock pile material. Geotechnical Testing Journal, 34(2). doi:10.1520/GTJ103111

Fala, O., Aubertin, M., Molson, J., Bussière, B., Wilson, G. W., & Martin, V. (2003). Numerical modelling ofunsaturated flow in uniform and heterogeous waste rock piles. Paper presented at the In proceedings of 6th international conference on acid rock drainage :application and sustainability of technologies., Carins, Australia.

Fala, O., Molson, J., Aubertin, M., & Bussière, B. (2005). Numerical Modelling of Flow and Capillary Barrier Effects in Unsaturated Waste Rock Piles. Mine Water and the Environment, 24(4), 172-185. doi:10.1007/s10230-005-0093-z

Fala, O., Molson, J., Aubertin, M., Dawood, I., Bussière, B., & Chapuis, R. P. (2012). A numerical modelling approach to assess long-term unsaturated flow and geochemical transport in a waste rock pile. International Journal of Mining, Reclamation and Environment, 27(1), 38-55. doi:10.1080/17480930.2011.644473

Fan, Y., Boukerkour, Y., Blanc, T., Umbanhowar, P. B., Ottino, J. M., & Lueptow, R. M. (2012). Stratification, segregation, and mixing of granular materials in quasi-two-dimensional bounded heaps. Physical Review E, 86(5), 051305.

Fan, Y., & Hill, K. (2011). Theory for shear-induced segregation of dense granular mixtures. New journal of physics, 13(9), 095009.

Fan, Y., Jacob, K. V., Freireich, B., & Lueptow, R. M. (2017). Segregation of granular materials in bounded heap flow: A review. Powder Technology, 312, 67-88.

Fei, M., Sun, Q., Hill, K., & Zhou, G. G. (2017). Simulation of size segregation in granular flow with material point method. Paper presented at the EPJ Web of Conferences.

Félix, G., & Thomas, N. (2004). Evidence of two effects in the size segregation process in dry granular media. Physical Review E, 70(5), 051307.

Feng, Y. Q., & Yu, A. B. (2007). Microdynamic modelling and analysis of the mixing and segregation of binary mixtures of particles in gas fluidization. Chemical Engineering Science, 62(1-2), 256-268. doi:10.1016/j.ces.2006.08.015

Fernlund, J. M. R. (2005). 3-D image analysis size and shape method applied to the evaluation of the Los Angeles test. Engineering Geology, 77(1-2), 57-67. doi:10.1016/j.enggeo.2004.08.002

Ferreira, T., & Rasb, W. (2012). ImageJ user guide: IJ 1.46 r.

Fines, P., G.W., W., Williams, D. J., Tran, A. B., & Miller, S. (2003). Field characterization of two full-scale waste rock piles. Paper presented at the Proceedings of the 6th International Conference on Acid Rock Drainage, Cairns, Australia.

Fines, P. E. (2006). Hydrological characterization of two full-scale waste rock piles. University of British Columbia,

Fox, Z., & Carraro, J. A. H. (2011). Peak and critical-state shear strength of mine waste rock. Paper presented at the 14th International Conference on Tailings and Mine Waste'10, October 17, 2010 - October 20, 2010, Vail, CO, United states.

Frossard, E., Hu, W., Dano, C., & Hicher, P.-Y. (2012). Rockfill shear strength evaluation: a rational method based on size effects. Géotechnique, 62(5), 415-427.

Fu, P., & Dafalias, Y. (2011). Study of anisotropic shear strength of granular materials using DEM simulation. International Journal for Numerical Analytical Methods in Geomechanics, 35(10), 1098-1126.

Fung, J. C., & Vassilicos, J. C. (2003). Inertial particle segregation by turbulence. Phys Rev E Stat Nonlin Soft Matter Phys, 68(4 Pt 2), 046309. doi:10.1103/PhysRevE.68.046309

Gamache-Rochette, A. (2004). Une étude de caractérisation en laboratoire et sur le terrain des écoulements de l'eau dans les roches stériles. École polytechnique de Montréal, École polytechnique de Montréal.

Gervais, D., Roy, C., Thibault, A., Pednault, C., & Doucet, D. (2014). Technical Report on the mineral resource and mineral reserve estimates for the Canadian Malartic Property. Retrieved from

Gharat, S. H. (2019). Flow and Segregation of Granular Materials during Heap Formation. In Progress in Fine Particle Plasmas (pp. 151): IntechOpen.

Gingold, R. A., & Monaghan, J. (1977). Smoothed particle hydrodynamics: theory and application to non-spherical stars. Monthly notices of the royal astronomical society, 181(3), 375-389.

Gorakhki, M. R., Bareither, C. A., & Scalia IV, J. (2022). Hydraulic conductivity testing and destructive sampling of field-scale mine waste test piles. Canadian Geotechnical Journal, 99(999), 1-12.

Govender, I. (2016). Granular flows in rotating drums: A rheological perspective. Minerals Engineering, 92, 168-175.

Gupta, A. K. (2016). Effects of particle size and confining pressure on breakage factor of rockfill materials using medium triaxial test. Journal of Rock Mechanics and Geotechnical Engineering, 8(3), 378-388. doi:10.1016/j.jrmge.2015.12.005

Hajizadeh Namaghi, H., Li, S., & Jiang, L. (2015). Numerical simulation of water flow in a large waste rock pile, Haizhou coal mine, China. Modeling Earth Systems and Environment, 1(1-2). doi:10.1007/s40808-015-0007-4

Hamzeloo, E., Massinaei, M., & Mehrshad, N. (2014). Estimation of particle size distribution on an industrial conveyor belt using image analysis and neural networks. Powder Technology, 261, 185-190.

Haselsteiner, R., Pamuk, R., & Ersoy, B. (2017). Aspects concerning the shear strength of rockfill material in rockfill dam engineering. geotechnik, 40(3), 193-203. doi:10.1002/gete.201600099

Hashim, M., Sharrock, G., & Saydam, S. (2008). A review of particle percolation in mining. Paper presented at the SHIRMS 2008: Proceedings of the First Southern Hemisphere International Rock Mechanics Symposium.

Hawley, M., & Cunning, J. (2017). Guidelines for Mine Waste Dump and Stockpile Design (M. Hawley & J. Cunning Eds.): Csiro Publishing.

Hazen, A. (1991). Discussion of “Dams on Sand Foundations” Transactions of the American Society of Civil Engineers, 73, 199-203.

Herasymuik, G., Azam, S., Wilson, G., Barbour, L., & Nichol, C. (2006). Hydrological characterization of an unsaturated waste rock dump. Paper presented at the Proceedings of the 59th Canadian geotechnical conference, Vancouver, BC, Canada.

Hockley, D., Noel, M., Rykaart, E., Hahn, S., & Paul, M. (2003). Testing of soil covers for waste rock in the Ronneburg WISMUT mine closure. Paper presented at the 6th International Conference on Acid Rock Drainage, Cairns, Australia.

Honkanadavar, N., Kumar, N., & Ratnam, M. (2014). Modeling the behaviour of alluvial and blasted quarried rockfill materials. Geotechnical Geological Engineering, 32(4), 1001-1015.

Huang, P., Miao, Q., Ding, Y., Sang, G., & Jia, M. (2021). Research on surface segregation and overall segregation of particles in a rotating drum based on stacked image. Powder Technology, 382, 162-172.

Huerta, D. A., & Ruiz-Suarez, J. C. (2004). Vibration-induced granular segregation: a phenomenon driven by three mechanisms. Phys Rev Lett, 92(11), 114301. doi:10.1103/PhysRevLett.92.114301

Iabichino, G., Barbero, M., Cravero, M., Fidelibus, C., & Usai, G. (2014). Experimental tests for the assessment of the shear strength of marble waste dumps. Environmental Earth Sciences, 71(7), 3259-3271.

Idelsohn, S. R., Oñate, E., Del Pin, F., & Calvo, N. (2006). Fluid–structure interaction using the particle finite element method. Computer methods in applied mechanics engineering, 195(17-18), 2100-2123.

Idelsohn, S. R., Oñate, E., & Pin, F. D. (2004). The particle finite element method: a powerful tool to solve incompressible flows with free‐surfaces and breaking waves. International journal for numerical methods in engineering, 61(7), 964-989.

Indraratna, B. (1994). The effect of normal stress-friction angle relationship on the stability analysis of a rockfill dam. Geotechnical and Geological Engineering, 12(2), 113-121.

Indraratna, B., Ionescu, D., & Christie, H. D. (1998). Shear Behavior of Railway Ballast Based on Large-Scale Triaxial Tests. Journal of Geotechnical and Geoenvironmental Engineering, 124(5), 439-449. doi:10.1061/(asce)1090-0241(1998)124:5(439)

Indraratna, B., Wijewardena, L., & Balasubramaniam, A. (1993). Large-scale triaxial testing of grey wacke rockfill. Géotechnique, 43(1), 37-51.

Inzerillo, L., Acuto, F., Di Mino, G., & Uddin, M. Z. (2022). Super-Resolution Images Methodology Applied to UAV Datasets to Road Pavement Monitoring. Drones, 6(7). doi:ARTN 171

10.3390/drones6070171

Itasca. (2019). PFC — particle flow code in 2 and 3 dimensions. Version 6.0, Documentation set of version 6.00.15. Retrieved from Minneapolis, Minnesota, USA.:

Iwashita, K., & Oda, M. (1998). Rolling resistance at contacts in simulation of shear band development by DEM. Journal of engineering mechanics, 124(3), 285-292.

Jain, A., Metzger, M. J., & Glasser, B. J. (2013). Effect of particle size distribution on segregation in vibrated systems. Powder Technology, 237, 543-553.

James, M., & Aubertin, M. (2017). Comparison of Numerical and Analytical Liquefaction Analyses of Tailings. Geotechnical Geological Engineering, 35(1), 277-291.

James, M., Aubertin, M., & Bussière, B. (2013). On the use of waste rock inclusions to improve the performance of tailings impoundments. Paper presented at the Proceedings of 18th International Conference on Soil Mechanics and Geotechnical Engineering, Paris, France.

Janoo, V. C. (1998). Quantification of shape, angularity, and surface texture of base course materials. Retrieved from Hanover, NH:

Jiang, M. J., Yu, H. S., & Harris, D. (2005). A novel discrete model for granular material incorporating rolling resistance. Computers and Geotechnics, 32(5), 340-357. doi:10.1016/j.compgeo.2005.05.001

Jiang, Y.-J., Fan, X.-Y., Li, T.-H., & Xiao, S.-Y. (2018). Influence of particle-size segregation on the impact of dry granular flow. Powder Technology, 340, 39-51. doi:10.1016/j.powtec.2018.09.014

Jiang, Y., Wang, L., Wu, Q., Sun, Z., Elmo, D., & Zheng, L. (2019). An improved shear stress monitoring method in numerical direct shear tests by particle flow code. Journal of Testing Evaluation, 48(6), 4136-4152.

Joseph, K. U. R. I. A. N., & Nagendran, R. (2007). Top down and bottom up approach for sustainability of waste management in developing countries. Paper presented at the Sardinia.

Just, S., Toschkoff, G., Funke, A., Djuric, D., Scharrer, G., Khinast, J., . . . Kleinebudde, P. (2013). Experimental analysis of tablet properties for discrete element modeling of an active coating process. AAPS PharmSciTech, 14(1), 402-411.

Katterfeld, A., & Wensrich, C. (2017). Understanding granular media: from fundamentals and simulations to industrial application. Granular Matter, 19(4). doi:10.1007/s10035-017-0765-y

Kenney, T., & Westland, J. (1993). Laboratory study of segregation of granular filter materials. Filters in geotechnical hydraulic engineering, 313-319.

Ketterhagen, W. R., Curtis, J. S., Wassgren, C. R., & Hancock, B. C. (2008). Modeling granular segregation in flow from quasi-three-dimensional, wedge-shaped hoppers. Powder Technology, 179(3), 126-143.

Ketterhagen, W. R., Curtis, J. S., Wassgren, C. R., Kong, A., Narayan, P. J., & Hancock, B. C. J. C. E. S. (2007). Granular segregation in discharging cylindrical hoppers: a discrete element and experimental study. 62(22), 6423-6439.

Khakhar, D., McCarthy, J., & Ottino, J. (1999). Mixing and segregation of granular materials in chute flows. Chaos: An Interdisciplinary Journal of Nonlinear Science, 9(3), 594-610.

Khola, N., & Wassgren, C. (2016). Correlations for shear-induced percolation segregation in granular shear flows. Powder Technology, 288, 441-452. doi:10.1016/j.powtec.2015.11.003

Kim, D., & Ha, S. (2014). Effects of Particle Size on the Shear Behavior of Coarse Grained Soils Reinforced with Geogrid. Materials (Basel), 7(2), 963-979. doi:10.3390/ma7020963

Krumbein, W. C. (1941). Measurement and geological significance of shape and roundness of sedimentary particles. Journal of Sedimentary Research, 11(2), 64-72.

Kudrolli, A. (2004). Size separation in vibrated granular matter. Reports on Progress in Physics, 67(3), 209-247. doi:10.1088/0034-4885/67/3/r01

Kuenen, P. H. (1956). Experimental abrasion of pebbles: 2. Rolling by current. The Journal of Geology, 64(4), 336-368.

Kumara, J., & Janaka, G. H. A. (2012). Image Analysis Techniques on Evaluation of Particle Size Distribution of Gravel. International Journal of Geomate. doi:10.21660/2012.5.1261

Kuo, H.-P., Tseng, W.-T., & Huang, A.-N. (2016). Controlling of Segregation in Rotating Drums by Independent End Wall Rotations. KONA Powder and Particle Journal, 33(0), 239-248. doi:10.14356/kona.2016004

Kwan, A. K., Mora, C., & Chan, H. (1999). Particle shape analysis of coarse aggregate using digital image processing. Cement Concrete Research, 29(9), 1403-1410.

Lahmira, B., Lefebvre, R., Aubertin, M., & Bussiere, B. (2016). Effect of heterogeneity and anisotropy related to the construction method on transfer processes in waste rock piles. J Contam Hydrol, 184, 35-49. doi:10.1016/j.jconhyd.2015.12.002

Lahmira, B., Lefebvre, R., Aubertin, M., & Bussiere, B. (2017). Effect of material variability and compacted layers on transfer processes in heterogeneous waste rock piles. J Contam Hydrol, 204, 66-78. doi:10.1016/j.jconhyd.2017.07.004

Landry, H., Laguë, C., & Roberge, M. (2006). Discrete element representation of manure products. Computers and Electronics in Agriculture, 51(1-2), 17-34. doi:10.1016/j.compag.2005.10.004

Langroudi, M. F., Soroush, A., & Shourijeh, P. T. (2015). A comparison of micromechanical assessments with internal stability/instability criteria for soils. Powder Technology, 276, 66-79.

Lanoix, M.-L. B., Pabst, T., & Aubertin, M. (2017). Characterization of the Hydrogeological Properties of a Sand Layer Placed on an Experimental Waste Rock pile. Paper presented at the GeoOttawa 2017, Ottawa.

Larsson, S. (2019). Particle methods for modelling granular material flow. Luleå University of Technology,

Lehouiller, P., Lampron, S., Gagnon, G., Houle, N., & Bouchard, F. (2020). NI 43-101 TECHNICAL REPORT, CANADIAN MALARTIC MINE, QUÉBEC, CANADA. Retrieved from

Lenart, S., Koseki, J., Miyashita, Y., & Sato, T. (2014). Large-scale triaxial tests of dense gravel material at low confining pressures. Soils and Foundations, 54(1), 45-55. doi:10.1016/j.sandf.2013.12.005

Lessard, G. (2011). Essais d'infiltration sur la halde à stériles Petit-Pas de la mine Tio, HavreSt-Pierre. École Polytechnique de Montréal, Montreal, Canada.

Li, L. P., Lan, H. X., & Peng, J. B. (2020). Loess erosion patterns on a cut-slope revealed by LiDAR scanning. Engineering Geology, 268. doi:ARTN 105516

10.1016/j.enggeo.2020.105516

Li, M., Wilkinson, D., & Patchigolla, K. (2005). Comparison of particle size distributions measured using different techniques. Particulate Science Technology, 23(3), 265-284.

Liao, C.-C., & Huang, Y.-Y. (2021). Experimental investigate the effect of liquid distribution state on size segregation of wet granular materials in rotating drums. Powder Technology, 381, 561-566.

Linero, S., Fityus, S., Simmons, J., Azéma, E., Estrada, N., & Dixon, J. (2020). Influence of particle size-shape correlation on the shear strength of scaled samples of coarse mine waste. Paper presented at the Slope Stability 2020.

Linero, S., Fityus, S., Simmons, J., Lizcano, A., & Cassidy, J. (2017). Trends in the Evolution of Particle Morphology with Size in Colluvial DepositsOverlying Channel Iron Deposits. . Paper presented at the EPJ Web of Conferences.

Linero, S., Palma, C., & Apablaza, R. (2007). Geotechnical Characterisation of Waste Material in Very High Dumps with Large Scale Triaxial Testing. Paper presented at the 2007 International Symposium on Rock Slope Stability in Open Pit Mining and Civil Engineering.

Lucy, L. B. (1977). A numerical approach to the testing of the fission hypothesis. The astronomical journal, 82, 1013-1024.

Lumbroso, D., McElroy, C., Goff, C., Collell, M. R., Petkovsek, G., & Wetton, M. (2019). The potential to reduce the risks posed by tailings dams using satellite-based information. International journal of disaster risk reduction, 38, 101209.

Mahmood, F. N., Barbour, S. L., Kennedy, C., & Hendry, M. J. (2017). Nitrate release from waste rock dumps in the Elk Valley, British Columbia, Canada. Science of the Total Environment, 605, 915-928.

Maknoon, M. (2016). slope stability analyses of waste rock piles under unsaturated conditions following large precipitations. (Ph.D), École Polytechnique de Montreal, University of Montreal,

Maknoon, M., & Aubertin, M. (2021). On the Use of Bench Construction to Improve the Stability of Unsaturated Waste Rock Piles. Geotechnical Geological Engineering, 39(2), 1425-1449.

Manso, J., Marcelino, J., & Caldeira, L. (2018). Crushing and oedometer compression of rockfill using DEM. Computers Geotechnics, 101, 11-22.

Mao, K., Wang, M. Y., Xu, Z., & Chen, T. (2004). DEM simulation of particle damping. Powder Technology, 142(2-3), 154-165.

Marachi, N. (1969). Strength and deformation characteristics of rockfill materials: University of California, Berkeley.

Marsal, R. J. (1967). Large scale testing of rockfill materials. Journal of the Soil Mechanics Foundations Division, 93(2), 27-43.

Marschi, N. D., Chan, C. K., & Seed, H. B. (1972). Evaluation of properties of rockfill materials. Journal of the Soil Mechanics Foundations Division, 98(1), 95-114.

Martin, V., Aubertin, M., Bussie`re, B., & Chapuis, P. R. (2004). Evaluation of unsaturated flow in mine waste rock. Paper presented at the 57th Canadian Geotechnical Conference and the 5th joint CGS-IAH Conference, Quebec City.

Martin, V., Bussière, B., Plante, B., Pabst, T., Aubertin, M., Medina, F., . . . Poaty, B. (2017). Controlling water infiltration in waste rock piles: Design, construction, and monitoring of a large-scale in-situ pilot test pile. Paper presented at the GeoOttawa 2017, Ottawa, Ontario, Canada.

Masad, E., Saadeh, S., Al-Rousan, T., Garboczi, E., & Little, D. (2005). Computations of particle surface characteristics using optical and X-ray CT images. Computational Materials Science, 34(4), 406-424. doi:10.1016/j.commatsci.2005.01.010

Massol-Chaudeur, S., Berthiaux, H., & Dodds, J. A. (2002). Experimental study of the mixing kinetics of binary pharmaceutical powder mixtures in a laboratory hoop mixer. Chemical Engineering Science, 57(19), 4053-4065.

Mbonimpa, M., Aubertin, M., Chapuis, R. P., & Bussière, B. (2002). Practical pedotransfer functions for estimating the saturated hydraulic conductivity. Geotechnical and Geological Engineering, 20(3), 235–259. doi:https://doi.org/10.1023/A:1016046214724

McLemore, V. T., Fakhimi, A., Zyl, D. v., Ayakwah, G. F., Anim, K., Boakye, K., . . . Viterbo, V. C. (2009). Literature review of other rock piles: characterization, weathering, and stability. Retrieved from

MEND. (2001). Manual report 5.4.2, Volume 1: Summary, Volume 2: Sampling and Analysis, Volume 3: Prediction, Volume 4: Prevention and Control, Volume 5: Treatment, Volume 6: Monitoring. Retrieved from Ottawa, Canada:

MEND. (2015). MEND Report 2.36.1 In-Pit Disposal of Reactive Mine Wastes: Approaches, Update and Case Study Results. Retrieved from 555 Booth St Ottawa, K1A 0G1:

Messerklinger, S., & Straubhaar, R. (2011). Filter Design for the Heightening of a High Earth Core Rockfill Dam: Taylor and Francis Group, London.

Milligan, V. (2003). Some uncertainties in embankment dam engineering. Journal of Geotechnical and Geoenvironmental Engineering, 129(9), 785-797.

Moffitt, K. (2000). Mine waste dump instability. University of British Columbia,

Mohammadi, M., Rai, P., Singh, U., & Singh, S. K. (2016). Investigation of Cycle Time Segments of Dragline Operation in Surface Coal Mine: A Statistical Approach. Geotechnical and Geological Engineering, 34(6), 1765-1774. doi:10.1007/s10706-016-9987-8

Monforte, L., Carbonell, J. M., Arroyo, M., & Gens, A. (2017). Performance of mixed formulations for the particle finite element method in soil mechanics problems. Computational Particle Mechanics, 4(3), 269-284.

Mora, C. F., Kwan, A. K. H., & Chan, H. C. (1998). Particle size distribution analysis of coarse aggregate using digital image processing. Cement and Concrete Research, 28(6), 921-932. doi:10.1016/s0008-8846(98)00043-x

Morin, K. A., Gerencher, E., Jones, C. E., & Konasewich, D. E. (1991). Critical literature review of acid drainage from waste rock. Retrieved from

Mosby, J., de Silva, S. R., & Enstad, G. G. (1996). Segregation of Particulate Materials – Mechanisms and Testers. KONA Powder and Particle Journal, 14(0), 31-43. doi:10.14356/kona.1996008

Navarro, H. A., & de Souza Braun, M. P. (2013). Determination of the normal spring stiffness coefficient in the linear spring–dashpot contact model of discrete element method. Powder Technology, 246, 707-722. doi:10.1016/j.powtec.2013.05.049

Neuner, M., Smith, L., Blowes, D. W., Sego, D. C., Smith, L. J. D., Fretz, N., & Gupton, M. (2013). The Diavik waste rock project: Water flow through mine waste rock in a permafrost terrain. Applied Geochemistry, 36, 222-233. doi:10.1016/j.apgeochem.2012.03.011

Nguyen, D. H., Azema, E., Sornay, P., & Radjai, F. (2015). Effects of shape and size polydispersity on strength properties of granular materials. Phys Rev E Stat Nonlin Soft Matter Phys, 91(3), 032203. doi:10.1103/PhysRevE.91.032203

Nichol, R. S. (1986). Rock segregation in waste dumps. Paper presented at the Proceedings of the international conference on flow-through rock drains.

Ohm, H.-S., & Hryciw, R. D. (2013). Translucent Segregation Table Test for Sand and Gravel Particle Size Distribution. Geotechnical Testing Journal, 36(4). doi:10.1520/gtj20120221

Ovalle, C., & Dano, C. (2020). Effects of particle size–strength and size–shape correlations on parallel grading scaling. Géotechnique Letters, 10(2), 191-197.

Ovalle, C., Frossard, E., Dano, C., Hu, W., Maiolino, S., & Hicher, P.-Y. (2014). The effect of size on the strength of coarse rock aggregates and large rockfill samples through experimental data. Acta Mechanica, 225(8), 2199-2216. doi:10.1007/s00707-014-1127-z

Oyanguren, P. R., Nicieza, C. G., Fernández, M. I. Á., & Palacio, C. G. (2008). Stability analysis of Llerin Rockfill Dam: An in situ direct shear test. Engineering Geology, 100(3-4), 120-130. doi:10.1016/j.enggeo.2008.02.009

Pankaj, S., Mahure, N., Gupta, S., Sandeep, D., & Devender, S. (2013). Estimation of shear strength of prototype rockfill materials. Int. J. Eng. Sci, 2, 421-426.

Paulick, M., Morgeneyer, M., & Kwade, A. (2015). Review on the influence of elastic particle properties on DEM simulation results. Powder Technology, 283, 66-76. doi:10.1016/j.powtec.2015.03.040

Pearce, S., Lehane, S., & Pearce, J. (2016). Waste material placement options during construction and closure risk reduction—quantifying the how, the why and the how much. Paper presented at the the 11th International Conference on Mine Closure, Australian Centre for Geomechanics.

Pedretti, D., Mayer, K. U., & Beckie, R. D. (2020). Controls of uncertainty in acid rock drainage predictions from waste rock piles examined through Monte-Carlo multicomponent reactive transport. Stochastic Environmental Research and Risk Assessment, 34(1), 219-233. doi:10.1007/s00477-019-01756-1

Pentland, A. (1927). A method of measuring the angularity of sands. Proceedings Transactions of the Royal Society of Canada, 21(3), 43.

Peregoedova, A. (2012). Étude experimentale des propriétés hydrogéologiques des roches stériles à une échelle intermediaire de laboratoire. École polytechnique (Montréal, Québec), Montreal.

Peregoedova, A., Aubertin, M., & Bussière, B. (2014). Evaluation of the water retention curve of mine waste rock using laboratory tests and predictive models. Paper presented at the Georegina 201, Regina,Canada.

Pieretti, M., Karlsson, T., Arvilommi, S., & Muniruzzaman, M. (2022). Challenges in predicting the reactivity of mine waste rocks based on kinetic testing: Humidity cell tests and reactive transport modeling. Journal of Geochemical Exploration, 237. doi:10.1016/j.gexplo.2022.106996

Potyondy, D. O. (2015). The bonded-particle model as a tool for rock mechanics research and application: current trends and future directions. Geosystem Engineering, 18(1), 1-28.

Price, W. A., & M., A. (2010). The Flooded Tailings Impoundment at the Equity Silver Mine. . Paper presented at the British Columbia Mine Reclamation Symposium.

Puell Ortiz, J., & Shukla, S. K. (2017). Methodology for a dump design optimization in large-scale open pit mines. Cogent Engineering, 4(1). doi:10.1080/23311916.2017.1387955

Puhalovich, A., & Coghill, M. (2011). Management of mine wastes using pit void backfilling methods—current issues and approaches. Mine Pit Lakes: Closure Managament Australian Centre for Geomechanics: Crawley, Australia, 3-14.

Quine, R. L. (1993). Stability and deformation of mine waste dumps in north-central Nevada: University of Nevada, Reno.

Qureshi, A., Maurice, C., & Öhlander, B. (2016). Potential of coal mine waste rock for generating acid mine drainage. Journal of Geochemical Exploration, 160, 44-54. doi:10.1016/j.gexplo.2015.10.014

Rai, P., Yadav, U., & Kumar, A. (2011). Productivity Analysis of Draglines Operating in Horizontal and Vertical Tandem Mode of Operation in a Coal Mine—A Case Study. Geotechnical and Geological Engineering, 29(4), 493-504. doi:10.1007/s10706-011-9398-9

Raschke, S. A., & Hryciw, R. D. (1997). Grain-Size Distribution of Granular Soils by Computer Vision. Geotechnical Testing Journal, 20(4). doi:10.1520/gtj10410j

Raymond, G. P., & Davies, J. R. (1978). Triaxial tests on dolomite railroad ballast. Journal of the Geotechnical Engineering Division, 104(6), 737-751.

Raymond, K. E., Seigneur, N., Su, D., & Mayer, K. U. (2021). Investigating the Influence of Structure and Heterogeneity in Waste Rock Piles on Mass Loading Rates—A Reactive Transport Modeling Study. Frontiers in Water, 3. doi:10.3389/frwa.2021.618418

Riley, N. A. (1941). Projection sphericity. Journal of Sedimentary Research, 11(2), 94-95.

Ristow, G. H. (1994). Particle Mass Segregation in a Two-Dimensional Rotating Drum. Europhysics Letters (EPL), 28(2), 97-101. doi:10.1209/0295-5075/28/2/004

Roessler, T., Richter, C., Katterfeld, A., & Will, F. (2019). Development of a standard calibration procedure for the DEM parameters of cohesionless bulk materials–part I: Solving the problem of ambiguous parameter combinations. Powder Technology, 343, 803-812.

Roskilly, S. J., Colbourn, E. A., Alli, O., Williams, D., Paul, K. A., Welfare, E. H., & Trusty, P. A. (2010). Investigating the effect of shape on particle segregation using a Monte Carlo simulation. Powder Technology, 203(2), 211-222.

Rousseau, M., & Pabst, T. (2022). Topology optimization of in-pit codisposal of waste rocks and tailings to reduce advective contaminant transport to the environment. Structural and Multidisciplinary Optimization, 65(6). doi:10.1007/s00158-022-03266-1

Sadek, M. A., & Chen, Y. (2014). Microproperties Calibration of Discrete Element Models for Soil-Tool Interaction. Paper presented at the Tech. rep., 2014 ASABE and CSBE/SCGAB Annual International Meeting, Montreal, Quebec, Canada.

Saeed, M. K., & Siraj, M. S. (2019). Mixing study of non-spherical particles using DEM. Powder Technology, 344, 617-627. doi:10.1016/j.powtec.2018.12.057

Santos, D. A., Barrozo, M. A. S., Duarte, C. R., Weigler, F., & Mellmann, J. (2016a). Investigation of particle dynamics in a rotary drum by means of experiments and numerical simulations using DEM. Advanced Powder Technology, 27(2), 692-703. doi:10.1016/j.apt.2016.02.027

Santos, D. A., Duarte, C. R., & Barrozo, M. A. S. (2016b). Segregation phenomenon in a rotary drum: Experimental study and CFD simulation. Powder Technology, 294, 1-10. doi:10.1016/j.powtec.2016.02.015

Seiden, G., & Thomas, P. J. (2011). Complexity, segregation, and pattern formation in rotating-drum flows. Reviews of Modern Physics, 83(4), 1323.

Shanthi, C., Porpatham, R. K., & Pappa, N. (2014). Image analysis for particle size distribution. International Journal of Engineering Technology, 6(3), 1340-1345.

Shen, P., Zhang, L. M., & Zhu, H. (2016a). Rainfall infiltration in a landslide soil deposit: Importance of inverse particle segregation. Engineering Geology, 205, 116-132. doi:10.1016/j.enggeo.2015.09.008

Shen, Z., Jiang, M., & Thornton, C. (2016b). DEM simulation of bonded granular material. Part I: contact model and application to cemented sand. Computers Geotechnics, 75, 192-209.

Shepherd, R. G. (1989). Correlations of Permeability and Grain Size. Ground Water, 27(5), 633-638. doi:10.1111/j.1745-6584.1989.tb00476.x

Shi, W.-c., Zhu, J.-g., Chiu, C.-f., & Liu, H.-l. (2010). Strength and deformation behaviour of coarse-grained soil by true triaxial tests. Journal of Central South University of Technology, 17(5), 1095-1102. doi:10.1007/s11771-010-0602-5

Shimosaka, A., Nousou, I., Shirakawa, Y., & Hidaka, J. (2013). Effect of particle shape on size segregation of particles. Chemical Engineering Transactions, 32, 2143-2148.

Simoni, A., & Houlsby, G. T. (2006). The Direct Shear Strength and Dilatancy of Sand–gravel Mixtures. Geotechnical and Geological Engineering, 24(3), 523-549. doi:10.1007/s10706-004-5832-6

Simons, T. A. H., Weiler, R., Strege, S., Bensmann, S., Schilling, M., & Kwade, A. (2015). A Ring Shear Tester as Calibration Experiment for DEM Simulations in Agitated Mixers – A Sensitivity Study. Procedia Engineering, 102, 741-748. doi:10.1016/j.proeng.2015.01.178

Smith, L. J. D., Blowes, D. W., Jambor, J. L., Smith, L., Sego, D. C., & Neuner, M. (2013a). The Diavik Waste Rock Project: Particle size distribution and sulfur characteristics of low-sulfide waste rock. Applied Geochemistry, 36, 200-209. doi:10.1016/j.apgeochem.2013.05.006

Smith, L. J. D., Moncur, M. C., Neuner, M., Gupton, M., Blowes, D. W., Smith, L., & Sego, D. C. (2013b). The Diavik Waste Rock Project: Design, construction, and instrumentation of field-scale experimental waste-rock piles. Applied Geochemistry, 36, 187-199. doi:10.1016/j.apgeochem.2011.12.026

Sneed, E. D., & Folk, R. L. (1958). Pebbles in the lower Colorado River, Texas a study in particle morphogenesis. The Journal of Geology, 66(2), 114-150.

Sozzi, A., Zambon, M., Mazza, G., & Salvatori, D. (2021). Fluidized bed drying of blackberry wastes: Drying kinetics, particle characterization and nutritional value of the obtained granular solids. Powder Technology, 385, 37-49.

Spitz, K., & Trudinger, J. (2019a). Approaches to Waste Rock Disposal: Issues and Risks. In Mining and the Environment (pp. 705-718): CRC Press.

Spitz, K., & Trudinger, J. (2019b). Mining and the environment: from ore to metal: CRC Press.

St-Arnault, M., Vriens, B., Blaskovich, R., Aranda, C., Klein, B., Ulrich Mayer, K., & Beckie, R. D. (2020). Geochemical and mineralogical assessment of reactivity in a full-scale heterogeneous waste-rock pile. Minerals Engineering, 145. doi:10.1016/j.mineng.2019.106089

Stephens, D., & Bridgwater, J. (1978a). The mixing and segregation of cohesionless particulate materials Part I. Failure zone formation. Powder Technology, 21(1), 17-28.

Stephens, D., & Bridgwater, J. (1978b). The mixing and segregation of cohesionless particulate materials part II. Microscopic mechanisms for particles differing in size. Powder Technology, 21(1), 29-44.

Stockwell, J., Smith, L., Jambor, J. L., & Beckie, R. (2006). The relationship between fluid flow and mineral weathering in heterogeneous unsaturated porous media: A physical and geochemical characterization of a waste-rock pile. Applied Geochemistry, 21(8), 1347-1361. doi:10.1016/j.apgeochem.2006.03.015

Su, H., Fu, Z., Gao, A., & Wen, Z. (2019). Numerical Simulation of Soil Levee Slope Instability Using Particle-Flow Code Method. Natural Hazards Review, 20(2). doi:10.1061/(asce)nh.1527-6996.0000327

Sulsky, D., Chen, Z., & Schreyer, H. L. (1994). A particle method for history-dependent materials. Computer Methods in Applied Mechanics and Engineering, 118(1-2), 179-196. doi:10.1016/0045-7825(94)90112-0

Sun, Y., Indraratna, B., & Nimbalkar, S. (2014). Three-dimensional characterisation of particle size and shape for ballast. Géotechnique Letters, 4(3), 197-202.

Sutherland, K., & Grabinsky, M. (2003). Evaluating segregation in granular filters for earth dams. Paper presented at the 56th Canadian geotechnical conference.

Sutherland, K. J. (2003). Quantifying and controlling segregation in earth dam construction: National Library of Canada= Bibliothèque nationale du Canada, Ottawa.

Sylvain, K., Pabst, T., & Dimech, A. (2019). Waste rock valorization in monolayer covers with elevated water table. Paper presented at the 18th Global Joint Seminar on Geo-Environmental Engineering.

Tachie-Menson, S. (2006). Characterization of the acid-Producing potential and investigation of its effect on weathering of the Goathill North Rock Pile at the Questa Molybdenum Mine. New Mexico Institute of Mining and Technology, New Mexico.

Takahashi, T., Nakagawa, H., Harada, T., & Yamashiki, Y. (1992). Routing Debris Flows with Particle Segregation. Journal of Hydraulic Engineering, 118(11), 1490-1507. doi:10.1061/(asce)0733-9429(1992)118:11(1490)

Tanaka, T. (1971). Segregation models of solid mixtures composed of different densities and particle sizes. Industrial Engineering Chemistry Process Design Development, 10(3), 332-340.

Tang, P., & Puri, V. (2004). Methods for minimizing segregation: a review. Particulate Science Technology, 22(4), 321-337.

Tang, P., & Puri, V. (2005). An innovative device for quantification of percolation and sieving segregation patterns–Single component and multiple size fractions. Particulate Science Technology, 23(4), 335-350.

Tang, P., & Puri, V. (2007). Segregation quantification of two-component particulate mixtures: effect of particle size, density, shape, and surface texture. Particulate Science Technology, 25(6), 571-588.

Teufelsbauer, H., Wang, Y., Chiou, M. C., & Wu, W. (2009). Flow–obstacle interaction in rapid granular avalanches: DEM simulation and comparison with experiment. Granular Matter, 11(4), 209-220. doi:10.1007/s10035-009-0142-6

Thakur, S. C., Ooi, J. Y., & Ahmadian, H. (2016). Scaling of discrete element model parameters for cohesionless and cohesive solid. Powder Technology, 293, 130-137. doi:10.1016/j.powtec.2015.05.051

Thoeni, K., Servin, M., Sloan, S. W., & Giacomini, A. (2019). Designing waste rock barriers by advanced numerical modelling. Journal of Rock Mechanics Geotechnical Engineering, 11(3), 659-675.

Tickell, F. G. (1932). The Examination of Fragmental Rocks. Nature, 129(3258), 528-529. doi:10.1038/129528b0

Tirapelle, M., Volpato, S., & Santomaso, A. C. (2021). Shear-induced particle segregation in binary mixtures: Verification of a percolation theory. Particuology, 57, 214-222.

Tomaschitz, J. d. O. P., Mannich, M., & Ota, J. J. (2018). Experimental results for guidance and design criteria of horizontal end-dumping type river closure. Rbrh, 23(0). doi:10.1590/2318-0331.231820180036

Tripathi, A., & Khakhar, D. V. (2013). Density difference-driven segregation in a dense granular flow. Journal of Fluid Mechanics, 717, 643-669. doi:10.1017/jfm.2012.603

Tsuji, Y., Tanaka, T., & Ishida, T. (1992). Lagrangian numerical simulation of plug flow of cohesionless particles in a horizontal pipe. Powder Technology, 71(3), 239-250. doi:10.1016/0032-5910(92)88030-l

Vangla, P., Roy, N., & Gali, M. L. (2018). Image based shape characterization of granular materials and its effect on kinematics of particle motion. Granular Matter, 20(1), 1-19.

Villain, L. (2014). Reclamation of acid-generating waste rock by in-pit backfilling and sealing: An evaluation of the Kimheden mine site, northern Sweden. Luleå tekniska universitet,

Villain, L., Sundström, N., Perttu, N., Alakangas, L., & Öhlander, B. (2014). Evaluation of the effectiveness of backfilling and sealing at an open-pit mine using ground penetrating radar and geoelectrical surveys, Kimheden, northern Sweden. Environmental Earth Sciences, 73(8), 4495-4509. doi:10.1007/s12665-014-3737-0

Vriens, B., Peterson, H., Laurenzi, L., Smith, L., Aranda, C., Mayer, K. U., & Beckie, R. D. (2019). Long-term monitoring of waste-rock weathering at the Antamina mine, Peru. Chemosphere, 215, 858-869.

Wadell, H. (1932). Volume, shape, and roundness of rock particles. The Journal of Geology, 40(5), 443-451.

Wadell, H. (1933). Sphericity and roundness of rock particles. The Journal of Geology, 41(3), 310-331.

Wang, D., Servin, M., Berglund, T., Mickelsson, K. O., & Rönnbäck, S. (2015). Parametrization and validation of a nonsmooth discrete element method for simulating flows of iron ore green pellets. Powder Technology, 283, 475-487. doi:10.1016/j.powtec.2015.05.040

Wang, J.-J., Zhang, H.-P., Tang, S.-C., & Liang, Y. (2013). Effects of Particle Size Distribution on Shear Strength of Accumulation Soil. Journal of Geotechnical and Geoenvironmental Engineering, 139(11), 1994-1997. doi:10.1061/(asce)gt.1943-5606.0000931

Weil, R. R., Brady, N. C., & Weil, R. R. (2016). The nature and properties of soils: Pearson.

Westfeld, P., Mader, D., & Maas, H. G. (2015). Generation of TIR-attributed 3D Point Clouds from UAV-based Thermal Imagery. Photogrammetrie Fernerkundung Geoinformation(5), 381-393. doi:10.1127/1432-8364/2015/0274

Westland, J. (1988). A study of segregation in cohesionless soil. University of Toronto, Toronto, Canada.

Wickland, B. E., Wilson, G. W., & Wijewickreme, D. (2010). Hydraulic conductivity and consolidation response of mixtures of mine waste rock and tailings. Canadian Geotechnical Journal, 47(4), 472-485. doi:10.1139/T09-115

Wijekoon, C., Goodwin, P., & Hsiang, T. (2008). Quantifying fungal infection of plant leaves by digital image analysis using Scion Image software. Journal of microbiological methods, 74(2-3), 94-101.

Williams, D., & Rohde, T. (2008). Rainfall infiltration into and seepage from rock dumps—a review. Paper presented at the Rock Dumps 2008: Proceedings of the First International Seminar on the Management of Rock Dumps, Stockpiles and Heap Leach Pads.

Williams, D. J. (1996). Lateral thinking on mine site rehabilitation. Paper presented at the Proceedings of National Environmental Law Association Conference.

Williams, D. J. (2001). Assessment of embankment parameters.

Wilson, D., Amos, R. T., Blowes, D. W., Langman, J. B., Ptacek, C. J., Smith, L., & Sego, D. C. (2018). Diavik waste rock project: A conceptual model for temperature and sulfide-content dependent geochemical evolution of waste rock – Laboratory scale. Applied Geochemistry, 89, 160-172. doi:10.1016/j.apgeochem.2017.12.007

Wilson, D., Smith, L., Atherton, C., Smith, L. J., Amos, R. T., Barsi, D. R., . . . Blowes, D. W. (2022). Diavik Waste Rock Project: Geostatistical Analysis of Sulfur, Carbon, and Hydraulic Conductivity Distribution in a Large-Scale Experimental Waste Rock Pile. Minerals, 12(5), 577.

Wu, P.-K., Matsushima, K., & Tatsuoka, F. (2008). Effects of specimen size and some other factors on the strength and deformation of granular soil in direct shear tests. Geotechnical Testing Journal, 31(1), 45-64.

Xiao, Y., Long, L., Matthew Evans, T., Zhou, H., Liu, H., & Stuedlein, A. W. (2019). Effect of Particle Shape on Stress-Dilatancy Responses of Medium-Dense Sands. Journal of Geotechnical and Geoenvironmental Engineering, 145(2). doi:10.1061/(asce)gt.1943-5606.0001994

Xu, M., Guo, N., & Yang, Z. (2021). Particle shape effects on the shear behaviors of granular assemblies: irregularity and elongation. Granular Matter, 23(2), 1-15.

Xu, W.-J., Wang, S., Zhang, H.-Y., & Zhang, Z.-L. (2016). Discrete element modelling of a soil-rock mixture used in an embankment dam. International Journal of Rock Mechanics Mining Sciences, 86, 141-156.

Xu, W., Xu, Q., & Hu, R. (2011). Study on the shear strength of soil–rock mixture by large scale direct shear test. International Journal of Rock Mechanics and Mining Sciences, 48(8), 1235-1247. doi:10.1016/j.ijrmms.2011.09.018

Xu, Y., Kafui, K., Thornton, C., & Lian, G. (2002). Effects of material properties on granular flow in a silo using DEM simulation. Particulate Science Technology, 20(2), 109-124.

Xu, Y., Williams, D., & Serati, M. (2017). Investigation of Shear Strength and Breakdown of Mine Waste Rock. Paper presented at the 51st US Rock Mechanics/Geomechanics Symposium.

Yan, Z., Wilkinson, S. K., Stitt, E. H., & Marigo, M. (2015). Discrete element modelling (DEM) input parameters: understanding their impact on model predictions using statistical analysis. Computational Particle Mechanics, 2(3), 283-299. doi:10.1007/s40571-015-0056-5

Ye, Z., Yahyaei, M., Hilden, M., & Powell, M. (2022). A laboratory-scale characterisation test for quantifying the size segregation of stockpiles. Minerals Engineering, 188, 107830.

Zevgolis, I. E. (2018). Geotechnical characterization of mining rock waste dumps in central Evia, Greece. Environmental Earth Sciences, 77(16), 1-18.

Zhang, J., Hu, Z., Ge, W., Zhang, Y., Li, T., & Li, J. (2004). Application of the Discrete Approach to the Simulation of Size Segregation in Granular Chute Flow. Industrial & Engineering Chemistry Research, 43(18), 5521-5528. doi:10.1021/ie034254f

Zhang, J., Wang, X., Yin, Z.-Y., & Liang, Z. (2020). DEM modeling of large-scale triaxial test of rock clasts considering realistic particle shapes and flexible membrane boundary. Engineering Geology, 279, 105871.

Zhang, S., & Liu, W. (2017). Application of aerial image analysis for assessing particle size segregation in dump leaching. Hydrometallurgy, 171, 99-105. doi:10.1016/j.hydromet.2017.05.001

Zhang, S., Liu, W., & Granata, G. (2018). Effects of grain size gradation on the porosity of packed heap leach beds. Hydrometallurgy, 179, 238-244. doi:10.1016/j.hydromet.2018.06.014

Zhang, S., Zhao, L., Wang, X., & Huang, D. (2021). Quantifying the effects of elongation and flatness on the shear behavior of realistic 3D rock aggregates based on DEM modeling. Advanced Powder Technology, 32(5), 1318-1332.

Zhang, Z. (2016). Particle overlapping error correction for coal size distribution estimation by image analysis. International Journal of Mineral Processing, 155, 136-139.

Zhao, Y., Zhou, H., Feng, X., & Cui, Y.-J. (2012). Effects of water content and particle crushing on the shear behaviour of an infilled-joint soil. Géotechnique, 62(12), 1133-1137.

Zheng, J., & Hryciw, R. D. (2015). Traditional soil particle sphericity, roundness and surface roughness by computational geometry. Géotechnique, 65(6), 494-506.

Zhou, W., Lai, Z., Ma, G., Yang, L., & Chen, Y. (2016). Effect of base roughness on size segregation in dry granular flows. Granular Matter, 18(4). doi:10.1007/s10035-016-0680-7

Zhu, D., Tu, S., Ma, H., Wei, H., Li, H., & Wang, C. (2019). Modeling and calculating for the compaction characteristics of waste rock masses. International Journal for Numerical Analytical Methods in Geomechanics, 43(1), 257-271.

Zhu, H., Zhou, Z., Yang, R., & Yu, A. (2008). Discrete particle simulation of particulate systems: a review of major applications and findings. Chemical Engineering Science, 63(23), 5728-5770.

Ziaie Moayed, R., Alibolandi, M., & Alizadeh, A. (2016). Specimen size effects on direct shear test of silty sands. International Journal of Geotechnical Engineering, 1-8. doi:10.1080/19386362.2016.1205166

Zigan, S., Thorpe, R. B., Tuzun, U., & Enstad, G. G. (2007). Air current segregation of alumina powder. Particle & Particle Systems Characterization, 24(2), 124-135.

Zigan, S., Thorpe, R. B., Tuzun, U., Enstad, G. G., & Battistin, F. (2008). Theoretical and experimental testing of a scaling rule for air current segregation of alumina powder in cylindrical silos. Powder Technology, 183(1), 133-145.

APPENDIX A WASTE ROCK BASIC PROPERTIES

Table A.1: Specific gravity of waste rock sample with diameters ranged between 5 mm and 50 mm (ASTM C127)

	Sample 1	Sample 2	Sample 3
Mass of oven-dried sample and container (g)	6595.6	6811.3	6619.7
Mass of container (g)	708.8	931.6	738.9
Mass of oven-dried sample (g) (A)	5886.8	5879.7	5880.8
Mass of SSD (g) (B)	5904	5901.8	5900.9
Apparent mass of saturated test sample in water (g) (C)	3748.8	3750	3749.3
G_S (OD) = A / (B - C)	2.7314	2.7325	2.7332
G_S (SSD)= B / (B - C)	2.7394	2.7427	2.7426
G_S (apparent) = A / (A - C)	2.7534	2.7608	2.7590
Absorption (%) = [(B - A) / A]×100	0.2922	0.3759	0.3418

Table A.1: Specific gravity of waste rock sample with particles < 5 mm (ASTM D854)

	Sample 1	Sample 2	Sample 3
Mass of oven-dried sample and container (g)	458.1	460.4	458.4
Mass of container (g)	285.4	290.6	287.6
M_s (g)	172.7	169.8	170.8
$M_{\rho ws,t}$ (g) at 22.6℃	816.1	802.8	816.2
$M_{\rho w,t}$ (g) at 22.6℃	705.8	694.7	707.5
G_t at 22.6℃	2.7676	2.7520	2.7504
The temperature coefficient K	0.99943	0.99943	0.99943
$G_{20℃}$	2.7669	2.7513	2.7496

M_s: the mass of the oven dry waste rock;

$M_{\rho w,t}$: mass of the pycnometer and water at the test temperature;

$M_{\rho ws,t}$: the mass of pycnometer, water, and waste rock at the test temperature.

Table A.2: Specific gravity of waste rock sample with particle diameters ranged between 0 and 50 mm

	Sample 1	Sample 2	Sample 3
R	97.15	97.19	97.18
P	2.85	2.81	2.82
$G_{1@20°C}$	2.7534	2.7608	2.7590
$G2_{@20°C}$	2.7669	2.7513	2.7496
G_s (at 20°C)	2.7538	2.7605	2.7587
The averager Gs of waste rock (0 ~ 50 mm) at 20°C	2.7577		

R: the percent of waste rock retained on the 5 mm sieve;

P: the percent of waste rock passing the 5 mm sieve;

$G_{1@20°C}$: the apparent specific gravity of waste rock retained on the 5 mm sieve as determined using ASTM C127, corrected to 20°C;

$G_{2@20°C}$: the specific gravity of waste rock passing the 5 mm sieve determined using ASTM D854.

APPENDIX B MEASURED AND SIMULATED REPOSE ANGLE

Table B.1: Measured repose angles (θ) of waste rock in laboratory repose angle tests.

Tests	H (cm)	L1 (cm)	L2 (cm)	L3 (cm)	L4 (cm)	R (cm)	H / R (-)	Radian (-)	Angle (°)
1	19.50	24.00	25.00	26.00	28.00	44.25	0.441	0.415	23.78
2	19.75	31	28	19	24	44.50	0.444	0.418	23.93
3	20.73	24	20	23	27	46.50	0.446	0.419	24.02
4	21.60	30	23	14	27	46.50	0.465	0.435	24.92
5	20.35	28	26	24	30	43.00	0.473	0.442	25.33
6	19.40	35	25	20	26	43.50	0.446	0.420	24.04
7	21.10	27	31	26	25	42.75	0.494	0.458	26.27
8	20.80	22	32	33	26	41.75	0.498	0.462	26.48
9	22.85	20	26	32	30	43.00	0.531	0.488	27.99
10	21.45	27	27	28	29	42.25	0.508	0.470	26.92

Table B.2: Simulated laboratory repose angle tests

	Simulated repose angle θ (°)											
	μ = 0.1											
μ_r	C1	C2	C3	C4	C5	C6	C7	C8	C9	C10	mean	Standard deviation
0.1	12.62	11.30	12.47	11.91	11.28	10.80	12.08	11.37	12.09	11.93	11.78	0.58
0.2	12.15	12.79	13.00	12.37	12.10	11.85	13.52	12.55	12.88	13.43	12.66	0.56
0.3	14.19	13.05	13.34	11.96	11.72	12.36	13.00	12.14	12.35	12.79	12.69	0.74
0.4	12.54	13.98	14.71	12.21	11.85	11.91	13.85	11.48	12.48	13.87	12.89	1.12
	μ = 0.2											
0.1	18.68	20.18	23.78	20.63	19.79	22.73	22.31	21.53	22.88	22.58	21.51	1.63
0.2	25.02	24.28	28.83	23.24	25.61	25.19	25.54	24.36	25.90	24.51	25.25	1.48
0.3	26.60	26.53	29.05	24.80	25.04	31.64	25.69	28.67	27.73	26.23	27.20	2.11
0.4	24.10	26.08	30.11	26.15	26.40	26.17	26.91	28.29	27.27	26.40	26.79	1.58
	μ = 0.3											
0.1	22.46	25.51	26.05	25.74	25.35	24.20	27.46	26.73	25.69	26.26	25.55	1.39
0.2	29.12	29.95	32.72	30.84	30.96	29.65	32.64	31.35	30.65	30.78	30.87	1.17
0.3	31.27	32.89	34.93	31.65	33.69	34.25	34.31	32.64	34.54	31.47	33.16	1.37
0.4	31.27	33.24	35.20	34.78	34.61	32.77	34.39	36.04	36.21	33.04	34.15	1.56
	μ = 0.4											
0.1	26.24	27.86	28.07	27.65	27.45	25.46	29.25	27.00	27.99	28.94	27.59	1.14
0.2	33.41	34.42	34.12	32.03	34.37	32.64	34.99	32.72	35.90	34.30	33.89	1.18
0.3	34.82	36.79	38.97	35.55	37.41	36.31	36.81	36.39	37.04	34.19	36.43	1.35
0.4	36.88	37.42	40.10	37.35	39.08	37.86	40.59	35.85	40.23	39.54	38.49	1.63

Table B.3: Simulated field repose angle tests in Canadian Malartic mine

μ_r	Repose angle θ (°)						
	μ = 0.2						
	C1	C2	C3	C4	C5	Mean	Standard deviation
0.2	28.3	31.2	26.7	30.2	29.8	29.2	1.7
0.4	26.5	33.0	30.1	32.6	29.2	30.3	2.6
0.6	30.1	33.5	27.9	32.8	30.8	31.0	2.2
0.8	30.5	33.9	33.1	32.8	30.4	32.1	1.6
	μ = 0.4						
0.2	32.9	33.6	32.7	35.0	32.7	33.4	1.0
0.4	36.3	37.4	35.8	37.1	37.0	36.7	0.7
0.6	36.5	38.1	37.4	38.6	37.7	37.7	0.8
0.8	37.3	40.9	38.2	41.2	37.2	38.9	2.0
	μ = 0.6						
0.2	34.6	37.9	30.9	36.4	36.7	35.3	2.7
0.4	36.9	38.3	36.2	36.5	38.5	37.3	1.1
0.6	38.1	40.8	38.2	40.9	38.8	39.4	1.4
0.8	40.2	42.0	38.4	40.7	40.5	40.4	1.3
	μ = 0.8						
0.2	35.8	35.5	36.5	36.2	35.0	35.8	0.6
0.4	38.5	38.1	41.7	38.3	38.5	39.0	1.5
0.6	40.9	39.3	44.6	42.7	42.7	42.0	2.0
0.8	42.8	41.5	43.5	46.8	43.9	43.7	1.9

Table B.4: Calibrated field repose angle tests in Canadian Malartic (CM) mine with $\mu = \mu_r = 0.44$. Ten simulations were repeated ten times with different random seeds.

Case	θ1	θ2	θ3	θ4	Mean	Standard deviation
1	33.2	31.7	36	38.7	34.9	3.1
2	38	38.8	36.1	39.8	38.2	1.6
3	38.5	35.4	39.5	36.3	37.4	1.9
4	37.9	39	39.7	43.8	40.1	2.6
5	39	40.4	38.2	38.8	39.1	0.9
6	38.1	38.1	37.5	36.6	37.6	0.7
7	36.8	43.1	33.3	36.9	37.5	4.1
8	35.3	40.7	32.8	34.3	35.8	3.4
9	38.3	33.7	36.3	35	35.8	2.0
10	35.4	41.5	33.8	38.4	37.3	3.4

Table B.5: Simulated field repose angle tests in Quebrada Blanca mine

μ_r	Repose angle (°)						
	$\mu = 0.2$						
	C1	C2	C3	C4	C5	Mean	Standard deviation
0.2	31.0	27.5	27.2	29.2	28.9	28.7	1.5
0.4	31.3	28.8	27.0	28.0	29.3	28.9	1.6
0.6	32.6	29.5	29.5	29.1	30.1	30.2	1.4
0.8	34.2	30.7	31.0	31.8	31.2	31.8	1.4
	$\mu = 0.4$						
0.2	34.1	32.7	28.9	32.9	33.0	32.3	2.0
0.4	36.3	33.3	33.6	36.3	35.7	35.0	1.5
0.6	37.9	38.2	36.2	37.7	38.6	37.7	0.9
0.8	37.4	37.1	37.9	38.8	40.3	38.3	1.3
	$\mu = 0.6$						
0.2	33.3	32.9	36.5	36.4	34.0	34.6	1.7
0.4	36.0	35.3	37.6	37.8	41.1	37.6	2.3
0.6	40.1	37.5	38.4	38.9	38.4	38.6	1.0
0.8	40.6	37.1	39.3	38.2	42.5	39.5	2.1
	$\mu = 0.8$						
0.2	36.2	37.0	31.4	37.4	32.7	34.9	2.7
0.4	41.2	37.5	37.4	37.8	37.8	38.3	1.6
0.6	41.3	44.1	39.0	39.0	38.0	40.3	2.5
0.8	38.8	43.4	40.9	39.2	39.0	40.3	2.0

Table B.6: Calibrated field repose angle tests in Quebrada Blanca mine with $\mu = \mu_r = 0.47$. Ten simulations were repeated ten times with ten different random seeds.

Case	θ1 (°)	θ2 (°)	θ3 (°)	θ4 (°)	Mean	Standard deviation
1	39.3	39.8	39.3	39.2	39.4	0.3
2	37.1	35.2	38.5	36.8	36.9	1.4
3	38.4	36.6	36.2	37.8	37.3	1.0
4	41	36.1	35.5	37.2	37.5	2.5
5	34.1	37.3	34.6	36.6	35.7	1.5
6	38.9	39.7	38.3	33	37.5	3.0
7	38.3	35	38.2	37.8	37.3	1.6
8	41.6	39.6	37.3	35.8	38.6	2.6
9	38.2	36.7	35	32	35.5	2.7
10	39.7	40.6	34.4	33.6	37.1	3.6

APPENDIX C MEASURED AND SIMULATED SEGREGATION PROPERTIES

Table C.1: Raw PSD curves data of the measured waste rock at the top of the slope in laboratory segregation tests. T1 – T5 indicated the tests 1 to 5.

Fraction (mm)	Passing (%) - Top section (S1)						
	T1	T2	T3	T4	T5	mean	Standard deviation
88.9	100.0	100.0	100.0	100.0	100.0	100.0	0.0
80	84.8	80.5	100.0	83.0	94.7	88.6	7.5
70	75.5	70.6	91.3	74.8	86.9	79.8	7.9
60	71.6	61.6	86.7	71.4	80.4	74.3	8.6
50	68.6	56.3	82.3	61.8	75.2	68.8	9.3
38.1	68.6	55.2	80.7	59.2	74.5	67.7	9.4
25.4	51.5	44.7	63.9	46.3	60.2	53.3	7.6
19.05	28.3	24.7	33.3	28.0	32.9	29.4	3.2
14	14.5	10.7	15.7	13.0	15.5	13.9	1.8
9	5.8	3.7	5.5	5.1	6.9	5.4	1.0
8	0	0	0	0	0	0	0

Table C.2: Raw PSD curves data of the measured waste rock at the middle of the slope in laboratory segregation tests. T1 – T5 indicated the tests 1 to 5.

Fraction (mm)	Passing (%) - Middle section (S2)						
	T1	T2	T3	T4	T5	mean	Standard deviation
88.9	100.0	100.0	100.0	100.0	100.0	100.0	0.0
80	88.6	90.5	79.4	82.0	89.3	86.0	4.4
70	63.0	76.4	66.0	62.3	66.0	66.7	5.1
60	57.8	68.7	59.6	56.8	62.5	61.1	4.3
50	55.6	66.1	56.9	52.3	58.5	57.9	4.6
38.1	53.5	63.2	55.7	50.5	56.6	55.9	4.2
25.4	43.1	45.3	41.6	37.3	39.7	41.4	2.8
19.05	23.1	25.4	22.2	18.7	20.5	22.0	2.3
14	10.0	11.9	9.8	7.5	8.1	9.4	1.5
9	3.8	5.1	3.4	2.4	2.6	3.5	1.0
8	0	0	0	0	0	0	0

Table C.3: Raw PSD curves data of the measured waste rock at the bottom of the slope in laboratory segregation tests. T1 – T5 indicated the tests 1 to 5.

Fraction (mm)	Passing (%) - Bottom section (S3)						
	T1	T2	T3	T4	T5	mean	Standard deviation
88.9	100.0	100.0	100.0	100.0	100.0	100.0	0.0
80	70.8	73.4	81.0	79.6	79.5	76.8	4.0
70	55.7	56.1	62.6	63.2	63.7	60.2	3.6
60	48.0	45.8	52.3	50.5	53.8	50.1	2.9
50	44.0	39.9	45.9	48.5	46.9	45.0	2.9
38.1	41.0	37.2	42.9	46.7	44.2	42.4	3.2
25.4	29.9	26.5	29.7	34.2	30.3	30.1	2.5
19.05	14.7	13.4	18.8	22.2	16.3	17.1	3.1
14	7.1	6.7	8.9	10.3	7.9	8.2	1.3
9	3.0	2.9	4.2	4.4	3.5	3.6	0.6
8	0	0	0	0	0	0	0
9	3.8	5.1	3.4	2.4	2.6	3.5	1.0
8	0	0	0	0	0	0	0

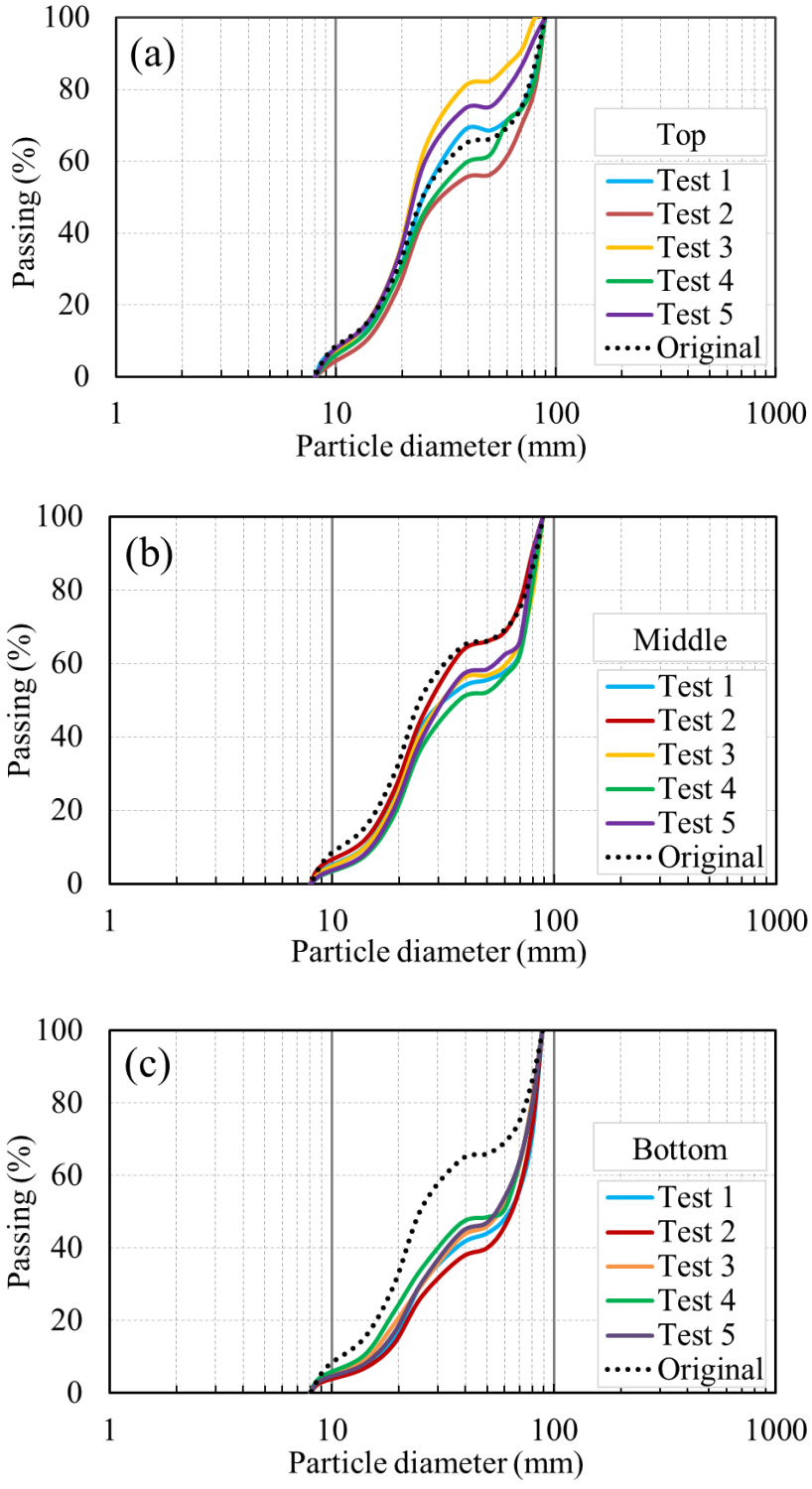

Figure C.1: PSD curves of waste rock in the (a) top, (b) middle, and (c) bottom section of the slope in the laboratory segregation tests.

Table C.4: Grading characteristics of the waste rock in the top, middle, and bottom section of the slope in segregation tests.

Top section (S1)								
Test	D_{95} (mm)	D_{90} (mm)	D_{80} (mm)	D_{60} (mm)	D_{50} (mm)	D_{30} (mm)	D_{15} (mm)	D_{10} (mm)
1	85.8	81.1	64.3	28.9	22.5	17.0	12.2	9.8
2	80.0	71.8	69.4	28.2	22.9	16.9	12.2	9.9
3	83.3	76.1	68.8	32.9	24.1	17.4	12.3	9.9
4	79.8	68.5	61.2	31.0	23.2	17.2	12.2	10.0
5	85.7	73.5	71.3	34.5	24.9	18.4	13.0	10.7
Mean	82.9	74.2	67.0	31.1	23.5	17.4	12.4	10.1
Standard deviation	2.9	4.8	4.1	2.7	1.0	0.6	0.3	0.4
Middle section (S2)								
Test	D_{95} (mm)	D_{90} (mm)	D_{80} (mm)	D_{60} (mm)	D_{50} (mm)	D_{30} (mm)	D_{15} (mm)	D_{10} (mm)
1	85.8	84.1	80.1	63.2	50.8	22.1	15.9	13.5
2	81.8	79.8	70.9	46.5	33.0	20.5	15.2	12.7
3	84.3	81.4	73.0	47.8	34.0	20.9	15.0	12.7
4	81.9	80.0	74.3	63.4	34.1	21.5	15.5	13.1
5	81.6	78.8	74.8	35.9	28.5	19.8	14.6	12.2
Mean	83.1	80.8	74.6	51.4	36.1	20.9	15.3	12.8
Standard deviation	1.9	2.0	3.4	11.8	8.5	0.9	0.5	0.5
Bottom section (S3)								
Test	D_{95} (mm)	D_{90} (mm)	D_{80} (mm)	D_{60} (mm)	D_{50} (mm)	D_{30} (mm)	D_{15} (mm)	D_{10} (mm)
1	85.0	81.5	76.6	61.1	50.0	23.7	16.3	13.0
2	84.8	82.0	79.6	70.1	62.4	27.1	17.0	13.8
3	85.7	84.1	79.1	68.9	57.8	24.0	16.4	13.3
4	86.2	82.1	77.2	68.6	58.0	23.8	15.9	13.0
5	85.1	83.7	80.5	59.4	48.6	24.5	16.9	14.2
Mean	85.4	82.7	78.6	65.6	55.4	24.6	16.5	13.5
Standard deviation	0.6	1.1	1.6	5.0	5.9	1.4	0.4	0.5

Table C.5: Raw PSD curves data of the waste rock in the top, middle, and bottom section of the slope in simulated laboratory segregation tests. Simulations were repeated five times (C1 – C5) with different random seeds.

D (mm)	Passing (%)														
	Top section (S1)					Middle section (S2)					Bottom section (S3)				
	C1	C2	C3	C4	C5	C1	C2	C3	C4	C5	C1	C2	C3	C4	C5
8	0	0	0	0	0	0	0	0	0	0	0	0	0	0	0
9	9	9	9	8	7	4	5	5	5	6	5	5	6	5	5
12	14	15	15	15	13	8	9	9	8	10	9	8	8	9	8
15	22	22	20	21	20	12	13	14	13	15	12	11	12	12	11
17	32	32	30	31	27	19	22	22	21	23	17	16	17	18	16
20	40	41	37	39	36	25	29	27	25	31	22	20	21	23	20
23	51	50	47	49	45	32	38	37	34	41	28	26	28	29	26
26	58	57	53	56	52	36	44	43	41	48	33	29	33	32	32
28	60	60	56	58	55	37	46	45	42	50	34	30	34	34	34
31	62	63	58	60	56	39	48	46	45	52	37	32	37	37	36
34	68	66	61	63	59	43	51	49	49	57	40	34	40	39	38
36	72	68	67	68	63	46	55	55	53	61	43	37	43	42	42
39	73	70	68	69	66	48	57	57	54	62	43	38	44	42	44
42	75	71	68	69	67	48	57	57	55	63	45	38	46	43	45
44	76	71	68	70	67	49	57	58	56	65	47	38	46	43	46
47	77	71	69	71	67	49	61	59	57	65	49	40	47	44	49
50	77	71	69	73	67	49	62	62	57	66	50	42	47	45	51
52	79	73	71	75	67	51	65	62	57	67	52	45	47	45	52
55	79	76	71	77	67	51	66	63	59	69	53	46	48	48	54
58	79	76	77	79	67	53	66	63	60	70	56	48	50	50	57
61	79	76	80	79	67	57	67	68	60	70	60	49	52	52	63
63	79	76	80	84	70	60	69	69	60	73	62	50	53	53	65
66	82	76	80	87	73	63	72	77	65	73	64	55	56	57	68
69	82	76	80	90	76	69	76	77	67	76	69	59	59	60	72
71	86	89	85	90	80	73	81	77	72	78	70	61	66	63	74
74	86	94	85	94	93	76	81	82	79	78	70	64	71	66	75
77	86	94	92	94	93	76	89	85	85	85	80	69	72	79	75
79	86	94	92	94	93	79	89	85	89	92	82	79	81	86	77
82	92	100	92	100	93	85	96	92	96	96	93	91	83	90	84
85	92	100	100	100	93	92	96	96	96	100	95	95	93	90	94
88	100	100	100	100	100	100	100	100	100	100	100	100	100	100	100

Table C.6: Grading characteristics of the waste rock in the top, middle, and bottom section of the slope in the calibration for CM mine ($\mu = \mu_r = 0.44$).

Top section (S1)								
Test	D_{95} (mm)	D_{90} (mm)	D_{80} (mm)	D_{60} (mm)	D_{50} (mm)	D_{30} (mm)	D_{15} (mm)	D_{10} (mm)
1	85.8	81.1	64.3	28.9	22.5	17.0	12.2	9.8
2	80.0	71.8	69.4	28.2	22.9	16.9	12.2	9.9
3	83.3	76.1	68.8	32.9	24.1	17.4	12.3	9.9
4	79.8	68.5	61.2	31.0	23.2	17.2	12.2	10.0
5	85.7	73.5	71.3	34.5	24.9	18.4	13.0	10.7
Mean	82.9	74.2	67.0	31.1	23.5	17.4	12.4	10.1
Standard deviation	2.9	4.8	4.1	2.7	1.0	0.6	0.3	0.4
Middle section (S2)								
Test	D_{95} (mm)	D_{90} (mm)	D_{80} (mm)	D_{60} (mm)	D_{50} (mm)	D_{30} (mm)	D_{15} (mm)	D_{10} (mm)
1	85.8	84.1	80.1	63.2	50.8	22.1	15.9	13.5
2	81.8	79.8	70.9	46.5	33.0	20.5	15.2	12.7
3	84.3	81.4	73.0	47.8	34.0	20.9	15.0	12.7
4	81.9	80.0	74.3	63.4	34.1	21.5	15.5	13.1
5	81.6	78.8	74.8	35.9	28.5	19.8	14.6	12.2
Mean	83.1	80.8	74.6	51.4	36.1	20.9	15.3	12.8
Standard deviation	1.9	2.0	3.4	11.8	8.5	0.9	0.5	0.5
Bottom section (S3)								
Test	D_{95} (mm)	D_{90} (mm)	D_{80} (mm)	D_{60} (mm)	D_{50} (mm)	D_{30} (mm)	D_{15} (mm)	D_{10} (mm)
1	85.0	81.5	76.6	61.1	50.0	23.7	16.3	13.0
2	84.8	82.0	79.6	70.1	62.4	27.1	17.0	13.8
3	85.7	84.1	79.1	68.9	57.8	24.0	16.4	13.3
4	86.2	82.1	77.2	68.6	58.0	23.8	15.9	13.0
5	85.1	83.7	80.5	59.4	48.6	24.5	16.9	14.2
Mean	85.4	82.7	78.6	65.6	55.4	24.6	16.5	13.5
Standard deviation	0.6	1.1	1.6	5.0	5.9	1.4	0.4	0.5

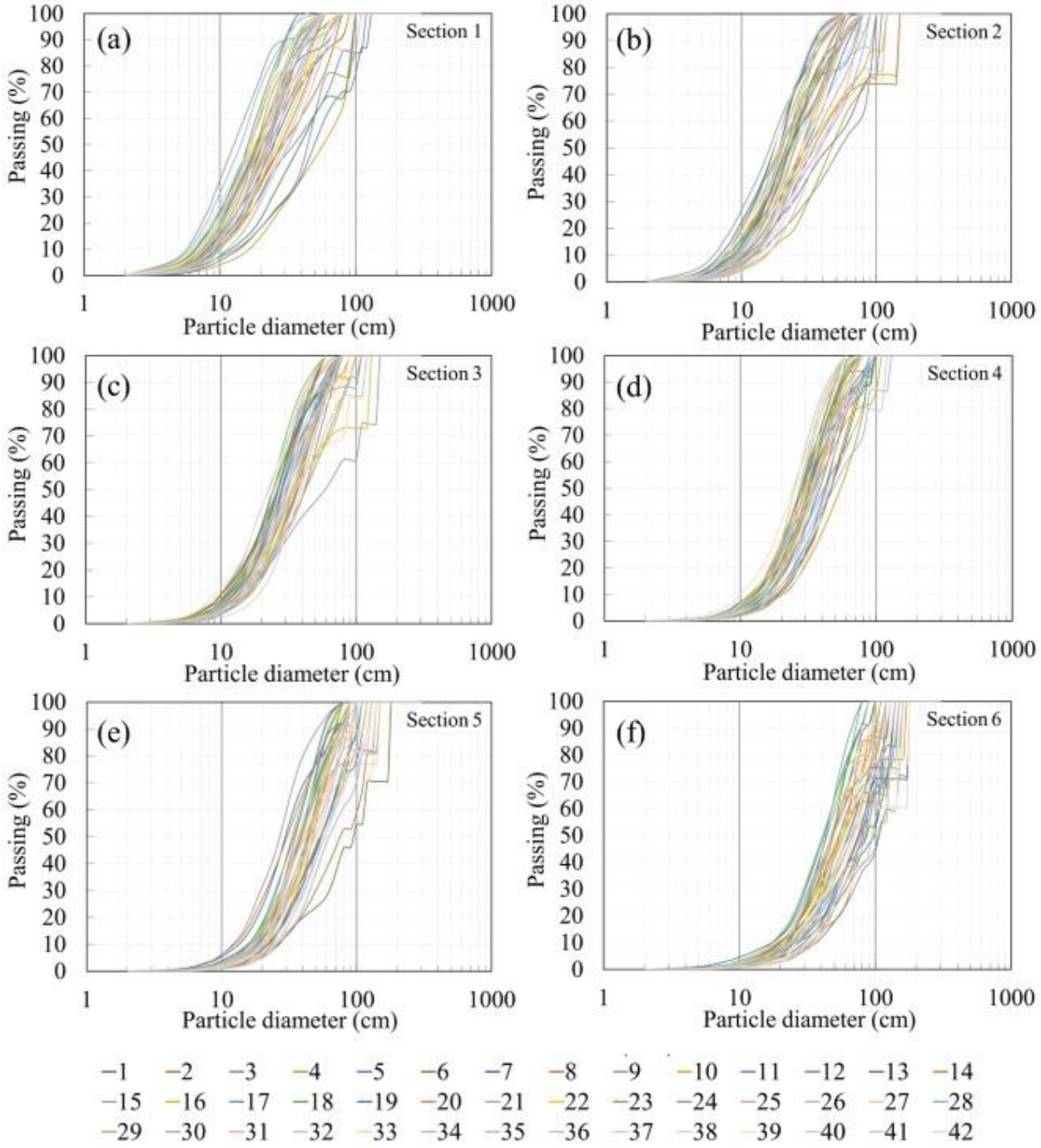

Figure C.2: Characterized 42 PSD curves of waste rock along the slope from (a) secttion 1 (top) to (f) section 6 (bottom) in Canadian Malartic (CM) mine using image analysis.

Table C.7: Segregation degree (χ) in each section of the slope in CM mine

PSD No.	χ (S1)	χ (S2)	χ (S3)	χ (S4)	χ (S5)	χ (S6)
1	-0.46	-1.06	-0.64	-0.31	0.41	0.30
2	-1.08	-1.40	-0.85	-0.46	0.21	0.29
3	-0.37	-0.22	-0.49	-0.63	-0.12	0.58
4	-0.02	-0.04	-0.28	-0.05	-0.03	0.17
5	0.00	-0.18	-0.55	-0.27	-0.25	0.50
6	-0.70	-0.53	-0.37	-0.11	0.14	0.40
7	-0.36	-0.71	-0.35	-0.24	-0.15	0.57
8	-0.29	0.16	-0.30	-0.21	-0.15	0.39
9	-1.25	-1.04	0.22	-0.08	-0.52	0.21
10	-0.63	-0.29	-0.34	-0.10	-0.15	0.42
11	-0.47	-0.94	-0.62	-0.25	0.01	0.46
12	-1.34	-1.11	-0.58	-0.20	0.18	0.42
13	-0.69	-0.79	-0.24	0.01	0.19	0.26
14	-1.53	-1.31	-0.77	-0.76	-0.29	0.34
15	-1.25	-0.97	-0.35	-0.47	-0.30	0.48
16	-0.84	-0.76	0.14	-0.30	0.02	0.40
17	-1.68	-0.89	-0.58	-0.57	-0.24	0.18
18	-0.64	-0.41	-0.32	-0.24	0.09	0.48
19	-1.16	-0.72	-0.85	-0.49	0.12	0.44
20	-0.78	-0.69	-0.43	-0.35	0.12	0.54
21	-0.70	-0.39	-0.53	-0.39	-0.10	0.60
22	-0.62	-0.49	-0.26	-0.35	0.14	0.41
23	-0.80	-0.56	-0.42	-0.04	0.12	0.38
24	-0.93	-0.66	-0.52	-0.31	0.22	0.28
25	-1.17	-1.04	-1.01	-0.56	-0.14	0.14
26	-0.59	-0.29	-0.03	-0.11	0.06	0.60
27	-0.75	-0.20	-0.22	-0.21	0.24	0.16
28	-1.04	-0.74	-0.20	0.22	-0.08	0.55
29	-1.09	-0.88	-0.56	-0.40	0.04	0.19
30	-0.78	-0.34	-0.37	-0.25	0.27	0.49
31	-0.31	-0.13	-0.39	-0.57	0.03	0.48
32	-0.91	-0.16	-0.22	0.13	0.11	0.18
33	-0.40	-0.37	0.08	-0.21	0.30	0.61
34	-0.47	-0.47	0.10	-0.12	0.20	0.61
35	-0.17	-0.20	-0.30	-0.27	0.24	0.30
36	-0.75	-0.63	-0.28	-0.36	0.10	0.32
37	-0.88	-0.58	-0.24	-0.11	0.27	0.48
38	-0.74	-0.39	-0.15	-0.20	0.02	0.61
39	-1.08	-1.03	-0.37	-0.34	0.05	0.52
40	-0.49	-0.40	-0.47	-0.36	0.35	0.30
41	-1.12	-0.94	-0.43	-0.31	0.17	0.42
42	-1.17	-1.20	-0.95	-0.83	-0.10	0.38

Table C.8: Grading characteristics of waste rock in the whole slope in CM mine analyzed using image analysis.

PSD	D_{95}	D_{90}	D_{80}	D_{60}	D_{50}	D_{30}	D_{15}	D_{10}	C_U	C_C
1	174.1	136.3	113.9	73.7	60.1	35.7	22.6	18.2	4.1	1.0
2	140.8	116.8	108.2	69.6	59.0	39.2	24.6	19.2	3.6	1.1
3	174.9	149.7	104.0	71.0	57.2	39.0	23.7	18.0	3.9	1.2
4	133.4	117.7	88.3	63.2	52.4	33.8	21.6	17.3	3.7	1.0
5	128.4	108.9	95.4	56.6	47.5	30.3	18.9	14.9	3.8	1.1
6	80.0	71.7	57.7	42.4	35.6	24.1	15.6	12.5	3.4	1.1
7	174.8	98.3	67.6	42.0	33.8	22.0	14.5	11.5	3.7	1.0
8	117.2	81.3	63.3	42.3	34.5	22.5	14.9	11.9	3.6	1.0
9	141.5	108.9	86.9	53.1	40.2	25.6	16.5	13.3	4.0	0.9
10	110.2	98.9	78.7	52.5	43.3	28.0	17.5	14.0	3.7	1.1
11	139.7	120.7	89.9	62.7	52.4	33.9	21.1	16.5	3.8	1.1
12	76.8	69.3	57.5	44.5	38.0	26.7	17.6	14.4	3.1	1.1
13	80.2	65.8	53.2	37.0	32.2	22.7	15.1	12.1	3.0	1.1
14	85.1	67.9	53.4	37.3	32.8	23.8	16.2	13.2	2.8	1.1
15	113.9	102.2	66.1	44.4	36.5	25.4	16.9	13.6	3.3	1.1
16	108.2	86.5	69.9	47.7	38.4	26.5	17.7	14.3	3.3	1.0
17	69.4	59.6	52.2	37.7	32.7	23.1	16.0	13.1	2.9	1.1
18	153.1	83.9	58.6	39.9	33.7	23.2	16.0	13.4	3.0	1.0
19	117.1	107.4	84.0	54.7	44.9	29.3	19.0	15.6	3.5	1.0
20	162.5	123.0	82.9	52.6	44.9	30.2	19.9	16.2	3.3	1.1
21	141.7	126.1	96.9	56.7	45.8	29.4	19.2	15.5	3.7	1.0
22	111.9	80.9	63.6	46.9	39.5	28.0	19.6	16.2	2.9	1.0
23	74.4	65.9	53.9	36.5	31.4	21.5	14.7	11.8	3.1	1.1
24	129.6	95.9	72.6	49.7	41.9	28.8	19.8	16.4	3.0	1.0
25	90.8	82.4	62.9	43.0	35.4	23.9	15.9	12.9	3.3	1.0
26	142.3	121.0	87.6	52.4	42.5	28.9	20.0	16.4	3.2	1.0
27	141.5	112.8	74.4	49.4	38.6	26.1	18.1	14.9	3.3	0.9
28	131.1	116.1	82.9	51.4	42.1	28.2	18.6	15.2	3.4	1.0
29	88.3	68.5	53.0	36.2	31.6	22.6	15.6	12.9	2.8	1.1
30	150.3	131.2	98.3	64.0	54.0	36.9	22.7	18.6	3.4	1.1
31	101.3	94.7	73.2	50.7	40.2	27.7	18.9	15.5	3.3	1.0
32	113.9	101.3	72.2	51.5	42.9	28.9	18.8	15.1	3.4	1.1
33	149.9	142.3	125.2	65.6	51.6	30.9	19.9	16.2	4.0	0.9
34	139.8	117.1	88.5	57.7	46.2	29.3	19.3	15.7	3.7	0.9
35	77.8	66.1	53.6	37.0	31.6	22.0	15.8	13.3	2.8	1.0
36	78.7	71.8	58.6	38.0	33.2	23.7	16.4	13.5	2.8	1.1
37	123.5	99.0	80.8	56.4	49.1	34.8	23.9	19.3	2.9	1.1
38	175.9	171.8	71.0	46.6	37.4	26.3	18.0	14.8	3.1	1.0
39	174.1	147.6	117.1	64.1	51.8	31.1	19.6	15.8	4.1	1.0
40	118.2	97.9	75.9	53.7	45.2	30.6	20.9	17.3	3.1	1.0
41	154.1	96.6	83.5	56.0	46.7	30.4	19.3	15.2	3.7	1.1
42	93.2	84.0	65.9	45.1	36.9	26.0	17.4	14.0	3.2	1.1

Table C.9: Grading characteristics of waste rock in section 1 in CM mine analyzed using image analysis.

PSD	D_{95}	D_{90}	D_{80}	D_{60}	D_{50}	D_{30}	D_{15}	D_{10}	C_U	C_C
1	97.4	94.8	89.4	50.9	39.2	24.3	15.7	12.0	4.2	1.0
2	75.4	70.7	61.5	39.2	29.7	17.9	10.9	8.6	4.5	0.9
3	97.9	95.8	91.6	50.7	45.0	30.3	17.3	13.1	3.9	1.4
4	116.6	113.2	92.5	73.2	57.9	32.8	20.1	16.1	4.5	0.9
5	126.1	122.3	102.6	59.5	50.6	31.5	17.5	13.8	4.3	1.2
6	58.5	49.4	35.9	25.1	20.7	13.4	8.9	7.3	3.4	1.0
7	84.2	75.1	51.4	31.0	24.8	15.9	9.8	8.0	3.9	1.0
8	68.6	58.9	50.3	34.5	28.4	17.9	11.9	9.6	3.6	1.0
9	46.7	32.7	21.9	15.2	12.9	8.9	6.4	5.5	2.8	1.0
10	84.4	75.7	49.2	29.1	23.4	15.3	9.9	8.1	3.6	1.0
11	116.6	113.1	73.5	48.2	35.3	19.6	11.9	9.4	5.1	0.8
12	34.8	31.6	25.3	18.5	16.1	11.5	7.8	6.5	2.9	1.1
13	71.3	62.7	36.3	22.7	18.7	12.6	8.8	7.4	3.1	1.0
14	51.5	43.1	32.1	21.5	18.5	12.9	8.8	7.2	3.0	1.1
15	48.6	37.8	32.5	22.7	18.9	13.4	9.3	7.8	2.9	1.0
16	51.7	43.5	34.4	23.5	18.2	12.2	8.4	7.0	3.4	0.9
17	35.2	32.3	26.6	19.2	16.6	11.5	7.7	6.3	3.0	1.1
18	47.3	37.4	32.8	23.8	19.6	14.1	9.7	7.9	3.0	1.1
19	51.8	43.7	34.2	23.6	20.4	14.9	10.2	8.5	2.8	1.1
20	53.4	46.9	36.4	26.2	22.3	15.4	10.6	8.9	2.9	1.0
21	52.9	45.9	36.3	28.9	25.2	17.8	12.3	10.1	2.9	1.1
22	59.9	55.7	47.2	32.7	26.8	18.0	12.2	9.9	3.3	1.0
23	44.5	35.6	27.3	19.6	17.1	12.1	7.9	6.5	3.0	1.2
24	55.5	51.0	42.1	28.8	23.6	16.4	11.1	9.3	3.1	1.0
25	56.0	51.9	43.8	25.7	21.8	15.0	10.0	8.3	3.1	1.1
26	50.5	41.0	34.6	26.6	23.2	17.1	11.6	9.6	2.8	1.1
27	54.9	49.8	39.5	23.9	20.8	14.9	10.4	8.9	2.7	1.0
28	36.1	31.3	23.6	16.7	14.2	9.8	6.8	5.8	2.9	1.0
29	43.8	36.4	31.3	22.5	19.0	13.5	9.0	7.5	3.0	1.1
30	54.9	49.9	39.8	27.1	23.2	17.2	11.1	9.0	3.0	1.2
31	106.4	102.8	55.2	39.4	32.6	20.9	14.1	11.3	3.5	1.0
32	53.4	46.8	35.9	23.8	19.5	13.3	8.8	7.3	3.3	1.0
33	50.2	40.4	33.1	23.5	20.8	15.3	10.6	9.0	2.6	1.1
34	51.4	42.8	34.7	25.7	21.8	15.3	10.4	8.7	2.9	1.0
35	67.7	58.6	50.9	36.1	29.9	19.2	12.5	10.0	3.6	1.0
36	66.8	49.6	34.5	24.8	21.6	15.3	10.2	8.4	3.0	1.1
37	62.4	53.7	39.1	29.0	24.3	16.2	10.7	8.8	3.3	1.0
38	36.4	33.6	27.9	19.8	17.2	12.2	8.3	6.8	2.9	1.1
39	45.1	35.8	27.5	19.2	16.8	11.8	8.0	6.7	2.9	1.1
40	72.7	65.4	54.9	38.7	31.7	20.3	13.9	11.2	3.4	1.0
41	52.8	45.7	32.0	19.9	16.6	10.9	7.3	6.0	3.3	1.0
42	52.2	44.4	34.5	23.6	20.1	13.4	8.6	6.9	3.4	1.1

Table C.10: Grading characteristics of waste rock in section 2 in CM mine analyzed using image analysis.

PSD	D_{95}	D_{90}	D_{80}	D_{60}	D_{50}	D_{30}	D_{15}	D_{10}	C_U	C_C
1	66.7	55.3	37.5	26.8	22.9	16.3	10.4	8.4	3.2	1.2
2	56.1	52.3	44.6	29.0	23.0	15.0	9.5	7.5	3.9	1.0
3	107.9	105.7	101.5	73.8	54.8	30.6	16.5	12.5	5.9	1.0
4	147.8	145.6	141.2	57.1	47.7	31.5	19.0	15.0	3.8	1.2
5	97.7	95.4	90.9	61.8	45.0	24.1	13.9	11.0	5.6	0.9
6	68.3	57.7	41.4	27.6	22.8	15.4	10.3	8.5	3.3	1.0
7	44.0	36.1	29.9	20.7	17.6	12.2	8.3	6.8	3.0	1.1
8	148.1	146.2	142.3	45.8	34.8	22.2	13.9	10.8	4.2	1.0
9	49.4	38.8	30.4	19.2	16.3	10.9	7.3	6.1	3.2	1.0
10	116.3	112.7	80.6	43.0	31.3	18.3	11.3	9.1	4.7	0.9
11	58.0	54.0	46.0	29.6	22.9	15.1	9.8	7.9	3.7	1.0
12	51.2	42.4	31.9	20.7	17.7	12.6	8.8	7.3	2.8	1.0
13	51.2	42.3	31.7	21.7	19.0	12.9	9.2	7.7	2.8	1.0
14	50.8	41.7	34.1	24.6	21.3	15.1	10.2	8.4	2.9	1.1
15	54.7	49.4	38.9	27.3	23.2	16.7	11.4	9.6	2.8	1.1
16	51.1	42.2	33.0	23.0	20.3	14.5	10.1	8.6	2.7	1.1
17	74.6	69.1	53.4	26.5	21.9	15.4	10.5	8.7	3.0	1.0
18	68.5	58.1	43.5	28.7	23.5	16.3	11.4	9.6	3.0	1.0
19	71.3	62.6	52.9	36.6	30.1	19.1	12.8	10.3	3.5	1.0
20	61.5	54.7	43.1	25.7	22.2	16.5	11.9	9.9	2.6	1.1
21	83.5	76.8	63.0	40.0	32.5	21.2	14.4	11.7	3.4	1.0
22	66.9	58.0	49.6	34.8	29.7	20.0	14.3	11.7	3.0	1.0
23	54.1	48.1	37.0	24.1	19.8	13.5	8.9	7.3	3.3	1.0
24	65.7	57.3	48.3	33.6	28.5	20.7	14.9	12.3	2.7	1.0
25	54.3	48.6	37.7	29.0	24.7	17.8	12.2	10.0	2.9	1.1
26	95.9	91.8	54.7	33.1	28.4	20.8	14.7	12.1	2.7	1.1
27	117.9	115.9	111.8	36.2	28.8	19.7	13.8	11.2	3.2	1.0
28	41.6	35.7	29.9	22.1	19.7	14.6	10.3	8.7	2.5	1.1
29	43.8	36.9	33.3	26.3	22.9	16.3	10.9	9.0	2.9	1.1
30	86.2	82.3	72.7	50.1	37.8	22.3	14.0	11.1	4.5	0.9
31	76.3	72.6	65.2	48.0	38.8	26.7	18.2	15.2	3.2	1.0
32	117.6	115.2	110.5	48.4	36.0	20.4	13.1	10.6	4.6	0.8
33	47.0	37.4	33.4	25.5	22.0	15.9	11.2	9.5	2.7	1.0
34	48.2	37.7	32.9	24.1	21.5	16.1	11.3	9.4	2.6	1.1
35	82.8	57.0	47.4	31.5	25.1	18.9	14.1	11.6	2.7	1.0
36	67.5	57.0	42.2	25.7	22.2	16.2	11.1	9.2	2.8	1.1
37	68.5	58.7	48.5	34.1	30.1	22.1	15.7	13.1	2.6	1.1
38	64.2	55.0	41.5	29.2	24.4	17.5	12.2	10.0	2.9	1.1
39	37.8	34.7	28.5	20.5	17.8	13.0	9.0	7.4	2.8	1.1
40	74.1	68.1	56.6	36.9	32.5	23.7	16.5	13.9	2.7	1.1
41	51.3	42.7	33.7	22.9	19.0	14.1	9.5	7.9	2.9	1.1
42	46.7	37.1	32.1	22.9	19.4	13.4	9.2	7.6	3.0	1.0

Table C.11: Grading characteristics of waste rock in section 3 in CM mine analyzed using image analysis.

PSD	D_{95}	D_{90}	D_{80}	D_{60}	D_{50}	D_{30}	D_{15}	D_{10}	C_U	C_C
1	81.3	71.4	56.4	39.9	33.9	23.3	15.7	13.0	3.1	1.0
2	66.0	58.4	53.0	42.1	36.7	25.8	17.0	14.1	3.0	1.1
3	75.0	70.1	60.2	47.8	41.6	27.7	16.5	13.4	3.6	1.2
4	103.8	87.0	73.6	52.1	42.8	27.1	18.8	15.2	3.4	0.9
5	71.9	63.9	51.5	34.0	28.9	20.2	13.6	11.0	3.1	1.1
6	69.6	59.4	45.1	30.8	26.0	18.0	12.5	10.4	3.0	1.0
7	69.3	59.2	46.0	29.8	24.4	17.6	11.8	9.9	3.0	1.1
8	93.9	57.7	45.3	31.4	26.7	18.0	12.0	9.8	3.2	1.0
9	148.0	146.1	142.2	77.9	58.9	30.0	18.1	14.9	5.2	0.8
10	70.0	60.0	53.7	40.9	34.5	22.0	14.3	11.5	3.5	1.0
11	71.4	62.8	53.2	37.2	31.4	21.2	14.5	11.8	3.2	1.0
12	55.3	50.6	41.3	31.1	26.9	18.6	13.1	10.7	2.9	1.0
13	55.8	51.6	43.1	32.7	28.9	21.2	15.1	12.5	2.6	1.1
14	56.2	52.3	44.6	32.8	28.3	20.7	14.7	12.1	2.7	1.1
15	105.7	101.4	56.3	41.0	35.1	25.7	17.5	14.7	2.8	1.1
16	128.1	126.3	122.6	48.7	36.8	25.6	17.4	14.5	3.4	0.9
17	65.7	56.6	45.5	32.5	28.3	20.5	14.5	11.9	2.7	1.1
18	70.8	61.5	45.2	29.7	24.6	18.2	13.7	11.3	2.6	1.0
19	54.8	49.6	39.2	30.7	26.9	19.6	14.1	11.4	2.7	1.1
20	64.0	57.4	50.3	36.7	31.8	22.4	15.7	12.9	2.8	1.1
21	65.8	56.8	46.0	32.7	28.4	20.6	14.7	11.9	2.7	1.1
22	82.6	69.4	54.7	39.7	34.0	24.0	18.0	15.0	2.6	1.0
23	52.6	45.2	35.7	26.7	22.6	16.1	11.4	9.6	2.8	1.0
24	68.6	59.0	51.2	36.6	32.1	23.4	17.3	14.8	2.5	1.0
25	54.0	47.9	37.2	28.6	24.5	18.7	12.8	10.6	2.7	1.2
26	94.5	88.7	75.8	49.4	36.6	26.9	19.0	15.6	3.2	0.9
27	84.2	77.4	58.8	39.2	34.0	24.9	17.2	14.7	2.7	1.1
28	69.8	59.9	52.8	38.8	33.6	23.8	17.2	14.8	2.6	1.0
29	57.9	52.6	41.9	30.6	26.1	19.4	14.0	11.4	2.7	1.1
30	71.5	63.0	54.8	42.0	36.1	26.0	17.9	14.9	2.8	1.1
31	73.5	67.0	54.7	35.3	30.3	21.4	15.2	12.6	2.8	1.0
32	72.9	65.7	56.2	43.7	37.5	26.6	17.1	14.4	3.0	1.1
33	116.9	113.8	87.2	49.4	36.0	23.7	16.1	13.4	3.7	0.9
34	116.7	113.3	71.8	50.3	42.6	28.1	18.0	14.9	3.4	1.1
35	59.0	51.9	37.9	28.6	24.4	19.3	14.0	11.3	2.5	1.2
36	68.9	59.1	49.2	34.6	30.7	22.3	15.3	12.6	2.7	1.1
37	91.5	71.9	57.6	45.3	39.2	29.1	21.3	18.2	2.5	1.0
38	73.0	66.1	54.8	37.1	32.3	23.2	17.1	14.3	2.6	1.0
39	81.8	76.8	68.6	43.1	33.8	22.3	15.6	13.4	3.2	0.9
40	66.8	58.1	50.0	35.7	31.0	22.4	16.5	14.2	2.5	1.0
41	72.9	65.9	53.3	35.3	31.2	22.7	15.5	12.6	2.8	1.2
42	54.5	49.0	38.0	26.9	22.6	16.0	10.8	8.8	3.1	1.1

Table C.12: Grading characteristics of waste rock in section 4 in CM mine analyzed using image analysis.

PSD	D_{95}	D_{90}	D_{80}	D_{60}	D_{50}	D_{30}	D_{15}	D_{10}	C_U	C_C
1	95.6	91.2	71.6	54.4	47.4	33.3	22.2	18.3	3.0	1.1
2	93.9	78.3	68.8	53.2	46.8	33.8	23.1	19.0	2.8	1.1
3	66.7	58.5	52.6	40.7	35.0	24.1	15.7	12.6	3.2	1.1
4	87.6	85.3	80.5	63.7	54.9	37.3	25.5	19.9	3.2	1.1
5	91.8	72.5	57.8	44.9	38.4	27.0	18.8	15.2	2.9	1.1
6	58.7	56.0	50.6	39.8	34.2	23.3	16.5	14.1	2.8	1.0
7	63.5	56.9	48.9	34.6	29.2	20.5	14.5	11.7	2.9	1.0
8	81.0	57.9	49.2	34.1	28.6	20.1	14.3	11.7	2.9	1.0
9	87.4	84.8	78.8	53.4	42.2	27.9	19.4	15.6	3.4	0.9
10	106.2	102.4	75.7	45.2	36.4	25.1	16.7	13.9	3.2	1.0
11	88.9	83.8	65.3	49.3	43.2	31.0	20.9	16.9	2.9	1.2
12	68.2	58.8	51.0	36.7	32.9	25.1	17.8	15.2	2.4	1.1
13	83.9	75.5	55.8	36.2	32.2	24.0	17.0	14.6	2.5	1.1
14	55.4	50.8	41.5	32.3	28.8	21.5	15.6	13.2	2.4	1.1
15	63.7	57.6	51.5	39.1	34.2	25.0	18.4	15.1	2.6	1.1
16	68.8	59.1	50.9	35.6	30.0	21.3	15.1	12.4	2.9	1.0
17	56.3	52.6	45.2	33.2	28.5	21.0	15.3	12.8	2.6	1.0
18	63.3	56.6	48.2	33.9	28.6	20.3	14.9	12.5	2.7	1.0
19	84.8	79.3	58.1	37.4	33.1	24.4	17.1	14.8	2.5	1.1
20	71.8	63.7	53.7	37.8	33.3	24.5	17.2	14.5	2.6	1.1
21	83.5	76.8	63.0	40.0	32.5	21.2	14.4	11.7	3.4	1.0
22	59.9	55.9	48.0	35.4	31.8	24.7	19.0	15.9	2.2	1.1
23	95.0	90.1	52.6	33.0	28.1	20.3	14.8	12.1	2.7	1.0
24	93.5	76.0	59.3	42.8	36.1	27.1	19.4	16.4	2.6	1.0
25	73.3	66.7	56.2	40.9	34.0	22.0	14.7	12.1	3.4	1.0
26	71.9	63.8	55.2	42.7	37.0	28.5	20.6	17.3	2.5	1.1
27	82.9	76.1	62.6	39.6	33.9	24.4	18.0	14.9	2.7	1.0
28	126.2	122.4	86.0	61.0	49.9	32.8	23.5	19.3	3.2	0.9
29	56.2	52.4	44.8	33.9	30.1	22.6	16.4	13.9	2.4	1.1
30	82.9	75.7	61.3	48.3	42.1	28.9	19.5	16.1	3.0	1.1
31	54.7	49.4	38.8	31.1	27.4	20.3	14.6	12.0	2.6	1.1
32	117.5	115.1	110.2	56.0	47.1	31.2	20.8	17.0	3.3	1.0
33	55.5	51.0	42.0	31.7	27.7	19.5	14.4	11.9	2.7	1.0
34	84.7	78.3	55.7	35.5	30.9	22.2	15.7	12.9	2.7	1.1
35	53.8	47.5	37.1	29.1	25.2	20.1	15.4	13.3	2.2	1.0
36	59.7	53.9	42.3	32.3	28.8	21.7	15.6	13.0	2.5	1.1
37	85.2	80.3	59.2	49.6	44.7	34.4	25.5	20.4	2.4	1.2
38	59.1	55.2	47.4	35.0	31.2	23.6	17.1	14.5	2.4	1.1
39	74.0	68.0	57.5	42.5	36.2	27.1	19.5	16.1	2.6	1.1
40	67.1	58.6	52.0	39.0	34.4	26.0	17.9	15.4	2.5	1.1
41	85.1	80.2	53.5	40.3	35.0	25.9	18.0	14.9	2.7	1.1
42	55.3	50.5	41.1	29.3	24.4	17.7	12.2	10.1	2.9	1.1

Table C.13: Grading characteristics of waste rock in section 5 in CM mine analyzed using image analysis.

PSD	D_{95}	D_{90}	D_{80}	D_{60}	D_{50}	D_{30}	D_{15}	D_{10}	C_U	C_C
1	178.3	176.6	173.2	113.3	94.7	62.1	33.0	26.7	4.3	1.3
2	147.3	144.5	118.8	101.2	76.3	50.3	32.4	26.1	3.9	1.0
3	96.7	93.5	86.1	64.5	54.9	38.5	26.1	20.9	3.1	1.1
4	105.5	101.0	87.6	65.7	54.1	35.0	22.0	17.6	3.7	1.1
5	84.2	77.8	62.0	46.2	38.8	27.9	19.0	15.4	3.0	1.1
6	82.0	73.3	58.4	45.5	39.1	28.7	20.2	16.8	2.7	1.1
7	74.1	68.2	55.8	35.0	30.6	22.2	15.9	13.3	2.6	1.1
8	71.9	63.9	53.2	36.4	31.1	21.3	15.0	12.4	2.9	1.0
9	60.6	53.9	41.4	31.2	27.3	19.4	14.4	12.0	2.6	1.0
10	79.4	71.8	58.3	43.9	37.1	27.5	19.1	15.9	2.8	1.1
11	105.5	101.0	85.4	63.6	54.4	36.9	26.1	22.0	2.9	1.0
12	75.4	70.8	61.6	49.7	44.0	32.5	23.5	19.9	2.5	1.1
13	82.9	70.0	55.9	44.2	38.3	28.9	21.3	18.3	2.4	1.0
14	67.1	58.6	52.4	40.1	35.5	28.0	21.1	18.0	2.2	1.1
15	83.2	74.6	58.0	43.6	37.0	28.0	20.3	16.8	2.6	1.1
16	74.7	69.3	59.2	46.0	39.3	29.6	21.9	18.8	2.4	1.0
17	65.6	58.1	51.9	39.6	34.5	25.0	18.3	15.4	2.6	1.0
18	94.2	77.7	60.5	45.4	38.1	27.6	20.4	17.5	2.6	1.0
19	115.6	111.2	101.4	65.0	55.4	38.1	26.2	21.5	3.0	1.0
20	127.1	124.2	94.9	53.9	48.4	37.0	27.0	23.1	2.3	1.1
21	85.1	80.3	69.0	51.1	43.7	31.9	24.0	19.1	2.7	1.0
22	115.6	111.2	67.1	51.0	45.1	33.4	24.7	21.2	2.4	1.0
23	71.9	63.8	53.9	38.0	33.9	25.7	18.7	15.8	2.4	1.1
24	147.3	144.6	88.4	64.5	54.3	36.4	26.2	21.9	2.9	0.9
25	87.0	84.0	75.4	51.5	41.7	28.7	19.8	16.2	3.2	1.0
26	85.8	81.5	69.0	52.0	46.0	33.7	23.9	20.3	2.6	1.1
27	147.8	145.6	141.3	66.0	53.4	31.5	22.2	19.1	3.5	0.8
28	71.2	62.3	55.0	43.3	37.7	29.2	21.9	18.6	2.3	1.1
29	83.1	76.5	63.8	46.4	38.4	27.8	19.6	16.7	2.8	1.0
30	137.4	134.8	109.1	78.6	63.2	45.3	30.6	24.6	3.2	1.1
31	96.3	92.7	73.8	53.2	42.0	29.7	21.2	17.6	3.0	0.9
32	90.0	79.7	73.1	59.7	49.5	33.0	24.1	19.8	3.0	0.9
33	138.2	136.4	132.7	57.9	49.7	34.2	24.5	20.5	2.8	1.0
34	107.1	104.2	77.1	56.4	46.3	31.4	22.6	19.1	2.9	0.9
35	81.6	75.1	63.0	47.3	40.0	27.3	18.9	15.8	3.0	1.0
36	93.9	77.3	62.5	45.3	37.6	27.9	20.6	17.7	2.6	1.0
37	125.0	120.0	95.4	68.7	56.5	41.0	29.5	25.7	2.7	1.0
38	84.1	78.0	64.8	47.7	40.1	28.3	20.2	16.9	2.8	1.0
39	127.3	124.6	88.1	67.5	58.4	36.7	24.2	20.3	3.3	1.0
40	126.8	123.6	105.3	70.5	58.5	41.6	29.2	25.1	2.8	1.0
41	94.8	89.7	83.6	67.4	58.4	40.4	27.3	22.5	3.0	1.1
42	93.9	86.4	58.7	43.8	37.1	28.9	22.1	19.5	2.3	1.0

Table C.14: Grading characteristics of waste rock in section 6 in CM mine analyzed using image analysis.

PSD	D_{95}	D_{90}	D_{80}	D_{60}	D_{50}	D_{30}	D_{15}	D_{10}	C_U	C_C
1	137.0	133.9	127.2	107.8	86.3	61.0	34.1	27.5	3.9	1.3
2	118.4	116.9	113.8	93.2	78.8	64.5	41.8	33.3	2.8	1.3
3	178.2	176.4	172.8	140.4	106.4	69.9	45.5	36.7	3.8	0.9
4	136.4	132.8	126.6	73.4	55.0	37.1	25.3	20.1	3.6	0.9
5	147.0	144.0	116.2	103.7	96.8	51.9	35.9	26.2	4.0	1.0
6	94.0	84.8	72.6	56.2	49.3	35.5	25.0	19.6	2.9	1.1
7	178.3	176.5	173.1	73.9	63.4	42.2	26.6	21.2	3.5	1.1
8	115.3	110.5	76.7	63.5	55.9	38.2	24.6	19.2	3.3	1.2
9	115.3	110.6	101.8	71.3	57.0	36.1	24.3	20.1	3.5	0.9
10	115.7	111.4	99.6	78.3	67.5	46.4	29.6	23.3	3.4	1.2
11	146.3	142.6	133.8	89.6	81.6	57.3	36.6	29.5	3.0	1.2
12	94.4	78.8	68.0	54.0	49.2	39.6	28.7	24.6	2.2	1.2
13	84.3	78.3	65.1	49.1	42.3	30.7	21.6	17.0	2.9	1.1
14	116.1	112.1	84.1	58.2	49.4	34.1	25.8	21.7	2.7	0.9
15	118.5	117.1	114.1	84.7	74.2	48.7	30.0	24.3	3.5	1.2
16	106.1	102.1	85.1	68.4	59.0	40.0	27.8	23.4	2.9	1.0
17	74.4	68.7	58.9	48.7	43.6	33.2	25.2	21.0	2.3	1.1
18	158.0	156.0	152.0	56.8	49.1	34.8	26.2	22.0	2.6	1.0
19	125.8	121.7	109.5	85.3	74.9	53.0	37.8	31.0	2.7	1.1
20	167.7	165.4	160.8	88.8	76.7	53.9	39.8	33.0	2.7	1.0
21	147.0	144.0	128.9	121.7	104.6	60.7	40.4	32.9	3.7	0.9
22	116.2	112.5	100.9	66.1	57.4	41.6	28.8	24.1	2.7	1.1
23	76.2	72.4	64.9	51.1	44.5	32.0	22.3	17.9	2.9	1.1
24	126.3	122.7	95.5	64.8	55.5	43.4	31.3	25.7	2.5	1.1
25	97.3	94.6	87.8	59.1	50.6	34.6	24.5	19.9	3.0	1.0
26	147.8	145.6	141.1	104.8	94.7	50.4	31.6	25.7	4.1	0.9
27	116.1	112.1	77.1	56.8	50.4	37.6	25.2	21.1	2.7	1.2
28	137.6	135.2	130.4	93.0	83.7	50.8	31.9	24.8	3.8	1.1
29	105.3	100.6	79.5	49.1	41.6	29.9	21.0	17.1	2.9	1.1
30	157.0	154.1	128.2	95.2	79.3	57.8	41.8	34.7	2.7	1.0
31	135.9	131.8	96.5	74.9	65.9	43.7	29.5	25.4	3.0	1.0
32	114.3	108.5	83.7	55.3	48.2	34.5	24.8	20.9	2.6	1.0
33	156.0	152.0	145.6	95.6	80.7	64.2	41.6	33.1	2.9	1.3
34	146.5	143.0	134.6	87.7	79.9	56.4	36.7	30.1	2.9	1.2
35	83.6	77.1	63.9	48.5	41.7	30.0	20.9	17.4	2.8	1.1
36	83.8	78.7	71.8	57.5	48.7	33.3	24.2	20.3	2.8	1.0
37	127.4	124.7	97.6	77.0	69.2	53.3	41.0	34.9	2.2	1.1
38	178.7	177.5	174.9	88.4	68.9	44.6	30.6	26.4	3.3	0.9
39	177.9	175.8	171.6	140.7	88.3	57.8	38.3	31.2	4.5	0.8
40	113.7	98.2	89.5	70.0	61.6	42.8	28.7	24.0	2.9	1.1
41	158.1	156.2	152.5	83.2	67.5	44.7	28.8	22.7	3.7	1.1
42	124.3	89.1	82.2	65.1	56.7	41.1	30.1	26.6	2.4	1.0

Table C.15: Measured and simulated slope angles of waste rock cones in laboratory segregation tests.

	Measured slope angle (°)	Simulated slope angle (°)
Case 1	24.4	24.7
Case 2	25	23.5
Case 3	24.9	26.5
Case 4	24.9	25.2
Case 5	24.3	26.4
Average	24.7	25.2
Standard deviation	0.3	1.2

APPENDIX D VERIFICATION OF SIMULATION MODEL

Simulation case 1: Particle velocity monitoring during free-fall movement

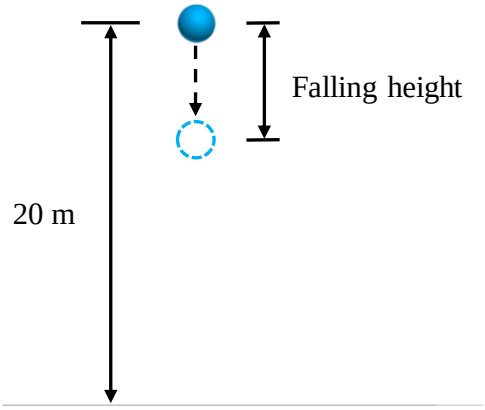

Figure D.1: One ball with a diameter of 2 m was dropped freely from an elevation of 20 m. Particle velocity (v) and falling height (h) was monitored. A timestep of $1\times e^{-4}$ was used in the simulation.

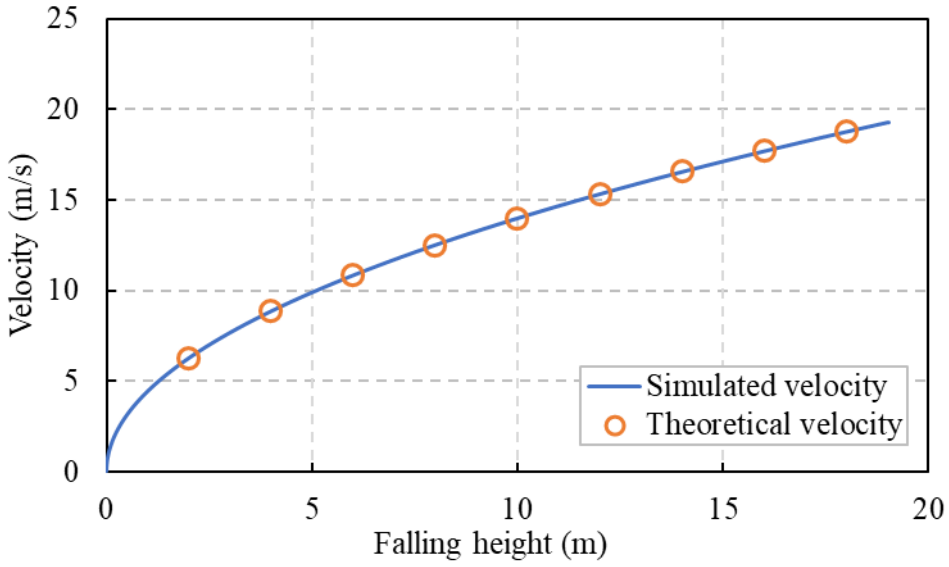

Figure D.2: Particle velocity (v) as a function of falling height (h). The simulated velocity matched well the theoretical velocity $v=\sqrt{2gh}$.

Simulation case 2: Collision between two balls

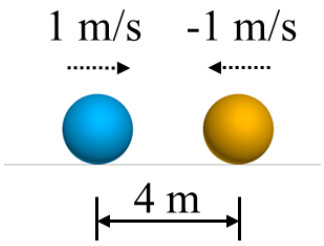

Figure D.3: Collision between two balls on the ground. Ball 1 (in blue) was applied an initial velocity of 1 m/s (toward right) and Ball 2 (in yellow) was applied an initial velocity of -1 m/s (toward right). Particle velocity and displacement were monitored in particle flow process without friction or energy dissipation. The velocities of two balls were presented in figure D.4.

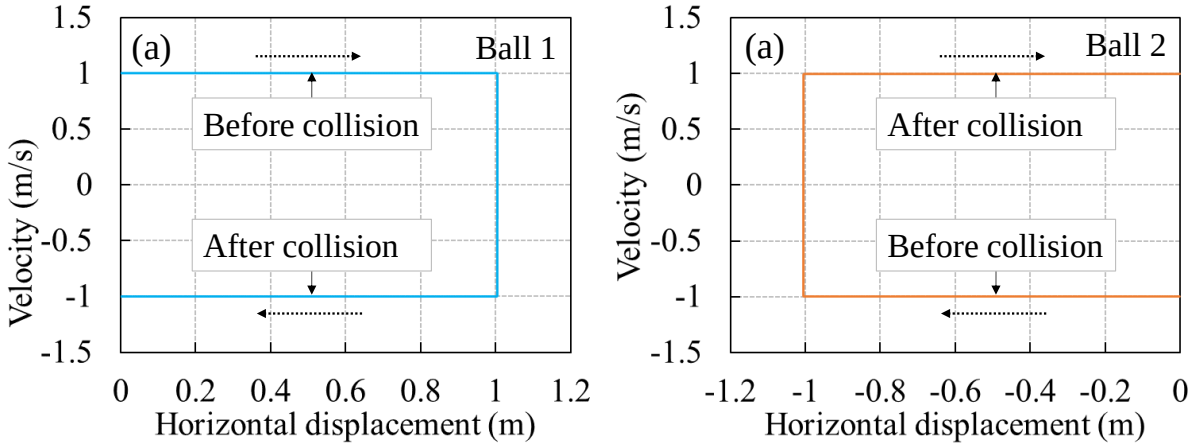

Figure D.4: Velocities of ball 1 and ball 2 in the collision process. The simulations correctly predicted that the two balls rebounded in the opposite direction at the same speed (1m/s).

APPENDIX E PSD CURVES OF SIMULATED WASTE ROCK PARTICLES IN PFC3D

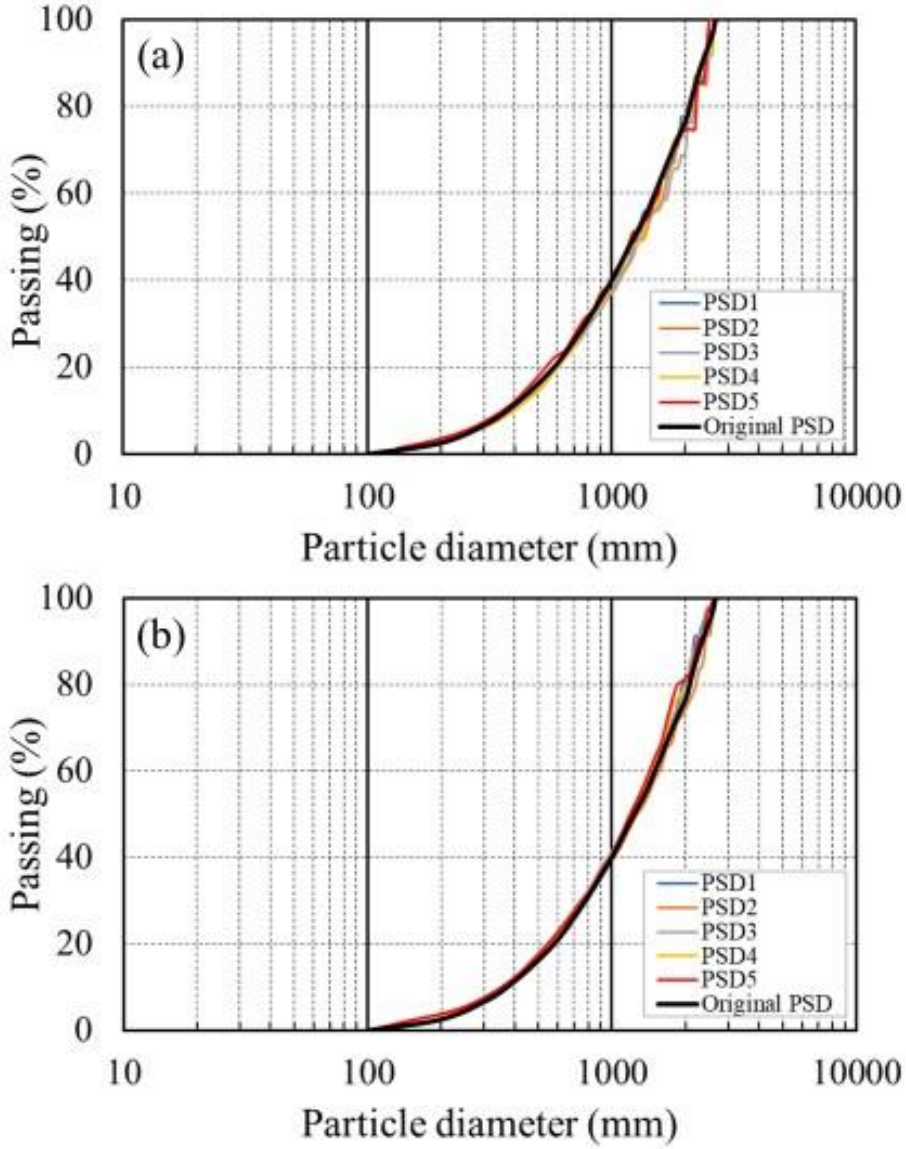

Figure E.1: PSD curves of generated particles in (a) end-dumping method and (b) push-dumping method simulations. PSD1-5 indicated PSD curves generated with five different random seeds.

APPENDIX F SIMULATIONS WITH DIFFERENT BASE LAYERS

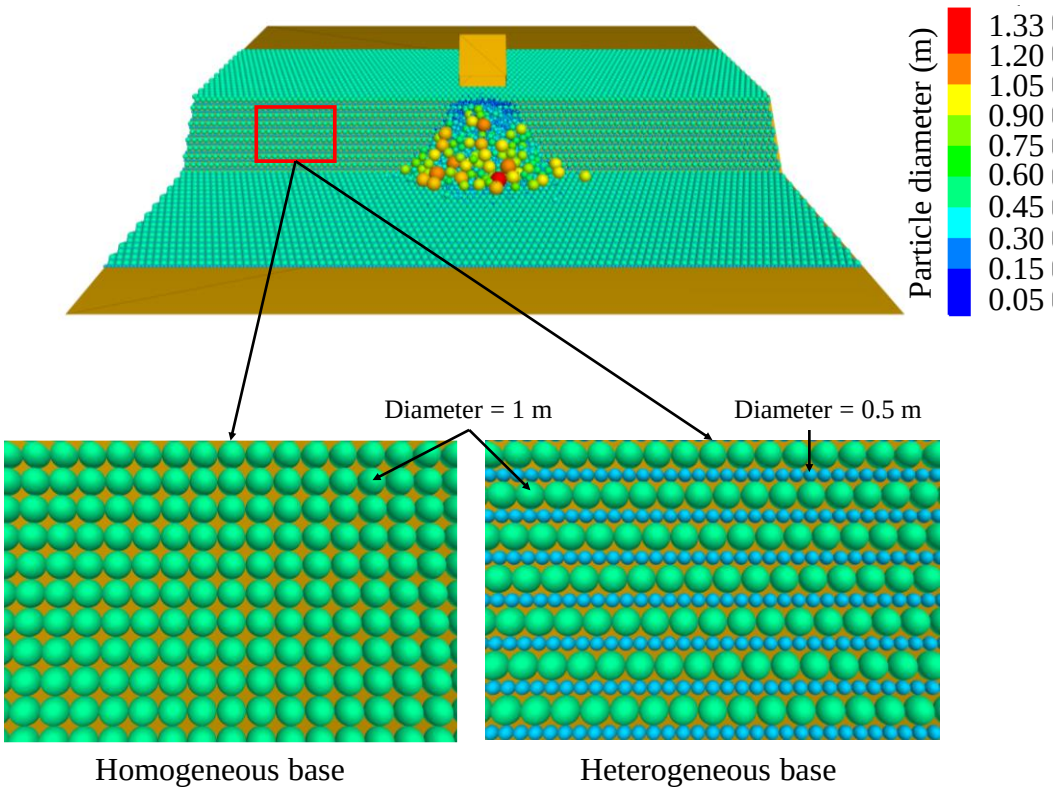

Figure F.1: Setting of the base layer in field scale simulations. Homogeneous base layer contained particles with a diameter of 1 m. Heterogenous base layer contained particles with diameters of 0.5 m and 1 m. Other settings were the same to case A1 in Chapter 6. Simulations with the two kinds of base layers are presented in Figure F.2.

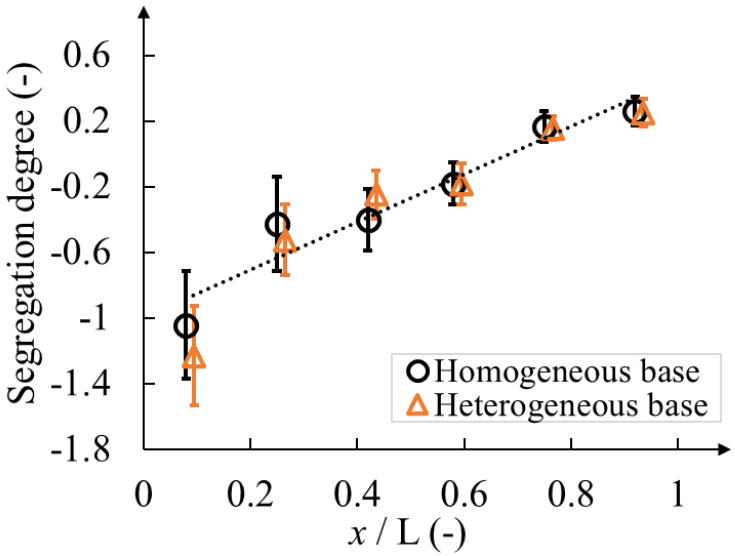

Figure F.2: Segregation degree of waste rock along the slope with homogeneous (in black) and heterogenous (in orange) base layers.